Iodine in Sea Ice and the Polar Atmosphere

Helen M. Atkinson

Submitted to the School of Environmental Sciences, University of East Anglia, in candidature for the degree of Doctor of Philosophy

August 2011

Abstract

The volatilisation of iodine from the ocean and release to the atmosphere in the ice-covered polar regions has been studied. Laboratory experiments involving sea ice- and ice associated- diatoms have shown how the extreme conditions experienced in sea ice brine channels may lead to an increase in production of organic forms of iodine. Trends were observed in production by different classes of enzymes, active in the oxidative metabolism of the cell. An enhancement in trace gas concentrations due to the concentration effect of solvent volume reduction has also been demonstrated.

Field campaigns have been undertaken in both the Arctic and Antarctic. Ship-based measurements in the Weddell Sea have implicated I_2 as a key species in the mechanism of enhancement of atmospheric iodine in this region. Organic and inorganic forms of iodine were measured in seawater, sea ice and the atmosphere. On the Brunt ice shelf, enhanced concentrations of CH_3I and C_2H_5I were measured in the snow firn air, with a diurnal profile, suggesting the snow may be a source of these compounds. These measurements have implications for atmospheric mixing ratios of IO, measured from the ship and validated by satellite data, and new particle formation. This is the first combined *in situ* study in Antarctica of organic and inorganic iodine compounds in sea water, ice and air.

On the Western Antarctic Peninsula, IO was detected in the atmosphere, and seawater measurements of iodocarbons have demonstrated how organic compounds of iodine are enhanced during the phytoplankton bloom; these measurements are also a first.

Iodine emissions in the sea ice zone were also quantified in two campaigns in the Arctic environment. High concentrations of halocarbons were measured in the brine of sea ice, with respect to the water below, in the Arctic Ocean. High atmospheric halocarbon mixing ratios and flux calculations have demonstrated the effect on the atmosphere above. In the Canadian sub-Arctic, where the ice had quite different physical properties, halocarbon concentrations were the highest ever recorded for some compounds, due to extreme concentration in very cold ice.

The enhancement of organic forms of iodine in sea ice has therefore been demonstrated. I_2 has been implicated as a key species in iodine emissions. Therefore, understanding has been furthered on the chemistry of iodine in sea ice and polar atmosphere.

List of Contents

List of Figures

List of Tables

Acknowledgements

Firstly I would like to thank my supervisors, Howard Roscoe, Peter Liss and Claire Hughes for their knowledge, support and guidance. Claire's contribution has been invaluable, and I'm very grateful for the opportunities she has given me. Howard's support has been unwavering, I couldn't have asked for a better primary supervisor, and he has become a close friend, climbing buddy and an inspiration – though being left in the dust of an old man with a false hip has been embarrassing at times.

This work was funded by the National Environment Research Council; additional funding for conference attendance has come from the Association of Polar Early Career Scientists (APECS) and the Research Council of Norway. My research has been supported by data from other researchers; I would like to thank Rosie Chance at the University of York / UEA for iodide and iodate measurements, Ru-Jin Huang at the University of Mainz for inorganic iodine data, Brian Davison at Lancaster University for particle and ozone data, and Anja Schönhardt at Bremen University for satellite data.

I feel very fortunate to have studied at two fine institutions, BAS and UEA. BAS have given me a huge amount of academic, logistical, financial and practical support, and to have worked for an institution which gives you the chance to go snowboarding in Antarctica after a hard day in the lab has been a privilege to say the least. I would especially like to thank Claire Allen for advice on diatoms, Ted Maksym for teaching me about sea ice, Andrew Fleming for sea ice maps, and the atmospheric chemistry group for help both with science and climbing mountains. For assistance in the field I would like to thank all staff on board both the RRS Ernest Shackleton and RRS James Clark Ross, and all at Rothera in 2009/10 season, with particular thanks to Sian Henley and Claire Lehman for making it fun. I am also indebted to many people at UEA, my particular thanks go to the LGMAC group for the loan of equipment and use of lab facilities, Rosie Chance for advice on all things iodine, Martin Johnson for help with the maths, Jan Strauss and Sophie Chollet for providing diatoms, Sarah Yeates for being a wonderful friend, and everyone at 452 for the best dinner parties.

To my parents for my upbringing, education and continued support as I persist in living as a student – I know I owe you a great deal. To my brothers – I'm so proud of you both. To my friends in Leeds – I've missed you and I'm so looking forward to spending more time with you all. Clare, Andy, Holly and Mandy, my best friends in the world – thank you. Finally I would like to dedicate this PhD to my grandmother, without whom I wouldn't be who I am.

Chapter 1. Iodine, sea ice and diatoms

Iodine is essential to mammalian health, being a necessary element in thyroid hormones; deficiency of this element in the human diet can lead to goitre and mental retardation [*Hetzel et al.*, 1987]. The source of iodine is ultimately the ocean; it is transferred via the atmosphere to land, where it is taken up by plants and so works its way up the food chain [*Fuge and Johnson*, 1986].

One way in which iodine is transferred from the ocean to land is via sea ice. Iodine may be concentrated by sea ice formation processes, or by reactions related to the metabolism of marine organisms [*Manley*, 2002]. In the atmosphere, iodine may be responsible for depleting tropospheric ozone [*Chameides and Davis*, 1980], contribute to new atmospheric particle formation [*O'Dowd et al.*, 2002], and subsequently impact climate.

The role of sea ice in concentrating iodine, the marine biological processes which may result in production of volatile forms of iodine, and the atmospheric chemistry following release of these compounds, are discussed in this section, and investigated further in this study.

1.1 The atmospheric chemistry of iodine

The enhancement of iodine in the atmosphere above the sea ice of the Weddell Sea has been the subject of investigation since ground based [*Saiz-Lopez et al.*, 2007a] and satellite measurements [*Saiz-Lopez et al.*, 2007b; *Schönhardt et al.*, 2008] revealed this region as having the highest global atmospheric concentrations of iodine monoxide (IO). An iodine–selective mechanism must exist which concentrates and volatilises iodine in preference to bromine in the ocean: bromide is at least 1000 times more abundant than iodide in seawater, whereas atmospheric mixing ratios of (up to 20 pptv) IO are similar to those of bromine monoxide (BrO) in Antarctica.

IO has only recently been measured in the Arctic, during the COmbined iodine and Bromine Release on the Arctic atmosphere (COBRA) field campaign [*Mahajan et al.*, 2010b] at levels of up to 3.4±1.2 pptv. These IO mixing ratios are however almost an order of magnitude lower than Antarctic concentrations.

BrO has been detected in similar amounts over both Southern- and Arctic Ocean sea ice [*Schönhardt et al.*, 2008], implying similar release mechanisms exist in both polar

regions for compounds of bromine. These are assumed to be heterogeneous reactions involving sea-salt bromide on sea-ice, snow or marine aerosol surfaces [eg *Barrie et al.*, 1988; *McConnell et al.*, 1992; *Vogt et al.*, 1996].

IO and BrO are formed by the reaction of iodine and bromine radicals with ozone respectively, and these reactions lead to ozone depletion in the troposphere [*Chameides and Davis*, 1980; *Davis et al.*, 1996] which is particularly pronounced when both halogens are present [*Read et al.*, 2008; *Saiz-Lopez et al.*, 2007b].

The oxidising capacity of the atmosphere may also be altered by reactions involving HO_x ($OH + HO_2$) and NO_x ($NO + NO_2$) [*Chameides and Davis*, 1980]; examples of ozone depletion mechanisms are given in cycles 1 to 3. That is not to say that ozone depletion events will always occur when high concentrations of the halogen oxides are present – there must be a well defined and long lived boundary layer to hold these reactive species in the same air parcel.

Cycle 1
$$I + O_3 \rightarrow IO + O_2$$
$$IO + HO_2 \rightarrow HOI + O_2$$
$$\underline{HOI + h\nu \rightarrow OH + I}$$
net: $$O_3 + HO_2 \rightarrow OH + 2O_2$$

Cycle 2
$$I + O_3 \rightarrow IO + O_2$$
$$IO + NO_2 (+M) \rightarrow IONO_2 (+M)$$
$$\underline{IONO_2 + h\nu \rightarrow I + NO_3}$$
net: $$O_3 + NO_2 \rightarrow O_2 + NO_3$$

Cycle 3
$$I + O_3 \rightarrow IO + O_2$$
$$\underline{IO + IO \rightarrow I + O_2}$$
net: $$2O_3 \rightarrow 3 O_2$$
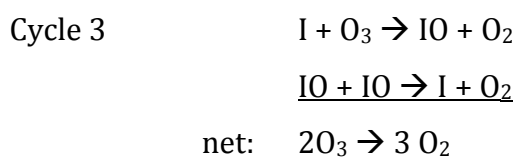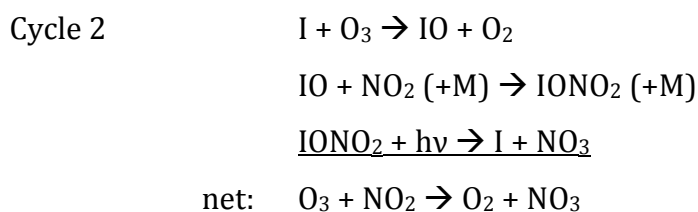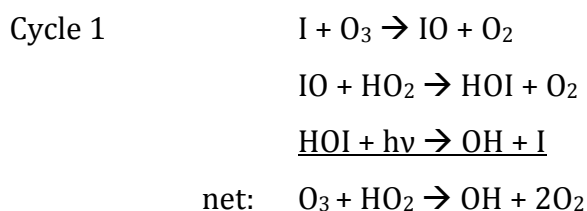
Identical reaction cycles to the above exist for bromine, and these cycles are especially effective at depleting ozone in the polar spring. Reactive forms of bromine build up on the surface of the snowpack and frozen aerosol surfaces during the long polar night. When the sun comes up and photolysis can occur, these compounds are broken down to release halogen radicals and the ozone depletion cycles can be responsible for the complete removal of all the ozone in the boundary layer. This well known phenemenon, termed the bromine explosion [*Platt and Janssen*, 1995], has been observed in both the Arctic [*Barrie et al.*, 1988] and Antarctic [*Kreher et al.*,

1997]; a simplified scheme is shown in figure 1, and a full review of the history of ozone depletion and the mechanisms involved can be found in *Simpson et al.* [2007].
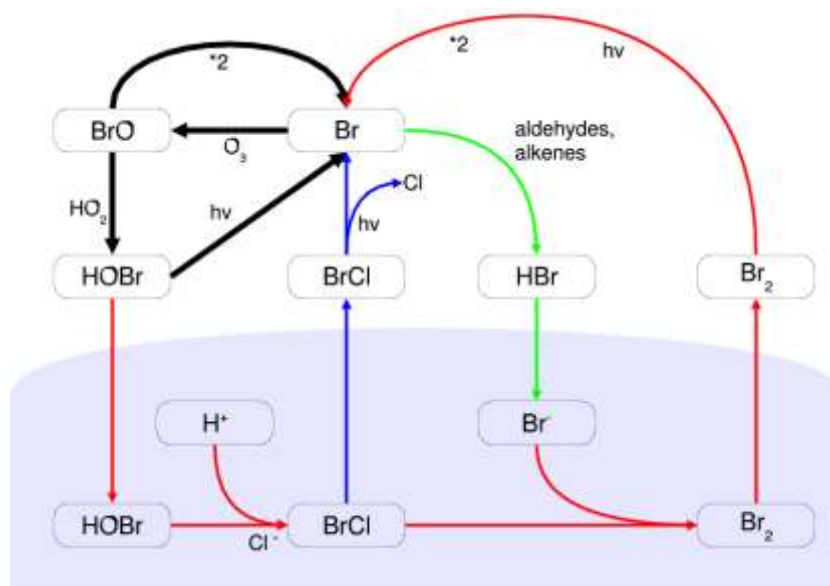
Figure 1. The bromine explosion, taken from *Simpson et al.* [2007], where the shaded area represents the aerosol and the area above the atmosphere.

1.2 New particle formation

IO may self react to form stable clusters of iodine oxides, which have the potential to grow to form new particles [*O'Dowd et al.*, 2002]. This makes the atmospheric chemistry of iodine extremely interesting with respect to the potential for new particle formation in the marine atmospheric environment.

It has long been known that iodine is enriched in marine aerosol [*Duce et al.*, 1963; *Reifenhauser and Heumann*, 1992], and bursts of new particles have been observed in temperate coastal areas where high concentrations of atmospheric iodine are also present [*Allen et al.*, 1999; *Carpenter et al.*, 1999; *O'Dowd et al.*, 2002]. The potential for growth of these new particles to become cloud condensation nuclei (CCN) makes understanding this pathway an important aspect of climate change research, as marine aerosols and clouds scatter incoming solar radiation, and hence have a negative effect on global radiative forcing [*Slingo*, 1990].

A number of field campaigns, laboratory experiments and modelling studies aimed at determining the pathway of new particle formation via iodine oxides have previously been undertaken. Smog chamber experiments carried out by *O'Dowd et al.* [2002] under marine atmospheric conditions showed new particle formation from the photolysis products of a mixture of CH_2I_2 and ozone in air. The production of new

particles proceeded in two steps: first, a thermodynamically stable cluster on the nm scale formed by homogeneous nucleation of iodine oxides. Rapid growth due to condensation and/or coagulation then caused the particle to grow to 3-4 nm in size; these quasi-stable particles then collided by diffusion with larger, pre-existing particles.

Recent work has postulated the OIO self reaction to be a dominant pathway leading to particles with the stoichiometry I_2O_4 [*Burkholder et al.*, 2004; *Pechtl et al.*, 2006; *Pirjola et al.*, 2005]. An alternative modelling study showed I_2O_5 [*Saunders and Plane*, 2006] to be the dominant species, but it is now believed that stable dimers of I_2O_4 reacting with itself and with I_2O_3 are the key pivotal species [*Saunders et al.*, 2010].

Saiz Lopez et al. [2006] used a coupled photochemical – aerosol growth model to investigate the role of I_2 in new particle formation at Mace Head, and showed the I_2/IO ratio could only be explained if I_2 was emitted at the coast; this was supported by observations of I_2 by broadband cavity ring down spectroscopy (BBCRDS) and inductively coupled plasma mass spectrometry (ICP-MS) [*Saiz-Lopez et al.*, 2006]. Iodine-induced new particle formation has also been reported at Roscoff, France [*McFiggans et al.*, 2010] and O Grove, Spain [*Mahajan et al.*, 2010a]; at the latter, simultaneous measurements of I, I_2 and ultrafine particles were made; the importance of I_2 is discussed further in section 1.7.

The aforementioned locations are all coastal sites where beds of kelp are exposed at low tide, and it has been suggested that stress to the macroalgal species following exposure to sunlight and ozone triggers the release of volatile forms of iodine as a defense mechanism [*Küpper et al.*, 1998].

The iodine content of aerosols over the Southern Ocean and Weddell Sea has not been measured, though *Davison et al.* [1996b] observed particle bursts during a cruise in the Weddell Sea, and the presence of IO over the Antarctic continent suggests reactive iodine recycling from the snowpack via aerosol [*Saiz-Lopez et al.*, 2007b].

1.3 Sea ice formation and the presence of brine channels

As the temperature of the atmosphere drops in autumn, the surface of the ocean cools. If the temperature falls below -1.8°C, ice crystals begin to form [*Weeks and Ackley*, 1982]. These crystals coalesce to form frazil or grease ice; when a continuous sheet of ice has built up this is known as nilas. This will only remain on calm water, in

more turbulent seas motion will cause the nilas ice to break into 'pancakes', so called due to the ridges around the edges of large ice floes formed as they move against one another [*Eicken and Lange*, 1989; *Weeks and Ackley*, 1982]. As the temperature drops further, the pancakes grow and are brought together until eventually pack ice is formed [*Lange et al.*, 1989]. Growth of the ice can now only occur vertically. Columnar ice grows, increasing the thickness of the ice from the bottom, as heat is transported from the warm ocean to the cold atmosphere. The bottom of the growing columnar ice is known as the skeletal layer, and is characterised by its high porosity and relatively high temperature, just below that of the water underneath which is fixed at the freezing point of seawater (-1.8°C) [*Weeks and Ackley*, 1982].

The formation of ice crystals causes the expulsion of salts as pure water freezes out of the mixture of water and salts in seawater. This leads to an increasingly concentrated brine which is expelled both vertically and horizontally. Thus sea ice is a mixture of ice crystals, brine inclusions at grain boundaries between the crystals, and brine channels [*Eide and Martin*, 1975]. The latter range in size from a few μm to a few cm in diameter (but normally less than 1 mm) [*Weissenberger et al.*, 1992] and form a three-dimensional network in the ice, providing a unique habitat for life, and a transport route for ions and trace gases dissolved in the brine.

The brine and ice are in equilibrium; as the temperate drops, the brine becomes more concentrated and the relative volume taken up by the matrix is reduced. As the concentration of the brine increases, it will melt the ice around it and the brine will tend to melt its way down through the ice, assisted by gravity. This equilibrium between ice and brine leads to a gradient in brine volume, which can be represented by equations 1 and 2 [*Frankenstein and Garner*, 1967].

$$\overline{} \qquad \text{when} \qquad\qquad (1)$$

$$\overline{} \qquad \text{when} \qquad\qquad (2)$$

Where V_b is brine volume, S_i is salinity and θ is temperature.

Thus by measuring the temperature and bulk salinity of the ice, the brine volume can be calculated. It has been ascertained that below $\sim$-5°C and below $\sim$5‰ total bulk salinity, which corresponds to a brine volume of $\sim$5%, the brine channels close off to form pockets. When this percolation threshold has been passed, transport of

compounds though the brine channels is not possible. This is known as the 'rule of 5s' [*Golden et al.*, 1998].

Equations 1 and 2 are empirical expressions which are widely used in sea ice work. An alternative method of brine volume calculation is to use the theoretical density-volume fraction equations of Cox and Weeks [1983] which would allow for the calculation of gas volume and porosity. However, this requires the bulk density of the ice sampled as an input, which can be difficult to ascertain in the field. Therefore, the Frankenstein and Garner equations have been chosen.

1.4 Brine channel biology

Sutherland [1852] was the first to describe life in sea ice, as "minute vegetable forms of exquisite beauty". It is probable that Sutherland was referring to diatoms, which make up a substantial component of the sea ice community [*Buinitsky*, 1977]. The brine channels within sea ice provide a habitat for a specialised community of bacteria, algae and plankton - mainly phytoplankton and picoplankton, with some zooplankton able to swim into the larger channels to graze [*Bergström et al.*, 1990; *Daly*, 1990].

There is some debate as to how biological organisms are incorporated into sea ice [*Horner et al.*, 1992 and references therein]. Laboratory experiments by *Garrison* [1989] showed that frazil ice crystals rising through the Southern Ocean as the ice forms around Antarctica in the autumn scavenge cells from the water column, thus concentrating them in the ice. Tidal motion forcing water through the brine channels may also result in the deposition of microalgae [*Ackley et al.*, 1987] as may smaller scale circulation features such as Langmuir cells [*Garrison and Buck*, 1989].

Some species thrive in the ice and have adapted physiologically to the conditions in this network, where favourable conditions such as protection from grazers and less variable light levels than may be experienced in the upper turbulent layer of the ocean are present [*Horner et al.*, 1992]. The sea ice community forms a large component of the food web in ice covered areas. It would appear diatoms are particularly well suited to life in the ice - as sea ice ages, the population shifts to favour psychrophilic organisms such as small pennate diatoms as well as other algal species, bacteria and viruses [*Thomas and Dieckmann*, 2002].

Sea ice present in the summer in Antarctica is a large area of primary productivity, providing an area hugely supportive of algae and krill. It is also used by seals and penguins as a breeding area [*Ackley et al.*, 2003].

Sea ice assemblages can be split into 3 main types: surface, interior and bottom, which are further sub-categorised by their characteristics depicted in figure 2 and described below.
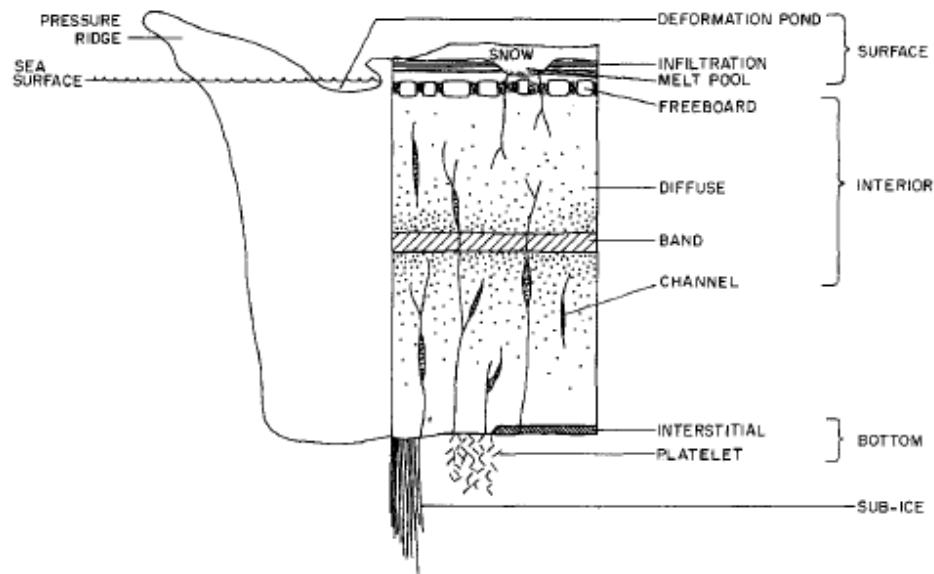
Figure 2. Sea ice communities, taken from *Horner et al.* [1992].

Surface communities were first described as a yellow to brown layer, 15-20 cm thick on Antarctic pack ice by *Meguro* [1962], who suggested its presence to be due to the weight of snow depressing the ice, allowing the surface to become flooded by sea water and resulting in infiltration of the snow by organisms in the seawater. Often these surface areas have chlorophyll a (Chl *a*) concentrations much higher than that of the seawater however, which would imply an in-situ bloom.

Freeboard or gap layer communities result from brine drainage from the top most layer of the ice as the surface warms. Algal growth increases, heat may be trapped by this biomass (by metabolism or trapping of incoming solar radiation due to the layer being darker than the surrounding ice) and so the ice melts further, allowing the phytoplankton to bloom in an area 10–30cm below the surface of the ice [*Haas et al.*, 2001]. Gap layers have only been observed in the Antarctic.

The most common habitat in sea ice for diatoms is the brine channels. When the ice starts to melt and the channels enlarge they are flushed with water from the sea

below which brings a fresh supply of nutrients and the phytoplankton bloom. The diatoms secrete an exopolymeric substance (EPS) [*Deming*, 2002; *Krembs et al.*, 2002] which allows them to remain attached to the ice and in some cases each other (see section 1.3.2). Band communities, more common in the Antarctic than in the Arctic, are formed when new ice is added underneath an existing bottom ice community by accretion [*Hoshiai*, 1977], or by incorporation from the biologically-rich water during freezing after the autumn phytoplankton bloom [*Ackley et al.*, 1979].

The interstitial assemblage is in the very bottom layer of the ice, which is congelation ice, and extends from the skeletal layer upwards as much as 20 cm. The vertical extent is controlled by decreasing nutrient availability and increasing salinity [*Arrigo and Sullivan*, 1992]. This well studied community is usually dominated by pennate diatoms in fast ice and centric diatoms in pack ice [*Horner et al.*, 1992 and references therein].

Platelet ice forms underneath congelation ice layer and is home to algal species which have been scavenged from the water column as platelets rise close to ice shelves [*Dieckmann et al.*, 1986]. The platelet layer forms due to the decreasing currents and sheer near an ice shelf. Nutrient supply in the platelet area is higher than in the interstitial area above, whereas radiation is lower; the differing physical environment owing to the nature of the ice crystals also contributes to making these quite different environments. Thereby, unique species flourish which are suited to these conditions, which they do in abundance, as has been observed in McMurdo Sound and the Weddell Sea [*Bunt*, 1964; 1968; *Palmisano and Sullivan*, 1985]. Platelet ice is the most porous of the sea ice-types; it ranges from a few cm to several m thick and is approximately 20% ice and 80% seawater. It is characterised by rapid nutrient exchange, high porosity and Chl *a* concentrations exceeding 1000 µg l^{-1} [*Bunt and Lee*, 1970].

1.4.1 Chlorophyll and diatom concentrations associated with sea ice

The open waters of the Southern Ocean are relatively low in phytoplankton due to deep mixing, variable light levels, low iron and silicate concentrations and grazing pressure [*Boyd*, 2002; *Daly et al.*, 2001; *Moline and Prezelin*, 1996]. Typical Chl *a* concentrations range between 0.05 and 1.5 µg l^{-1} [*Arrigo et al.*, 1998; *El-Sayed*, 2005], however Chl *a* concentrations are higher (1 to > 30 µg l^{-1}) in continental shelf and ice edge areas [*El-Sayed*, 2005]. The area around the Antarctic Peninsula in particular,

one of the most productive areas of the Southern Ocean, is home to large communities of phytoplankton, which form the base of a food web which includes zooplankton, birds and mammals.

In much of Antarctic pack ice the Chl *a* concentration is normally less than 10 μg l^{-1} [*Horner et al.*, 1992] but communities such as those described in section 1.4 can be responsible for concentrations of 100 μg l^{-1} [eg *Garrison et al.*, 2003], and 10 times this in platelet ice which is the most diatom rich. Surface communities with snow cover have been reported to have Chl *a* concentrations of up 400 μg Chl *a* l^{-1} [*Kristiansen and Syvertsen*, 1990; *Meguro*, 1962].

1.4.2 Survival by extremophiles

Recent work [*Deming*, 2002; *Krembs et al.*, 2002] has shown that psychrophilic diatoms survive in the unique environment of sea ice brine channels by the production of EPS, which acts as a cryoprotectant. EPS contains mycosporine-like amino acids which act to protect the organisms from the low temperatures [*Hannach and Sigleo*, 1998]. Concentration of dissolved organic material (DOM) has been closely linked to the production of EPS.

Diatoms are auto- and hetero-trophic, allowing them to live in these sealed off environments once the conditions are such that the 'rule of 5s' determines the brine network is no longer connected to the seawater below which would provide a supply of nutrients. Diatoms held inside brine pockets will multiply until all the nutrients have been used up. Following this it is possible resting spores may be formed until more nutrients become available.

Grant and Horner [1976] reported Arctic ice diatoms able to withstand salinities of 5‰ to 60‰. *Barlow et al.* [1988] demonstrated how diatoms living in brine channels adapt to the decreasing light levels experienced as the ice thickness increases and the habitable channels become further removed from the sunlight, which will also be in short supply during the coldest months – the number of photosynthetic units is increased and the flow of electrons through the electron transport chain is decreased in order to maintain an effective absorption cross section. The concentration of light harvesting pigments Chl *a*, Chl *c* and fucoxanthin remain constant.

Thus diatoms living within sea ice must endure extreme conditions – limited light and nutrients, high salinity and low temperatures. The chemical environment may also

become quite hostile to life – low CO_2 and high O_2 concentrations combined with pH levels as high as 11 [*Thomas et al.*, 2010]. Species which live, and indeed thrive, in these environments must therefore be able to photosynthesise in an alkaline environment, and in the presence of harmful oxidants such as H_2O_2 and OH, the toxic photochemical products of high O_2 concentrations [*Vincent and Roy*, 1993]. Diatoms have antioxidative enzymes, and those isolated from sea ice have been shown to have high activities of these enzymes [*Arrigo and Thomas*, 2004] which may have implications for this study.

1.5 Sea ice diatoms as a source of volatile iodine

A mechanism of enhancement, volatilisation and release of iodine may be provided by sea ice diatoms. Diatoms which live in brine channels may release halogenated volatile organic compounds, the so-called halocarbons, which, following release from the ice surface and photolysis, may contribute to the presence of halogen radicals in the atmosphere. Whilst it is possible that other organisms living in sea ice brine channels also release halocarbons, little evidence for this exists in the literature, and such considerations are beyond the scope of this thesis.

The production of halocarbons by diatoms is well established [*Sturges et al.*, 1992; *Tokarczyk and Moore*, 1994], via enzymes active in the oxidative metabolism of the cell [*Manley*, 2002; *Moore et al.*, 1996]. It is not known what physiological function the halocarbons perform, however iodine is a useful anti-oxidant; it is a large, easily polarisable atom which may be of particular use in the harsh environment experienced by sea ice diatoms [*Arrigo and Thomas*, 2004]. Therefore, halocarbon production may be a by-product of the use of iodine in the oxidative metabolism of the cell. Halocarbons may also be produced as a defence mechanism in response to grazing [*Manley*, 2002].

It has been shown that the polyhalogenated compounds are produced via a different mechanism to those with only one halogen atom; different anti-oxidative enzymes are responsible. Monohalogenated organic compounds are produced by methyl transferase activity, and polyhalocarbons are proposed to be by-products of halogenation of organics by haloperoxidases [*Manley*, 2002; *Moore*, 2003].

Halocarbons emitted by sea ice diatoms may permeate through sea ice if the brine channels are interconnected (section 1.3). On the surface of the ice, halocarbons may

be released into the atmosphere, and thus the flux from source to atmosphere is driven by a concentration gradient. Once in the atmosphere, the halocarbons are photolysed and iodine atoms are released, to be involved in atmospheric chemistry as described in sections 1.1 and 1.2. This process is depicted in figure 3.
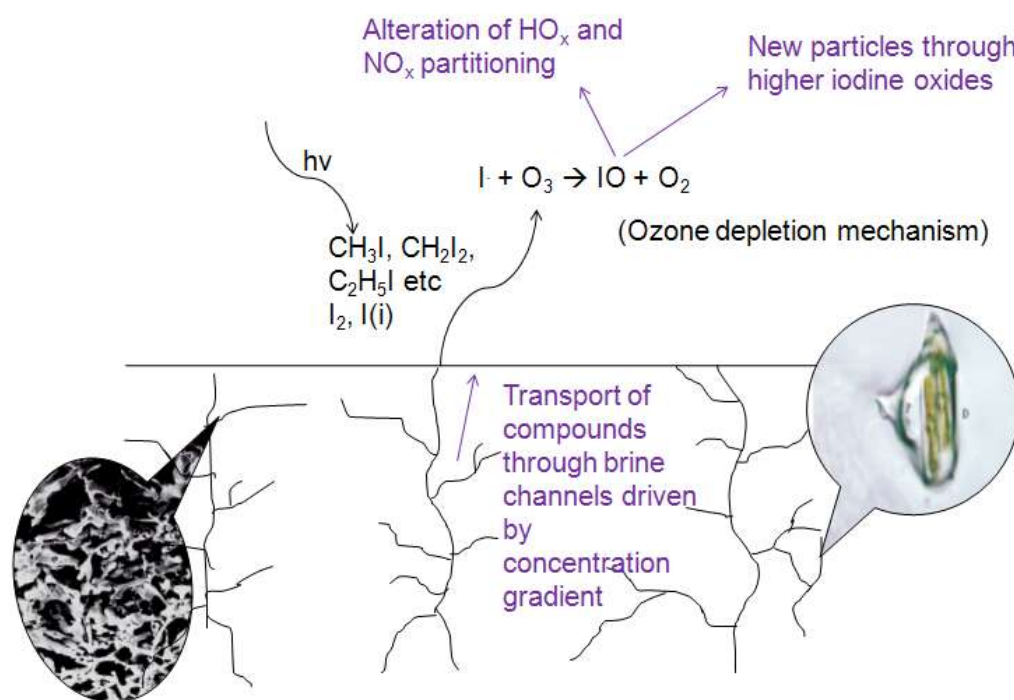
Figure 3. The mechanism of biological sources of iodine emissions in the sea ice zone. Left insert shows a cast of the 3-dimensional structure of brine channels [*Weissenberger et al.*, 1992] and the right insert shows a photograph of a diatom inside a brine channel [*Krembs et al.*, 2002].

Laboratory experiments have sought to further understand and quantify these halocarbon emissions. Polar diatoms, and in particular the ice-associated diatom *Porosira Glacialis*, which has a bipolar distribution [*Hasle*, 1976], have consistently been shown to emit more halocarbons, and accumulate more iodide, than other diatom species. *Tokarczyk and Moore* [1994] measured production of $CHBr_3$, CH_2Br_2, $CHBr_2Cl$ and CH_2ICl from *Porosira Glacialis*, rates of $CHBr_3$, $CHBr_2Cl$ and CH_2Br_2 production were $211 – 347$, $0.25 – 5$ and $31 – 34 \times 10^{-9}$ pmol cell^{-1} hour^{-1} respectively. Further work by Moore and co-workers [*Moore et al.*, 1996] showed iodocarbon production by the Arctic diatoms *Nitzschia* sp. (CCMP 580), *Nitzschia arctica*, *Porosira glacialis*, and *Navicula* sp. (CCMP 545). Production rates were found to be higher than those of phytoplankton in temperate waters. *Porosira Glacialis* was shown to produce

$CHBr_3$, CH_2Br_2, CH_2ICl, CH_3I, C_2H_5I and CH_2IBr, with the highest production rates observed during exponential growth.

Manley and de la Cuesta [1997] tested 15 species of diatom for CH_3I production and found it in 5. Their study used enhanced iodide concentrations (0.5μM) to ensure iodocarbon production was not iodide limited. *Hill and Manley* [2009] measured the production of reactive bromine and iodine, in the form of HOBr and HOI, in cultures of 11 species of diatom, 5 of which were polar. 6 of the 11 produced significant quantities of reactive iodine, most of them polar. *De la Cuesta and Manley* [2009] investigated iodide assimilation and efflux in 10 species of diatom, *Porosira Glacialis* gave the highest cellular release rates with values of 7916 x 10^{-9} pmol cell^{-1} hour^{-1} under nitrate replete conditions. Where halocarbon production has been monitored over the life cycle of diatoms, rates have been highest during exponential growth [*Moore et al.*, 1996], and less during stationary and dying phases, which could help account for the higher atmospheric mixing ratios of IO in the spring when the ice melts, the phytoplankton bloom is seeded, and the growth of diatoms begins.

Whilst alternative pathways of iodocarbon production have been proposed, involving light [*Spokes and Liss*, 1996], humic material [*Carpenter et al.*, 2005] and ozone [*Martino et al.*, 2009], biological production is thought to be the dominant source. Enzymatic production of HOI and HOBr by diatoms has also been suggested [*Hill and Manley*, 2009], which may then react with dissolved organics to produce the halocarbons. Diatoms have been shown to be capable of accumulating iodide [*de la Cuesta and Manley*, 2009], and to play a role in the conversion of iodate to iodide [*Chance et al.*, 2007]. Iodide and iodate concentrations in seawater are discussed further in section 1.9. I_2 emissions from sea ice algae have also been suggested by a recent modelling study [*Saiz-Lopez and Boxe*, 2008] to be the main precursor of the observed IO in coastal Antarctica, the pathway and release mechanism involved biology as the iodine source, iodine accumulation in sea ice and subsequent release from the ice surface. I_2 emissions are discussed in more detail in section 1.7.

1.6 Polar field measurements of halocarbons

There have been numerous studies aimed at measuring halocarbons in the polar regions, and previous measurements in polar waters and air are summarised in tables 1 and 2 respectively.

Enhanced halocarbon concentrations have been measured in sea ice brine and ice covered waters. *Fogelqvist and Tanhua* [1995] measured enhanced concentrations of CH_3I, C_2H_5I and 1- & 2-C_3H_7I, and the presence of CH_2ICl and C_4H_9I, in sea ice brine in the Weddell Sea. *Fogelqvist* [1985] found bromoform to be supersaturated (above the expected equilibrium between trace gas concentrations in surface seawater and the atmosphere above) in the Arctic Ocean, with the highest concentrations found in waters next to ice, suggesting a strong source from the ice or the ice edge, and *Carpenter et al.* [2007] found enhanced iodocarbon concentrations in Southern Ocean waters from ice melt characterised by low salinity. Work by Hughes and co-workers as part of the long term monitoring Rothera Time Series data [*Hughes et al.*, 2009] has shown the seasonality of bromocarbon production to be correlated to the phytoplankton bloom on the Antarctic Peninsula, which is in turn dependent on sea ice conditions. Environmental factors which may influence halocarbon production by sea ice algae include light intensity, nutrient availability, salinity and temperature.

Atmospheric halocarbon concentrations are not especially enhanced in the polar regions however. For example, a global study by Rasmussen *et al.* [1982] showed mean (and range) CH_3I concentrations of 2 (1-3) pptv. To date, halocarbon measurements have been unable to account for the iodine atom flux necessary to maintain the high concentrations of IO found in Antarctica [*Carpenter et al.*, 2007 and references therein].

Extremely high mixing ratios of atmospheric halocarbons were measured in the Canadian sub-Arctic [*Carpenter et al.*, 2005] close to the town of Kuujjuarapik, on the east coast of Hudson Bay. These measurements are especially interesting as they were made in the absence of open leads and, for the iodocarbons, were the highest concentrations ever recorded in the atmosphere. The authors proposed an abiotic mechanism, supported by laboratory experiments, for the production of CH_3I, C_2H_5I and CH_2I_2 via the reaction of HOI with humic material in the quasi-liquid layer (QLL) on the surface of sea ice. The origin of HOI in the QLL was suggested to be atmospheric deposition or from reactions of the type HOBr + I$^-$ → HOI + Br$^-$.

Kuujjuarapik was revisited for the COBRA field campaign, and results for halocarbons in sea ice will be reported in this study. Mixing ratios of atmospheric halocarbons have previously been reported elsewhere [*Mahajan et al.*, 2010b] and the fluxes necessary to account for these were also much larger than have ever been measured.

However simultaneous IO measurements and a subsequent modelling study suggested open leads in the sea ice were the origin of the halocarbons, which were in turn the precursors for the IO.

Reference	Compound	Location	Mean	Range
Dyrssen and Fogelqvist [1985]	$CHBr_3$	Arctic	29	
Fogelqvist [1985]	$CHBr_3$	Arctic	38	22 - 54
Klick and Abrahamsson [1992]	CH_2ICl	Southern Ocean (Atlantic)	1.44	<22.7
	$1\text{-}C_3H_7I$		0.76	<15.9
	$2\text{-}C_3H_7I$		0.71	<21.2
	$CHBr_3$		10.7	4 – 24.5
Moore and Tokarczyk [1993]	CH_3I	NW Atlantic 60-32°N		<0.7 - 61.3
	CH_2ICl			0.57 - 21.7
	$CHBr_3$			3.9 – 7.9
Krysell [1991]	$CHBr_3$	Arctic	16	12 - 27
Reifenhauser and Heumann [1992]	CH_3I	Antarctic 60-66°S	18.3	1.4 - 52.8
	CH_2ICl			<1.37
Schall and Heumann [1993]	CH_3I	Arctic algae field	7.25	<0.07 - 38
	CH_2I_2		23.10	<2 - 102
	CH_2ICl		0.40	<0.02 -1.03
	$1\text{-}C_3H_7I$		7.00	<0.47 - 29
	$2\text{-}C_3H_7I$		8.82	<0.55 - 50.2
	CH_3I	Arctic coastal water 78°N	3.52	<0.07-10.56
	CH_2ICl		1.71	0.63-3.82
	CH_2I_2		6.34	<0.93-12.7
	$1\text{-}C_3H_7I$		2.35	0.35-6.06
	$2\text{-}C_3H_7I$		3.53	0.41-12.6
Fogelqvist and Tanhua [1995]	CH_3I	Weddell Sea ice pore water	38.0	34.5-40.9
	C_2H_5I		27.3	26.2-17.6
	$1\text{-}C_3H_7I$		235	218-259
	$2\text{-}C_3H_7I$		7.06	
	$CHBr_3$		22	21 - 23
	$CHBr_2Cl$		2.6	2.5-2.6
Happell and Wallace [1996]	CH_3I	Greenland/Norwegian seas	0.43	0.18-0.88
Schall et al. [1997]	CH_3I	Southern Ocean 62-72°S	2.1	0.07-8.8
	CH_2ICl		0.56	0.05-1.8
	CH_2I_2		<0.75	
	$1\text{-}C_3H_7I$		1.18	<0.29-1.94
	$CHBr_3$		15	<0.2 - 59
	$CHBr_2Cl$		1.9	0.3 - 7
Moore and Groszko [1999]	CH_3I	NW Atlantic		<0.7 - 7
Chuck et al. [2005]	CH_3I	Atlantic 50N-65S	4.37	0.25-18.7
	CH_2ICl		2.54	0.09-14.2
	$CHBr_3$		5.1	0.1 – 30.7
	$CHBr_2Cl$		0.7	0.1 – 12.2

Table 1. Previous measurements of halocarbons in polar waters (all values in pM) (continued on next page)

Carpenter et al. [2007]	$CHBr_3$	Southern Ocean	57	44-78
	CH_2I_2	(Weddell)	4.2	1.7-8.2
	CH_2IBr		0.8	0.2-1.4
	CH_2ICl		0.7	0.2-2.4
Hughes et al. [2009]	$CHBr_3$	Antarctic Peninsula		<276
	CH_2Br_2			<30

Table 1 (continued). Previous measurements of halocarbons in polar waters (all values in pM)

Reference	Compound	Location	Mean	Range
Rasmussen [1982]	CH_3I	Global	2	1-3
Reifenhäuser and	CH_3I	Antarctic 60-66°S	2.4	0.6-7.9
Heumann [1992]	$CHBr_3$	Antarctic Peninsula	6.3	
	$CHBr_2Cl$		3.8	
	CH_2Br_2		3.7	
Schall and Heumann	CH_3I	Arctic	1.04	<0.004-2.12
[1993]	CH_2I_2		0.46	<0.08-1.02
	CH_2ICl		0.07	<0.004-0.18
	$1-C_3H_7I$		0.2	<0.02-0.28
	$2-C_3H_7I$		2.0	<0.02-5.98
	$CHBr_3$		0.45	<0.02 – 1.19
	$CHBr_2Cl$		0.33	<0.01 – 1.00
	CH_2Br_2		0.45	<0.008 – 1.00
Yokouchi et al. [1996]	$CHBr_3$	Alert, Canada	1.9	0.25 – 5.7
	$CHBr_2Cl$		0.24	0.07 – 0.51
	CH_2ICl		0.01	<0.005 – 0.05
Moore and Groszko [1999]	CH_3I	NW Atlantic	1.7	
Carpenter et al. [2003]	CH_3I	Cape Grim	2.6	1.0 – 7.3
	CH_2ICl		0.04	0.0 – 0.39
	$CHBr_3$		2.6	0.7 – 8.0
	$CHBr_2Cl$		0.19	0.05 – 0.78
	CH_2Br_2		0.43	0.10 – 1.39
Carpenter et al. [2005]	CH_2I_2	Hudson Bay, Quebec	1.4	<3.3
	CH_2IBr		3.7	<3.7
	CH_2ICl			<0.4
Hughes et al. [2009]	$CHBr_3$	Antarctic Peninsula	2.7	
	CH_2Br_2		0.4	
Mahajan et al. [2010]	CH_3I	Hudson Bay, Quebec		<3.83
	CH_2IBr			<0.11
	CH_2ICl			<0.165

Table 2. Previous measurements of halocarbons in the polar atmosphere (all values in pptv)

1.7 The importance of I_2 and inorganic iodine species

Field measurements in ice covered waters are rare; as was discussed in section 1.2, most have been made in temperate coastal locations [eg *Carpenter et al.*, 1999;

Furneaux et al., 2010] and here the link between iodocarbons, IO and new particle bursts has been demonstrated [*Allen et al.*, 1999; *Carpenter et al.*, 1999].

The importance of I_2 in supplying an iodine atom flux to the atmosphere has recently become apparent [*Huang et al.*, 2010; *Mahajan et al.*, 2010a] with suggestions that it dominates the flux and is the most important precursor for new particle formation in the marine environment [*Mahajan et al.*, 2010a; *McFiggans et al.*, 2004; *Saiz-Lopez and Plane*, 2004; *Saiz-Lopez et al.*, 2007b]. I_2 is a highly reactive species, reacting quickly with organic material in seawater [*Truesdale and Spencer*, 1974; *Wong*, 1991] and being photolysed quickly in the atmosphere to provide two iodine atoms.

A study at O Grove, Galicia, Spain [*Mahajan et al.*, 2010a] showed I_2 to be present at levels of 350 ±100 pptv. Huang et al. [2010] also detected up to 300 pptv I_2 at Mace Head, where HOI and ICl (collectively termed activated iodine compounds (AIC)) were also measured. AIC showed a maximum concentration of 30.2 pptv at night and 6.0 pptv during the day.

HOI and ICl are also involved in ozone depletion cycles; HOI is formed from the reaction of IO with HO_2, uptake onto aerosol and reaction with Cl^- may then yield ICl, the release of which may further enhance ozone depletion [*Vogt et al.*, 1999]. If HOI is taken up onto sea salt aerosols it liberates Cl^- at a significant rate [*McFiggans et al.*, 2002]. HOI may also react with Br^- present in fresh sea salt aerosol, producing BrO and HOBr. HOBr may then react with sea salt which leads to autocatalytic release of Br_2 [*Vogt et al.*, 1996]. Hence this heterogeneous iodine chemistry may lead to liberation of chlorine and bromine from sea salt aerosols.

Some debate exists as to how I_2 may be released into the polar atmosphere. A modelling study suggested that the enhancement of iodine compounds over Southern Ocean sea ice proceeds via accumulation of I^- by sea ice algae followed by I_2 release via the reaction HOI + I^- + H^+ → I_2 + H_2O [*Saiz-Lopez and Boxe*, 2008]. The equilibrium will be driven in favour of the products by the high volatility of I_2 and thus iodine is removed from seawater, volatilised and released into the atmosphere. An alternative abiotic mechanism has been proposed by *O'Driscoll et al.*[2008]. A solution of nitrite and iodide, both present in sea salt, releases I_2 and NO if the solution undergoes a freeze thaw cycle. This reaction had previously been known to occur in weakly acidic solutions, the authors of this study have suggested H^+ ions rejected from the ice phase are concentrated in liquid micropockets, allowing the reaction to proceed.

1.8 Why the difference?

Different conditions in Arctic and Antarctic waters and sea ice may contribute to the inhomogeneous distribution of atmospheric IO and BrO in the polar regions [*Schönhardt et al.*, 2008]. The Arctic Ocean is a deep basin of seawater (figure 4), which, until recently, was ice covered year-round. It is surrounded by large continental shelves and shallow smaller seas which are ice covered only in winter. Most of the water exchange occurs with the North Atlantic. Until recently, between 50 to 90% of Arctic ice was multi-year and over 2 m thick, though these numbers are declining rapidly as the global climate warms. More than 90% of the sea ice of the Southern Ocean is first year and up to about 1 m thick, averaging 0.4 m, though some multi-year ice of much greater thickness is present, especially in the Weddell Sea which stays ice covered even in summer [*Arrigo and Thomas*, 2004]. Southern Ocean waters are influenced by deep waters from more temperate areas of the globe and thus have a larger supply of nutrients. These differences, summarised in table 3, have important implications for the sea ice biota.

Property	Arctic	Antarctic
Maximum ice cover	14×10^6 km^2	20×10^6 km^2
Minimum ice cover	7×10^6 km^2	4×10^6 km^2
Age of ice	mainly multi-year	mainly one year
Ice thickness	> 2 m	~0.4 m
Ice salinity	low	high
Ice type	mainly columnar	mainly granular
Space for organisms	low	high
Melting process	at air-ice interface	at water-ice interface
Platelet ice	absent	present
Land fast ice	over shallow water	mainly over deep water

Table 3. Comparison of Arctic and Antarctic sea ice properties (modified from *Spindler* [1990]).

Granular ice contains about twice as much brine volume than columnar ice and so Antarctic sea ice is richer in biology than that of the Arctic [*Horner et al.*, 1992]. In ice packs not attached to land, snow aids primary production by depressing the ice surface, causing flooding, which may lead to the formation of gap layers. Snow only serves to reduce primary production in land fast sea ice by reducing available light

[*Welch and Bergmann*, 1989]. Surface flooding due to heavy snow cover occurs on 15-30% of pack ice in Antarctica [*Wadhams et al.*, 1987], subsequent algal growth is a function of reduced light intensity due to the snow cover and increased nutrient supply due to the flooding caused by its weight. The ice of the Arctic, held as it is by the continental shelves, is thick and mainly columnar, and has little chance of surface flooding so gap layers are not common. In contrast, Antarctic sea ice is characterised by high porosity and high biological activity [*Garrison and Buck*, 1989], and the sea ice of the Weddell Sea is particularly prone to gap layer formation. The presence of algal species known to concentrate and emit volatile compounds of iodine close to the ice-atmosphere interface may result in an increased flux of these compounds to the atmosphere.
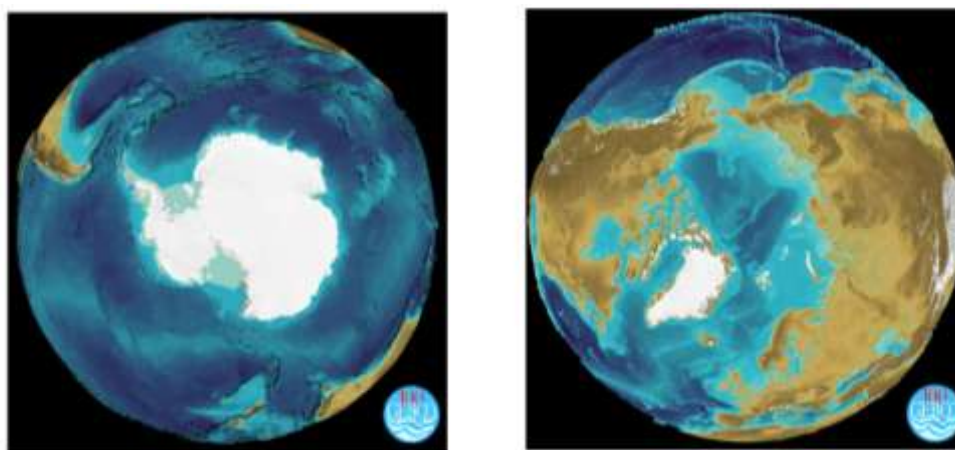
Figure 4. Images showing the marked difference in the bathymetry of the Southern and Arctic Oceans [courtesy General Bathymetric Chart of the Oceans]

As has been discussed, the atmospheric chemistry of iodine oxides is complex and involves recycling on aerosol and the snowpack in the polar regions. In the Arctic, where the sea ice area is surrounded by land on which vegetation grows, it is possible for iodine to be absorbed by plants and so work its way up the food chain. Conversely, in Antarctica the iodine lands on the snow, is reactivated (as shown by extraordinarily high concentrations of IO in the Antarctic snowpack [*Frieß et al.*, 2010]) then is deposited again and the cycle continues. The lack of plants to absorb the iodine, and animals to eat them, prevents the removal of iodine in the Antarctic environment.

1.9 Iodide / Iodate

As alluded to briefly in section 1.5, diatoms have been shown to play a role in the conversion of iodate to iodide [*Chance et al.*, 2007]. The concentration of total iodine in the open ocean ranges from 0.44 to 0.49 μM [*Küpper et al.*, 1998]. This is in the form of iodate (IO_3^-), iodide (I^-), molecular iodine (I_2), hypo-iodous acid (HOI), and various iodocarbons [*Truesdale*, 1995]. Iodine mainly exists in the first two forms, the thermodynamically stable form, iodate, dominates in the open ocean. However, in the photic zone iodide can account for up to 50% of total iodine [*Wong*, 1991], and it is kinetically stable once formed [*Luther et al.*, 1995]. High iodide concentrations have been reported in biologically rich waters by numerous studies [*Campos et al.*, 1996; *Jickells et al.*, 1988; *Nakayama et al.*, 1989; *Tsunogai and Sase*, 1969].

In the Southern Ocean, a study by *Bluhm* [2010] measured high iodide concentrations after the phytoplankton bloom, but depleted concentrations during it, indicating a correlation between iodide production and seasonal variations in diatom distribution. *Chance et al.* [2007] demonstrated the ability of cold water diatoms to reduce iodate to iodide. The ability to do so varied between species, with *Nitzschia sp.* cultures able to remove all of the iodate present in the medium, followed by production of iodide of up to 3nmol I^- μg Chl a^{-1} day^{-1} (under enhanced concentrations of iodate - which may be present in hypersaline brine channels). Not all of the iodate could be accounted for however, suggesting another pathway of iodine conversion, presumably iodocarbon production or uptake to the diatom particulate. Other diatom species took up iodate, only some produced iodide.

However, no clear correlation has been found between the highest iodide/iodate ratios and the highest concentrations of biomass [*Spokes and Liss*, 1996]. Possible alternative pathways are via photochemistry or bacteria. A laboratory study in deionised seawater in the presence of light and organic matter concluded the conversion of iodate to iodide can be driven by radiation, is not biologically driven, but organic matter must be present. The reaction proceeded with a lag time of two hours, suggesting iodide production is a secondary process following some initial photochemical product [*Spokes and Liss*, 1996]. *Francois* [1987] showed humic material may reduce iodate to form iodine-containing organic matter; it is possible that photodissociation of this would yield I^-.

1.10 The concentration effect

When considering the concentration of ions and trace gases dissolved in sea ice brine, the effect of reducing the volume of the liquid phase of the medium must be considered. Any enhancement in concentrations due to this effect may then be separated from production processes occurring within the ice. Furthermore, when compounds become supersaturated, bubbles may nucleate, which are then included along ice crystal boundaries [*Bari and Hallett*, 1974; *Cox and Weeks*, 1982]. If the ice is not porous enough to allow these gases to escape they will remain trapped in the ice. The diffusivity of halogenated gases is sea ice has been measured to be 1.3×10^{-4} cm^2 s^{-1} ($\pm 40\%$) [*Loose et al.*, 2011], however at low temperatures (-15°C) this can be as low as 4×10^{-6} cm^2 s^{-1} [*Gosink et al.*, 1976] in sea ice and through freshwater ice is $\sim 10^{-10}$ cm^2 s^{-1} [*Hemmingsen*, 1959] which is 5 orders of magnitude slower than molecular gas diffusion in water.

1.11 Summary

If diatoms capable of accumulating iodide, releasing iodocarbons or volatile inorganic forms of iodine reside in sea ice, reactive forms of iodine may thus build up in sea ice brine channels. If the ice is porous enough to allow these compounds to escape, the brine channel community may be a source of atmospheric iodine.

Once released into the atmosphere, these iodine compounds are broken down by solar radiation to yield iodine radicals. Iodine oxides may then form when iodine reacts with ozone, via catalytic ozone depletion mechanisms. IO may self react to form higher iodine oxides which are insoluble - these may contribute to an increased number of small particles in the atmosphere. A larger number of small particles scatters sunlight more effectively, and hence the presence of iodine oxides in the atmosphere may impact global radiative forcing.

The sea ice formation process itself may also contribute towards increased fluxes of iodocarbons, by concentrating the trace gases into a small volume of brine. Therefore the physical properties of the sea ice may play a role in controlling how easily these compounds are released.

1.12 Aims of this study

The overarching aim of this study is to investigate why such high mixing ratios of IO are present over Antarctica, with particular focus on the Weddell Sea area where the highest IO levels are found. Measurements will also be made in other polar locations in order that a comparative study can be undertaken.

The hypothesis that sea ice diatoms concentrate and volatilise iodine from the ocean will be investigated. Halocarbons will be measured in seawater, sea ice and air in order to ascertain whether ice which contains diatoms is a source of halocarbons. Concentrations of inorganic compounds of iodine will also be measured in the sea ice, and compared to seawater concentrations. Chl *a* analysis will be used as an indication of algae distribution in the ice. Physical properties of the ice will determine the continuity of the brine channel network, providing a pathway for the iodine compounds from sources to the atmosphere.

The relative contribution of organic and inorganic iodine compounds to the IO budget will be investigated; the importance of I_2 and AIC has recently been shown in temperate locations but is as yet unknown in the polar regions. Simultaneous atmospheric measurements of I_2, AIC, halocarbons and IO will quantify the emission of compounds of iodine into the atmosphere in the sea ice zone. New particle formation will be measured to assess the impact of these emissions.

Saturation anomalies, flux calculations and a modelling study will be used to interpret the measurement of organic and inorganic iodine compounds in sea water, ice and air, and the resultant IO and new particles which arise. Being able to compare these measurements to similar measurements in the Arctic will further understanding, and potentially raise more interesting questions.

In the laboratory, controlled experiments on sea ice and polar diatoms will investigate factors which may cause an enhancement in halocarbon concentrations under sea ice conditions. The combination of field measurements and laboratory experiments will help determine whether any enhancement in concentration of iodine compounds in the polar regions can be explained via the biological [*Saiz-Lopez and Boxe*, 2008] or abiotic [*Carpenter et al.*, 2005] mechanisms discussed above.

Work presented in this thesis

Chapters 3 and 4 report results from laboratory experiments aimed at determining the effect of the extreme sea ice environment on halocarbon production by diatoms. Various aspects of brine channel conditions were simulated; halocarbon concentrations were monitored whilst changing halide ion concentrations, and during sea ice formation at low temperatures and relevant light intensities. Experiments were also carried out on a naturally occurring ice algae community on the Antarctic Peninsula, demonstrating these results are not confined to laboratory conditions which may not be representative of the natural environment, but rather may be applied to natural systems.

Chapter 5 reports results from a cruise in the Weddell Sea, where organic and inorganic compounds of iodine were measured and quantified. Chl *a* analysis was used an indication of algae distribution in the ice. The physical properties of the ice determined the continuity of the brine channel network, providing a pathway for the iodine compounds from source to atmosphere. IO and new particle formation were also measured to assess the impact of compounds released from the ice on the atmosphere above. Saturation anomalies, flux calculations and a modelling study have been used to interpret the measurements. This is the first combined *in situ* study in Antarctica of organic and inorganic iodine compounds in sea water, ice and air, and the resultant IO and new particles which arise.

Chapter 6 reports results from a second ship-based field campaign which was carried out in the Arctic Ocean north of the Greenland and Norwegian seas, as a melting ice floe on the edge of the Arctic pack was followed for 9 days while it drifted south-west and melted. Halocarbon concentrations are also reported from the sea ice brine, the water below the ice, and the air above. This ice may represent that of all Arctic ice in the future, being first year, less than 1m thick and very porous. Results are also reported from ice of the Canadian sub-Arctic in early spring, which was thicker, colder, and less porous. Fluxes, loss processes, production pathways, and effects of ice conditions are discussed.

Chapter 7 presents a small data set of field measurements collected on the Antarctic Peninsula, which shows the presence of iodocarbons in seawater. Detailed depth profiles through the water column of iodocarbons, and bromocarbons, are presented, alongside atmospheric measurements of IO.

Chapter 8 summarises the results from chapters 3-7, and by comparing the measurements made it is hoped the understanding of the chemistry of iodine associated with sea ice and diatoms has been furthered. Work is suggested which may continue to improve this understanding.

Chapter 2. Materials and methods

Four field campaigns were carried out during this study, and a summary of the locations and measurements made is given in table 5. Where measurements were made in collaboration with other groups, these are denoted in brackets in the table and discussed in the relevant results chapters. Laboratory studies were carried out at UEA in the UK and at Rothera, a research station on the Antarctic Peninsula, which involved subjecting sea ice- and cold water diatoms to the conditions they may experience in sea ice brine channels; results are reported in Chapters 3 and 4. Chapter 5 reports results from the Weddell Sea cruise, and Chapter 6 summarises results from the two Arctic field campaigns, COBRA and JR219. Chapter 7 reports field data from Rothera, a small data set which was collected whilst the laboratory experiments of chapters 3 and 4 were being out. Sampling and analysis techniques common to multiple studies are discussed in this chapter, whereas experiment-specific materials and methods are included in the relevant results chapters.

2.1 Halocarbons in sea ice, water and air

2.1.1 Gas chromatography mass spectrometry

Gas chromatography–mass spectrometry (GCMS) is a means by which a mixture of volatile compounds can be separated and quantified. A gaseous sample is carried in a flow of inert gas (in this case helium) along a column. Differing affinities between the compounds and the coating of the column means each compound is retained inside the column for a different length of time, and thus the compounds are separated. A mass spectrometric detection technique allows for identification of the compounds which exit the column, based on the mass / charge ratio of the ions of which the compound is composed. After ionisation and fragmentation, the sample is deflected by a magnet, and scanning the magnetic field preferentially directs ions to the detector.

In this study, halocarbon analysis was carried out with an Agilent GC 6890N and Mass Selective Detector 5975. The GCMS method had been developed by previous users (Claire Hughes and Frances Hopkins, UEA) and optimised for halocarbon analysis.

The GC was fitted with a 60 m, 0.32μm film thickness capillary column (DB-VRX, J&W). The GC oven was held at 36°C for 5 min at the start of the GC run, then heated up to 200°C at 20°C min^{-1}, held at 200°C for 2 min and then heated to 240°C at 40°C

min^{-1}. In total 10 halocarbons were measured: CH_3I, C_2H_5I, $CHBr_3$, CH_2ICl, 2-C_3H_7I, CH_2I_2, CH_2IBr, $CHBr_2Cl$, 1-C_3H_7I and CH_2Br_2.

The MS operated with an electron ionisation detector in single ion mode (SIM). SIM is a selective detection technique – only selective ions are measured, and thus the time available to measure each is increased, and a higher precision is achieved.

Limits of detection (LoD) and retention times were different during different experiments and are given in the relevant chapters. Calibrations were carried out at the start and end of every campaign and experimental period, and an example of the calibration curves obtained are shown in figure 5. Liquid standards were used for the calibration, injecting (with a Hamilton microlitre syringe) a known concentration of standards (Sigma) dissolved in methanol (Fisher) into 40 ml pre-purged seawater in a gas-tight glass syringe. The standards were prepared in the UK, and stored in amber glass vials with Thames Restec mini-inert valve caps. The primary standard was prepared gravimetrically, the second and tertiary (working) standards were prepared by serial dilution of microlitre volumes. When used in the field they were stored at -20°C, for a maximum of 8 months.

The performance of the GCMS was validated by tuning with the inbuilt autotune function. The autotune was carried out at the start of every field campaign and experimental period. The method uses an internal calibration compound, perfluorotributylamine (PFTBA).

The sensitivity of the instrument was monitored in between calibrations by injecting every sample with a known concentration of deuterated 1-iodopropane and deuterated methyl iodide dissolved in methanol, which was checked for contamination at regular intervals. System sensitivity drift may occur due to a build up of deposition products on ion source walls, ion repeller and lens; the analysis of the deuterated compounds ensures quality control and consistent data.

Field campaign	Location	Date	Measurement	Technique
COBRA	Kuujjuarapik, Quebec	February – March 2008	Halocarbons	GCMS (York)
			Diatom distribution	Microscopy
			Chl *a*	Fluorometry
			Sea ice physics (brine volume)	Temperature and salinity measurements
Weddell Sea	Southern Ocean, Weddell Sea, Brunt Ice Shelf	January - March 2009	Halocarbons	GCMS
			I_2, HOI and ICl	Denuder tubes (Mainz)
			Diatom distribution	Microscopy
			Chl *a*	Fluorometry
			Sea ice physics (brine volume)	Temperature and salinity measurements
			Iodide	Cyclic voltammetry (York)
			Iodate	Spectrometry (York)
			IO	Mini max DOAS
Rothera	Antarctic Peninsula	Dec 2009 – March 2010	Halocarbons	GCMS
			Diatom distribution	Microscopy
			Chl *a*	Fluorometry
			Laboratory experiments	See details in text
			IO	Mini max DOAS
Arctic (JR219)	Arctic Ocean / Greenland / Norwegian seas	June – July 2010	Halocarbons	GCMS
			Chl *a*	Fluorometry (Oxford)
			Sea ice physics	Temperature and salinity measurements

Table 4. Summary of field campaign measurements

Air samples were collected directly onto Markes (Ltd) three-bed solid sorbent tubes containing Tenax, Carbograph and Carboxen were used, details of how ambient air was drawn through these tubes are given in the relevant results chapters. In order to extrapolate from concentrations in pM for water samples to pptv in air, the following formula was applied:

[pptv] = ((([pM]*0.04*extraction efficiency)/volume of air)/n

Where 0.04 is the volume of the water sample used for calibration in litres, n is the number of moles per litre of air at the relevant atmospheric temperature and pressure, and extraction efficiencies are $CH_3I = 1$; $C_2H_5I = 1$; $CHBr_3 = 0.5$; $CH_2ICl = 0.6$; $2\text{-}C_3H_7I = 0.6$; $CH_2I_2 = 0.4$; $CH_2IBr = 0.6$; $CHBr_2Cl = 0.6$; $1\text{-}C_3H_7I = 0.6$; $CH_2Br_2 = 0.6$ (Claire Hughes, personal communication).

2.1.2 Purge and trap

In order to transfer the halocarbons present in a water sample into the GCMS, a technique called purge and trap is used. This involves bubbling up to 1 L oxygen-free nitrogen (OFN) through the filtered water sample (40 ml unless otherwise stated) in a custom-made glass purge tube. The halocarbons were then trapped in one of two ways.

In the first method, Markes adsorbent tubes were used, held between 0°C and 4°C by a Peltier cooler. The tubes were then loaded into an UltrA autosampler connected to a Markes Unity thermal desorption unit, which is in turn connected to the GCMS. Halocarbons are desorbed from the tubes in the Ultra system, re-focussed on a cold trap held at -10°C in the Unity system, and transferred to the GC column in a stream of helium at a flow rate of 2 ml min^{-1} by rapidly heating the cold trap to 290°C.

In the second method, a trap cooled to -150°C by suspension above liquid nitrogen was used to trap and focus the halocarbons; the trap was heated with boiling water to extract the compounds for halocarbon analysis, with helium at the same flow rate.

OFN flow rates through the purge tube were 95 ml min^{-1} for 10 mins in the former method and 40 ml min^{-1} for 15 mins in the latter. Particles and water vapour were removed from the purge-gas stream using glass wool and a counterflow Nafion dryer respectively.
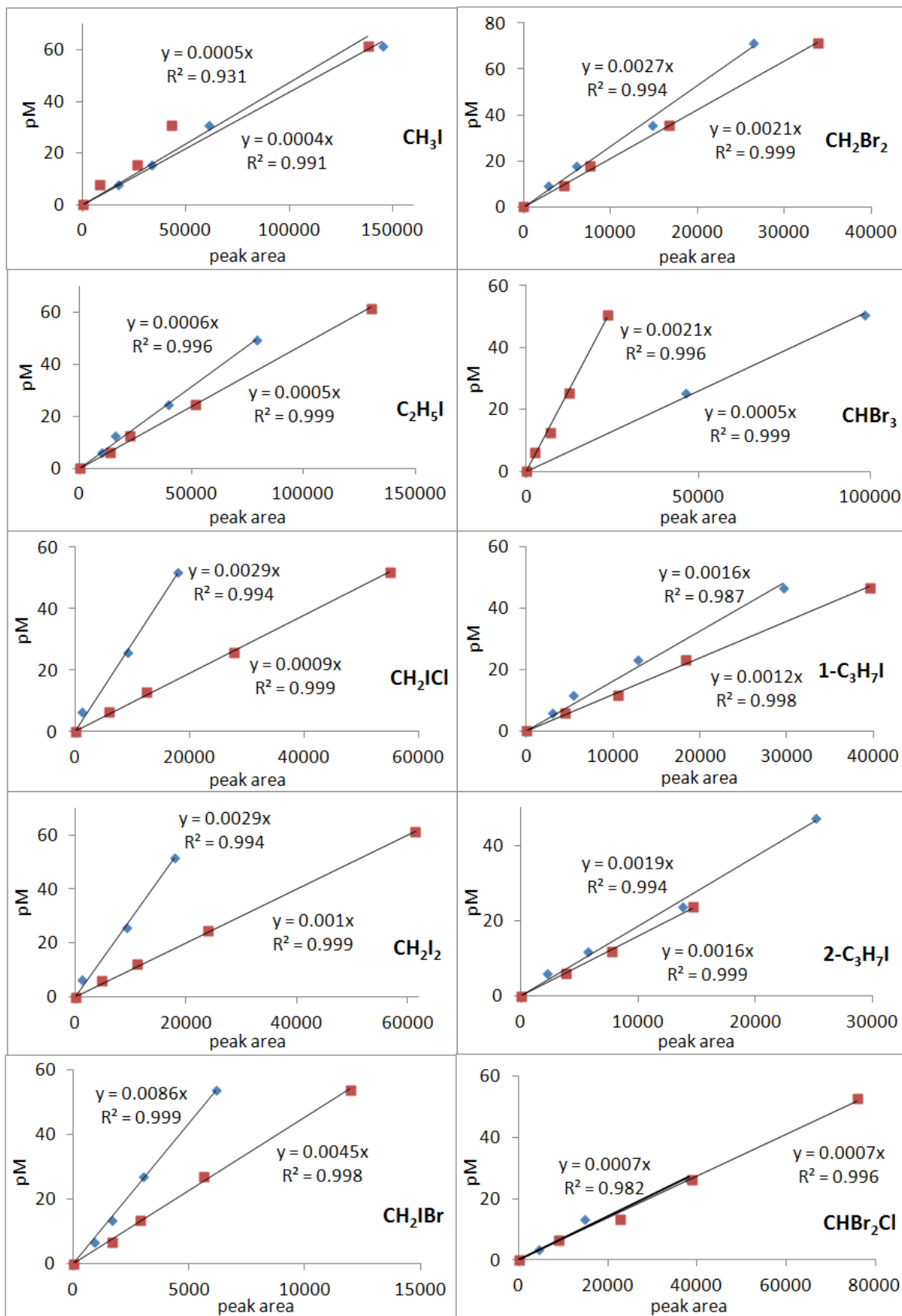
Figure 5. Examples of straight line fits to known standard concentrations obtained with similar GCMS instruments in August (blue diamonds) and November (red squares) 2010.

2.2 Iodide and iodate concentrations in seawater and ice

Iodide and iodate concentrations in seawater and sea ice were measured at UEA within 9 months of the relevant field campaign. The water samples were frozen in plastic centrifuge tubes, transported at -20°C and stored at -20°C at UEA.

Iodide concentrations were measured using cathodic stripping square wave voltammetry (CSSWV) as detailed in *Luther et al.* [1988], LoD was 0.08 nM and precision, determined by errors in duplicate water samples, was between 0.4% and 4.7%. An Eco-chemie μAutolab Type II voltammeter was used, with an IME 663 control unit and a Metrohm 663 VA hanging mercury drop electrode in SMDE mode.

Iodate concentrations were measured spectrophotometrically using the method of *Jickells et al.* [1988], LoD was 30 nM and precision was between 6.1 and 12.9%.

2.3 Chlorophyll a concentrations in seawater and ice

For all experiments except the COBRA field campaign, Chl *a* was measured using a Turner AU-10 fluorometer fitted with a red-sensitive photomultiplier tube (10-AU-600), a blue lamp (10-089, equivalent to F4T4.5B), a blue excitation filter (340-500 nm) and a red emission filter (>665 nm). Fluorescence was measured following extraction of the sample from the filter paper overnight (in darkness at 4 °C) in 10 ml of 90% acetone buffered with $MgCO_3$. Unless otherwise stated, filter papers used were Whatmann GF/F glass fibre filters, 47mm diameter. Chl *a* concentrations were corrected for interference from phaeophytin *a* (a breakdown product of Chl *a*) by measuring fluorescence before and after acidification with 8% HCl and calibrated using a pure Chl *a* standard (Chl *a* from *Anacystis nidulans* - 1mg diluted in 90% buffered acetone, Sigma-Aldrich), the concentration of which was determined spectrophotometrically.

2.4 Cell numbers and volumes, and photosynthetic efficiency

Cell volumes and numbers were measured on the Coulter Counter, and a phyto-pulsed amplitude modulation (phyto-PAM) fluorometer was used to measure fluorescence before and after laser excitation. Briefly, a cuvette containing DRS is subjected to a pulse of light which saturates the PSII reaction centres of the chlorophyll, suppressing photochemical quenching which reduces fluorescence yield. The ratio of variable to maximal fluorescence (F_v/F_m) gives an indication of the

photosynthetic efficiency of the diatoms, which in turn is an indication of their health [*Genty et al.*, 1989].

2.5 Atmospheric mixing ratios of I_2, ICl and HOI

Molecular and inorganic iodine compounds were measured using denuder tubes as detailed in *Huang and Hoffman* [2009]. Briefly, 1,3,5-trimethoxybenzene (1,3,5-TMB) coated brown borosilicate glass (50 cm length × 6 mm internal diameter) denuder tubes were used for the collection of gaseous HOI and ICl (collectively termed AIC), and α-cyclodextrin/$^{129}I^-$ (α-CD/$^{129}I^-$) coated denuder tubes were used for the collection of gaseous I_2.

The denuder tubes were mounted on the foremast of the ship at a height of approximately 10 m above sea level, connected to a pump and mass flow controller, and air was sampled for 3 hours at a rate of 500 ml min^{-1}. The denuder tubes were then capped with polypropylene end-caps, stored at -20°C, transported back to Mainz University, and analysed within 8 months by GCMS by Ru-Jin Huang.

The samples were analysed using a GCMS (Trace GC / PolarisQ, Thermo Finnigan Italia S.p.A, Rodano, Italy) with a 30 m × 0.25 mm and 0.25 μm film thickness fused-silica capillary column (Rtx®-5MS, Restek Co., Bad Homburg, Germany). Helium (99.999% purity) was used as a carrier gas, with a flow rate of 1.0 mL min^{-1}. 1 μL of the sample (or standard) was injected by an AS 3000 Thermo Finnigan autosampler. The temperature of the injector was set to 250°C and the temperature of the transfer line was set to 300°C. The GC oven temperature was held at 50°C for 3 min, ramped at 30°C min^{-1} to 220°C and held there for another 3 min. The MS was in EI mode, data acquisition was performed in full scan mode (*m/z* range 45–450) for identification and characterization of the derivatives, and in selected ion monitoring (SIM) mode for quantification.

Triplicate analyses by GCMS on the same tube gave a relative standard deviation (RSD) of 0.12% or less for AIC and 0.054% or less for I_2 analysis. On the basis of 90 litre sample volume, the LoD obtained for previous but similar measurements to this work was 28.6 ppqv for AIC and 94.6 ppqv for I_2, respectively. However, samples prepared to correct for interference, by treating tubes in a similar manner to the sampling tubes without drawing any air through them, gave a background 'blank' of 1.2 ppt for I_2 and 0.25 ppt for AIC.

2.6 Column densities and mixing ratios of IO

IO was monitored using a mini-MAX DOAS, a miniature Multiple Axis (i.e. vertically scanning) UV-visible Differential Optical Absorption Spectrometer, whose spectra are analysed by the method of *Platt et al.* [1979]. The instrument [*Hönninger and Platt*, 2002] of the Hoffman-Heidelberg design, using an Ocean Optics USB-2000, was set to measure at wavelengths from 337 to 481 nm with a spectral resolution of about 0.7 nm. IO was analysed from 409 to 474 nm, and BrO from 341 to 356 nm.

The DOAS analyses were performed by Dr Howard Roscoe (BAS) with the WinDOAS program, analysed with references near local noon at 90° elevation. Median slant amounts during each day with prolonged sunny periods were calculated, at four different elevation angles. During the Weddell Sea cruise, elevation angles of 4°, 8°, 15° and 50° were chosen. 4° was the lower limit chosen to avoid looking at the ice surface as the ship rolled a little, though the ship's movement was very restricted when surrounded by sea ice. 50° was the upper limit as this was the maximum permitted by the mounting location. At Rothera, where no such restrictions were necessary, the elevation angles ranged from 2° to 90°.

Median slant amounts at the three lowest elevations were subtracted from that at the highest elevation value, and divided by the appropriate differences in air mass factors (AMFs) to produce the vertical amounts. AMFs were supplied by Francois Hendrick of BIRA (personal communication). Mixing ratios were then calculated within an assumed boundary layer height, see relevant results chapters for more details.

IO column densities as measured by satellite during the campaign period are also presented for comparison. Measurements were made from the ENVISAT satellite-based SCIAMACHY (SCanning Imaging Absorption spectroMeter for Atmospheric ChartographY) instrumentation [*Schönhardt et al.*, 2008]. The technique measures the absorption by IO of backscattered radiation upwelling from the atmosphere with a UV-Vis-NIR spectrometer. The data was analysed by Anja Schönhardt at Bremen University.

2.7 Brine volume of sea ice

The temperature (handheld temperature probe) and bulk *salinity* (Hach sensION5 ISFET conductivity meter with internal temperature correction, resolution of 0.1 g l^{-1} and accuracy of 0.1 psu between -2.0 and 35.0°C) of the sea ice were measured in

order to calculate brine volume, according to the empirically derived equations 1 and 2 of *Frankenstein and Garner* [1967] as discussed in section 1.3.

2.8 Normalisation of bulk ice concentrations

Different methods were employed during this study to sample sea ice brine, and details are given in the relevant materials and methods sections in the results chapters. Where the bulk ice, rather than the liquid brine, was sampled, it is then necessary to normalise the bulk ice concentrations to liquid brine volume in order that the two methods can be compared.

As it is assumed that the biological and chemical activity of interest is occurring in the liquid phase of the sea ice, the change in volume of this liquid phase must be accounted for. Therefore where bulk ice was sampled, equation 3 gives initial concentrations in the brine

$$[x]_{brine} = [x]_{bulk} / \text{brine volume} \qquad (3)$$

where $[x]_{brine}$ is the concentration of the compound of interest in the brine and $[x]_{bulk}$ is the measured concentration in the bulk ice sample.

It is then necessary to correct for brine salinity to allow for concentration or dilution effects within and between cores and relative to the underlying seawater, as changes in concentration may be correlated with salinity variations in the brine channels. Equations 4 and 5 are used, the latter is employed when it was not possible to measure brine salinity

$$R[x]_{brine} = ([x]_{brine} / S_{brine}) * S_{ref} \qquad (4)$$

$$S_{brine} = S_{bulk} / \text{brine volume} \qquad (5)$$

where $R[x]_{brine}$ is the normalised and salinity corrected concentration of compound x, S_{brine} is brine salinity, S_{ref} is the salinity of the underlying seawater and S_{bulk} is the salinity of the bulk ice sample.

There are a number of different methods of normalising concentrations in bulk ice samples to concentrations in the brine. One can either normalise solely to brine volume, or solely in line with salinity. However it was felt that the above method took into consideration all aspects of how trace gases may become concentrated in sea ice. Thus by applying these equations and looking at the vertical profiles of halocarbon

concentrations throughout the ice depth, any variation in compound concentration must then be due to chemical and biological processes occurring *in situ* in the brine channels.

Chapter 3. Halocarbon Production by Polar Diatoms During Sea Ice Formation

3.1. Introduction

In order to study the factors affecting halocarbon production by polar diatoms, seawater containing *Porosira Glacialis*, an ice-associated diatom which has a bipolar distribution [*Hasle*, 1976], was frozen in Tedlar sampling bags. Halocarbon concentrations were monitored during the freezing and melting of the seawater, and physiological measurements were made to understand how diatoms survive when seawater freezes and they are incorporated into the brine channels. The change in conditions experienced by the diatoms is not simply the temperature – as the seawater freezes the concentrations of dissolved ions and trace gases will increase as the volume of the liquid phase decreases.

For each experiment, a filtered 'control' bag was used to account for this reduction in brine volume. Though it is possible to estimate what halocarbon concentrations may be in the liquid phase of the ice simply by multiplying by brine volume, loss processes may be occurring, such as uptake by bacteria and loss to the walls of the bag. The filtered control accounts for these. Another control, a bag held at ambient temperature, was also used, to assess halocarbon concentrations by the same subculture of diatoms which were not frozen.

Similar experiments were also carried out on cultures of two Antarctic ice diatoms, *Fragilariopsis Cylindrus and Fragilariopsis sp.*, collected from the Weddell Sea and Antarctic Peninsula respectively, and on a naturally occurring ice algae community on the Antarctic Peninsula to show these results are not confined to the laboratory, but rather may be applied to natural systems. This chapter aims to further understand how halocarbon concentrations become enhanced in sea ice brine.

3.2. Materials and methods

Cultured diatom stocks of *Porosira Glacialis* (kindly provided by Sophie Chollet, UEA), *Fragilariopsis Cylindrus* (collected from the Weddell Sea and kindly provided by Jan Strauss, UEA) *and Fragilariopsis sp.*, (collected from the Antarctic Peninsula and kindly provided by Claire Hughes, UEA) were grown in F/2 medium. F/2 is a widely used seawater medium enriched with nitrate ($NaNO_3$), phosphate ($NaH_2PO_4{:}H_2O$), silicate ($Na_2SiO_3{:}9H_2O$), trace metals ($FeCl_3{:}6H_2O$, $Na_2EDTA{:}2H_2O$, $CuSO_4{:}5H_2O$,

$Na_2MoO_4:2H_2O$, $ZnSO_4:7H_2O$, $CoCl_2:6H_2O$ and $MnCl_2:4H_2O$) and vitamins (thiamine HCl (vit. B_1), biotin (vit. H) and cyanocobalamin (vit. B12)) and was made up following the method of *Guillard and Ryther* [1962] and *Guillard* [1975], at 4°C in 3 litre glass conical flasks (experiment 1 and Rothera experiments) or 25 litre polycarbonate flasks (experiments 2 and 3).

Diatom-rich seawater (DRS) was transferred into 5 litre SKC Tedlar sampling bags with dual stainless steel fittings (experiments 1 – 3) or 3 litre SKC Tedlar sampling bags with a single polypropylene fitting (Rothera experiments). Tedlar is a polyvinyl fluoride film, and the bags are made from two sheets of the film glued together. DRS was transferred to the bags via a ~2 m long piece of Teflon tubing, after rinsing three times. Any air in the bag was then carefully removed by holding the valve open at the top of the bag and applying pressure to the liquid.

For the filtered experimental controls, DRS was filtered under a vacuum of 130 Pa. All equipment and glassware were kept on ice to try to maintain cold temperatures during filtration and preparation. Once prepared, and the first sample had been taken for halocarbon analysis, the bags were moved to incubators as detailed in experimental description sections 3.2.1 to 3.2.4.. Four incubators were used:

Incubator 1: a 4°C cold room with a 12 hour light cycle and a photon flux of 85 μmol photon $m^{-2}\,s^{-1}$ from fluorescent tubes.

Incubator 2: a -15°C freezer with an LED array of blue, white and UV light, designed to be representative of the light in polar regions, with a photon flux of 15 μmol photon $m^{-2}\,s^{-1}$.

Incubator 3: a culture incubator which had an adjustable temperature setting, and a 24 hour light cycle with a photon flux of 35-40 μmol photon $m^{-2}\,s^{-1}$ from fluorescent tubes.

Incubator 4: a freezer set to -10°C, with the same LED array used in incubator 2

It is known that halocarbon production rates vary with light intensity [*Moore et al.*, 1996] and the light intensities in the incubators were designed to be similar to those which may be experienced in open water and sea ice conditions at the relevant temperatures.

At the sampling time (0, 24 and 48 hours after sample preparation unless otherwise stated, see results section 3.3), 50 ml (or 30 ml for -15°C samples where brine volumes were very much reduced) of the seawater / brine was drawn into a gas-tight syringe through the valve via a 2 cm length of Tygon tubing, after rinsing. Where much ice formation had occurred, it was first ensured that sufficient brine had drained down to the valve opening (by gravity), to avoid creating a vacuum inside the bag as the brine was removed. Duplicate samples from the same bag were used, except in experiment 1, where single samples were only possible at some times, and Rothera experiment 2 where duplicate bags were also used, and duplicate samples taken from each bag.

10 ml of the 50 ml removed was used for physiological measurements - cell volumes and numbers were measured on the Coulter Counter, and a phyto-PAM fluorometer was used to measure fluorescence before and after laser excitation as described in section 2.4.

The remaining 40 ml (or 20 ml) sample was then injected through a 25 mm Whatman GF/F filter paper, held in a gas tight plastic filter paper holder, directly into the custom-made glass purge tube at the start of the GCMS analysis set up as described in section 2.1.2. The liquid nitrogen method of trapping was used in experiments 1-3, whereas the Markes system of trapping on adsorbent tubes was used in the Rothera experiments.

Ten halocarbons were measured, shown in table 5, with retention times and limits of detection. A calibration was carried out approximately once every two months during the experimental period as detailed in section 1.2, agreement between calibrations was good and R^2 values of regression lines fit to the data were ≥0.94. Any drift in instrument sensitivity between the calibrations was accounted for by the addition of deuterated standards to every sample as described in section 2.2.1.

A summary of the experimental controls is given in sections 3.2.1 to 3.2.4 and table 6.

	CH_3I	C_2H_5I	$CHBr_3$	CH_2ICl	$2\text{-}C_3H_7I$
m/z	142	156	173	176	170
LoD	0.10	0.02	0.10	0.08	0.003
RT	4.05	6.3	10.7	8.3	7.5
	CH_2I_2	CH_2IBr	$CHBr_2Cl$	$1\text{-}C_3H_7I$	CH_2Br_2
m/z	268	222	129	170	174
LoD	0.15	0.22	0.24	0.001	0.10
RT	11.1	9.7	9.5	8.4	7.95

Table 5. Halocarbons analysed by GCMS, showing mass / charge ratio (m/z), limit of detection (LoD) in pM, and retention times (RT) in minutes.

3.2.1 Tedlar bag experiment 1

A preliminary experiment was carried out to determine whether the Tedlar bags were suitable experimental reaction vessels, as there were concerns over the Tedlar material being a source or a sink of halocarbons. Three controls were used, two of which were bags of seawater containing *Porosira Glacialis* (approx 5000 cells ml^{-1}), one (labelled Ambient) was placed in incubator 1, and the other (labelled Low T) in incubator 2. This allowed a comparison of halocarbon production at varying temperatures and light intensities. The third control bag containing identical, but filtered, seawater to remove the diatoms (labelled Low T (F)) which was also placed in incubator 2 in order to check that there were no emissions from the bag during the freezing process, to check for loss of any compounds to the bag walls, and also to ascertain if any other reactions were occurring during the freezing process which did not involve the diatoms. 1 litre DRS (or filtered DRS) was added to each bag. Due to the large reduction in brine volume in the low temperature bags, duplicate samples were only taken from the Ambient bag at 24 hours, and the percentage error associated with these halocarbon concentrations was applied to data from all bags.

3.2.2 Tedlar bag experiment 2

In Experiment 2, the effect of low temperatures on halocarbon production by *Porosira Glacialis* and *Fragilariopsis Cylindrus* was studied. 3 litres DRS was added to two bags for each species, (Ambient at +4°C, Low T at variable temperature, -3°C to -5°C) and 3 litres filtered DRS was added to a third bag to be used as a low temperature control

(Low T (F)). The Ambient bags were placed in incubator 1 for 4 days, then moved to incubator 2 for one night, then moved back to incubator 1.

The low temperature bags were held in incubator 3, the temperature of which was set to -3°C for the first 3 days of this experiment. However little ice formation was observed (see section 3.3.2 for further discussion), so the temperature was lowered to -5°C for 3 days. Following this, as the diatoms were still healthy, the temperature of the incubator was raised to +4°C for 3 days, in order that further observations could be made on temperature variations on the same population of algae.

3.2.3 Tedlar bag experiment 3

Fragilariopsis sp. was used for a study of halocarbon production at +4°C (Ambient) and -5°C (Low T), and a low temperature filtered control was used (Low T (F)). 3 litres DRS was added to each bag. The Ambient bag was kept in incubator 1, the Low T and Low T (F) bags were kept in incubator 3 at -5°C for the first 48 hours, and at +4 °C for the remaining 24 hours of the experiment, so that a comparison between the two conditions could be made.

3.2.4 Rothera tedlar bag experiments 1 and 2

During the austral summer of 2009 / 2010, similar experiments were carried out on algae collected from pieces of sea ice found in Ryder Bay, shown in figure 6. The ice (~50 cm^3 pieces) was collected from the side of a small boat and the liquid inside the brine channels was allowed to drain into a bucket. The brine which drained was collected, and inoculated in F/2 medium as described in section 3.2.

Two glass conical flasks were prepared with this inoculated natural community, in which algae then began to grow. The flasks were kept outside in flowing seawater tanks. Cultures were not made, so the resulting assemblages will have been a mixture of species present in the ice. As the light intensity and temperature may have been different in the tanks to that found in the ice, a different species may have come to dominate the community than was originally present. However, two assemblages of diatoms were successfully grown, labelled J and K, and Tedlar bag experiments were carried out. The assemblages were dominated by a *Fragilariopsis* species, and under inspection below the microscope appeared to be monocultures (figure 7), however the presence of other species is likely for the reasons mentioned above.
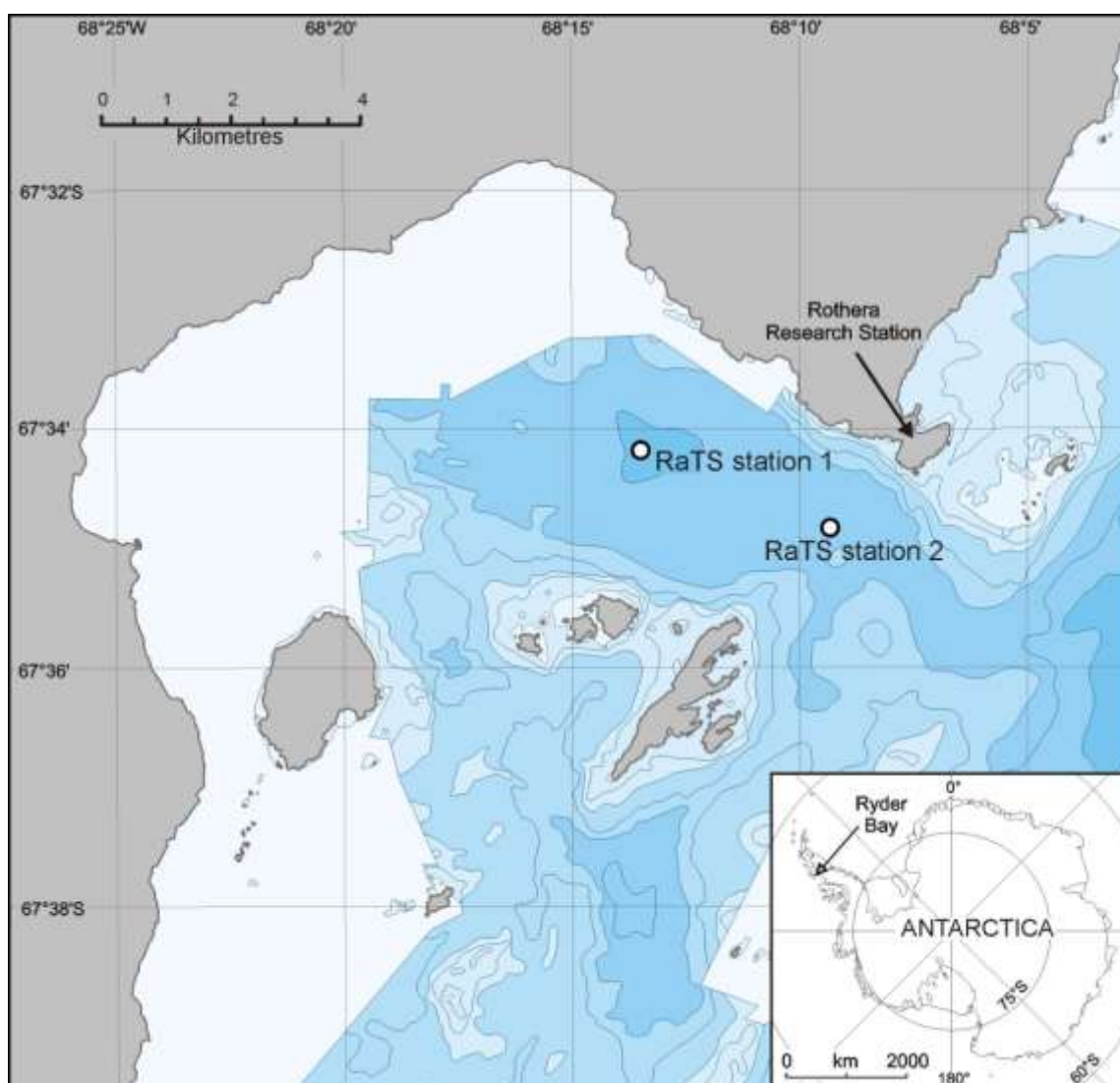
Figure 6. Map of Ryder Bay, where sea ice samples were collected, from which diatom assemblages were grown.

A different GCMS was used for halocarbon analysis, but the model, column, method and technique were identical. A calibration was carried out at the start and end of the experimental period, and instrument sensitivity drift was accounted for by the addition of deuterated standards to every sample (section 2.2.1).

Assemblage J was used in Rothera Tedlar bag experiment 1. Three bags were filled, each with 1.5 litres DRS (or filtered DRS). Bag 'Low T' was placed in incubator 4, a freezer set to -10°C. Bag 'Low T (F)' was a filtered low temperature control also placed in incubator 4, and the 'Ambient' bag was placed outside in the flowing seawater tanks. Here the temperature was approximately 0°C and light intensities corresponded to solar radiation. Day light hours were between 22 to 24 hours during the experimental period.

Rothera Tedlar bag experiment 2 was a repeat of Rothera Tedlar bag experiment 1, only 2 litres DRS was added to each bag, diatom assemblage K was used, and duplicate bags were placed under each control (Low T, Low T (F) and Ambient). In this way, errors associated with both natural variability and experimental technique were accounted for.

Exp	Species	Time (days)	Labels	Incubator	Temperature (°C)
1	PG	3	Ambient	1	4
			Low T	2	-15
			Low T (F)	2	-15
2	PG & FC	9	Ambient	1/2	4/-15
			Low T	3	-3 to -5
			Low T (F)	3	-3 to -5
3	Fsp	4	Ambient	1	4
			Low T	3	-5 to 4
			Low T (F)	3	-5 to 4
Rothera1	J	1	Ambient	Outdoors	0
			Low T	4	-10
			Low T (F)	4	-10
Rothera1	K	3	Ambient	Outdoors	0
			Low T	4	-10
			Low T (F)	4	-10

Table 6. Experimental controls in Tedlar bag experiments. PG = *Porosira Glacialis*, FC = *Fragilariopsis Cylindrus,* Fsp = *Fragilariopsis sp.*, J = Rothera assemblage J and K = Rothera assemblage K.

Figure 7. Diatom assemblages J (top panel) and K (middle and bottom panel), grown from a naturally occurring ice algae community from Ryder Bay, under the microscope.

3.3. Results

3.3.1 Physiological measurements

Information on the photosynthetic efficiency of the diatoms, and cell density and volume, help us to understand how the diatoms cope with the conditions in these extreme environments. In Tedlar bag experiment 2 in the Low T bags, the photosynthetic efficiency of the *Porosira Glacialis* remains stable at -3°C, drops a little at -5°C, and drops further at +4°C (figure 8), though it should be remembered that the high cell counts at this stage may mean the diatoms are coming towards the end of their growth stage, so a loss in photosynthetic efficiency is to be expected. This can be seen in the cell density plots in figure 9. The photosynthetic efficiency of the *Fragilariopsis Cylindrus* in the Low T bag (figure 8) seems more sensitive to temperature change, dropping down to $F_v/F_m = 0.32$, but increases again once the bags have been bought back to +4°C.

The results for photosynthetic efficiency in the Ambient bags are very interesting: the *Porosira Glacialis* drop in efficiency a little (from $F_v/F_m = 0.67$ to 0.5) over the first 4 days of the experiment, the large reduction in F_v/F_m then suggests cell death when the medium is frozen to -15°C, with a small increase in photosynthetic efficiency as some cells survive and start to grow again upon ice melt. The *Fragilariopsis Cylindrus* however show a similar reduction in photosynthetic efficiency at -15°C, but instantly recover upon ice melt.

As can be seen from figure 9, *Porosira Glacialis* stops growing at about 8000 – 9000 cells ml^{-1} at both temperatures. *Fragilariopsis Cylindrus* grows very slowly initially in the low temperature bag, despite being healthy, then shows a short lived growth spurt. Growth is seen in the ambient bag, which slows a little after the -15 °C freeze. Of particular interest is the large enhancement in cell numbers of *Fragilariopsis Cylindrus* when frozen to -15 °C, as they are incorporated into the reduced volume of the brine channel network, whereas the *Porosira Glacialis* cells are not as concentrated. This discrepancy could be due to the larger volume of the *Porosira Glacialis* cells; they are not as easily expelled from the ice matrix as it forms as the tiny *Fragilariopsis Cylindrus* are.
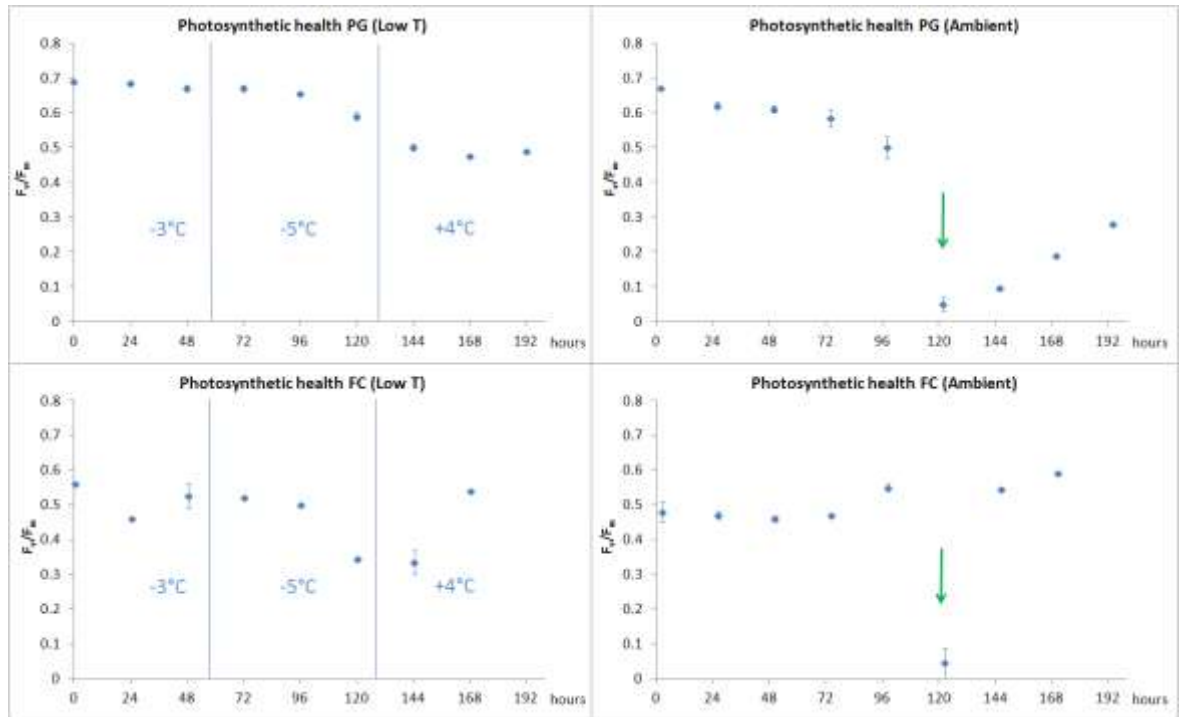
Figure 8. Photosynthetic efficiency represented by F_v/F_m for *Porosira Glacialis* and *Fragilariopsis Cylindrus* in Tedlar bag experiment 2. The Ambient bags were held at +4°C with the exception of the point denoted by the green arrow, which was taken after the seawater had been frozen down to -15°C overnight. Average and range of duplicate samples are shown.
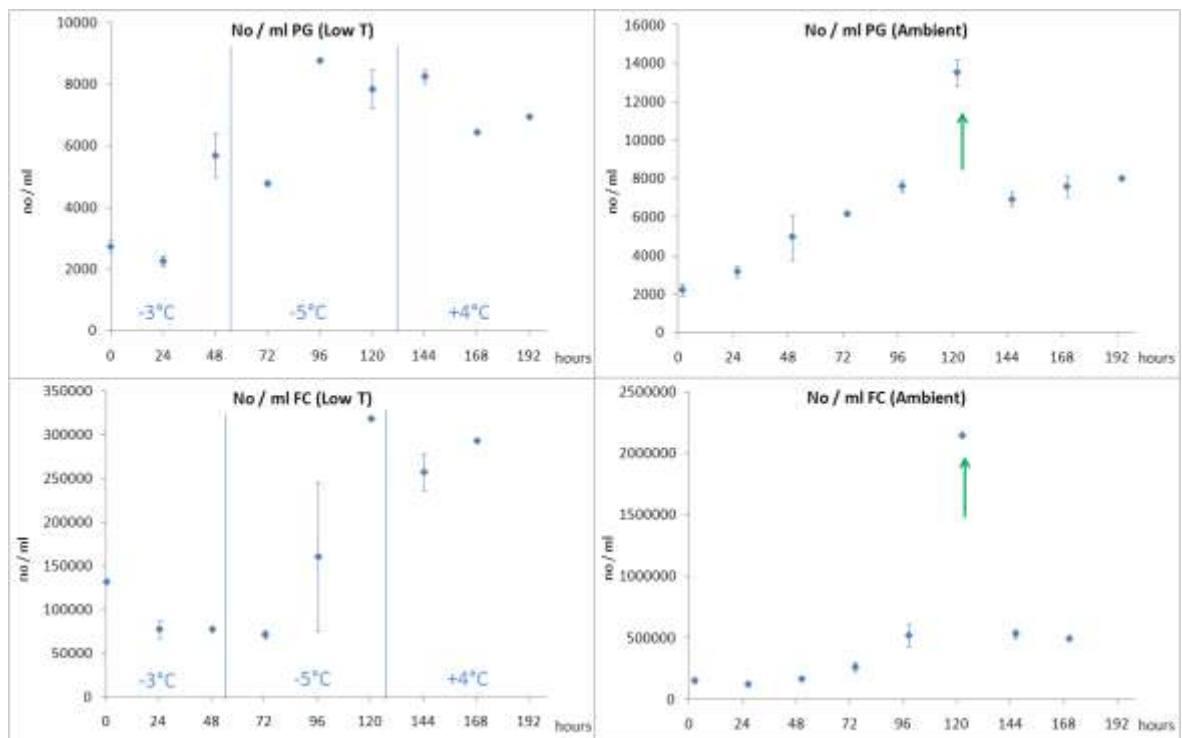
Figure 9. Cell densities of *Porosira Glacialis* and *Fragilariopsis Cylindrus* in Tedlar bag experiment 2. The Low T bags were held at the temperature shown in blue below the data points. The Ambient bags were held at +4°C with the exception of the point denoted by the green arrow, which was taken after the seawater had been frozen down to -15°C overnight. Average and range of duplicate samples are shown. Note the change in scale.

Cell volume measurements (figure 10) also tell an interesting story. In the low temperature bags, as would be expected during the exponential growth phase (at which the diatom stocks should have been at the start of the experiment), *Porosira Glacialis* reduces in volume over time (due to cell division) whereas *Fragilariopsis Cylindrus* cell size increases, which must be due to some reproductive growth. Cell volume results for the Ambient bags show how the different diatom species are affected by the freezing process. When *Porosira Glacialis* is frozen to -15°C, cell death results as the cells break open and cell volume is subsequently halved. The cell volume of *Fragilariopsis Cylindrus* however is unaffected by the freezing. This explains why the latter diatom species regain photosynthetic efficiency immediately after ice melt (figure 8), and higher cell densities are recorded at -15°C (figure 9) as the small *Fragilariopsis Cylindrus* are easily incorporated into the brine. The larger *Porosira Glacialis,* however, is not as easily expelled by the ice crystal formation; they are crushed within the ice lattice, cell lysis and death results.
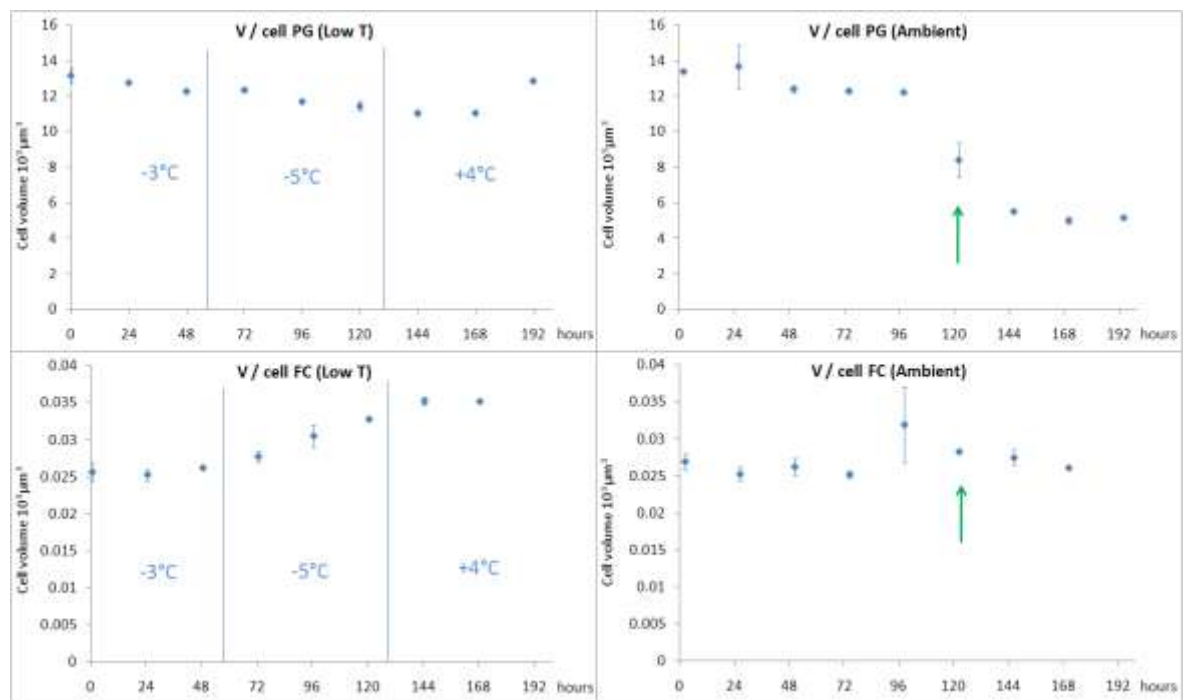
Figure 10. Cell volume of *Porosira Glacialis* and *Fragilariopsis Cylindrus* in Tedlar bag experiment 2. The Low T bags were held at the temperature shown in blue below the data points. The Ambient bags were held at +4°C with the exception of the point denoted by the green arrow, which was taken after the seawater had been frozen down to -15°C overnight. Average and range of duplicate samples are shown.

3.3.2 Halocarbon concentrations

Tedlar bag experiment 1

Halocarbon concentrations in cultures of *Porosira Glacialis* at -15°C and +4°C, and a filtered control at -15°C, are shown in figure 11. Some loss of C_2H_5I, $CHBr_3$, CH_2ICl, CH_2I_2, CH_2IBr, $CHBr_2Cl$ and CH_2Br_2 in the filtered control is possibly due to the walls of the bag, however halocarbon production is well in excess of this loss. A small amount of CH_3I, $1-C_3H_7I$ and $2-C_3H_7I$ appears to be produced in the absence of the diatoms, this could be due to emissions from the bag, or bacteria could be responsible, however the quantities emitted are small.

The concentrations which would be expected from the concentration effect in the low temperature bag, that is by the reduction in the volume of the liquid phase of the sea ice, is accounted for by the filtered control, as are any loss processes during the freezing process. At -15°C, at constant bulk salinity, brine volume is 6.1%; hence if all halocarbons are concentrated in the brine, a 16 fold increase in initial halocarbon concentrations is expected due to this phenomenon. However such a strong enhancement is not seen, indeed in the filtered control the concentrations often drop to 0. Where any enhancement in concentrations of halocarbons occurs, it is assumed to be due to diatom activity under the extreme conditions experienced in the sea ice brine.

Tedlar bag experiment 2

Porosira Glacialis and *Fragilariopsis Cylindrus* were used to study the effect of temperature on halocarbon production. For each species, a low temperature (Low T) a filtered low temperature control (Low T (F)) and an ambient control (Ambient) were prepared as detailed in section 3.2 and table 6.

The Low T and Low T (F) bags were held at -3°C in the incubator for the first 3 days of the experiment, and at -5°C for next 3 days. Very little ice formation was observed at -3°C, approximately 10% of the water was frozen in the bag containing *Porosira Glacialis*, and only a small number of frazil ice crystals were observed in the bag containing *Fragilariopsis Cylindrus*. This is interesting as *Fragilariopsis Cylindrus* is an ice diatom, and, as was discussed in section 1.4.2, ice diatoms secrete EPS, containing anti-freeze agents which may have prevented the bags from freezing. When held at
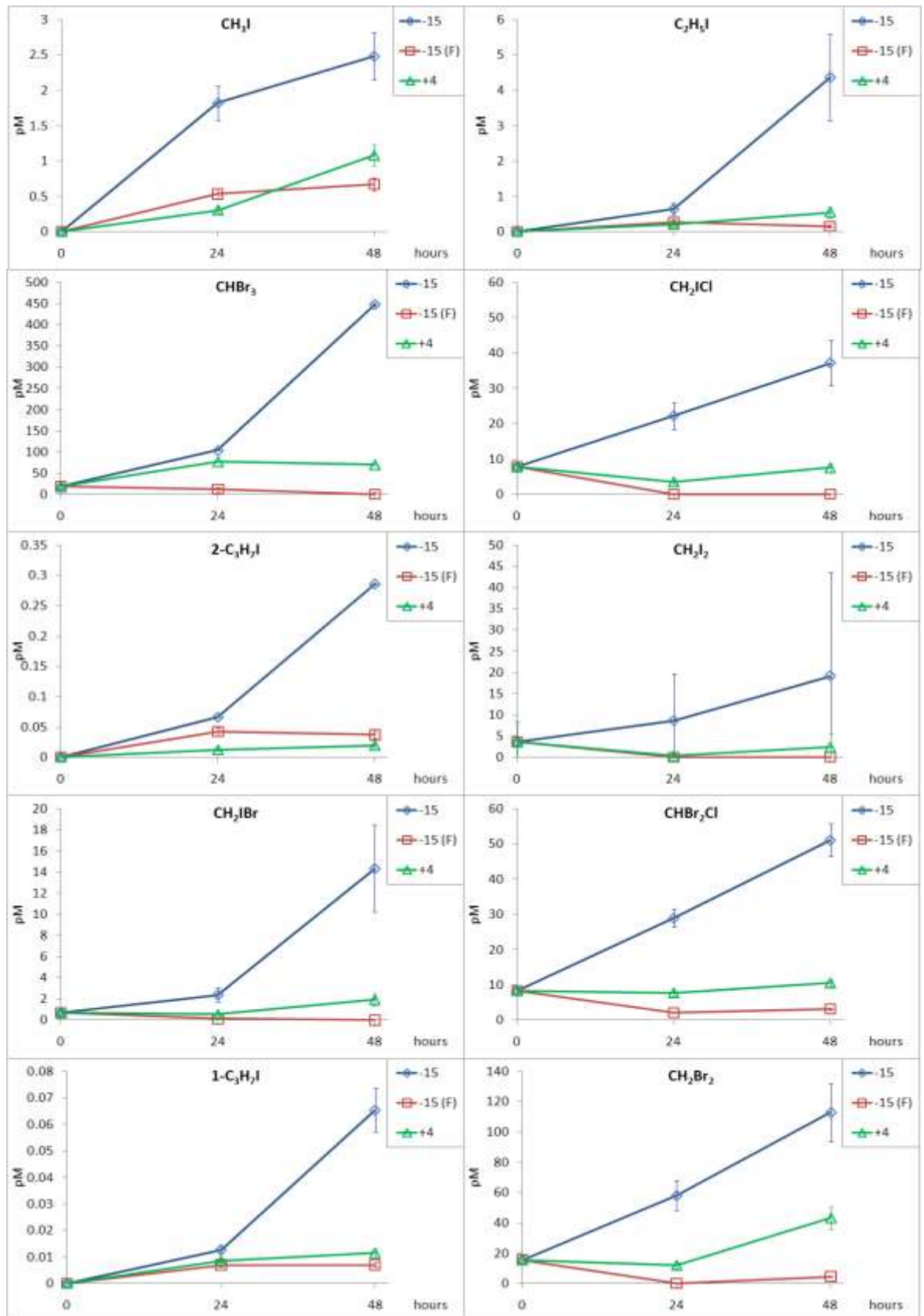
Figure 11. Halocarbon concentrations in Tedlar bags containing *Porosira Glacialis* held at -15°C and +4°C. A bag containing the same medium which had been filtered at 0.2μm was also held at -15°C.

-5°C, approximately 40% and 20% of the water was frozen in the bags containing *Porosira Glacialis* and *Fragilariopsis Cylindrus* respectively. The bags were then held at +4°C for the next 3 days, so as to ensure that the 4°C results are comparable: it may not be possible to compare the results from the bags in the 4°C degree cold room to the ones at -5°C in the incubator as the light intensities and cycles were different.

The diatoms in the bags remained healthy (a drop in F_v/F_m of <0.25) during the timescale of the experiment, though, as can be seen in figure 9, the diatoms reached the stationary growth phase and halocarbon production could have reduced as a result of this, as has been suggested by previous studies [eg *Tokarczyk and Moore*, 1994].

Porosira Glacialis

Halocarbon concentrations in cultures of *Porosira Glacialis* are shown in figures 12 to 16, with the upper panels showing halocarbon concentrations in the Low T and Low T (F) bags, and results for the Ambient bags shown in the lower panels, respectively. The halocarbon concentrations expected from the concentration effect of solvent volume reduction in the Ambient bags are shown by the dashed line. The concentration effect is not shown for the Low T bags as this is accounted for by the Low T (F) bag. Where concentrations do not increase in the Low T (F) bag at lower temperatures, other loss processes must be occurring, such as loss to the walls of the bag or uptake by bacteria.

Other than a slight increase in **CH_3I** concentration in the Low T (F) bag in the first 24 hours, concentrations decrease in all bags, possibly due to loss to the walls of the bag or uptake by bacteria. The initial production of CH_3I in the Low T (F) bag could be via chemical reaction with other species, or biological production from enzymes released from cell lysis during filtration. The release of CH_3I after the Ambient bag has been frozen and thawed supports release from cell lysis during freezing, supported by high concentrations of this compound at low temperature in Tedlar bag experiment 1 (figure 11)

After initial loss of **C_2H_5I** to the walls of the bag, production is then seen in the Low T bag at -3°C. This production stops at -5°C and values remain constant. When the Low T bag is moved to +4°C some production of C_2H_5I is observed, followed by some loss. The Ambient bag also shows a release of C_2H_5I after thawing from -15°C. The cause of

production of C_2H_5I after ice melt in all bags is not known, but release from the bag wall is possible.

CHBr₃ and **CH₂Br₂** concentrations follow a similar trend, production is observed to be independent of temperature in the Low T bag, and production in the Ambient bag is very similar. In Tedlar bag experiment 1 (figure 11), CH_2Br_2 production was observed at low and ambient temperatures, but $CHBr_3$ production was not observed at 4°C, the reason for this discrepancy is not known.

CH₂ICl and **CHBr₂Cl** production is not observed, but the effect of the trace gases being concentrated in the brine when the Ambient bag is frozen to -15°C is clearly seen. These compounds also showed little or no production at 4°C in Tedlar bag experiment 1 (figure 11).

CH₂I₂ and **CH₂IBr** concentrations show a similar pattern, increasing over time at low temperature, but no production is observed at 4°C. These compounds also showed little or no production at 4°C in Tedlar bag experiment 1 (figure 11).

1-C₃H₇I concentrations fall over the first 24 hours in the Low T and Low T (F) bags, then some production is observed, with highest production rate being seen at -3 °C. There is some release following the freeze-thaw of the Ambient bag, but concentrations are very low in all samples, and close to the limit of detection of the instrument.

2-C₃H₇I was not observed above the limit of detection in any of the experimental controls.

In the Ambient bag, the effect of freezing the medium clearly results in an increase in concentration of the dissolved trace gases. The magnitude of this increase is compound dependent; this may be due to loss to the walls of the bag, uptake by bacteria, or compounds being trapped in brine pockets which were sealed off from the brine network and thus were not sampled. For most compounds, the concentrations returned to their pre-frozen values upon ice thaw, however the concentrations of C_2H_5I and $1-C_3H_7I$ increased, possibly due to cell lysis as observed in figure 10. The trends between the different compounds are also apparent, with the bromocarbons $CHBr_3$ and CH_2Br_2, and the poly-iodocarbons CH_2I_2 and CH_2IBr showing similar patterns of production.

The trends between different compounds are interesting as different enzymes are thought to be responsible for production of different classes of compounds. Methyl transferases are thought to be responsible for monohalogen production whereas haloperoxidase enzymes have been shown to be responsible for production of polyhalocarbons. Haloperoxidases can be further sub-classified into bromoperoxidase and iodoperoxidase enzymes, responsible for production of bromocarbon and iodocarbon compounds respectively. Results from this experiment would suggest compounds produced by methyl transferase enzymes are more likely to be released after a freeze-thaw cycle (CH_3I, C_2H_5I and $1\text{-}C_3H_7I$).
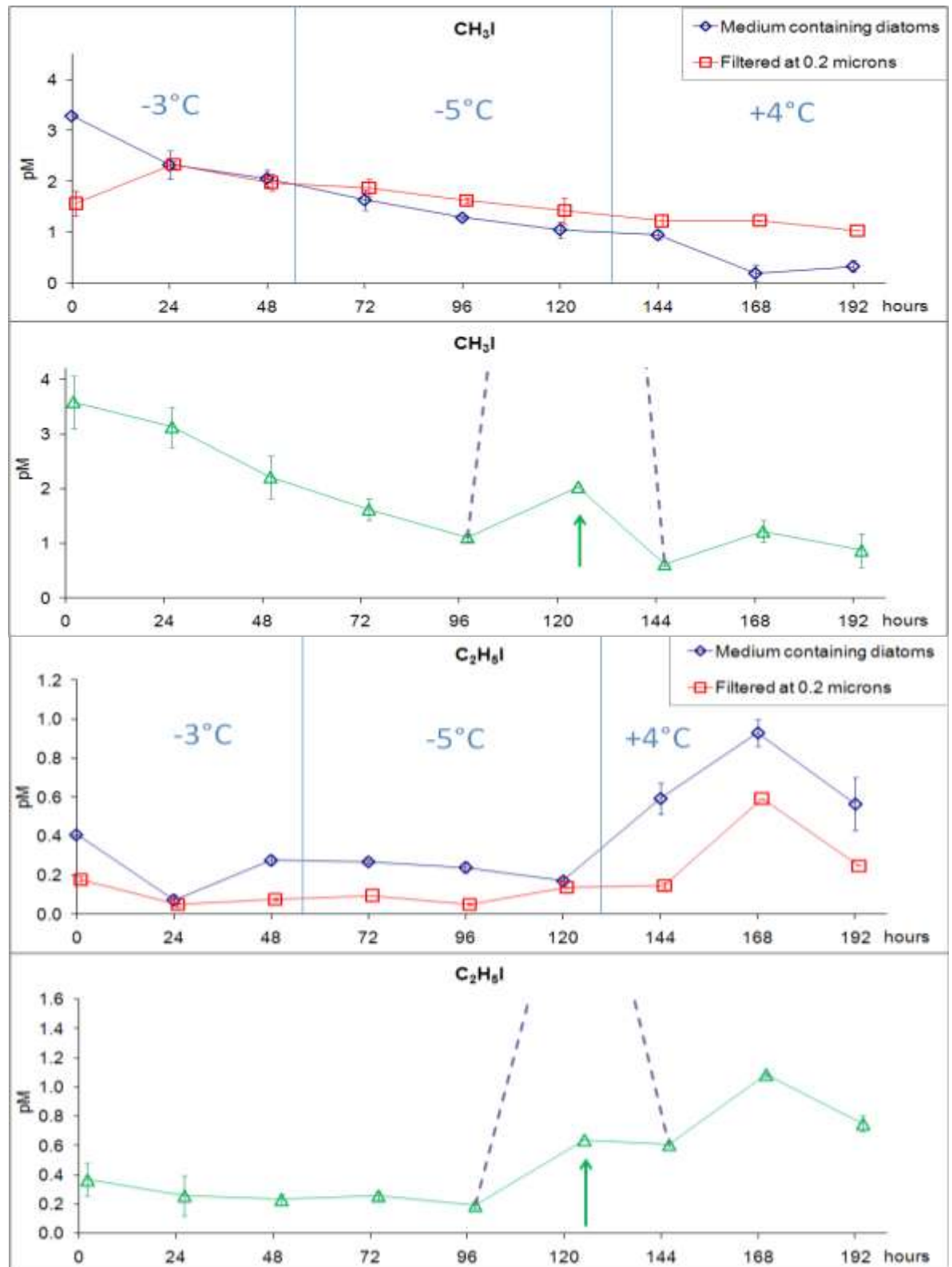
Figure 12. Concentrations of CH$_3$I and C$_2$H$_5$I in cultures of *Porosira Glacialis* in the low temperature bag (top panel, with filtered control) where the temperature is shown above the data, and in the ambient bag (bottom panel) which was held at 4°C except for the point denoted by the green arrow, which denotes concentrations after freezing to -15°C. The dashed line represents concentrations expected via the concentration effect. Average and range of duplicate samples are shown.
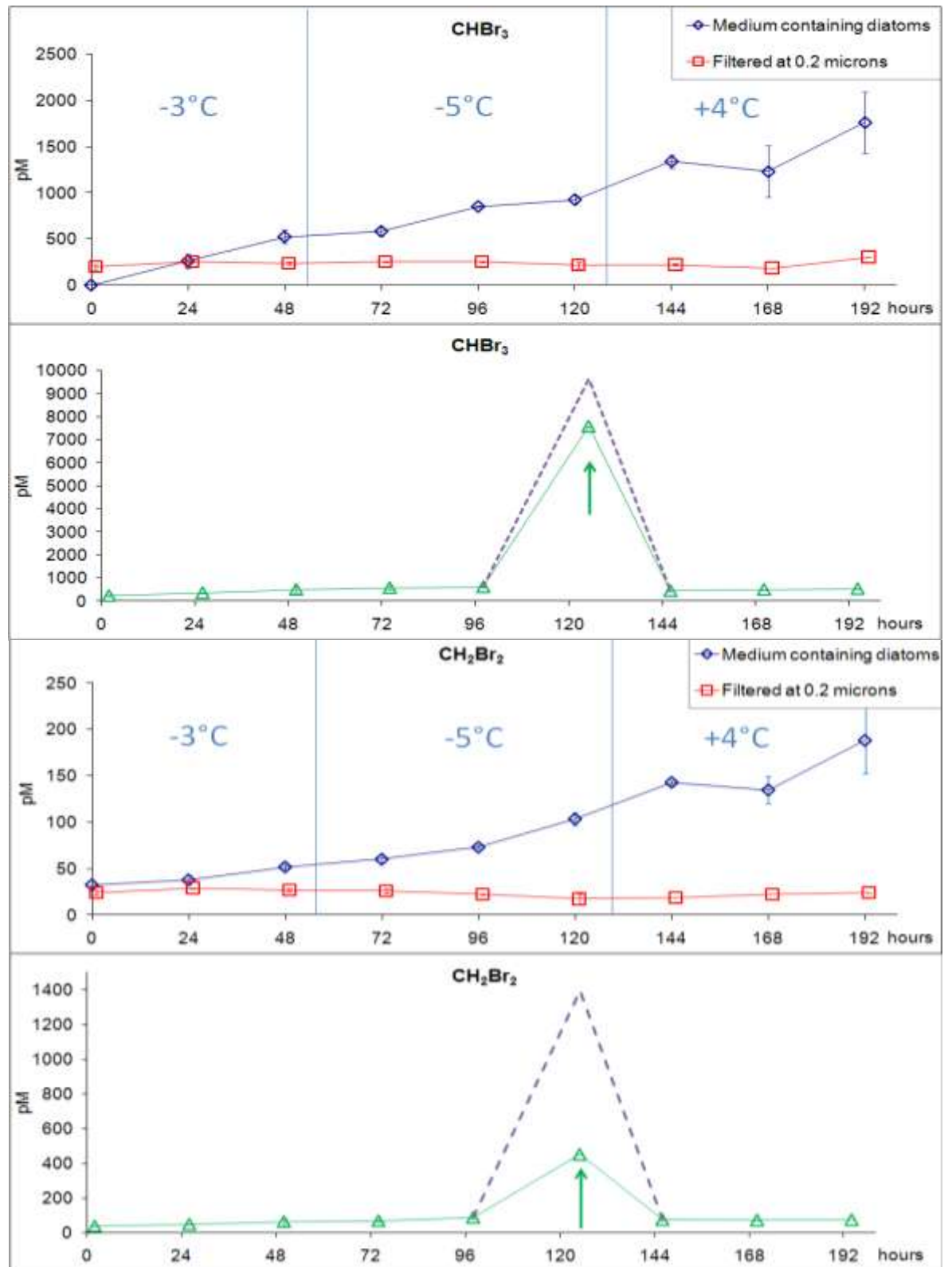
Figure 13. Concentrations of $CHBr_3$ and CH_2Br_2 in cultures of *Porosira Glacialis* in the low temperature bag (top panel, with filtered control) where the temperature is shown above the data, and in the ambient bag (bottom panel) which was held at 4°C except for the point denoted by the green arrow, which denotes concentrations after freezing to -15°C. The dashed line represents concentrations expected via the concentration effect. Average and range of duplicate samples are shown.
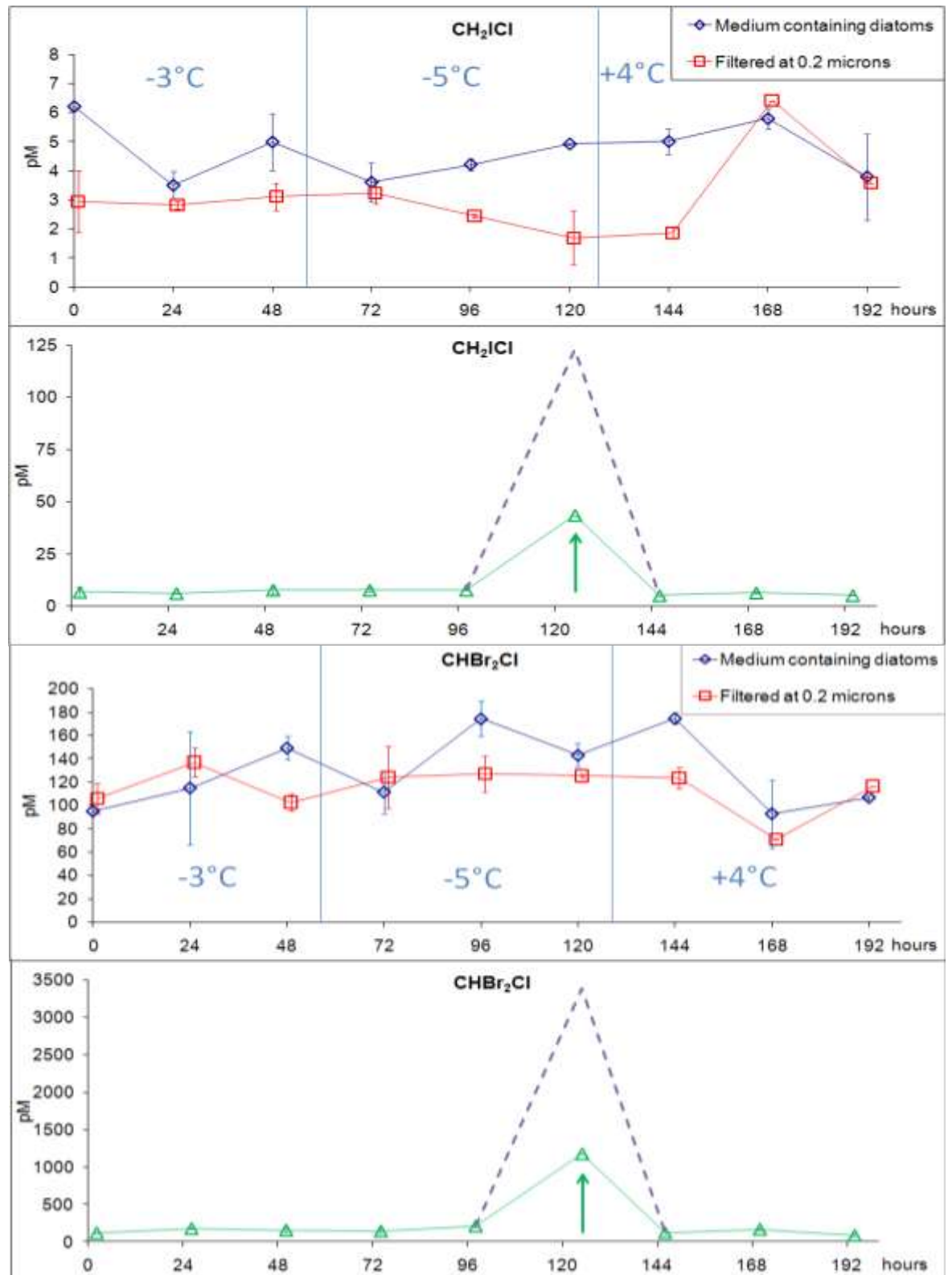
Figure 14. Concentrations of CH$_2$ICl and CHBr$_2$Cl in cultures of *Porosira Glacialis* in the low temperature bag (top panel, with filtered control) where the temperature is shown above the data, and in the ambient bag (bottom panel) which was held at 4°C except for the point denoted by the green arrow, which denotes concentrations after freezing to -15°C. The dashed line represents concentrations expected via the concentration effect. Average and range of duplicate samples are shown.
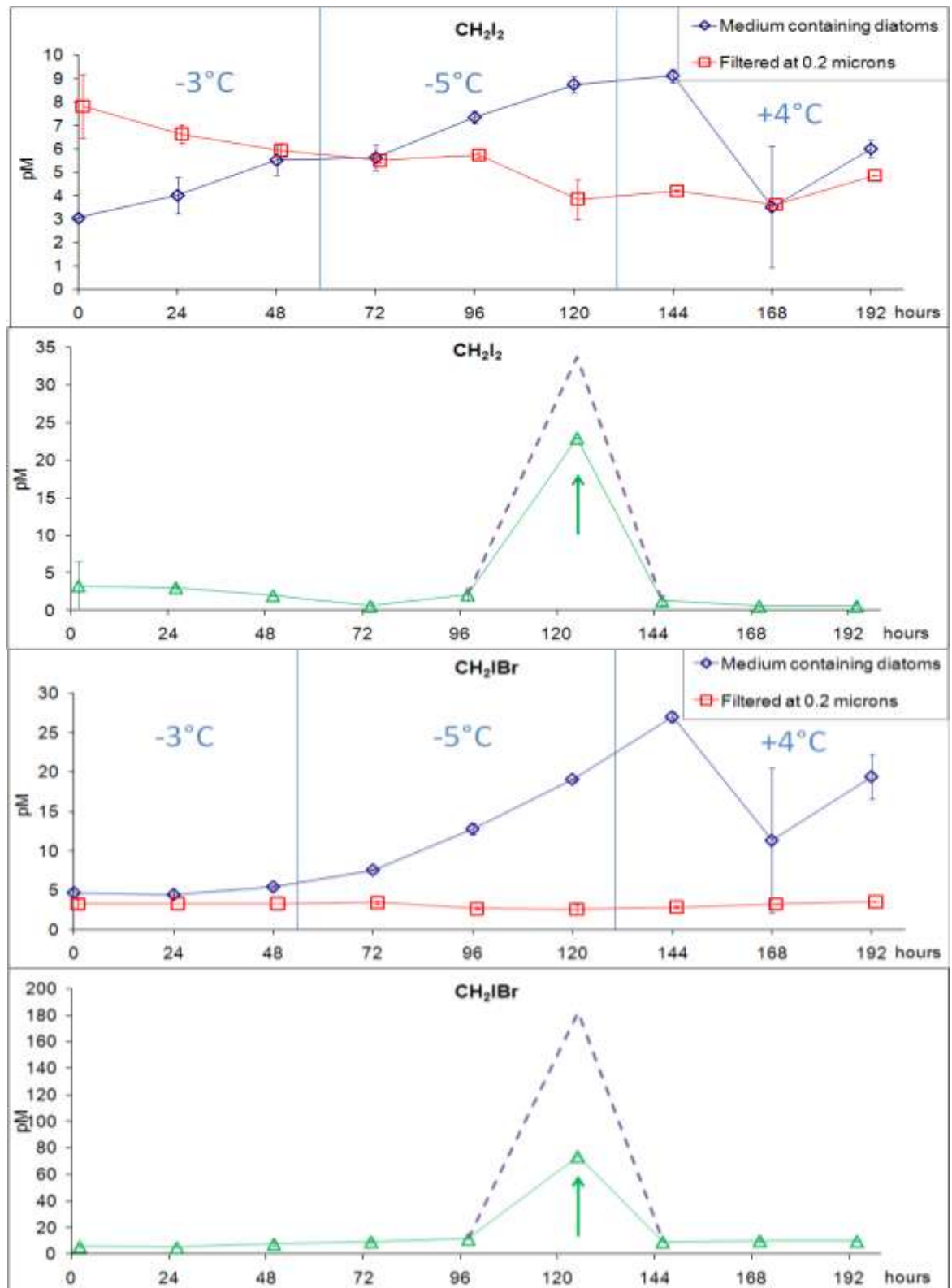
Figure 15. Concentrations of CH₂I₂ and CH₂IBr in cultures of *Porosira Glacialis* in the low temperature bag (top panel, with filtered control) where the temperature is shown above the data, and in the ambient bag (bottom panel) which was held at 4°C except for the point denoted by the green arrow, which denotes concentrations after freezing to -15°C. The dashed line represents concentrations expected via the concentration effect. Average and range of duplicate samples are shown.
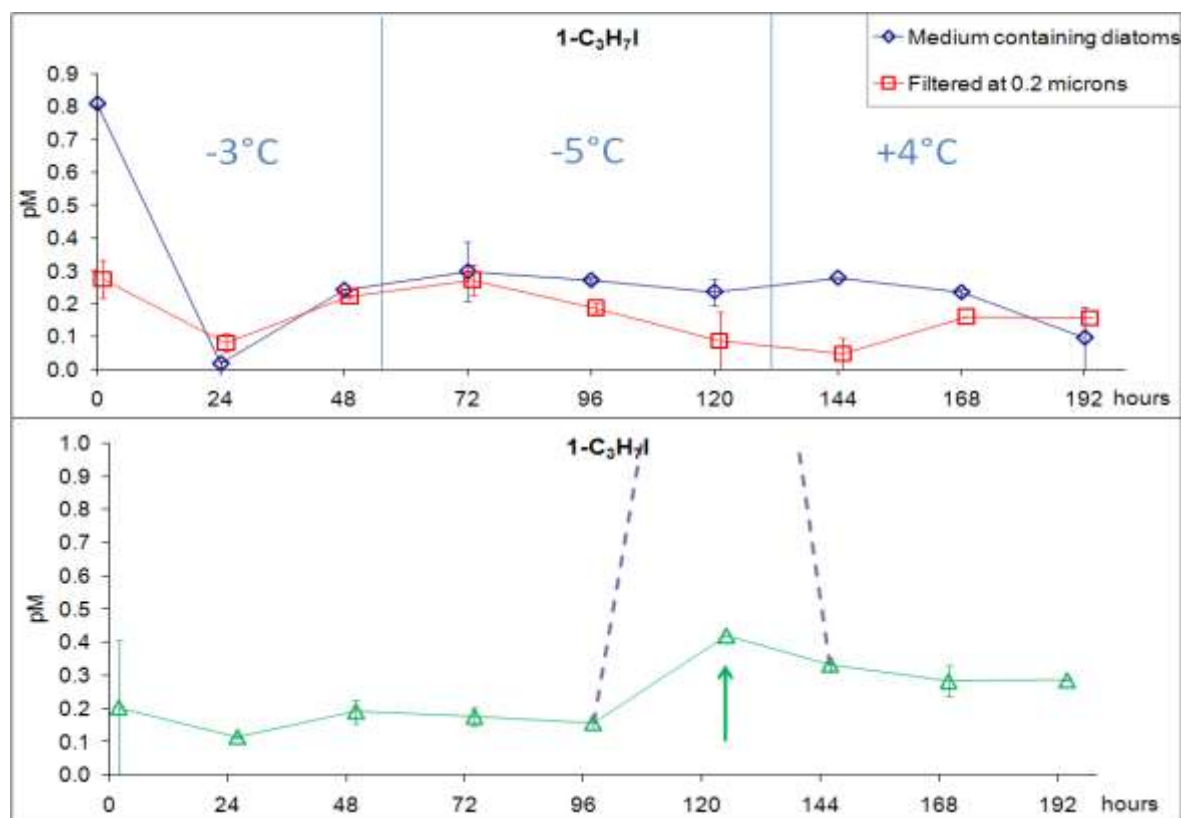
Figure 16. Concentrations of 1-C₃H₇I in cultures of *Porosira Glacialis* in the low temperature bag (top panel, with filtered control) where the temperature is shown above the data, and in the ambient bag (bottom panel) which was held at 4°C except for the point denoted by the green arrow, which denotes concentrations after freezing to -15°C. The dashed line represents concentrations expected via the concentration effect. Average and range of duplicate samples are shown.

Fragilariopsis Cylindrus

Concentrations of **C₂H₅I**, **CH₂IBr** and **CH₂ICl** in cultures of *Fragilariopsis Cylindrus* in Tedlar bag experiment 2 are shown in figures 17 and 18. No production of any of the other halocarbons measured was observed, and the concentrations over time show no change except for the concentration effect of freezing the ambient bag to -15°C.

As with the *Porosira Glacialis* cultures, there is a release of **C₂H₅I** upon ice melt at 168 hours. **CH₂IBr** production is observed at -5°C, less than expected via the concentration effect, but concentrations drop then increase after the freeze-thaw. **CH₂I₂** concentrations decrease over time, but remain higher in the low temperature bags than in the ambient bag. However, the concentrations in the low temperature bags do not differ between filtered and unfiltered bags, suggesting loss processes are occurring which are not due to the diatoms, such as uptake by bacteria or loss to the walls of the bag.
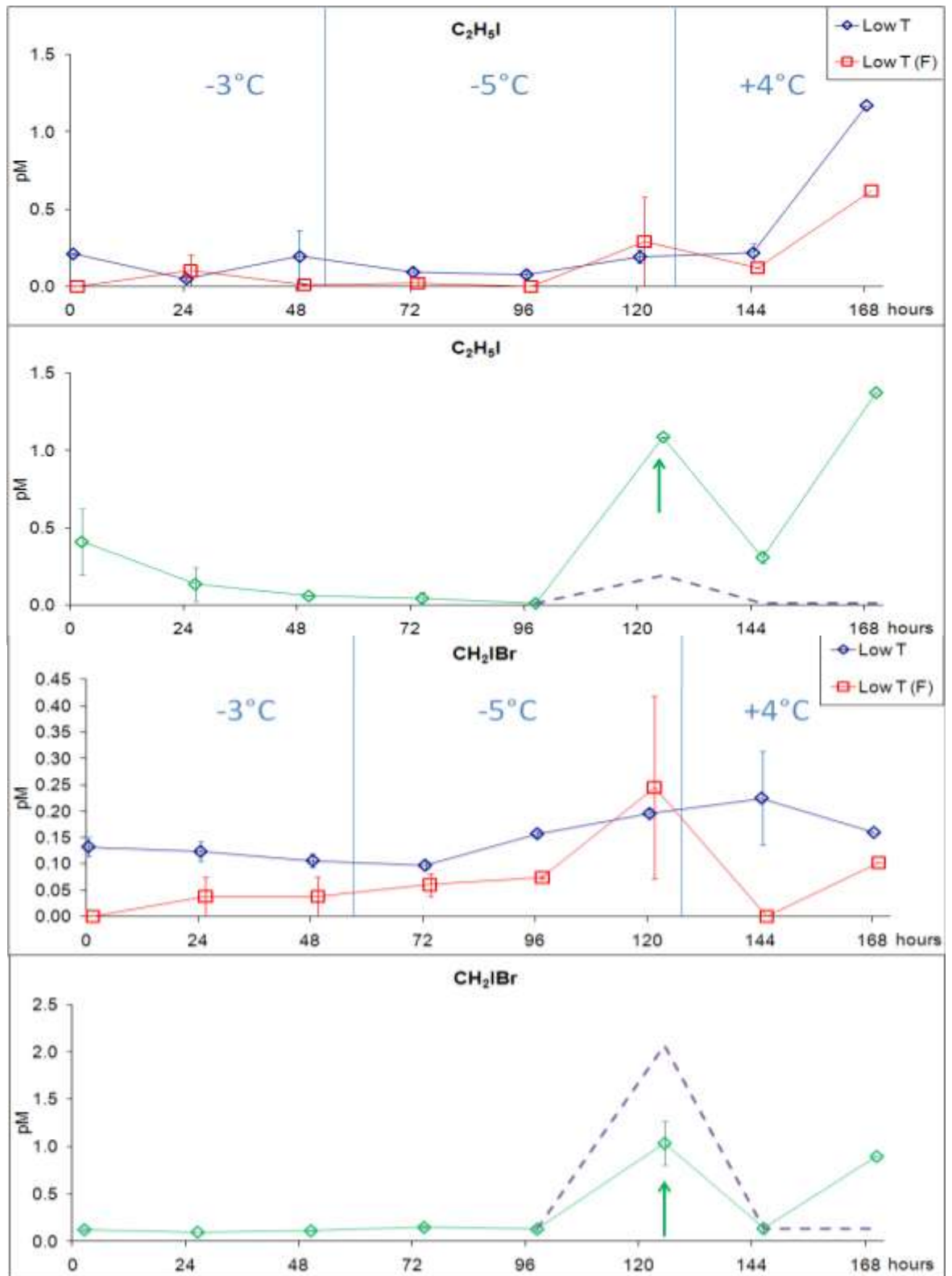
Figure 17. Concentrations of C_2H_5I and CH_2IBr in cultures of *Fragilariopsis Cylindrus* in the low temperature bag (top panel, with filtered control) where the temperature is shown above the data, and in the ambient bags (bottom panel) which were held at 4°C except for the point denoted by the green arrow, which denotes concentrations after freezing to -15°C. The dashed line represents concentrations expected via the concentration effect. Average and range of duplicate samples are shown.
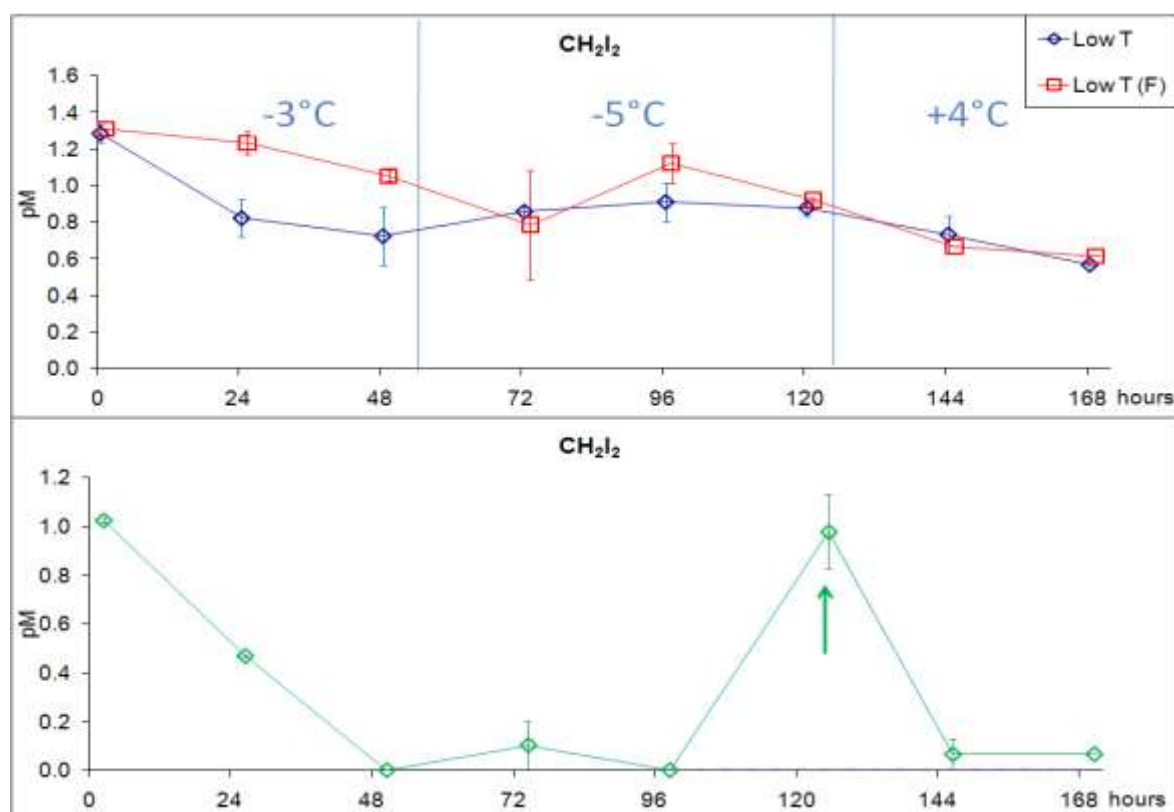
Figure 18. Concentrations of CH_2I_2 in cultures of *Fragilariopsis Cylindrus* in the low temperature bag (top panel, with filtered control) where the temperature is shown above the data, and in the ambient bags (bottom panel) which were held at 4°C except for the point denoted by the green arrow, which denotes concentrations after freezing to -15°C.

Tedlar bag experiment 3 *Fragilariopsis sp.*

The effect of temperature on halocarbon production by *Fragilariopsis sp.* was studied in Tedlar bags held at -5°C and +4°C for the Low T and Ambient controls respectively, and a Low T (F) control was also used. Considerably more ice formation occurred at -5°C in the bags containing *Fragilariopsis sp.* than in the bags containing *Porosira Glacialis* or *Fragilariopsis;* approximately 60% of the water was frozen after 48 hours. *Fragilariopsis sp.* is also an ice diatom, if the anti-freeze agents in EPS do prevent ice formation, it must be produced in different amounts by different species of diatom.

The Low T and Low T (F) bags were then moved to the 4°C cold room in order that a direct comparison between the two controls could be made. Figure 19 shows halocarbon concentrations in all bags. Increased halocarbon production occurs in the Low T bags, above that measured in the filtered control. However, once the ice has melted the concentrations drop to match those in the ambient bags, apart from C_2H_5I which once again shows substantial increase upon ice melt, and CH_2ICl which showed a significant increase in production in the low temperature bags.
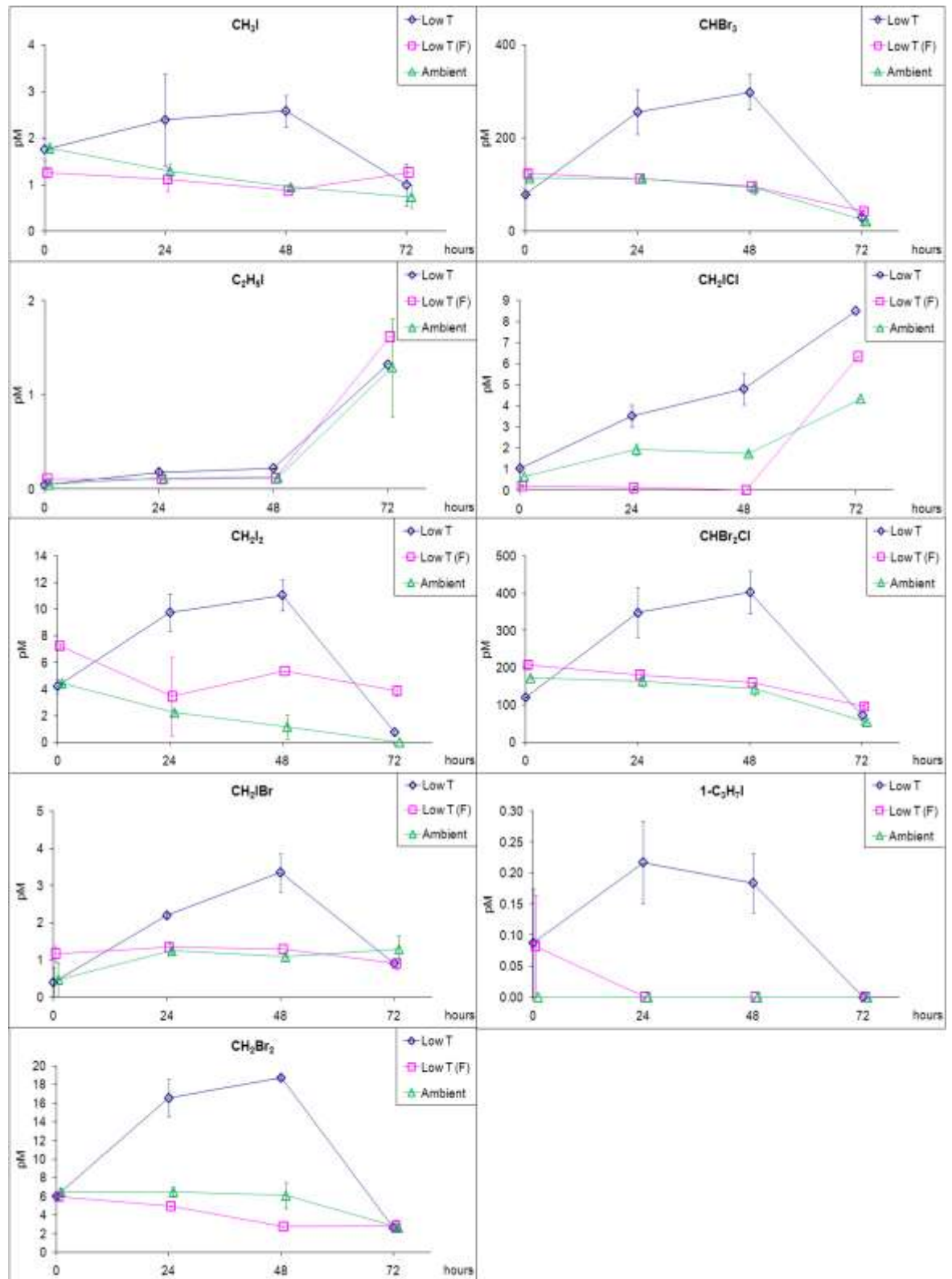
Figure 19. Halocarbon concentrations in Tedlar bags containing *Fragilariopsis sp..* Low T was held at -5°C for the first 48 hours of the experiment then moved to +4°C (Low T) and a filtered control bag (Low T (F)) was held under the same conditions, to check emissions from, or deposition to, the bag. The Ambient bag was constantly held at +4°C. Average and range of duplicate samples are shown.

3.3.3 Results from experiments on a naturally occurring Antarctic ice algae community

In order to study how applicable these laboratory experiments are to the natural environment, similar experiments were carried out on a naturally occurring Antarctic ice algae community. Diatom assemblages (J and K) were grown from sea ice brine collected in Ryder Bay (figure 6). The average and range of halocarbon concentrations in the sea ice pore water from which assemblage J were taken were 2.4 (1.9 to 3.1) pM CH_3I, 1.0 (0.7 to 1.3) pM C_2H_5I, 18.5 (17.9 to 18.8) pM $CHBr_3$, 0.6 (0.5 to 0.6) pM CH_2ICl, 0.1 (<LoD to 0.3) pM CH_2I_2, 1.6 (1.4 to 1.7) pM CH_2IBr, 1.1 (0.6 to 1.6) pM $CHBr_2Cl$ and 4.8 (4.2 to 5.3) pM CH_2Br_2. The concentrations of all iodocarbons except CH_3I are higher than those in the underlying seawater at the time, whereas bromocarbon concentrations in the ice brine are lower (average seawater concentrations at 7 depths from 0 to 100m, triplicate samples for each, were 4.1 pM CH_3I, 0.6 pM C_2H_5I, 33.1 pM $CHBr_3$, 0.4 pM CH_2ICl, 0.2 pM CH_2I_2 and 14.9 pM CH_2Br_2; CH_2IBr concentrations were below the LoD). This data supports iodocarbon, but not bromocarbon, production by algae living in sea ice.

Rothera Tedlar bag experiment 1

Initial cell densities of the Antarctic ice algae community, measured back in the UK after preservation with Lugol's iodine, were approximately 1500 cells ml^{-1}. Three bags were used, a low temperature bag (Low T) filled with DRS at -10°C in a freezer under the same LED array used in previous experiments, a filtered low temperature control (Low T (F)), and an Ambient bag placed outside in the flowing seawater tanks at approximately 0°C. Halocarbon concentrations are shown in figure 20. Due to time constraints, it was only possible to run this experiment for 24 hours, by which time approximately 60% of the water in the bags had frozen. Concentrations of **CH_3I**, **C_2H_5I**, **CH_2ICl**, **1-C_3H_7I**, **CH_2I_2**, **$CHBr_2Cl$** and **CH_2IBr** are all higher in the low temperature bags which contain diatoms (Low T).

Of particular interest is the much greater enhancement in iodocarbon concentrations compared to the bromocarbons in the Low T bags; the compounds may be released upon cell lysis during freezing, or production may increase due to the stresses of the freezing process. **CH_2IBr** concentrations are particularly high, which is interesting as very high concentrations of this compound were measured during the COBRA field campaign (see Chapter 6). **CH_2I_2** concentration results are also interesting; loss is

observed in the ambient bag, no production is seen in the filtered bag but there is some production in the frozen DRS.
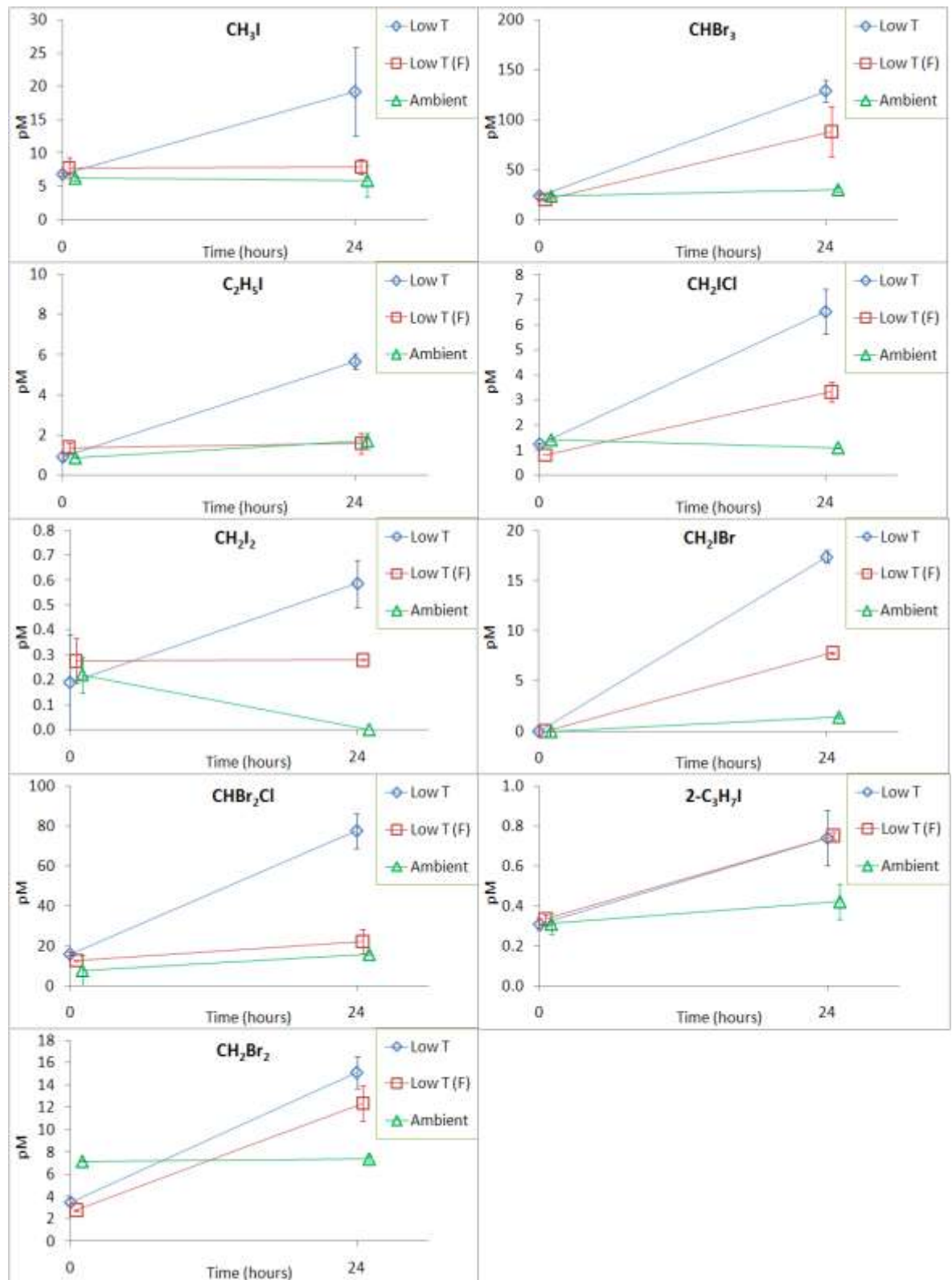
Figure 20. Concentrations of halocarbons a naturally occurring Antarctic ice algae community (Assemblage J) at -10°C (Low T), 0°C (Ambient), and a low temperature filtered control (Low T (F)). Average and range of duplicate samples are shown.

Rothera Tedlar bag experiment 2

The second Tedlar bag experiment at Rothera was a repeat of the first, but with duplicate bags used for each control. Duplicate samples were taken from each bag. Diatom assemblage K was used; 2 litres DRS (or filtered DRS) was added to each bag. Initial cell densities were approximately 1700 cells ml^{-1}. Concentrations of **CHBr$_3$**, **CH$_2$I$_2$**, **CH$_2$IBr**, **CHBr$_2$Cl**, **1-C$_3$H$_7$I** and **CH$_2$Br$_2$** are shown in figures 21 to 26 respectively; no significant production of the other halocarbons was observed. **CHBr$_3$** concentrations were higher in the ambient bags, **CH$_2$IBr** concentrations were higher in the frozen bags, whereas production of the other halocarbons shown in the figures was independent of temperature. However losses to the bag are significant at low temperature, as can be seen in reduction in concentrations in the Low T (F) bags, so enhanced concentrations in the bags containing DRS represent significant production by diatoms. The two assemblages (J and K) at Rothera showed different trends in iodocarbon and bromocarbon production. Whether this is due to a different species dominating the community, or whether the assemblages were at a different stage in their growth is not known.
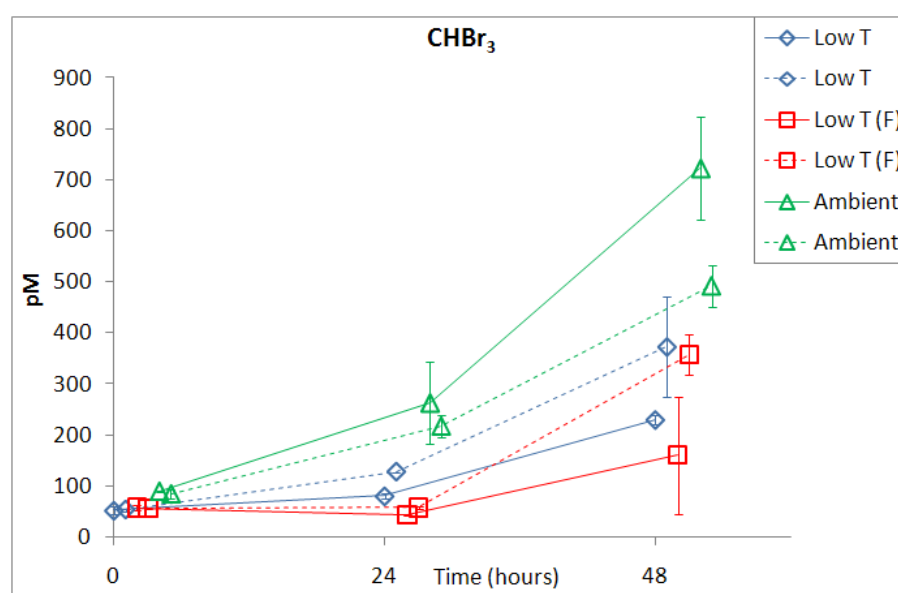
Figure 21. Concentrations of CHBr$_3$ in a naturally occurring Antarctic ice algae community (Assemblage K) at -10°C (Low T), 0°C (Ambient), and a low temperature filtered control (Low T (F)). Average and range of duplicate samples from duplicate bags (4 samples at each time point) are shown.
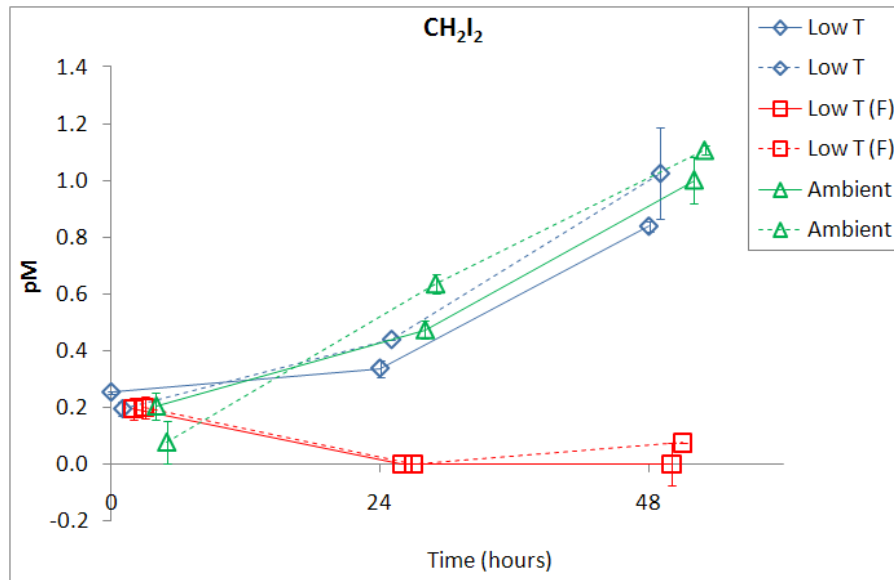
Figure 22. Concentrations of CH$_2$I$_2$ in a naturally occurring Antarctic ice algae community (Assemblage K) at -10°C (Low T), 0°C (Ambient), and a low temperature filtered control (Low T (F)). Average and range of duplicate samples from duplicate bags (4 samples at each time point) are shown.
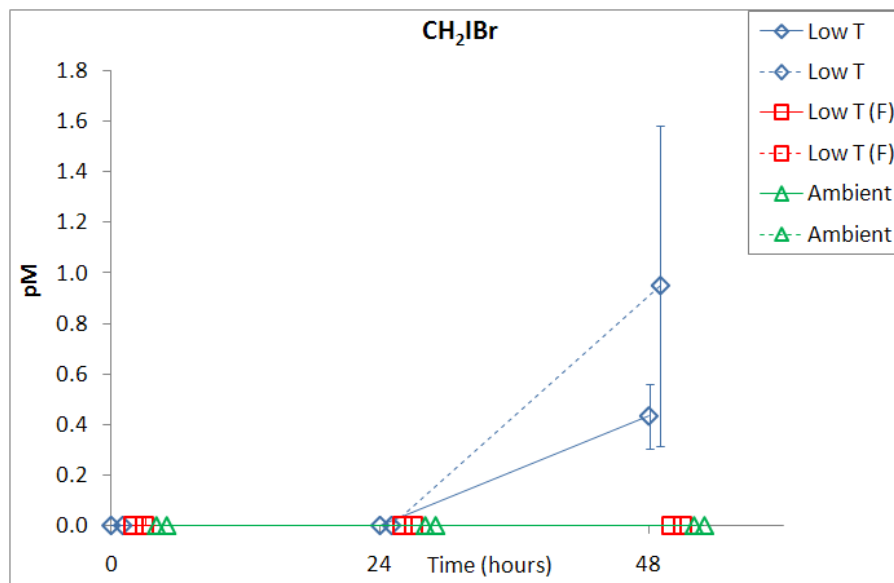
Figure 23. Concentrations of CH$_2$IBr in a naturally occurring Antarctic ice algae community (Assemblage K) at -10°C (Low T), 0°C (Ambient), and a low temperature filtered control (Low T (F)). Average and range of duplicate samples from duplicate bags (4 samples at each time point) are shown.
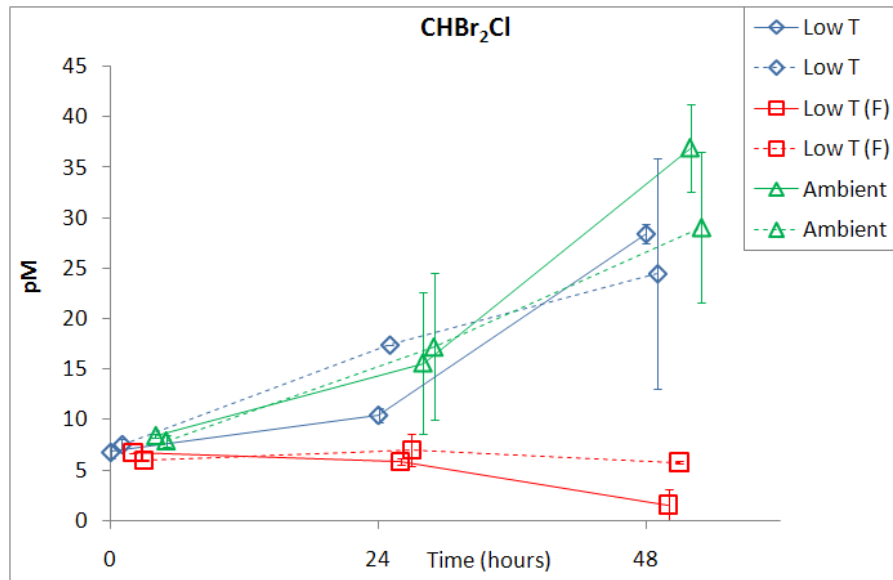
Figure 24. Concentrations of CHBr$_2$Cl in a naturally occurring Antarctic ice algae community (Assemblage K) at -10°C (Low T), 0°C (Ambient), and a low temperature filtered control (Low T (F)). Average and range of duplicate samples from duplicate bags (4 samples at each time point) are shown.
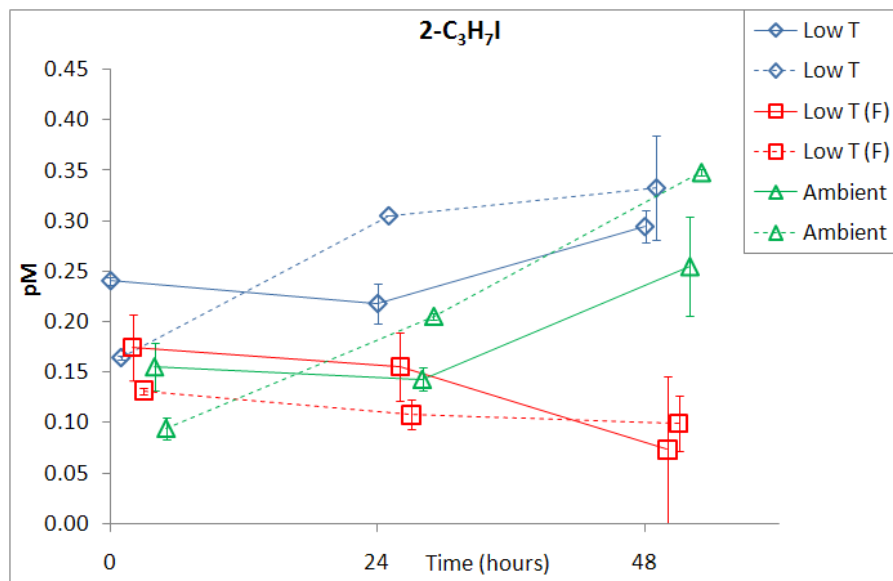
Figure 25. Concentrations of 2-C$_3$H$_7$I in a naturally occurring Antarctic ice algae community (Assemblage K) at -10°C (Low T), 0°C (Ambient), and a low temperature filtered control (Low T (F)). Average and range of duplicate samples from duplicate bags (4 samples at each time point) are shown.
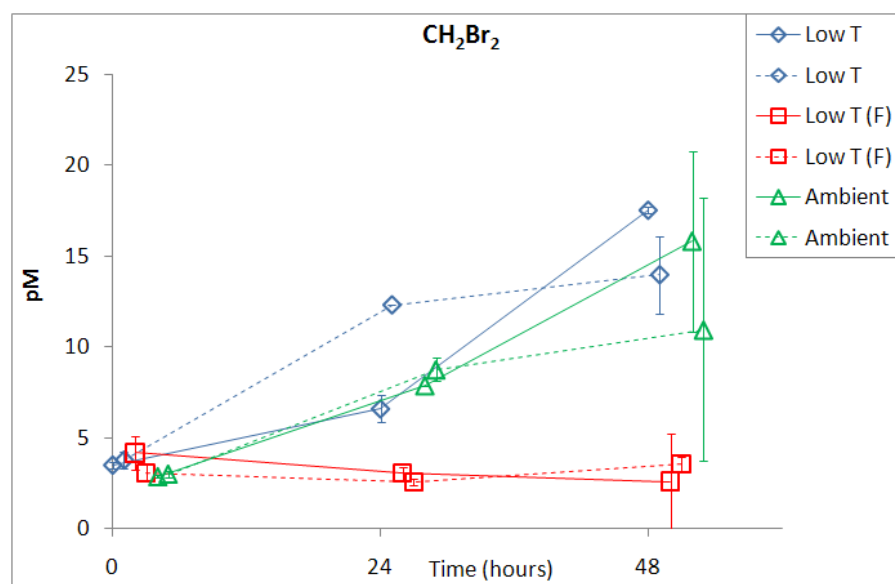
Figure 26. Concentrations of CH_2Br_2 in a naturally occurring Antarctic ice algae community (Assemblage K) at -10°C (Low T), 0°C (Ambient), and a low temperature filtered control (Low T (F)). Average and range of duplicate samples from duplicate bags (4 samples at each time point) are shown.

3.4. Discussion

CH₃I concentrations are higher in cultures of *Porosira Glacialis* at low temperature (-15°C) in experiment 1. The sharp increase in production in the first 24 hours, followed by a smaller increase between 24 and 48 hours, may a reflection of the amount of ice formation, subsequent reduction in volume of the brine and hence concentration of the halocarbons produced. It is also possible that halocarbon production by the diatoms under the stresses imposed by the freezing process slows; photosynthetic efficiency was not measured in this experiment so it is impossible to ascertain how this subculture reacted to the freezing process. CH₃I production is also observed in the Ambient bag, at a rate of approximately 0.02 pM hour⁻¹.

A loss of CH₃I over time in both bags containing *Porosira Glacialis* is observed in experiment 2. Although the concentration effect is clearly seen in the ambient bag, it is not as concentrated as would be expected from brine volume calculations (figure 12), and the increase is smaller in magnitude than for most other halocarbons. This may be due to nucleophilic attack by Cl⁻, the rate of which increases with salinity [*Elliott and Rowland*, 1993]; bacterial consumption or loss to the walls of the bag could also be responsible. No production of CH₃I is observed from either *Fragilariopsis* species in experiments 2 and 3. An increase in CH₃I concentration at -10°C is observed in the Antarctic ice algae community in Rothera experiment 1,

though the concentration effect is again smaller than expected, so similar loss processes could be occurring. Nevertheless, this leads to CH_3I concentrations of 26 pM, in reasonable agreement with field measurements of 35 - 41 pM in Weddell Sea ice brine [*Fogelqvist and Tanhua*, 1995].

C_2H_5I concentrations are higher in cultures of *Porosira Glacialis* at low temperature (-15°C) in experiment 1, though the much larger increase from 24 to 48 hours than in the first 24 hours of the experiment suggest C_2H_5I is first concentrated in the brine, and then released by diatoms under brine conditions. The maximum rate of change of C_2H_5I concentration in experiment 1 is 0.2 pM hour^{-1}, compared to an average production rate of 0.01 pM hour^{-1} under ambient conditions. In experiment 2, for both *Porosira Glacialis* and *Fragilariopsis Cylindrus,* there is a significant increase in concentrations of C_2H_5I after ice melt, also observed in the filtered control, so an abiotic mechanism to do with the freezing process may be responsible, as may emissions from the bag. Experiment 3 shows a similar trend, though the reason for the increase in concentrations in the ambient bag, which had not been frozen, is unclear. Results from the Rothera experiments show an increase in concentration of a magnitude expected when the brine volume is 11%, though the lack of a similar increase in the filtered control suggests some link to diatoms. Maximum concentrations recorded in the first Rothera experiment were 6.1 pM; lower than field measurements of 26 - 29 pM in Weddell Sea ice brine [*Fogelqvist and Tanhua*, 1995].

$CHBr_3$ concentrations are higher in cultures of *Porosira Glacialis* at low temperature (-15°C) in experiment 1, though the much larger increase from 24 to 48 hours than in the first 24 hours of the experiment suggest $CHBr_3$ is first concentrated in the brine, and then more is released by the diatoms under conditions experienced in the sea ice brine. Production is independent of temperature for *Porosira Glacialis* in Tedlar bag experiment 2, and $CHBr_3$ is not produced by either *Fragilariopsis* species in experiments 2 and 3. Maximum concentrations of up to 2000 pM were measured in the low temperature bags, and up to 7575 pM upon freezing to -15°C when brine volume is 6.1%. Results from the first Rothera experiment show an increase in $CHBr_3$ concentration in both frozen bags (filtered and unfiltered) suggesting no increase in production due to the diatoms under brine conditions for the naturally occurring Antarctic ice algae community. High production rates are seen in Rothera experiment 2, with the maximum rate of 27 pM hour^{-1} in the ambient bags which showed a

greater increase in concentration than the frozen bags, despite the solvent volume reduction in the latter. Maximum $CHBr_3$ concentrations in the Rothera experiments were 820 pM. $CHBr_3$ production by *Porosira Glacialis* is well documented, *Tokarczyk and Moore* [1994] recorded concentrations of up to 990 pM, though their experiments ran over several weeks, and *Moore et al.* [1996] recorded concentrations of up to 1400 pM. $CHBr_3$ production by naturally occurring communities at Rothera has previously been demonstrated as part of the RaTS data project [*Hughes et al.*, 2009]. The highest concentration of $CHBr_3$ measured in Arctic ice was 1451 pM when normalised to liquid water content [*Sturges et al.*, 1997]; Our results for the low temperature samples in experiment 2 are in good agreement with previous measurements.

CH_2ICl concentrations are high (up to 37 pM) at -15°C in experiment 1, well in excess of obvious loss processes observed in the other two bags. Low production is observed by *Porosira Glacialis* in the second experiment at -5°C, whereas no production is observed for *Fragilariopsis Cylindrus*. *Fragilariopsis sp.* show production of CH_2ICl, both at -5°C and 4°C, more so at the lower temperature. Whilst concentrations in the first Rothera experiment increase in both frozen bags, the unfiltered assemblages show a larger concentration increase, suggesting some increase due to the diatoms. Maximum production rates were recorded in Rothera experiment 1, of 0.23 pM hour^{-1}. CH_2ICl concentrations are high compared to field measurements where concentrations are up to 3 pM [*Chuck et al.*, 2005] but lower than those measured in the laboratory by *Moore et al.* [1996]) (up to 200 pM).

2-C_3H_7I concentrations are higher in cultures of *Porosira Glacialis* at low temperature (-15°C) in Tedlar bag experiment 1, though concentrations are very small. 2-C_3H_7I production was not observed above the limit of detection in any of the other experiments at UEA. In the first Rothera experiment, the concentrations in the low temperature bags do not differ between the unfiltered and filtered control. However, in the second Rothera experiment 2-C_3H_7I production was observed independent of temperature in a naturally occurring Antarctic ice algae community, with an average production rate of 0.003 pM hour^{-1} leading to a maximum concentration of 0.88 pM, much lower than field measurements of 7 pM in Weddell Sea ice brine [*Fogelqvist and Tanhua*, 1995].

CH$_2$I$_2$ concentrations show large errors in the frozen bag containing *Porosira Glacialis* in experiment 1, though concentrations are higher (up to 19 pM) than in the ambient bag and the filtered control, where some loss is seen. *Porosira Glacialis* also shows a higher production of CH$_2$I$_2$ at low temperatures in Tedlar bag experiment 2; *Fragilariopsis Cylindrus* shows no production over time though concentrations are higher in the low temperature bags. *Fragilariopsis sp.* shows no production of CH$_2$I$_2$. In the first Rothera experiment, a loss is observed in the ambient bag, no production is seen in the filtered bag but there is some production of CH$_2$I$_2$ in the frozen bag containing assemblage J. However, when assemblage K was used in the second experiment, CH$_2$I$_2$ production was observed at both temperatures. This is the first report of CH$_2$I$_2$ production by an Antarctic ice algae community, with average production rates of 0.016 pM hour^{-1} for both assemblages J and K. Any processes which lead to increased production of this highly labile compound are of interest to atmospheric chemists seeking to understand the release of reactive iodine. CH$_2$I$_2$ concentrations of 4.2 pM (1.7 – 8.2 pM) have been recorded in Antarctic waters [*Carpenter et al.*, 2007], of a similar magnitude to concentrations measured during these experiments.

CH$_2$IBr concentrations are higher in cultures of *Porosira Glacialis* at low temperature (-15°C) in experiment 1, though the much larger increase from 24 to 48 hours than in the first 24 hours of the experiment suggest CH$_2$IBr is first concentrated in the brine, and further production occurs when the diatoms are subject to the extreme conditions in the brine channels. The average increase in CH$_2$IBr concentration between 24 and 48 hours was 0.46 pM hour^{-1} leading to a maximum concentration of 14.3±4.1 pM. In experiment 2, low production was observed at -3 °C, there is a significant increase at -5 °C, which then stops at 4 °C. However, some production is observed in the ambient bag at 4 °C, which suggests the different light intensities of the two incubators may have an effect on production, or production may have stopped in the low temperature bags due to the diatoms coming towards the end of their exponential growth phase. Results from the Rothera experiments are interesting, showing increased concentrations of CH$_2$IBr when both assemblages J and K are frozen. CH$_2$IBr is a labile compound and, as with CH$_2$I$_2$, is of particular interest in the study of the volatilisation of iodine. The concentrations measured here are in excess of those measured by Carpenter et al (2007) in Antarctic waters of 0.8

pM (range 0.2–1.4 pM), but in good agreement with high concentrations in Arctic sea ice (up to 33 pM) measured by this group (paper in preparation).

CHBr$_2$Cl concentrations show an enhancement in the low temperature (-15°C) bags containing *Porosira Glacialis* in experiment 1, well in excess of observed loss in the filtered control. Concentrations were high (63 – 188 pM) but did not change significantly over time in any sample bags at any temperature in experiments 2 and 3, except due to brine volume reduction where concentrations reached 1178 pM. In the Rothera experiments, a concentration effect due to brine volume reduction was observed as expected in the first experiment, but the results for the second experiment are interesting – production of CHBr$_2$Cl is observed independent of temperature in a naturally occurring Antarctic ice algae community, at an average rate of 0.48 pM hour^{-1}. *Tokarczyk and Moore* [1994] noted extremely low production of CHBr$_2$Cl in their study of halocarbon production by *Porosira Glacialis*, and to our knowledge no other reports of its production exist.

1-C$_3$H$_7$I concentrations show a similar pattern to C$_2$H$_5$I concentrations – higher in the low temperature bags containing *Porosira Glacialis* in experiment 1 with a further increase after 24 hours, due to the diatoms under brine channel conditions. In experiment 2 some loss, possibly to the walls of the bag, is observed in all bags containing *Porosira Glacialis*, production is then observed at low temperature for 3 days, though concentrations are low, followed by some loss. In the Ambient bag, concentrations increase upon freezing to 0.42 pM at -15°C but then remain high upon ice melt, possibly due to cell lysis and compound release. No production of 1-C$_3$H$_7$I is observed from either *Fragilariopsis* species in experiments 2 and 3, and the only increase in concentrations in the Rothera experiments is due to the concentration effect of brine volume reduction, which resulted in maximum 1-C$_3$H$_7$I concentrations of up to 1.3 pM. These concentrations are much lower than field measurements of 217 - 259 pM in Weddell Sea ice brine [*Fogelqvist and Tanhua*, 1995].

CH$_2$Br$_2$ concentrations show a similar pattern to CHBr$_3$, though concentrations are an order of magnitude lower. CH$_2$Br$_2$ concentrations are higher in cultures of *Porosira Glacialis* at low temperature (-15°C) in experiment 1, though this could be due to the concentration effect. Production is independent of temperature for *Porosira Glacialis* in experiment 2 where average change in concentration over time of 0.86 pM hour^{-1} leads to maximum concentrations of 224 pM. CH$_2$Br$_2$ is not produced by either

Fragilariopsis species in experiments 2 and 3. Results from Rothera experiment 1 show an increase in concentration in both frozen bags (filtered and unfiltered) suggesting no increase in production due to the diatoms under extreme conditions in brine channels for the naturally occurring Antarctic ice algae community assemblage J. Assemblage K show CH_2Br_2 production independent of temperature an average rate of 0.2 pM hour^{-1}. These results are in reasonable agreement with those of *Tokarczyk and Moore* [1994] who measured CH_2Br_2 concentrations of up to 350 pM in *Porosira Glacialis* cultures, though less than those of *Moore et al.* [1996] who measured concentrations of up to 1600 pM, albeit over a longer experimental timescale.

3.5. Conclusions

Of particular interest to this study are the labile iodocarbons which are broken down rapidly by solar radiation to yield iodine radicals. The lifetimes for the most reactive iodocarbons on the Antarctic Peninsula at noon in summer are approximately 20 hours for CH_2ICl, a few hours for CH_2IBr and 20 minutes for CH_2I_2. These compounds can yield substantial amounts of reactive iodine, the longer-lived iodocarbons such as CH_3I cannot sustain a significant amount of iodine during their photolysis as the radical lifetime is limited by deposition to the surface or within aerosol on a shorter timescale. The potential for these reactive iodine species to be enhanced in concentration under sea ice conditions has been demonstrated.

Antarctic sea ice grows and recedes over an area of approximately 15×10^6 km^2 every year [*Cavalieri et al.*, 1999]. The halocarbons in this water are concentrated in the sea ice brine during ice formation, and the concentration effect may play a role in the transport of these compounds from the ocean to the atmosphere. Where phytoplankton communities are present in the water, this effect may be further enhanced by increased halocarbon production by the algae under the extreme conditions in the brine channels. To estimate the global contribution from such processes is beyond the scope of this thesis. However it has been demonstrated that both the concentration effect and increased halocarbon production by sea ice algae play a role in concentrating halocarbons in sea ice brine. More work is needed to understand fully the processes which lead to halocarbon release from sea ice.

When monitoring halocarbon concentrations in seawater containing diatoms, bromocarbon production rates were observed to be mostly independent of

temperature; increases in concentration at very low temperatures may be due to the concentration effect of brine volume reduction during sea ice formation.

CH_3I concentrations at low temperature were lower than those expected via the concentration effect; the enhancement which did occur was less than that of the other iodocarbons. This may be due to nucleophilic attack by Cl^-, the rate of which increases with salinity. C_2H_5I concentrations consistently increased upon ice melt, abiotic reactions could be occurring, but release of this compound from the material of the bag is also possible. The more reactive iodocarbons, CH_2ICl, CH_2I_2, CH_2IBr, 1- and 2-C_3H_7I all showed the potential to be produced in larger quantities under sea ice conditions, exceeding concentrations expected via the concentration effect.

CH_2ICl production increased under frozen conditions in the naturally occurring Antarctic communities, concentrations of CH_2I_2 and CH_2IBr increased in both *Porosira Glacialis* cultures and the naturally occurring community on the Antarctic Peninsula, whereas 1- and 2-C_3H_7I production only increased in *Porosira Glacialis* cultures.

3.6 Summary

It has been demonstrated that

- *Porosira Glacialis*, which is a relatively large diatom, does not survive when frozen in a seawater medium to -15°C.
- The much smaller *Fragilariopsis Cylindrus* is more easily incorporated into the brine channel network when seawater freezes, and though the photosynthetic efficiency is greatly reduced at -15°C, the diatom recovers upon ice melt.
- Both the increase in halocarbon production by diatoms under sea ice conditions and the concentration effect of solvent volume reduction provide a mechanism by which halocarbons may become concentrated in sea ice brine.
- Iodocarbons in seawater have the potential to be enhanced in concentration under sea ice conditions.
- Bromocarbons become less concentrated than iodocarbons in sea ice brine.
- Trends can be seen between concentrations of mono- and poly-halogenated organics, which can be traced back to their production by different classes of enzyme.
- C_2H_5I is released after ice melt, though this may be due to emissions from the sampling bags

The increase is iodocarbon concentrations in the sea ice brine may be due to increased production by diatoms under stressful conditions as they utilise iodide in this extreme environment. Concentrations may also become enhanced in the seawater medium when the diatom frustules break open upon cell death, and intracellular compounds are released.

These findings are important in understanding how the concentrations of iodine compounds are enhanced in sea ice brine channels. The measurements made on sea ice collected from Ryder Bay on the Western Antarctic Peninsula showed enhanced concentrations of iodocarbons, but not bromocarbons, in the brine. When the sea ice is porous enough to allow these compounds to escape, this provides a mechanism by which iodine may be enhanced in the atmosphere above sea ice.

Chapter 4. Production of Halocarbons by Polar Diatoms Subject to Salinity Stress

4.1 Introduction

Chapter 3 investigated halocarbon emissions during the freezing of a seawater medium containing diatoms; this chapter explores what factors of the freezing process may be responsible for a change in halocarbon concentrations. Cultures of the same three species of diatom used in chapter 3, *Porosira Glacialis, Fragilariopsis Cylindrus* and *Fragilariopsis sp.*, were used. These diatoms were placed under conditions of varying salinities, iodide and bromide concentrations, and halocarbon concentrations were monitored. Similar experiments were once again carried out carried out on a naturally occurring Antarctic ice algae community on the Antarctic Peninsula.

4.2. Materials and methods

Stocks of the cultured diatoms, *Porosira Glacialis, Fragilariopsis Cylindrus* and *Fragilariopsis sp.*, were grown in an incubator at 4°C and light intensity of 85 µphoton m^{-2} s^{-1} (measured in a flask of distilled water at the bench level) on a 12 hour light cycle, in the F/2 medium detailed in section 3.2, in 1 litre glass conical flasks. Seawater collected from the Weddell Sea was used, which was filtered and autoclaved before use. Axenic conditions were maintained during sample preparation, and all glassware was also autoclaved.

The Antarctic ice algae community (Rothera experiments) were grown in 3 litre glass conical flasks in flowing seawater tanks outside as detailed in section 3.2.4.

In order to prepare the samples used for the experiment, 25 ml diatom rich seawater (DRS) was added to a 50 ml culture tube containing 25 ml pre-purged distilled water (PPDW) or 25ml pre-purged seawater (PPSW) + a known quantity of baked NaCl (NaCl (Sigma Aldrich), baked in furnace to remove any organic material, at 300°C in pre-weighed (to ±0.01g precision) foil packages) + KI (Sigma Aldrich) or KBr (Sigma Aldrich) where relevant. The tubes were filled completely without a headspace to ensure trace gases remained in solution, and returned to the incubator.

After the appropriate time had elapsed, 40 ml of the solution was drawn into a gas tight syringe via a piece of Tygon tubing placed at the bottom of the culture tube to

avoid sampling water which had chance to de-gas when the tube was opened. This 40 ml sample was then injected through a 25 mm Whatman GF/F filter paper, held in a gas tight plastic filter paper holder, directly into the purge tube at the start of the GCMS analysis set up as described in section 2.1.2. The liquid nitrogen method of trapping was used in experiments involving *Porosira Glacialis, Fragilariopsis Cylindrus* and *Fragilariopsis sp.*, whereas the Markes system was used in the Rothera experiments. The remaining 10 ml DRS in the culture tube was immediately used for physiological measurements: cell volume, cell density and photosynthetic efficiency as detailed in section 3.2, except at Rothera where this was not possible. Three tubes were used for each control unless otherwise stated.

4.3. Experimental description and hypotheses

4.3.1 Experiments using *Porosira Glacialis*

During sea ice formation, diatoms in the ocean are incorporated into brine channels within the ice, experiencing salinity stress as the temperature drops and the brine becomes more concentrated. This results in increased concentrations of bromide and iodide. The following experiments subjected diatoms to variations in these conditions, and were carried out consecutively on sub cultures from the same stock of *Porosira Glacialis.* The experiments are summarised in table 7 and described in more detail below

Experiment 1 was designed to study the effect on halocarbon production of increasing salinity (35‰ to 65‰, from average seawater salinity to the maximum salinity of natural diatom habitats [*Grant and Horner*, 1976]). Experiment 2 was a repeat of experiment 1, but at high iodide concentrations, as the assumption is made that iodide is being accumulated in some way. If microalgae are capable of accumulating iodide in the same way macroalgae have been shown to [*Küpper et al.*, 1998] then iodide concentrations in brine channels could be 30 000 times that in the underlying seawater, and could reach 10^{-3}M, which is the high iodide value used in this experiment.

Experiments 3 and 4 were tests designed to ensure these results were comparable: changing salinity and iodide in the same experiment, both with a salinity which caused the diatoms to be stressed (65‰), and another which was so extreme that

cell lysis (rupture) occurred (85‰), respectively. Experiment 3 also investigated the effect of low salinity stress.

Experiment 5 varied bromide concentrations, which allows an insight into competition between the halogens for the enzyme active site. Following these extreme scenarios, experiment 6 used more reasonable levels of salinity (25‰ – 45‰) and iodide (10^{-5} M to 10^{-4}M) to be more representative of the natural environment.

4.3.2 Experiments using *Fragilariopsis Cylindrus* and *Fragilariopsis sp.*

Fragilariopsis Cylindrus, a Weddell Sea ice diatom, was subject to conditions of varying salinity, bromide and iodide concentration, to ascertain whether this species, which had not previously been known to produce halocarbons, could be encouraged to do so under the stressful conditions they may find in sea ice brine channels. One set of samples was held at ambient concentrations, one was subjected to high salinity (55‰), one to high salinity and high bromide (2400 μM) and another to high salinity and high iodide (10^{-4}).

A second Fragilariopsis species, *Fragilariopsis sp.,* collected from the Antarctic Peninsula in 2008, was checked for halocarbon production, and subjected to varying bromide concentrations (400 – 2400 μM) as bromocarbon production has been recorded in this area associated with ice melt [*Hughes et al.*, 2009].

Further experiments were not carried out with either *Fragilariopsis* species, following affirmation that neither species was of particular interest with respect to halocarbon production.

4.3.3 Experiments using a naturally occurring Antarctic ice algae community

During the austral summer of 2009/2010, similar experiments were carried out on algae collected from pieces of sea ice found in Ryder Bay, shown in figure 6. Details of the collection and growth of the diatom assemblages are identical to that described in section 3.2.4; only assemblage J was used. The assemblage was subjected to conditions of high salinity and high iodide concentrations, and halocarbon concentrations were monitored. The purpose of these experiments was to ascertain whether a natural community, not previously known to produce iodocarbons, could be encouraged to under sea ice conditions.

4.4. Results from experiments using *Porosira Glacialis*

Table 7 gives an overview of six experiments aimed at elucidating which conditions associated with sea ice may affect halocarbon production by *Porosira Glacialis* and a brief introduction to which compounds were affected by the changes.

Exp	Hypothesis	Compounds affected by changing experimental conditions
1	Increasing salinity increases halocarbon production	$CHBr_3$, CH_2IBr and CH_2Br_2 production suppressed by increasing salinity
2	Increasing salinity at high I^- concentration increases iodocarbon production	CH_3I, C_2H_5I and $1-C_3H_7I$ production enhanced by increasing salinity, CH_2I_2 and CH_2IBr production suppressed. $2-C_3H_7I$ production is independent of salinity. Bromocarbon production is now not observed
3	Low salinity stress may also increase iodocarbon production at high I^-	CH_3I, C_2H_5I, and $2-C_3H_7I$ production increases with high or low salinity stress
4	Cell lysis at high salinity and high I^- releases halocarbons	CH_3I, C_2H_5I, $1-C_3H_7I$ and CH_2IBr concentrations increase upon cell lysis. CH_2I_2 and CH_2ICl production observed at high I^- regardless of cell lysis
5	Bromocarbon production is affected by Br^- concentrations	No significant change in halocarbon production observed
6	Less extreme salinity, iodide and bromide concentration changes influence halocarbon production	CH_3I, C_2H_5I, $2-C_3H_7I$ and $1-C_3H_7I$ production is highest when iodide concentrations are high; and all except CH_3I increase with increasing salinity. Varying bromide concentration does not affect halocarbon production.

Table 7. Summary of all experiments using *Porosira Glacialis*

4.4.1 Physiological measurements

Cell numbers were monitored as the cultures were being grown up, and the diatoms were in their exponential growth phase before each experiment commenced. The F_v/F_m ratio obtained via fluorometry (section 3.2) was used as an indication of the photosynthetic efficiency of the diatoms, which is in turn an indication of their health. During exponential growth when the diatom stocks are at their most healthy, typical F_v/F_m ratios for *Porosira Glacialis* are between 0.5 and 0.65. Before each experiment reported in this study commenced, the photosynthetic efficiency of the *Porosira Glacialis* was above $F_v/F_m = 0.53$, and cell densities were between 2100 ± 210 and 5500 ± 550 cells ml^{-1}. Production rates have been corrected for this variation in cell density by taking the total average of cell numbers during the experimental period.

Physiological measurements enable us to understand how diatoms cope with the extreme conditions in the brine channels. For example, in experiment 1, at a salinity of 35‰ and 45‰ the photosynthetic efficiency of the *Porosira Glacialis* is not adversely affected (figure 27). At 55‰ an effect due is seen - the photosynthetic efficiency of the diatoms is adversely affected by the increase in salinity, but recovery is swift as the diatoms adapt to their environment within a few hours (the F_v/F_m ratio increased from 0.21 to 0.35 within the experimental sampling time between the triplicate samples, data not shown). However at 65‰ recovery from the salinity stress is not observed within the timescale of the experiment.

Cell volume measurements allow an insight into the effect on the cell size of the experimental conditions. For example in experiment 2, cell volume can be seen to decrease during the experiment with increasing salinity (figure 28). Figure 29 clearly shows the cell lysis which occurred in experiment 4 at high salinity (85‰), as cell volume halved. Split diatom frustules were also observed under the microscope.

Experiment 5, in which bromide concentrations were varied, gave unexpected results for diatom photosynthetic efficiency – though the salinity was held at 55‰, the F_v/F_m of the *Porosira Glacialis* was very variable, and decreased in all controls (figure 30). Whether this was due to the addition of the bromide is unclear.

In experiments 6 and 7, where salinities were altered by a small amount, neither the cell volume nor growth rate was altered by the change in experimental conditions, and the F_v/F_m values were not different between samples (data not shown).
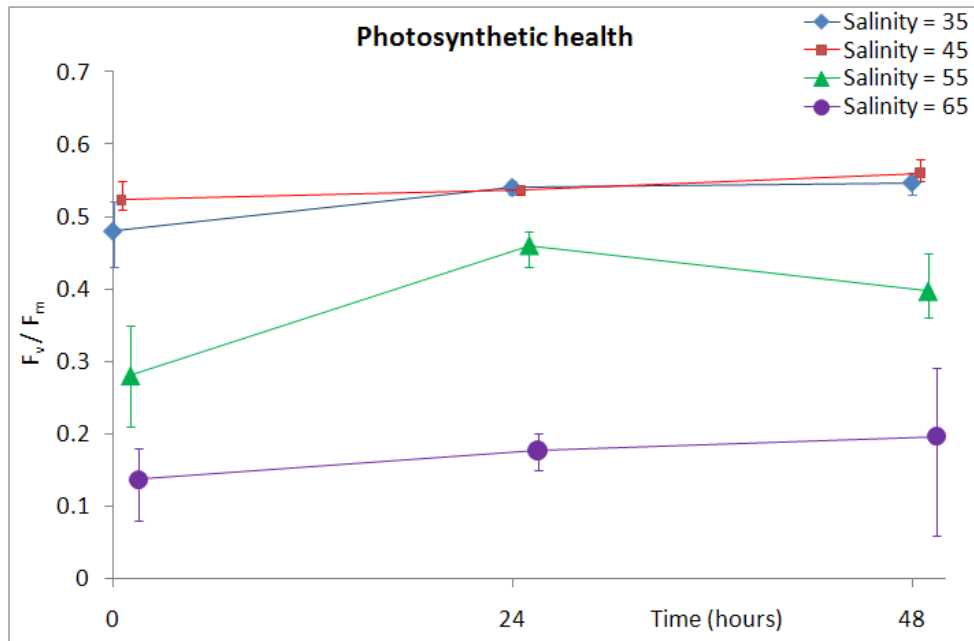
Figure 27. Photosynthetic efficiency of *Porosira Glacialis* in experiment 1. A decrease in photosynthetic efficiency is observed at higher salinity. The average and range of triplicate samples at each time is shown.
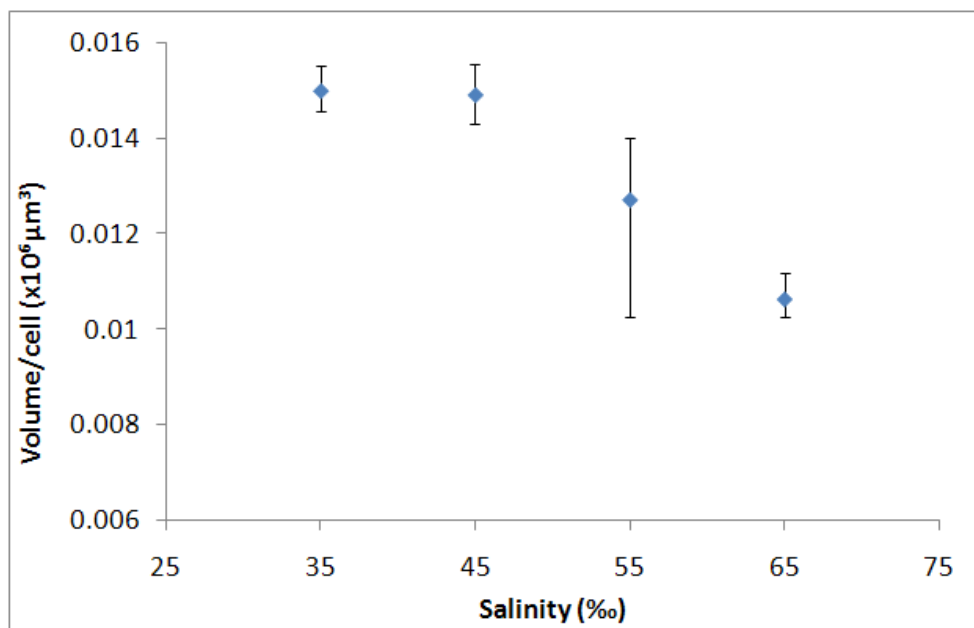
Figure 28. *Porosira Glacialis* cell volume after 48 hours in experiment 2. The average and range of triplicate samples is shown.
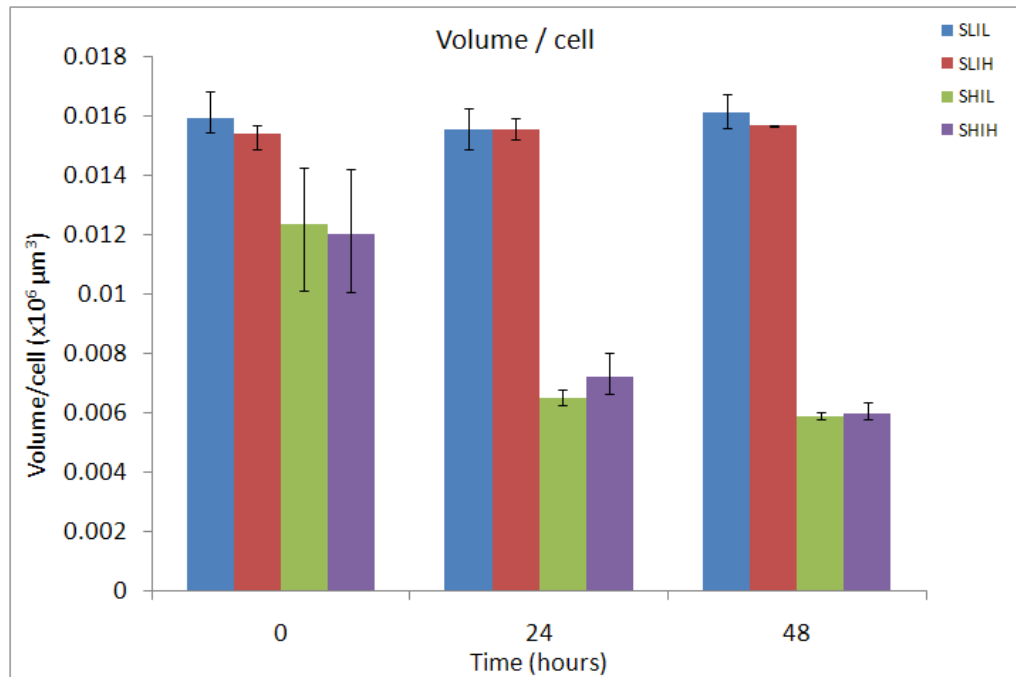
Figure 29. Cell volume of *Porosira Glacialis* in experiment 4, where S = salinity, L = low, I = iodide concentration and H = high. The average and range of triplicate samples at each time is shown.
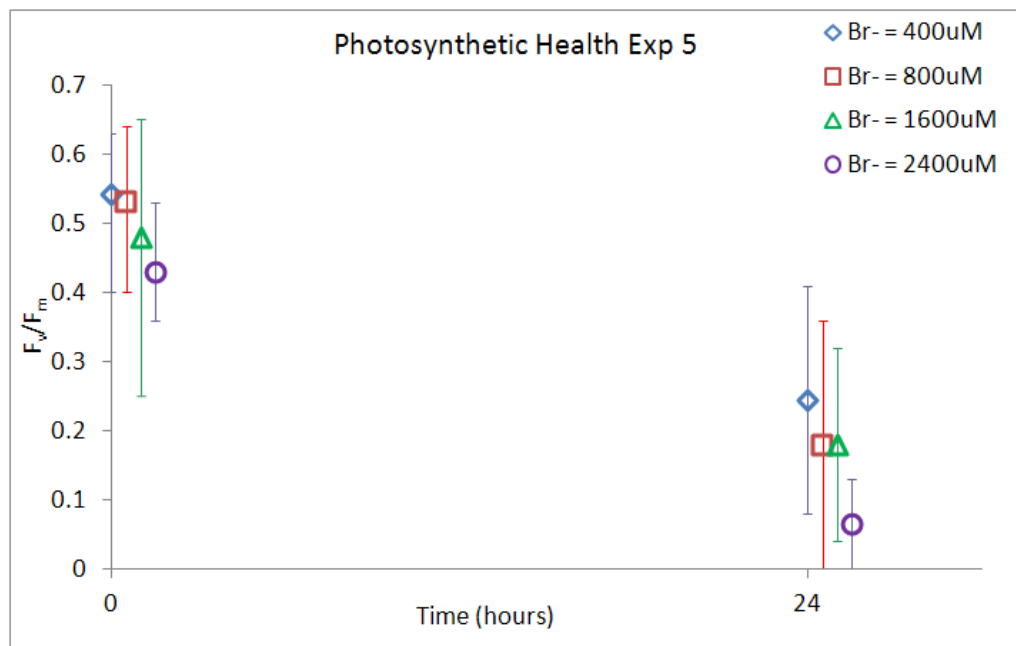
Figure 30. Photosynthetic efficiency of *Porosira Glacialis* shows a dramatic decrease during the first 24 hours of experiment 5 in all controls, where S = salinity, L = low, I = iodide concentration and H = high. The average and range of triplicate samples at each time is shown.

4.4.2 Halocarbon measurements

During the exponential growth phase of *Porosira Glacialis* cultures, before these experiments were started and when the diatoms were not stressed in any way, average production of $CHBr_3$, CH_2ICl, CH_2IBr, $CHBr_2Cl$ and CH_2Br_2 was 1755, 0.025, 0.075, 0.675 and 0.6 x 10^{-9} pmol cell^{-1} hour^{-1} respectively. Production of the other halocarbons was not observed.

Several blanks were prepared during the experimental period, made up of PPSW, PPDW, and a mixture of the two. F/2 nutrients were added, as were NaCl, KI and KBr, as per experimental conditions. Tubes were analysed after incubation for 0, 24 and 48 hours. No significant change in halocarbon concentrations was observed in any of the blank samples.

In the results presented below, halocarbon concentrations were measured at 0, 24 and 48 hours after diatoms were subjected to the stresses they may experience in sea ice brine channels, as listed in table 7. Production rates have then been calculated using data at 0 and 48 hours, with the full range of possible changes in concentration represented (maximum concentration at 0 hours deducted from minimum concentration at 48 hours and vice versa). Average cell numbers during the experiment were used to calculate a production rate per cell.

An alternative method is to calculate a halocarbon concentration per cell at both 0 and 48 hours, and divide by time to determine a production rate, however this method leads to negative production rates in most samples, as diatom growth rates far exceed halocarbon production rates, and thus the data is distorted. Where negative production rates are shown with the method chosen, this reflects an overall loss of halocarbon concentrations in the sample tubes during the experiment. This could be due to bacterial consumption as has been observed in culture experiments involving diatoms (Claire Hughes, private communication).

Experiment 1

When a salinity of 35‰ was maintained (figure 31), *Porosira Glacialis* produced CH_2IBr, $CHBr_3$ and CH_2Br_2. Production of these compounds was slightly suppressed when salinity was increased to 45‰, and the data was much more spread. When the salinity was increased further, production stopped. From the spread of data at 45‰ it looks as though a tipping point in the system responsible for production of CH_2IBr,

CHBr$_3$ and CH$_2$Br$_2$ was reached at this point. As enzymatic production of halocarbons has previously been demonstrated in work by other groups [*Manley*, 2002; *Moore et al.*, 1996], it is likely that the salinity stress caused denaturing of these enzymes.

When CH$_2$Br$_2$ and CH$_2$IBr concentrations are studied (figure 31), it can be seen that at higher salinities, initial (though reduced) production is seen during the first 24 hours of the experiment, after which loss processes dominate. This may represent a gradual shutting down of the anti-oxidative enzymatic systems responsible for halocarbon production [*Manley*, 2002].

Significant production of other halocarbons was not observed. Results from experiment 1 would suggest a decrease in production of CHBr$_3$, CH$_2$Br$_2$ and CH$_2$IBr in saline brine channels in sea ice.
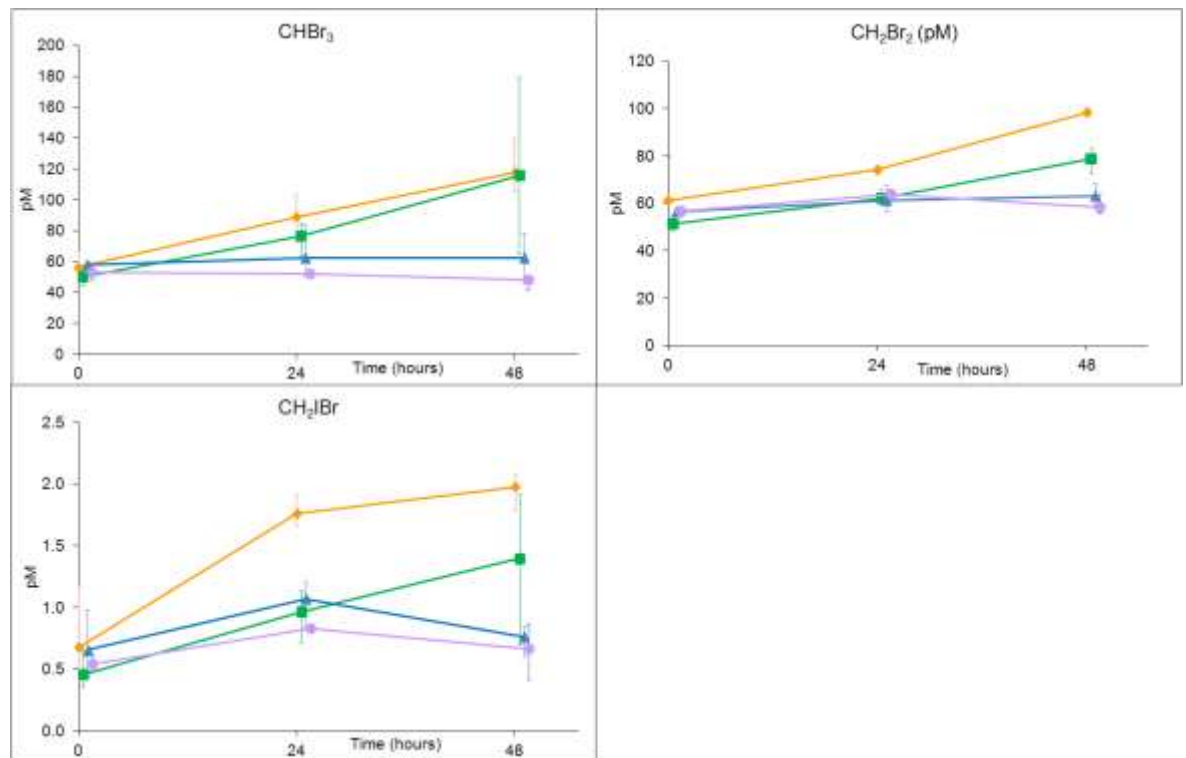
Figure 31. Concentrations of CHBr$_3$, CH$_2$IBr and CH$_2$Br$_2$ in seawater containing *Porosira Glacialis* in experiment 1 under conditions of ◆ S = 35‰, ■ S = 45‰, ▲ S = 55‰ and ● S = 65‰. The average and range of triplicate samples at each time is shown. Concentrations of other halocarbons were not affected (data not shown).
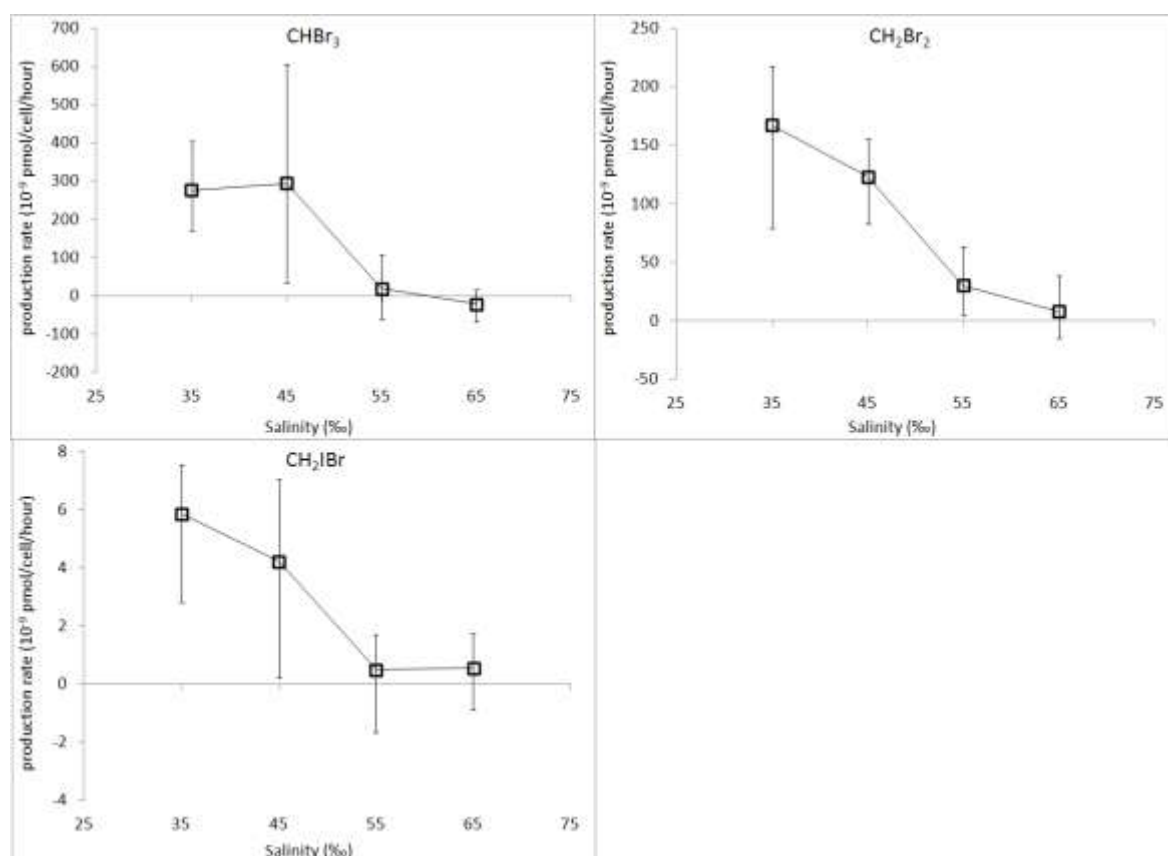
Figure 32. Production rates of CHBr$_3$, CH$_2$Br$_2$ and CH$_2$IBr by *Porosira Glacialis* in experiment 1, deduced from halocarbon production between 0 and 48 hours from data as shown in figure 31. Production rates of other halocarbons were not affected (data not shown).

Experiment 2

Experiment 2 is a repeat of experiment 1 but with an artificially high iodide concentration (10^{-3}M). It would appear that production of the bromocarbons is suppressed due to the addition of the iodide, as no significant production of CHBr$_3$, CH$_2$Br$_2$ and CHBr$_2$Cl is observed in any of the samples (data not shown). Production of some iodocarbons is however now observed (figures 33 and 34). CH$_3$I and 2-C$_3$H$_7$I are produced, but rates are unaffected by the change in salinity. Production of CH$_2$I$_2$ and CH$_2$IBr, the most reactive of the iodocarbons, is highest when salinity is 35‰, then decreases with increasing salinity. Production of C$_2$H$_5$I and 1-C$_3$H$_7$I is increased with increasing salinity, at these high iodide concentrations.

Agreement between the triplicate samples (error bars in figure 34) is good except in the S = 55‰ samples after 48 hours for CH$_3$I and C$_2$H$_5$I. This may represent a tipping point in the system responsible for production of these compounds being reached at this salinity. As discussed previously, this may be due to denaturing of enzymes.

Once again, changes in concentrations of some compounds (CH_2I_2, CH_2IBr and 2-C_3H_7I, figure 33) are time dependent – a slight increase in concentration occurs during the first day of the experiment but then loss processes dominate as production stops due to the stresses imposed by the experimental controls.
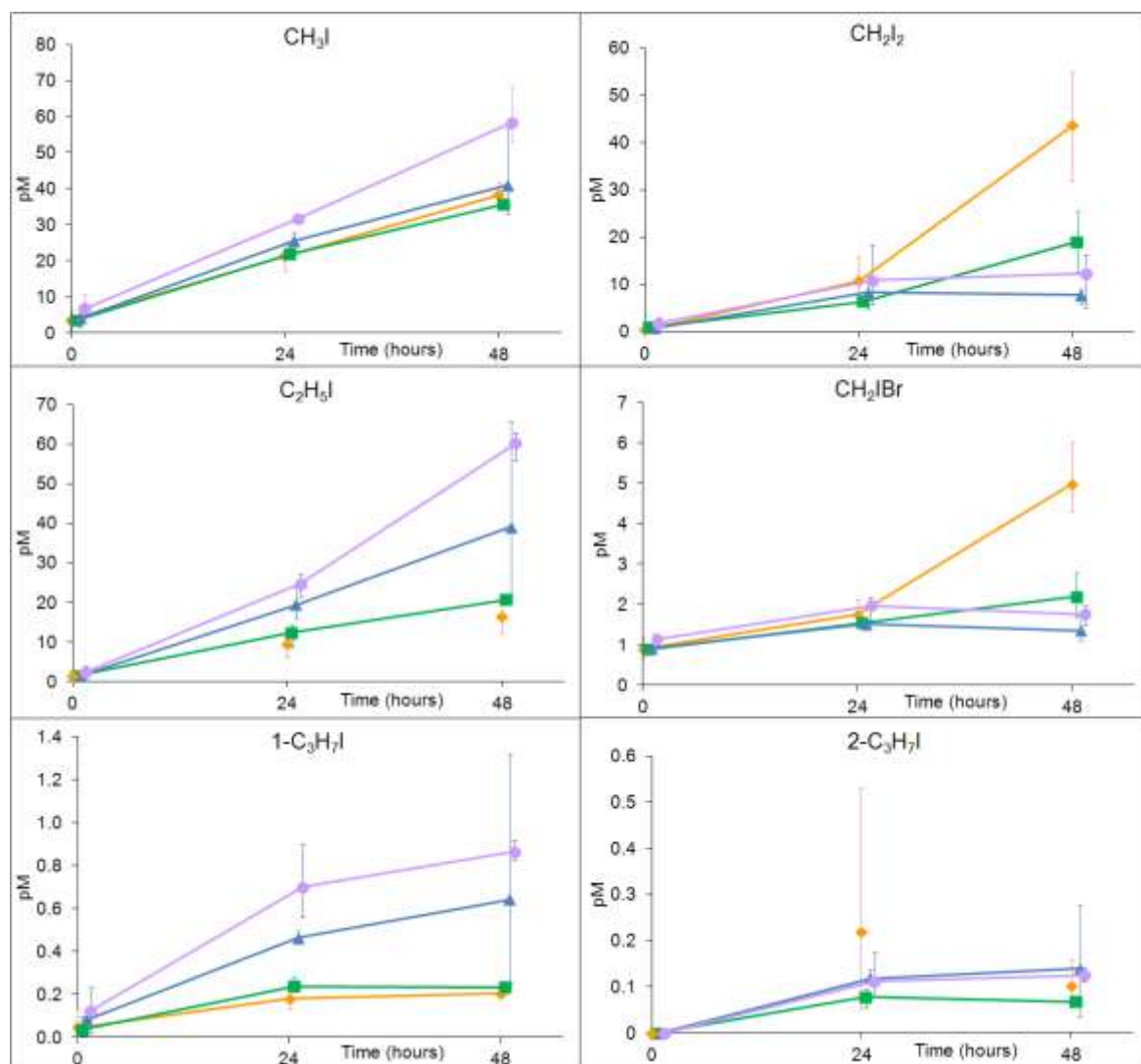
Figure 33. Concentrations of CH_3I, C_2H_5I, $1-C_3H_7I$, CH_2I_2, CH_2IBr and $1-C_3H_7I$ in seawater containing *Porosira Glacialis* in experiment 2, under conditions of high iodide concentration and ◆ S = 35 ‰, ■ S = 45 ‰, ▲ S = 55 ‰ and ● S = 65 ‰. The average and range of triplicate samples at each time is shown. Concentrations of other halocarbons were not affected (data not shown).

The different production pathways of the mono- and poly-halogenated compounds can be seen by the different responses of the two types of enzymes. The haloperoxidases, assumed to be responsible for production of polyhalocarbons [*Manley*, 2002; *Moore*, 2003], appear to utilise the additional iodide, however polyhalocarbon production is suppressed with increasing salinity. Methyl

transferases, responsible for monohalogen production, also utilise the additional iodide and high production rates are seen at ambient or slightly enhanced salinities.

The production of iodocarbons by diatoms, when iodide is available, is important in understanding how iodocarbon concentrations come to be enhanced in sea ice brine channels. Furthermore, the increase in production of C_2H_5I and $1\text{-}C_3H_7I$ when *Porosira Glacialis* is salinity stressed is an important result, and implies monoiodocarbon concentrations would be enhanced under conditions found in sea ice brine channels.
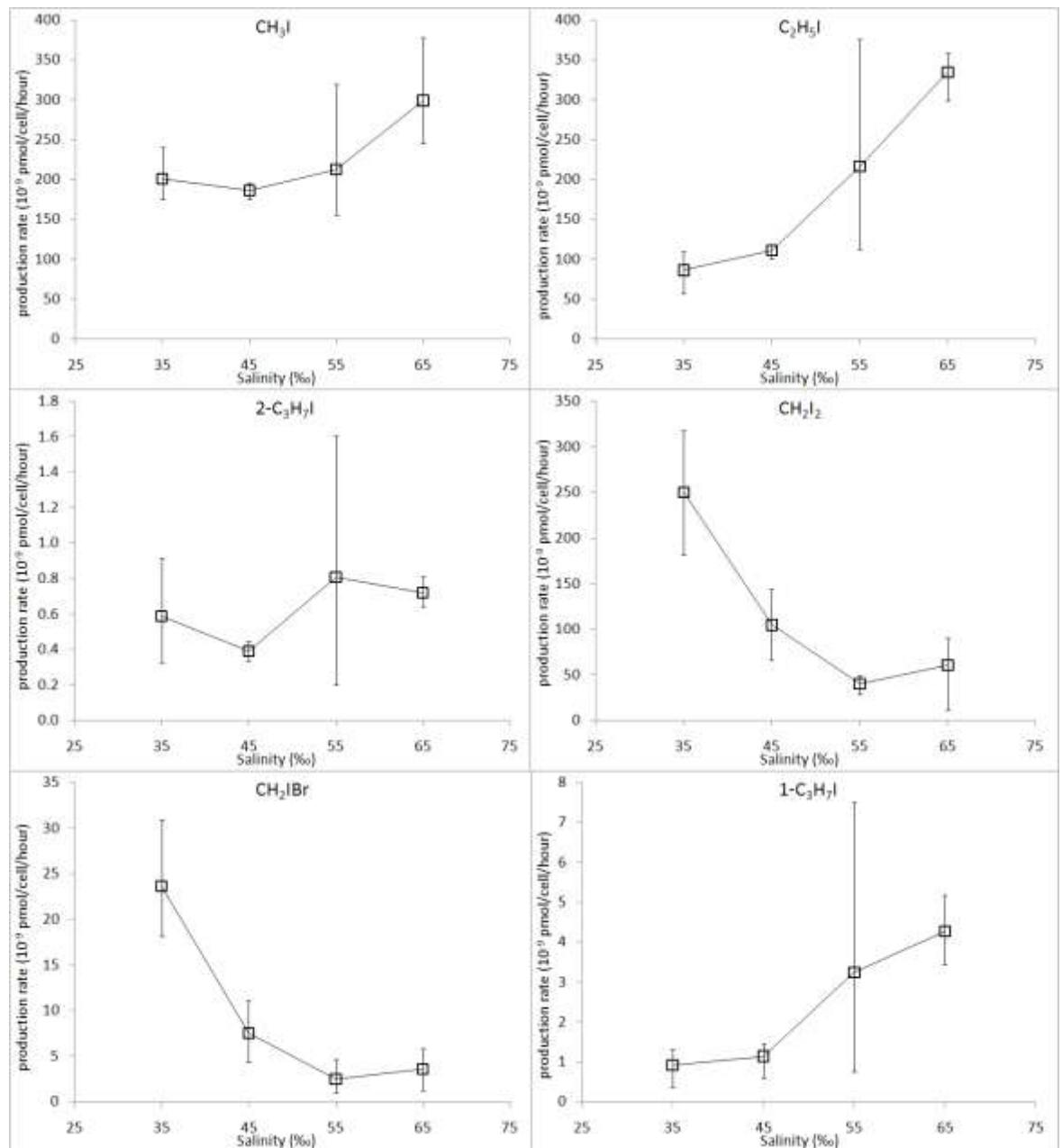
Figure 34. Production rates of halocarbons by *Porosira Glacialis* in experiment 2, deduced from the total change in concentration of halocarbons over 48 hours, with error bars representing maximum and minimum possible changes in concentration.

Experiment 3

The conditions in experiment 3 were designed to represent the environment diatoms may experience during ice melt (low salinity as the brine channels are infiltrated with fresh melt water, then a return to ambient seawater concentrations) and ice formation, allowing an insight into halocarbon production during the melting and freezing of sea ice.

Porosira Glacialis were used; One sample set was first subjected to a low salinity (17.5‰) for 2 hours; NaCl was then added to return the salinity to 35‰. In the second set of samples the salinity was increased to 65‰. High and low iodide concentrations were used for both salinity conditions.

Interestingly, the low salinity and high iodide samples produce the largest amounts of all mono-iodocarbons, showing it is stress and the presence of iodide which results in higher production of these compounds, as opposed to simply the increase in salinity. The production of bromocarbons was suppressed in all samples with an increase in either iodide concentration or salinity. $CHBr_3$ and $CHBr_2Cl$ concentrations were highest at lowest iodide (data not shown), again showing that bromocarbon production is suppressed at higher iodide concentrations and high salinity.
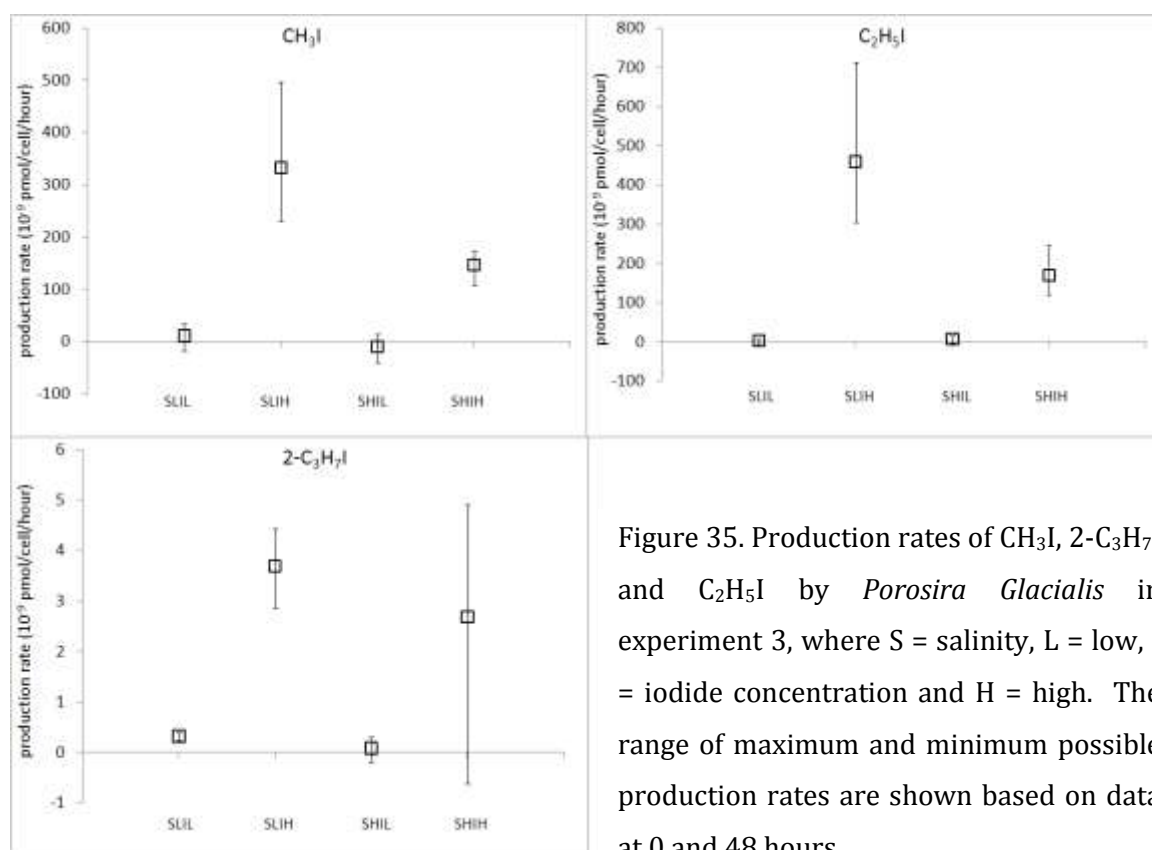
Figure 35. Production rates of CH_3I, $2\text{-}C_3H_7I$ and C_2H_5I by *Porosira Glacialis* in experiment 3, where S = salinity, L = low, I = iodide concentration and H = high. The range of maximum and minimum possible production rates are shown based on data at 0 and 48 hours.

Experiment 4

Questions which have yet to be answered involve the production routes of the different compounds, whether the enzymes are intra- or extra-cellular, and how the stress to, or health of, the diatoms affects production.

An extreme salinity of 85‰ salinity was used in experiment 4 to break open all the diatom frustules, the resultant F_v/F_m was <0.1, confirming cell death. Cell lysis occurred at high salinity in this experiment (figure 29) and broken frustules were also observed under the microscope.

High concentrations of CH_3I, C_2H_5I, $1-C_3H_7I$, and CH_2IBr were observed at high salinity and high iodide concentration (figures 36 and 37). The spread of data is large for the other halocarbon compounds and, although the tendency is for higher concentrations at high iodide, the difference is not significant.

Once again in this experiment the responses of the different types of enzyme can be seen clearly. Methyl transferase produces CH_3I, C_2H_5I, and $1-C_3H_7I$ when salinity and iodide are both high, whereas iodoperoxidase enzyme activity is more likely to produce polyhalocarbons (CH_2I_2, CH_2ICl and CH_2IBr) at high iodide, with less dependence on salinity.

A very interesting observation in this experiment is the high concentrations of CH_2I_2 upon cell lysis, which has not been shown to increase in concentration in previous experiments. A tentative conclusion is that *Porosira Glacialis* has high intracellular concentrations of CH_2I_2. The release of this compound upon cell death would have implications for iodine emissions in the sea ice environment, as this compound is the most labile of the iodocarbons, being photolysed rapidly to release two iodine atoms.
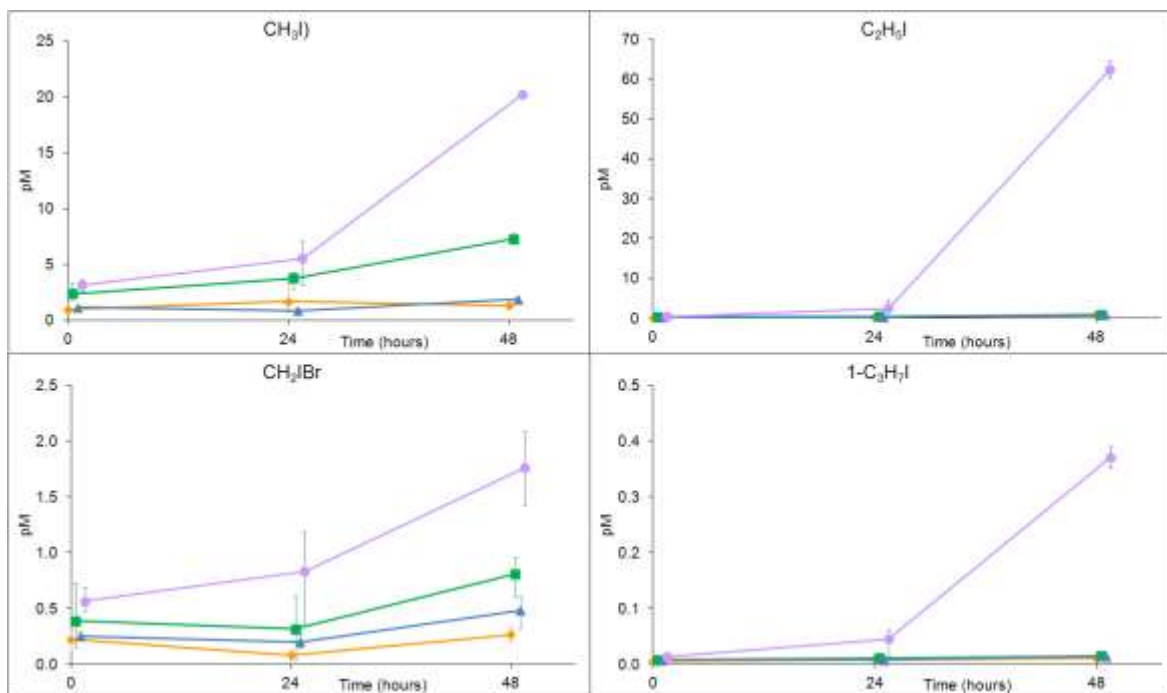
Figure 36. Concentrations of CH_3I, C_2H_5I, CH_2IBr and $1-C_3H_7I$ in seawater containing *Porosira Glacialis* in experiment 4 under conditions of ◆ low salinity and low I^-, ■ high salinity and low I^-, ▲ low salinity and high I^- and ● high salinity and high I^- in experiment 4 (where high salinity was 85‰). The average and range of triplicate samples at each time is shown.

Experiment 5

It has thus far been ascertained that changing iodide concentrations in a medium which contains *Porosira Glacialis* which have been salinity stressed affects the production of iodocarbons. Experiment 5 investigates whether the production of bromocarbons is affected by varying bromide concentrations. The salinity was held at 55‰, and the bromide changed from 400 to 2400 μM. As can be seen in figure 30, the photosynthetic efficiency of the diatoms was very variable and lower than in previous experiments at this salinity, and the reason for this is unclear. The experiment resulted in very little production of any halocarbons, but a very small amount of C_2H_5I was produced when bromide concentration was double that of seawater (1600 μM) and CH_2I_2 production seems to decrease with increasing bromide concentration (figure 38). The results of this experiment suggest that changing bromide concentrations does little to affect halocarbon production.
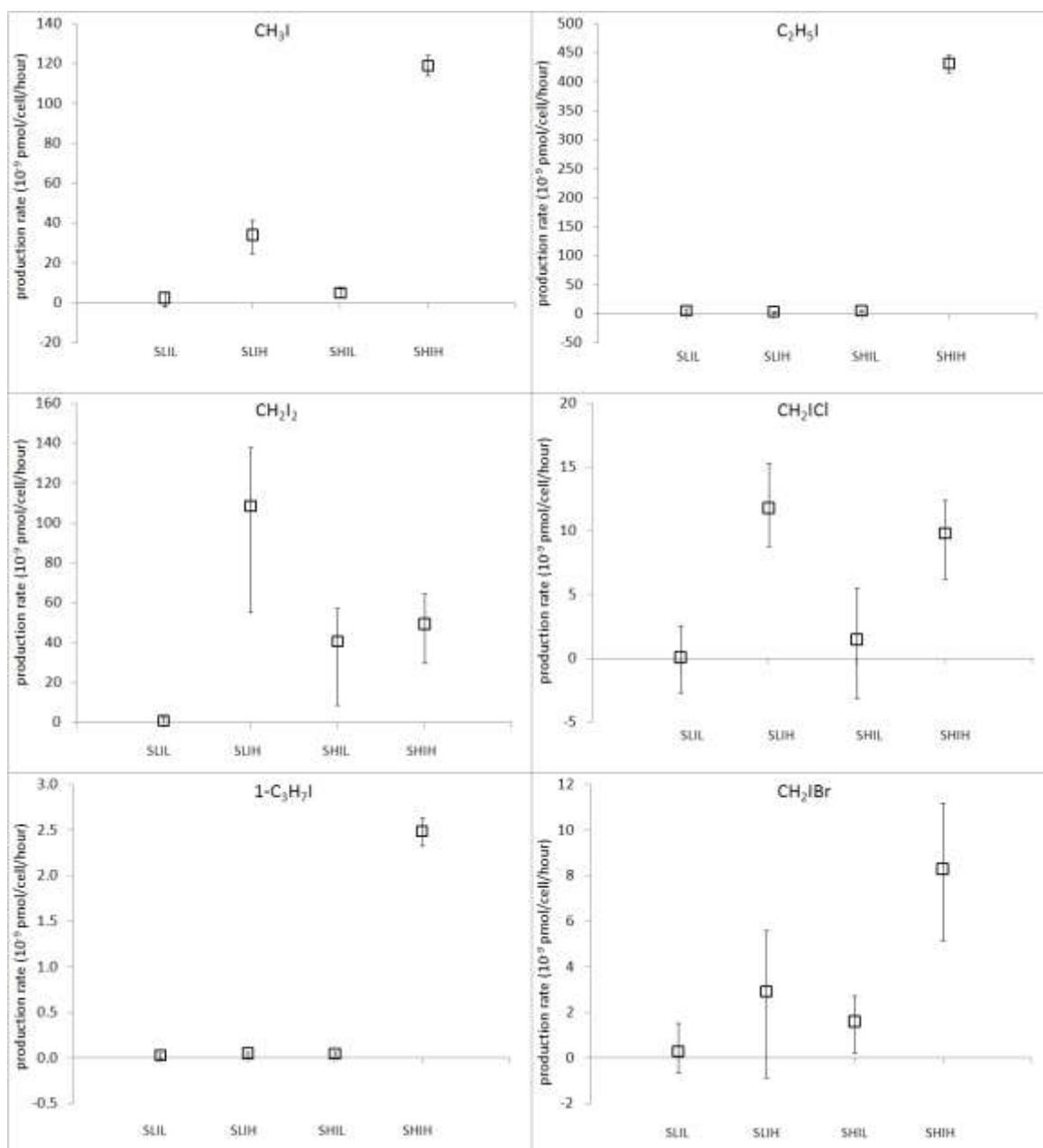
Figure 37. Production rates of halocarbons by *Porosira Glacialis* in experiment 4, where S = salinity, L = low, I = iodide concentration and H = high. The range of maximum and minimum possible production rates over 48 hours is shown.
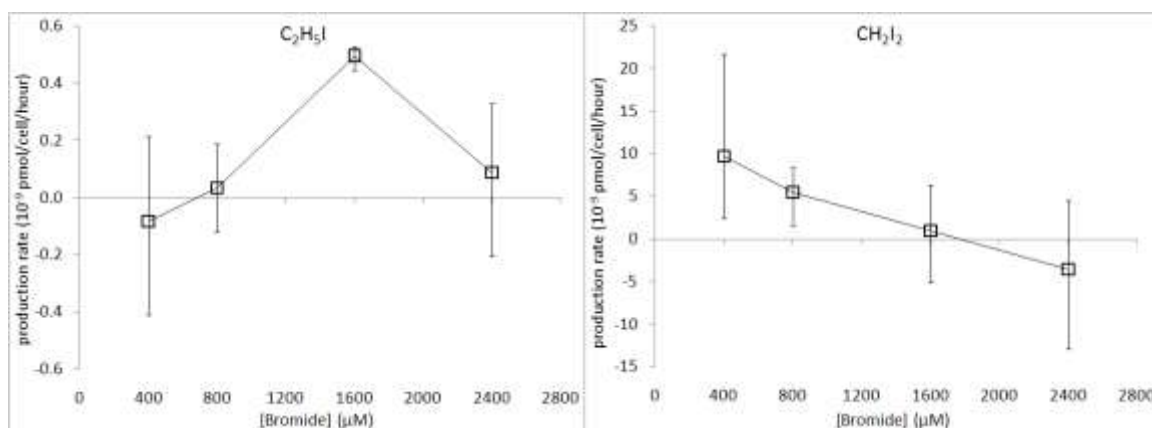
Figure 38. Production rates of C_2H_5I and CH_2I_2 by *Porosira Glacialis* experiment 5, with error bars representing maximum and minimum over 48 hours. Production rates of other halocarbons were not affected (data not shown).

Experiment 6

In experiment 6, the salinity was varied only slightly to reduce the stress experienced by *Porosira Glacialis*, and to be more representative of natural conditions, as although the salinity may reach 65‰ in brine channels, this increase does not occur instantaneously. Bromide and iodide concentrations were then either adjusted to be in line with salinity, or enhanced as detailed in table 8. A value three times that expected in line with salinity was chosen for bromide, as this is the highest bromide concentration recorded to date [*Rankin et al.*, 2002]. A higher value of iodide was chosen, as the assumption is made that the iodine is being concentrated in some way, whether it be by the biology, by the cold conditions, or by concentration in the sea ice brine.

Experiment 6 brought together many of the variables from previous experiments, and was designed to test questions which had arisen in an environment more representative of natural conditions. The key questions asked were:

- do mild changes in salinity affect iodocarbon production?
- within this less extreme salinity range, is iodocarbon production affected by the addition of iodide (or bromide)?
- how is bromocarbon production affected by the addition of bromide (or iodide)?

Due to the large number of variables in this experiment it was only possible to take measurements from duplicate samples.

The results from experiment 6 are shown in figure 39. Whilst bromocarbon production is slightly higher at high bromide and high salinity, the difference is not significant. Polyiodocarbon production shows no clear trend. The exciting result is in production of monoiodocarbons, which all show an increase in production when iodide concentrations are high. CH_3I production is highest at low salinity, whereas C_2H_5I, 1-C_3H_7I and 2-C_3H_7I production is all highest at high salinity and high iodide concentrations, This is another example of increased methyl transferase activity at high salinity and high iodide.

This experiment has shown how shows brine channel conditions may increase production of CH_3I, C_2H_5I, 2-C_3H_7I and 1-C_3H_7I.

Salinity	Br$^-$ (µM)	I$^-$ (µM)	
23	603	7.14	control
23	603	71.4	high iodide
23	1810	7.14	high bromide
33	844	10	control
33	844	100	high iodide
33	2530	10	high bromide
43	1090	16.3	control
43	1090	163	high iodide
43	3260	16.3	high bromide

Table 8. Bromide and iodide concentrations used in experiment 6. Seawater used to grow diatoms is north Atlantic seawater, where literature values for iodide concentrations are 100nM in areas of high algal density (*Wong* [1995]). The highlighted cells in the table are the values of bromide in line with salinity. The second sample in each salinity range is enhanced iodide, 1000 times the salinity normalised value. The lower iodide concentrations used in the control and high bromide samples is 100 times the salinity normalised value.
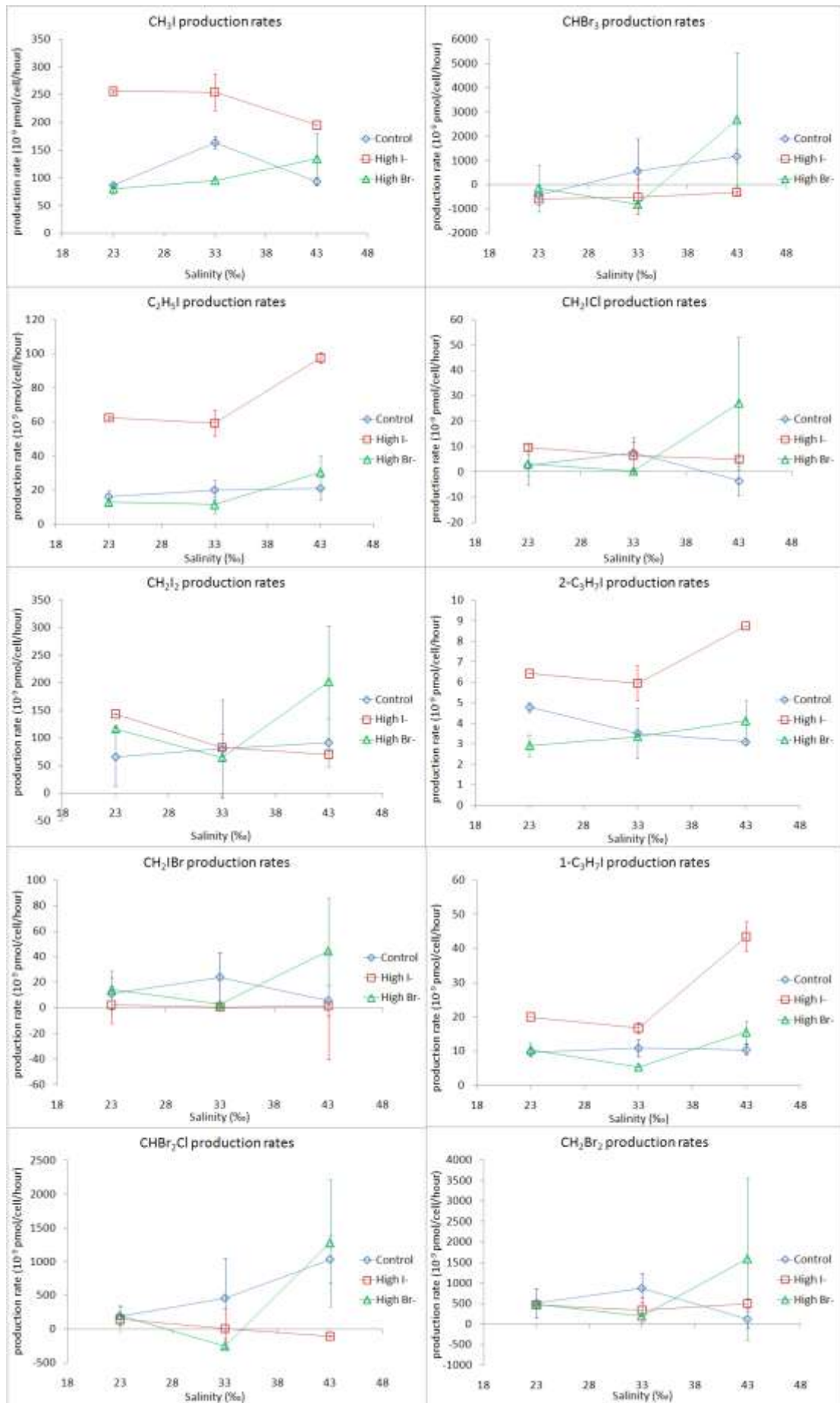
Figure 39. Halocarbon production rates by *Porosira Glacialis* in experiment 6, with error bars representing maximum and minimum possible production rates after 48 hours.

4.4.3 Discussion and comparison to literature values

CH₃I concentrations increased when *Porosira Glacialis* was salinity stressed and subject to high iodide concentrations in this study. The highest concentrations were recorded in experiments 2 and 3, with values of 58 (53 - 68) pM and 37 (29 -49) pM respectively. This compares to field measurements of 38 pM in Weddell Sea ice brine [*Fogelqvist and Tanhua*, 1995]. The highest production rate measured was 332 (230 – 496) x 10^{-9} pmol cell^{-1} hour^{-1} in experiment 3. *Manley and de la Cuesta* [1997] recorded values of 34.6 x 10^{-9} pmol cell^{-1} hour^{-1} for *Porosira Glacialis* in exponential growth phase which is in good agreement with our value of 10.9 x 10^{-9} pmol cell^{-1} hour^{-1} for the low salinity low iodide control in experiment 3.

C₂H₅I concentrations follow a similar trend to CH₃I concentrations in this study, suggesting similar production mechanisms. Concentrations were highest in experiments 2 and 4 (60.2 (55.8 – 62.8) pM and 62.4 (60.3 – 64.5) pM respectively when *Porosira Glacialis* was salinity stressed and iodide concentrations were high. This compares to field measurements by others of 27 pM in Weddell Sea ice brine [*Fogelqvist and Tanhua*, 1995]. The highest production rates of 460 (305 – 712) x 10^{-9} pmol cell^{-1} hour^{-1} were found in experiment 3.

CHBr₃ production was lower than expected during these experiments, and addition of any salts suppressed it. The highest recorded concentrations were in experiments 1 (118 (105 – 140) pM) and 5 (up to 120 pM but no production). The exception to the trend was in experiment 6, where high concentrations 509 (262 – 756) pM and a high production rate (2688 (-69.6 – 5447) x 10^{-9} pmol cell^{-1} hour^{-1}) were recorded under conditions of high salinity and high bromide concentrations but the spread of data is large. CHBr₃ production by *Porosira Glacialis* is well documented, *Tokarczyk and Moore* [1994] recorded concentrations of up to 990 pM, though their experiments ran over several weeks, and *Moore et al.* [1996] recorded concentrations of up to 1400 pM. The lower concentrations in this experiment could be due to the stresses of the experimental controls.

CH₂ICl concentrations were highest in experiment 2 where some production occurred in the first 24 hours, followed by loss, in all samples. The high salinity, high iodide samples had CH₂ICl concentrations of 13.8 (13.0 – 14.8) pM, which is close to maximum CH₂ICl values recorded in North Atlantic seawater of 17 pM [*Moore and Tokarczyk*, 1993]. Total production of CH₂ICl was highest in experiment 6 however,

under conditions of high salinity and high bromide concentration where rates of 27.2 (1.1 – 53.3) x 10^{-9} pmol cell^{-1} hour^{-1} were measured, though again the spread of data in this experiment was large and a more modest value of 9 x 10^{-9} pmol cell^{-1} hour^{-1} was recorded in both experiments 3 and 4. CH_2ICl concentrations are high compared to field measurements where concentrations are up to 3 pM [*Chuck et al.*, 2005] but lower than those measured in the laboratory by *Moore et al.* [1996] of up to 200 pM.

2-C_3H_7I concentrations were highest in all experiments which subjected *Porosira Glacialis* to high salinity and high iodide concentrations with values of 0.39 (0.34 – 0.44) pM in experiment 3, and values of up to 0.8 in all controls at high iodide concentrations in experiment 6. This compares to field measurements of 5.8 pM in Weddell Sea ice brine [*Fogelqvist and Tanhua*, 1995]. In experiment 6, maximum production rates were 8.74 x 10^{-9} pmol cell^{-1} hour^{-1}.

CH_2I_2 concentrations were suppressed by increasing salinity, but highest concentrations were recorded when iodide concentrations were high in experiments 2, 4 and 6. In experiment 2, CH_2I_2 concentrations reached 43.6 (32.1 – 55.0) pM and production rates were 250 (181 – 318) x 10^{-9} pmol cell^{-1} hour^{-1} in the low salinity high iodide samples. CH_2I_2 concentrations of 4.2 (1.7 – 8.2 pM) have been recorded in Antarctic waters [*Carpenter et al.*, 2007].

CH_2IBr concentrations showed a tendency to be highest at low salinity and high iodide concentrations, with highest concentrations (4.98 (4.32 – 6.01) pM) recorded in experiment 2, where production rates were 23.6 (18.1 – 30.9) x 10^{-9} pmol cell^{-1} hour^{-1}. Concentrations are higher than those of CH_2IBr by *Carpenter et al.* [2007] in Antarctic waters of 0.8 (0.2–1.4 M).

$CHBr_2Cl$ was not produced in significant amounts throughout the experimental period, concentrations reached 303 (41 – 565) pM in experiment 4, and calculated production rates were 1968 (51.3 – 3858) x 10^{-9} pmol cell^{-1} hour^{-1}, though the spread of data is too large for any conclusions to be drawn. *Tokarczyk and Moore* [1994] also noted extremely low production of $CHBr_2Cl$ in their study of halocarbon production by *Porosira Glacialis.*

1-C_3H_7I production was consistently shown to be highest in samples subject to high iodide and salinity, with the highest values recorded in experiment 6 of up to 4 pM in all high iodide samples. This compares to field measurements of 235 pM in Weddell

Sea ice brine [*Fogelqvist and Tanhua*, 1995]. Production rates measured in experiment 6 were 19.9, 16.8 and 43.5 x 10^{-9} pmol cell^{-1} hour^{-1} for salinities of 23, 33 and 43‰ respectively.

CH$_2$Br$_2$ production followed a similar trend to that of CHBr$_3$ in this study, which was expected as these two compounds have been suggested to be produced via a similar mechanism [*Manley*, 2002]. At low salinity in experiment 1, concentrations reached 98.2 (97.3 – 100) pM during production at 167 (78.9 – 218) x 10^{-9} pmol cell^{-1} hour^{-1}. Concentrations (up to 250 pM) in experiment 6 were higher, though no significant production was observed. These results are in reasonable agreement with those of *Tokarczyk and Moore* [1994] who measured CH$_2$Br$_2$ concentrations of up to 350 pM in *Porosira Glacialis* cultures, though *Moore et al.* [1996] measured concentrations of up to 1600 pM.

4.4.4. Summary of results from experiments using *Porosira Glacialis*

The key findings from experiments 1 – 6 can be summarised as follows:

- Salinity-induced stress to *Porosira Glacialis* resulted in decreased bromocarbon production.
- Production of the bromocarbons is also suppressed by the addition of iodide, suggesting iodide is able to outcompete bromide for the active site of the enzymes responsible for halocarbon production.
- Increasing bromide concentrations did not increase bromocarbon production.
- Whilst increasing salinity without increasing iodide concentrations also suppressed iodocarbon production, as soon as additional iodide was available, iodocarbon production increased.
- At high iodide, increasing salinity increased monoiodocarbon production, but decreased polyiodocarbon production.
- Low salinity controls show it is a change in salinity, as opposed to an increase, which results in increased iodocarbon production.
- Cell lysis caused CH$_3$I, C$_2$H$_5$I, 1-C$_3$H$_7$I and CH$_2$IBr concentrations to increase. suggesting these compounds reside within the diatom cell.
- Different responses of different enzyme types were clear, with the same patterns of production for monoiodocarbons (methyl transferase) and polyiodocarbons (iodoperoxidase).

These results have implications for the sea ice environment. As seawater freezes, trace gases and dissolved ions are concentrated in the brine channels. Brine channels are home to diatoms, which may use iodide as a cellular anti-oxidant. Iodide may be especially useful by survival mechanisms in this extreme environment. It has been shown that salinity changes and the presence of iodide cause iodocarbon concentrations to increase, hence iodocarbons may be a byproduct of the anti-oxidative metabolism of the cell. Bromocarbon production does not appear to be affected. Hence these processes may help us to understand why iodine compounds are concentrated and released in the sea ice environment, as any labile compounds released by sea ice diatoms may be released to the atmosphere if the ice is porous enough to allow the compounds to escape.

4.5. Results from experiments using *Fragilariopsis Cylindrus and Fragilariopsis sp.*

The F_v/F_m ratio obtained via fluorometry (section 3.2) was used as an indication of the photosynthetic efficiency of the diatoms. During exponential growth when the diatom stocks are at their most healthy, typical F_v/F_m ratios for *Fragilariopsis Cylindrus* are between 0.45 and 0.55. In this experiment, the F_v/F_m ratio was greater than 0.47 before the experiment commenced. Cell numbers were much higher than in the *Porosira Glacialis* experiments as this species is much smaller, initial cell numbers were 113×10^3 cells ml^{-1}. Production of halocarbons was extremely low, a little CH_2ICl, CH_2I_2, CH_2IBr, 1-C_3H_7I and CH_2Br_2 under ambient conditions, but net loss of all compounds as soon as concentration of any of the salts was increased. Production rates of CH_2ICl, CH_2I_2, CH_2IBr, 1-C_3H_7I and CH_2Br_2 under ambient conditions were 83 ± 56, 17 ± 36, 46 ± 65, 0.07 ± 0.05 and $0.013 \pm 0.024 \times 10^{-12}$ pmol cell^{-1} hour^{-1} respectively.

Fragilariopsis sp. was subjected to varying bromide concentrations (400 – 2400 μM). Production of $CHBr_2Cl$ (864 ($486 – 1125$) $\times 10^{-9}$ pmol cell^{-1} hour^{-1}) and CH_2Br_2 (3.57 (-$1.43 – 8.47 \times 10^{-9}$ pmol cell^{-1} hour^{-1}) was observed when bromide concentrations were equal to those of seawater (800 μM) but production decreased at other bromide concentrations (figure 40). No significant production of any other halocarbons was observed.
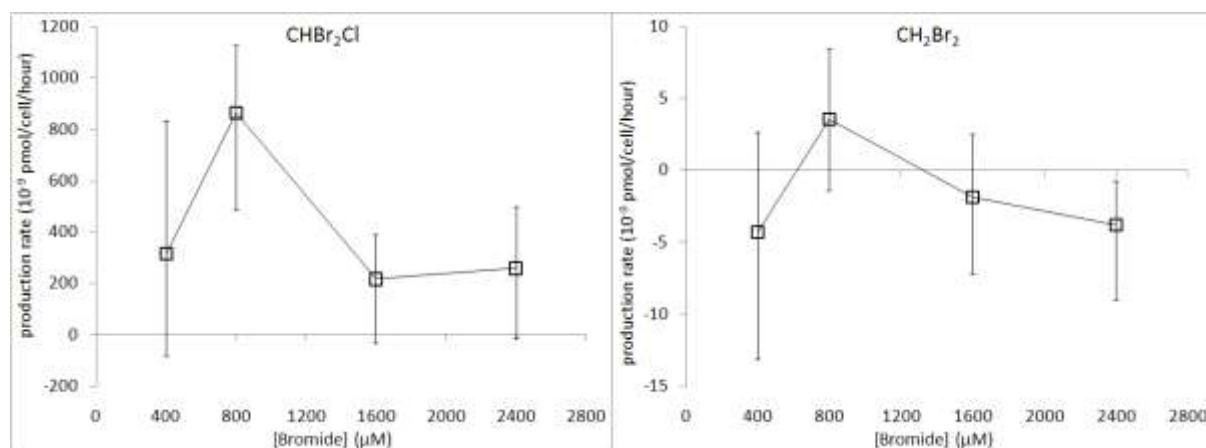
Figure 40. Bromocarbon production by *Fragilariopsis sp.* subject to varying bromide concentrations with error bars representing maximum and minimum possible production rates after 48 hours, production rates of other halocarbons were not affected (data not shown).

4.6. Results from a naturally occurring Antarctic ice algae community

4.6.1 Halocarbon measurements

Rothera experiment 1

Rothera experiment 1 was a repeat of experiment 4, using high and low salinity (35 to 65‰) and iodide concentrations (ambient and 10^{-3} M) in the same experiment. Production of CH_3I, CH_2I_2, C_2H_5I, CH_2ICl, $1-C_3H_7I$ and $2-C_3H_7I$ increased when salinity and iodide concentrations were high, production of bromocarbons was not observed.

Rothera experiment 2

Rothera experiment 1 showed increased concentrations of iodocarbons in seawater containing diatoms when salinity and iodide concentrations were high. Is this due to production by diatoms, or are abiotic reactions occurring, such as the reaction of I⁻ with organics in solution? To answer this question, KI and NaCl were added to assemblages of DRS, and DRS which had been filtered, at concentrations equal to the high salinity and high iodide control in Rothera experiment 1. Figure 42 shows enhanced production rates of CH_3I, C_2H_5I, and $1-C_3H_7I$ in seawater containing an ice algae community. CH_2I_2, CH_2ICl and $2-C_3H_7I$ are produced in equal amounts in both DRS and filtered DRS. Whilst every care was taken to ensure diatoms frustules were not broken during filtration, it is possible that some enzymes were released into solution during the filtration process; these enzymes could then be responsible for halocarbon production. Abiotic reactions between dissolved organic material and

iodide in the medium could also be responsible; such reactions are discussed further in section 6.1.
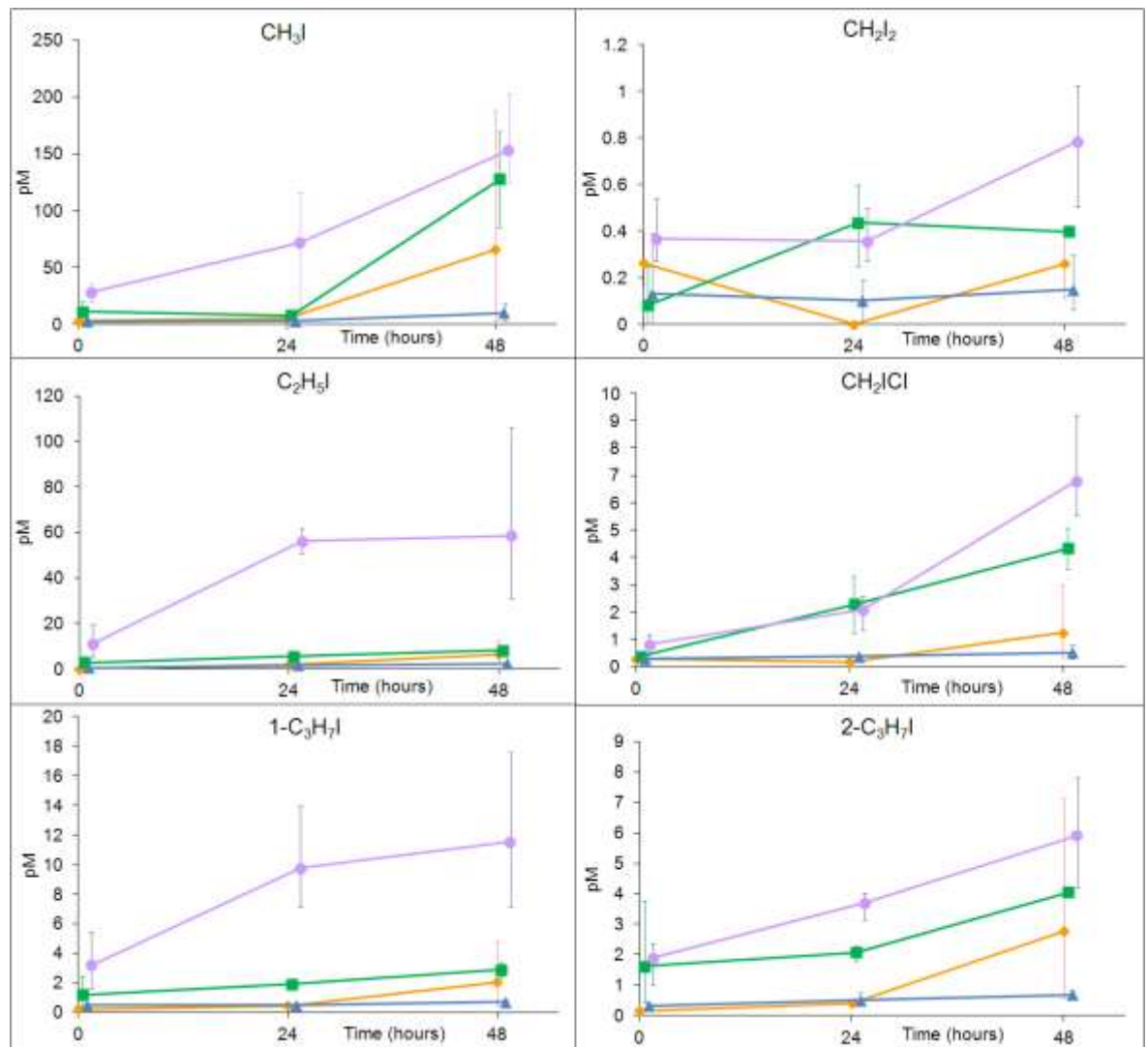
Figure 41. Concentration of halocarbons in an Antarctic ice algae community (assemblage J) under conditions of ◆ low salinity and low iodide, ■ low salinity and high iodide, ▲ high salinity and low iodide and ● high salinity and high iodide. The average and range of triplicate samples at each time is shown.
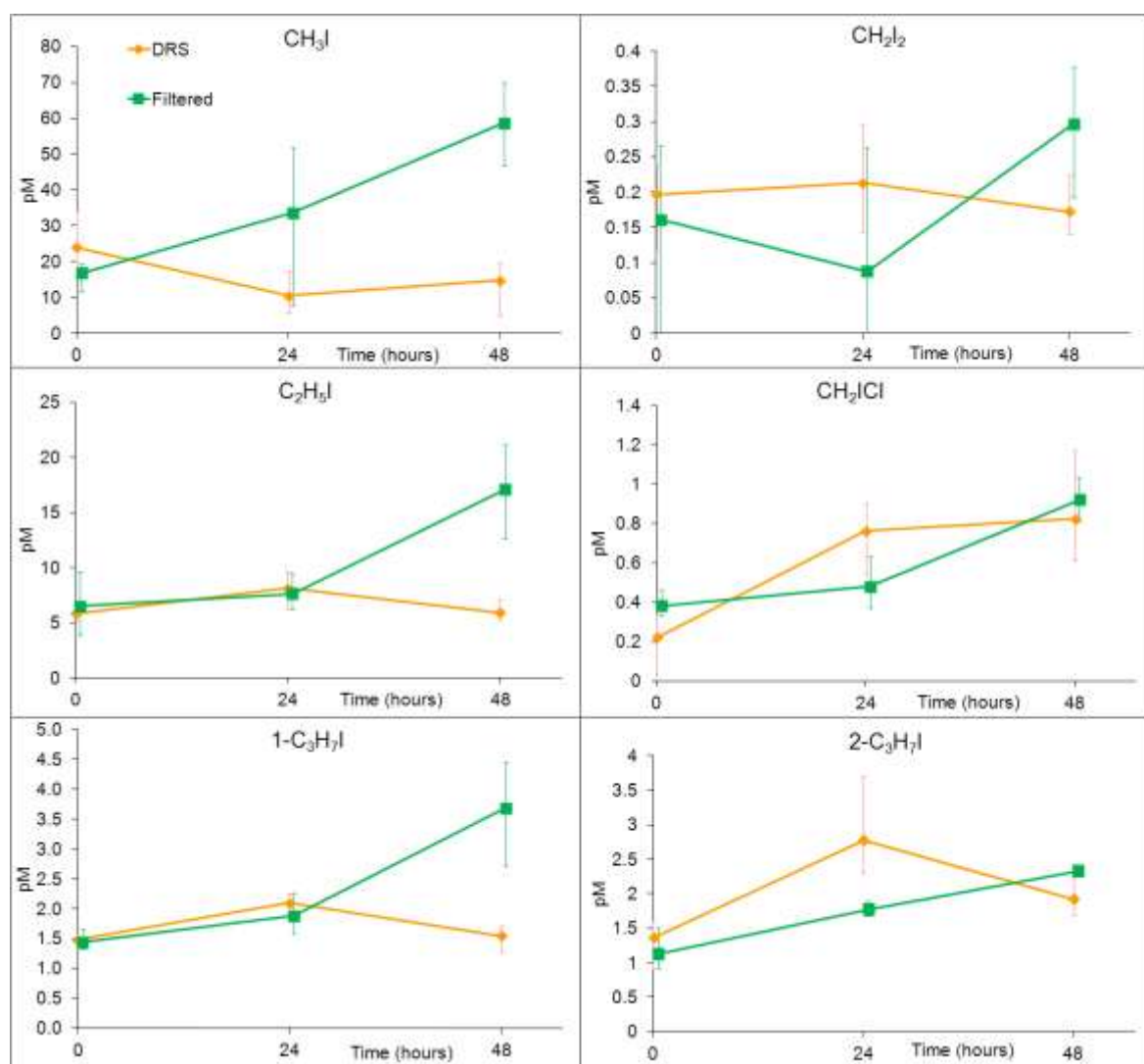
Figure 42. Concentration of halocarbons in seawater containing ■ an Antarctic ice algae community (assemblage K) and ◆ 0.2 μm filtered seawater under high salinity and high iodide conditions. The average and range of triplicate samples at each time is shown.

4.6.2 Summary of Rothera experiments

Results from the Rothera experiments show enhanced iodocarbon production in an Antarctic ice algae community under conditions of high salinity and high iodide concentrations. Increased production of the monoiodocarbons CH_3I, C_2H_5I, and 1-C_3H_7I is dependent on the presence of diatoms, so biotic production has been demonstrated. Production of CH_2I_2, 2-C_3H_7I and CH_2ICl increases in seawater when iodide and salinity are high after removal of the diatoms, so may be due to a reaction of iodide with humic material. However it is also possible that enzymes released during filtration may be responsible for halocarbon production, so these results do not allow any firm conclusions to be drawn, and more experiments are needed. It is interesting that once again the monoiodocarbons exhibit a different trend to the polyiodocarbons.

4.7. Discussion

It has been demonstrated that under the conditions experienced by diatoms in the sea ice environment (varying salinity, and high bromide and iodide concentrations), iodocarbon production increases. It is not known whether these compounds are produced directly by the diatoms, or whether they are the secondary compounds of other emissions. For example, HOI emissions may react with dissolved organics to produce the iodocarbons. Enzymatic production of HOI and HOBr by diatoms has previously been suggested [*Hill and Manley*, 2009]. The release of iodocarbons upon cell lysis suggests these compounds are formed within the cell, or formed rapidly from compounds within the cell.

Trends were observed between monoiodinated and polyiodinated compounds; this is significant as these different classes of compound have previously been shown to be produced by different types of enzyme. [*Manley*, 2002]. The methyl transferase enzyme responsible for monohalogen production activity and the haloperoxidase enzyme responsible for polyhalocarbon production are both antioxidative enzymes, likely to be particularly active in the harsh sea ice environment.

If diatoms are able to accumulate and concentrate iodine then this may be an iodine selective mechanism of volatilisation in the sea ice zone. The release of some compounds is due to salinity-induced stress, and production of these compounds may help the diatoms to survive in this extreme environment. It is also possible that another survival mechanism is occurring, such as the production of anti-freeze compounds, or the production of resting spores, of which iodocarbon production is simply by-product.

Whilst the cultures of *Porosira Glacialis*, *Fragilariopsis sp*., and *Fragilariopsis Cylindrus* were not free from bacteria (some bacterial contamination was observed via DAPI-staining), sterile technique was used during the experiments and autoclaved seawater was used for the medium. In this way, bacterial contamination was minimised in the experiments using cultures, whereas bacteria will be much more prolific in natural seawater communities. It is not known what effect bacteria may have had on halocarbon concentrations in these experiments.

4.7.1 Discussion of alternative production pathways of iodocarbons

Moore and Zafirou [1994] reported CH_3I production via photochemistry in seawater involving photolysis of humic material to yield methyl radicals which react with iodine atoms produced by oxidation of I^-. However the authors caution that this process would not be efficient due to competition for methyl radicals with the more abundant oxygen present in sunlit surface waters. An abiotic mechanism proposed by *Swanson et al.* [2002] following observations of iodocarbons above snow involves the photolysis of carbonyl compounds to produce alkyl radicals which react with iodine atoms formed from the reaction of iodide with OH. This mechanism may also be occurring in seawater and may explain monohalocarbon production.

Recent measurements of iodocarbons in the Canadian sub-arctic [*Carpenter et al.*, 2005], close to the coast of Hudson Bay but in the absence of open water or leads detectable by satellite, were postulated to be abiotic in origin. The mechanism, supported by laboratory experiments, suggested for the production of CH_3I, CHI_3 and CH_2I_2 proceeded via the reaction of HOI with humic material on the surface of sea ice. It is possible that similar reactions could be occurring in the experiments in this study. It is also possible that the increased concentration of halocarbons in these experiments is due to the reaction of I^- with organics. However the lack of enhancement of iodocarbons in the *Fragilariopsis* cultures when iodide concentrations are high would suggest this is not the case. Rothera experiment 2 also demonstrated the necessity of diatoms (or anything larger than the 0.2 μm filter pore size) in seawater for enhanced production of CH_3I, C_2H_5I and $1\text{-}C_3H_7I$. CH_2ICl formation could be due to photolysis of CH_2I_2, this reaction proceeds with a yield of 25–35% [*Jones and Carpenter*, 2005; *Martino et al.*, 2009].

4.8. Summary

The highest concentrations of atmospheric IO and BrO, which result from the presence of reactive halogen radicals in the atmosphere, are observed over the sea ice of the Southern Ocean during spring when the ice is melting [*Schönhardt et al.*, 2008], with another peak in autumn during ice formation. In this study, experiments were carried to ascertain whether sea ice diatoms produce reactive halogenated compounds, and whether the stresses of the extreme environment experienced within the brine channels caused an increase in production.

In these experiments, maximum production rates of CH_3I, C_2H_5I and $1\text{-}C_3H_7I$, produced by methyl transferase activity [*Manley*, 2002; *Moore et al.*, 1996], were observed when *Porosira Glacialis* were salinity stressed and iodide concentrations were enhanced. CH_2ICl, CH_2I_2, CH_2IBr and $2\text{-}C_3H_7I$, production also increased when iodide concentrations were enhanced, though very high salinities suppressed production. Polyhalogenated compounds are produced by haloperoxidase enzymes [*Manley*, 2002; *Moore*, 2003]. The trend in production within a similar class of compound is an interesting result.

Production of the bromocarbons tended to be greatest when salinity, bromide and iodide were all low. It may be that iodide is able to outcompete bromide for the active sites of enzymes responsible for halocarbon production. Therefore, enhancement in halogen ions increases production of iodocarbons but not bromocarbons. This may be because iodide is a useful cellular anti-oxidant; it is a large, easily polarisable atom, so of particular use in the harsh environment experienced by sea ice diatoms [*Arrigo and Thomas*, 2004]. The increase in concentrations of iodocarbons under sea ice conditions is in good agreement with the work of *Fogelqvist and Tanhua* [1995] who found enhanced iodocarbon, but not bromocarbon, concentrations in sea ice brine in the Weddell Sea.

By varying temperature, salinity, iodide and bromide concentrations, many aspects of the freezing process which may affect halocarbon production have been studied in chapters 3 and 4. The emerging picture is one of increased iodocarbon production by diatoms under sea ice conditions.

Chapter 5. Iodine Emissions from the Sea Ice of the Weddell Sea

5.1 Introduction

As discussed in chapter 1, the motivation for this research came from measurements of the highest global atmospheric concentrations of IO above the sea ice of the Weddell Sea and continent close by [*Saiz-Lopez et al.*, 2007a; *Saiz-Lopez et al.*, 2007b; *Schönhardt et al.*, 2008]. Chapters 3 and 4 have shown how sea ice formation may concentrate volatile compounds containing iodine into the ice brine, and how diatoms living in the brine channels may produce more iodocarbons due to the stresses of the sea ice environment. If the sea ice is porous enough to allow these compounds to escape, it may be a source of volatile iodine, and hence atmospheric iodine oxides.

From January to March 2009 a field campaign was undertaken on board a ship in the Southern Atlantic Ocean and Weddell Sea in order to further investigate in these processes. Organic and inorganic compounds of iodine were measured and quantified. Chl *a* analysis was used as an indication of algae distribution in the ice. The physical properties of the ice determined the continuity of the brine channel network, providing a pathway for the iodine compounds from sources to the atmosphere. IO and new particle formation were also measured to assess the impact of compounds released from the ice on the atmosphere above. Saturation anomalies, flux calculations and a modelling study have been used to interpret the measurements. This study is the first combined *in situ* study in Antarctica of organic and inorganic iodine compounds in sea water, ice and air, and the resultant IO and new particles which arise.

5.2. Description of field campaign

Measurements were made from 28th January to 5th March 2009 (figure 43) on the ice-strengthened RRS Ernest Shackleton (cruise ES033) sailing from Stanley in the Falkland Islands (51.6°S 57.6°W), via Signy (60.7°S 45.6°W), to the ice covered Weddell Sea. Several weeks were spent in the sea ice, which was up to 2 m thick, followed by three days moored against the Brunt Ice shelf (75.4°S 26.8°W), then returning via Signy to Stanley. Ice cores were taken between 5th and 14th February. Seawater and air were sampled at irregular intervals during the course of the

campaign. Between 19th and 22nd February, an experimental site was set up on the Brunt Ice shelf where air was continuously monitored.
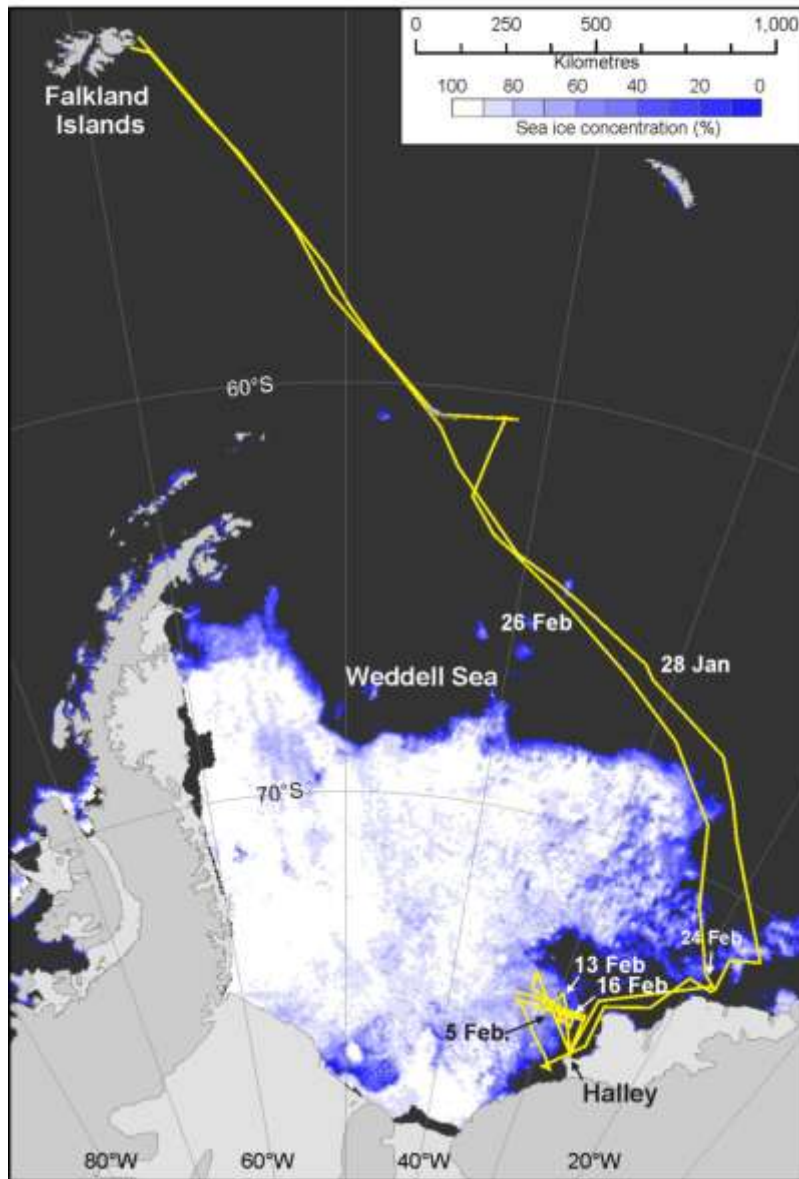
Figure 43. Cruise path of ES033 in the Southern Ocean and Weddell Sea, and ice cover on 21st February 2011. Ice cores were made between the 5th and 13th of February, and the ice shelf experiment was set up close to Halley.

5.3. Materials and methods

A summary of the measurements made during the field campaign is given in table 9. Where measurements were made in collaboration with other groups, this is denoted in brackets.

Analyte	Medium	Technique
Halocarbons	Air, water and ice	GCMS
I_2, HOI and ICl	Air	Denuder tubes (R.J. Huang; University of Mainz)
Chl *a*	Water and ice	Fluorometry
Iodide	Water and ice	Cyclic voltammetry (R. Chance; University of York / UEA)
Iodate	Water and ice	Spectrophotometry (R. Chance; University of York / UEA)
IO	Air	Mini-MAX-DOAS (H. Roscoe; BAS)
Sea ice physics (brine volume etc)	Ice	Temperature and salinity measurements
Ozone	Air	2B 205 ozone analyser (B. Davison; Lancaster University)
Particles	Air	Grimm 5.401 particle counter (B. Davison; Lancaster University)

Table 9. Measurements made during cruise ES033

5.3.1 Sample collection

Ice cores. Cores were made with a 1 m long, 9 cm diameter SIPRE corer (Mark II coring system, Kovacs Enterprises Inc). The cores were made within 50 m of the ship, ice was between 80 – 180 cm thick, and all but the first core (5th Feb) represent the full thickness of the ice; the first core was only the top metre of thicker ice, the remainder of the core could not be retrieved due to a temporary problem with the corer. Once brought up, the cores were immediately cut into 10 cm or 3 cm long sections in order that vertical profiles of concentrations through the ice could be ascertained. The middle section of the ice core was removed with a custom-made stainless steel 'mini-corer' with dimensions to exactly match those of the inside of a 100ml gas-tight syringe. The mini core was then immediately transferred to a syringe and left to melt at room temperature in the dark. It is acknowledged that cells could have been stressed due to the salinity changes experienced during ice melt. The conventional technique is to melt ice samples in seawater, however this was not appropriate for this study due to the necessity of keeping the ice in a gas-tight

container, in order to limit escape of the compounds. Furthermore, it would not be desirable to dilute halocarbon concentrations which are already close to the limit of detection of the GCMS. 4 ice cores were made during the campaign, from which a total of 43 samples were analysed.

Diatom-rich ice (DRI). On three occasions a small boat was used to collect ice samples where discolouration due to the presence of diatoms could clearly be seen (shown in figure 44); the presence of the ice algae was confirmed my microscopy. By leaning over the side of the boat, a total of 12 gas-tight syringes were filled with ice with a stainless steel scoop, and left to melt in the dark at room temperature. These diatom rich ice samples were in contact with lead water and were very porous.

Underway seawater (USW). Water samples from the ship's USW supply, which pumps water in to the wet lab from a depth of 6 m, were sampled at irregular intervals during the campaign. Samples were taken with a 100 ml gas-tight syringe directly from the pump outlet in the wet lab on the ship. This method ensured limited exposure to air of the water, and no bubbles were visible in the water after it had been allowed to run for a few minutes.

Air. A pump and vacuum gauge (-1 to +1 bar) were used to draw air through Markes sorbent tubes or denuder tubes for halocarbon analysis or I_2 and AIC in air respectively. A Tylan mass flow controller (MFC) (model F260-V) connected to a Tylan RO-32 power supply/display box was used to control the flow, the control box was modified to include a yellow/black twisted pair MFC output signal pickup on its front panel. This allows logging of the MFC flow read with a Gemini TinyTalk 2 logger. The pumping equipment was all set up below the bow of the ship and Tygon tubing was connected to an air sampling site on the forecastle, 10 m above sea level. The flow rate was checked with a flow meter regularly on both the inlet of the Markes sorbent tube (halocarbons) and the denuder tube (I_2 and AIC), which were deployed for 40 mins at a flow rate of 25 ml min^{-1}, and 3 hours at a rate of 500 ml min^{-1} respectively.

Air samples for halocarbon analysis were collected at irregular intervals throughout the duration of the cruise, when time permitted. Air samples for I_2 and AIC analysis were collected daily providing conditions permitted. Adverse conditions which prevented sampling on occasion were very rough seas which prevented the sampling

site being accessed, or wind direction being such that the air was directed past the ship's stack, thus potentially contaminating the sample with emissions from the ship.

Figure 44. Ice floes broken by the ship's passage through the sea ice of Weddell Sea, where an area of high algal biomass was clearly visible close to the surface of the ice.

5.3.2. Sample preparation and analysis

Melted ice and water samples for Chl *a* and iodide / iodate analysis were filtered through a 47μm Whatman GF/F filter paper, the filtered water was stored at -20°C on the ship and transported back to the UK for analysis. Water samples for halocarbon analysis were filtered through a 47μm Whatman GF/F filter paper directly into the glass purge tube at the start of the GCMS run as detailed in section 2.1, with the Markes thermal desorption unit used as the trapping method. The filter papers were wrapped in aluminium foil and stored at -80°C on the ship for Chl *a* analysis back in the UK.

Although the focus of this study is iodocarbons, the bromocarbons $CHBr_3$, $CHBr_2Cl$ and CH_2Br_2 were also measured and results for these are presented as supplementary information. In total 9 halocarbons were measured, shown in table 10, with retention times and limit of detection. CH_2I_2 unfortunately could not be measured due to a contamination problem, and this will be discussed further in section 5.5. A calibration was carried out at the start and end of the campaign as detailed in section 2.1. R^2 values for all calibration curves were above 0.96. The standards were prepared in the UK, and stored at -20°C. Measurement precision, determined by errors in duplicate water samples, was between 0.9% and 14.0%.

	CH₃I	C₂H₅I	CHBr₃	CH₂ICl	2-C₃H₇I
m/z	142	156	173	176	170
LoD	0.15	0.28	1.82	0.18	0.34
RT	6.4	8.5	12.8	10.4	9.6

	CH₂IBr	CHBr₂Cl	1-C₃H₇I	CH₂Br₂
m/z	222	129	170	174
LoD	0.12	0.83	0.33	0.77
RT	11.9	11.6	10.4	10.0

Table 10. Halocarbons analysed by GCMS, showing mass / charge ratio (m/z), limit of detection (LoD) in pM, and retention times (RT) in mins. The LoD improved during the course of the campaign for most compounds, LoD at the start of the campaign is given.

Iodide and iodate concentrations were measured by cyclic voltammetry and spectrophotometry back in the UK within 9 months of the field campaign as detailed in section 2.2.

Chl *a* was measured by fluorometry as detailed in section 2.3 within 15 months of the campaign, samples were stored at -80°C during this time.

Molecular and inorganic iodine compounds were measured via denuder tubes as detailed in section 2.5.

IO was monitored by mini-MAX DOAS as detailed in section 2.6 with references of: 9th Jan (for spectra from 7th to 15th Jan); 5th Feb (for spectra from 25th Jan to 10th Feb); 21st Feb (for spectra after 16th Feb) near local noon at 90° elevation. Median slant amounts during each day with prolonged sunny periods were measured at elevation angles of 4°, 8°, 15° and 50° Those at 4°, 8° and 15° were subtracted from the 50° value, and divided by the appropriate differences in AMFs to produce the vertical amounts. Mixing ratios were then calculated within an estimated boundary layer height of 200 m [*Renfrew and King*, 2000] which is typical of that over sea ice next to an ice shelf. The mini-MAX-DOAS was mounted on the bridge of the ship, looking out through a port-facing window, a height of approximately 15 m above sea level. IO column densities were also measured by satellite during the campaign period as detailed in section 2.6.

Particles were counted with a Grimm 5.401 particle counter attached to a differential mobility analyser to give particle size information.

Ozone was measured using a 2B Technology dual beam 205 ozone analyser. 10 minute averaged data is presented.

The **brine volume** of the sea ice was calculated as detailed in section 2.7.

Wind speed and direction were recorded with a Kestrel 4500 weather tracker when the ship was sailing, with compensation made for ship speed and heading. For the time period the ship was moored, and the ice shelf experiment was set up (see section 2.2.3 for details), the wind speed and direction data was that recorded at Halley, the BAS base located 12 km SSW of the ship.

Whilst on board the ship, wind direction was always monitored via the ship's instrumentation to ensure the ship's stack did not affect the integrity of any atmospheric samples.

5.3.3. Ice shelf experiment

The ship moored against the Brunt ice shelf close to Halley from 19th – 23rd February 2009. During this time an experimental site was set up on the ice shelf at 75.4°N, 26.6°W.

Denuder tubes were deployed to sample air at a height of 1 m above the snowpack, attached to an aluminium pole outside a tent housing a battery and pump, and connected to the denuder tubes via Teflon tubing. The pumping system used in this experiment was a BAS ex-ASSAY pumping/logger unit, with mass flow meter and miniature air pump. These units were modified to provide connection of Gemini TinyTalk 2 data loggers to the front panel. The air pump exhaust was also plumbed to a front panel bulkhead fitting for monitoring the air flow via an external flow meter. The ex-ASSAY pumping unit uses a Honeywell (MicroSwitch) airflow sensor Model AWM5101-VN (RS part number 395-184), which has a 1-5Vdc linear voltage output for the mass flow range 0 – 5 SLPM, with a ±3.0% reading linearity error. Near-continuous ambient air samples were taken for 3 days.

Ambient air was sampled for halocarbons regularly from a height of 1m above the snowpack by drawing air through a sorbent tube with a gas-tight syringe via a piece of Tygon tubing. Halocarbon emissions from the snowpack were also measured using a Teflon-lined plastic tube, 0.6m long, 0.1m diameter, pushed 20 cm into the snow with a valve at the top, through which air was drawn, through a Markes sorbent tube, with a gas-tight syringe.

5.3.4 Saturation anomalies, flux calculations and modelling of data

Saturation anomalies and fluxes were calculated in order to estimate the importance of the regional chemistry on the atmosphere above. Saturation anomalies, defined as the percentage departure from the expected equilibrium between trace gas concentrations in surface seawater and the atmosphere above were calculated via equation 6 where C_w is the seawater concentration, C_a is the atmospheric concentration and H is the temperature dependent dimensionless Henry's law constant (taken from *Sander* [1999]).

Saturation anomaly = 100% x $(C_w - C_a/H)/(C_a/H)$ (6)

The statistical language R was used for flux calculations as detailed in *Johnson* [2010]. Briefly, equation $F = K_w(C_a/H - C_w)$ was used where F is the flux, K_w is the transfer velocity, C_a is the air concentration, C_w the simultaneous water concentration, and H the Henry's law constant as above. Transfer velocities are dependent on wind speed, salinity and water temperature.

To calculate the flux of iodine necessary to reproduce the observed levels of I_2 and IO, the one-dimensional photochemistry and transport Tropospheric Halogen Chemistry Model (THAMO) was used by Alfonso Saiz-Lopez and Anoop Mahajan at the Laboratorio de Ciencias de la Atmósfera y el Clima (CIAC), details of which are given in *Saiz-Lopez et al.* [2008]. The model was run at a vertical resolution of 1 m up to a boundary layer height of 200 m. The vertical transport in the model is constrained using wind shear, calculated from wind speed measurements during the campaign and a surface roughness length, which was set at 5 x 10^{-5} m according to long-term observations at Halley Bay, Antarctica [*King and Anderson*, 1994]. The eddy diffusion coefficient (K_z) increased from 8 x 10^2 cm^2 s^{-1} at 1 m to a maximum of 3.2 x 10^5 cm^2 s^{-1} at 32 m. In addition to photochemical, gas-phase and heterogeneous reactions, THAMO also treats the formation of new iodine oxide particles (IOPs) using coagulation of higher oxides of iodine and uptake of condensable vapours on these new particles. A further description of the IOP formation routines can be found in *Mahajan et al.* [2010].

5.4. Results

As it is assumed that the biolgical and chemical activity of interest is occurring in the liquid phase of the sea ice, and bulk ice was sampled, values have been normalised to

sea ice brine volume and corrected for salinity as described in section 2.8. Chl *a* and halocarbon concentrations are reported in sections 5.4.1 and 5.4.2 respectively. Table 14 summarises complementary measurements to the halocarbon analysis, the results are discussed in section 5.4.3 to 5.4.8.

5.4.1 Chlorophyll a concentrations

Chl *a* data is only available for a limited number of samples. Two ice cores, each comprising 8 discrete sections, contained between 0.1 to 101.1 µg l^{-1} Chl *a* and results are shown alongside halocarbon concentrations in figures 45 and 46. The presence of diatoms in the ice was confirmed via microscopy, small pennate diatoms dominated the community. Chl *a* concentrations in 3 samples of diatom-rich ice were 11.4, 32.2 and 6.6 µg l^{-1}, much higher than that of the underlying seawater, where Chl *a* concentrations ranged from 0.05 to 0.22 µg l^{-1} (average 0.14 µg l^{-1} across 4 samples).

5.4.2 Halocarbon concentrations

An overview of halocarbon concentrations across all samples (water, air and ice) collected during the campaign is presented in table 11; the results from ice samples are then broken down into sample type: concentrations in diatom rich ice are shown in table 12, and those from ice cores in table 13 and figures 45 and 46. Halocarbon concentrations measured in the ship's USW supply are presented in figure 47, and box-whisker plots show a summary of concentrations in ice and water in figure 48. Atmospheric halocarbon mixing ratios in air are shown in figure 49. Results from the ice shelf experiment are presented in section 5.4.4.

Ice samples

Halocarbon profiles are shown in figures 45 and 46 alongside Chl *a* data where available. The core of the 5th February shows a peak in halocarbon concentrations close to the surface of the ice, and a corresponding peak in Chl *a*, supporting production of halocarbons by diatoms in surface communities as described in section 1.4. $CHBr_3$, CH_2ICl, $1\text{-}C_3H_7I$ and CH_2Br_2 concentrations all show enhanced concentrations from 60 – 70 cm, just below another area of high Chl *a*. The significant peak in mono-iodocarbons close to the surface of the ice is in good agreement with ice core data from the COBRA field campaign (see Chapter 6).

Compound	Sample type	20th percentile	Average	80th percentile	Max
CH_3I	Ice	1.2	4.8	4.2	149
	Water	0.03	0.1	0.2	0.3
	Air	0.01	0.1	0.11	0.5
C_2H_5I	Ice	5.3	30.6	24.4	739
	Water	0.1	1.1	1.8	5.0
	Air	0.0	0.2	0.4	2.1
$CHBr_3$	Ice	46.2	270	363	6850
	Water	5.9	19.0	26.5	71.3
	Air	0.9	3.3	3.3	41.0
CH_2ICl	Ice	0.0	9.6	5.0	455
	Water	0.0	0.2	0.3	1.1
	Air	0.0	0.07	0.0	4.3
$2\text{-}C_3H_7I$	Ice	0.0	9.9	4.6	311
	Water	0.0	0.2	0.36	0.9
	Air	0.0	0.03	0.0	0.6
CH_2IBr	Ice	0.0	6.3	0.0	406
	Water	<LoD	<LoD	<LoD	<LoD
	Air	0.0	0.03	0.0	1.0
$CHBr_2Cl$	Ice	2.1	6.7	10.0	49.4
	Water	0.1	0.6	0.8	2.1
	Air	0.0	0.4	0.4	5.7
$1\text{-}C_3H_7I$	Ice	2.5	14.3	13.3	258
	Water	0.0	0.7	1.2	2.9
	Air	0.0	0.07	0.0	2.9
CH_2Br_2	Ice	2.8	22.0	12.1	1270
	Water	0.0	2.2	2.9	6.7
	Air	0.6	1.1	1.7	5.3

Table 11. Halocarbon concentrations measured by GCMS during the cruise. In total, 55 ice samples, 37 water samples and 99 air samples were analysed, average and maximum values are given , minimum values are below LoD. Values are in pM for all ice and water samples, normalised to brine volume and corrected for salinity where relevant; values are in pptv for air samples.

	CH$_3$I	C$_2$H$_5$I	CHBr$_3$	CH$_2$ICl	2-C$_3$H$_7$I	CH$_2$IBr	CHBr$_2$Cl	1-C$_3$H$_7$I	CH$_2$Br$_2$
20th %	0.9	7.3	16.1	0.6	0.7	0.0	2.2	2.5	2.2
Average	3.9	30.9	189	3.2	3.36	3.2	5.8	14.4	5.3
80th %	8.6	30.5	166	4.8	3.5	3.2	9.4	12.2	7.9
Max	10.9	207	937	11.0	21.9	28.9	15.1	98.3	10.7

Table 12. Halocarbon concentrations in 12 samples of visibly discoloured diatom-rich ice from the Weddell Sea. Values have been brine volume normalised and salinity corrected. Minimum values are below LoD except for CH$_3$I (0.28 pM) and C$_2$H$_5$I (3.1 pM).

	CH$_3$I	C$_2$H$_5$I	CHBr$_3$	CH$_2$ICl	2-C$_3$H$_7$I	CH$_2$IBr	CHBr$_2$Cl	1-C$_3$H$_7$I	CH$_2$Br$_2$
20th %	1.3	5.3	56.3	0.0	0.0	0.0	2.1	2.5	3.8
Average	5.7	30.4	351	16.1	16.4	9.4	7.5	14.3	38.7
80th %	3.5	23.2	368	4.9	5.5	0.0	10.1	14.1	13.5
Max	149	739	6850	455	311	406	49.4	258	1270

Table 13. Halocarbon concentrations in 43 samples from 4 ice cores from the sea ice of the Weddell Sea. Values have been brine volume normalised and salinity corrected. Minimum values are below LoD. Data from table 12 is not included in table 13.

The core of 7th February shows good agreement between halocarbon concentration profiles. Concentrations of most compounds are enhanced in the top 20 cm of the ice. This could be due to emissions from the ice algae community or photochemical reactions, unfortunately Chl *a* data is not available for this core. Another peak in halocarbon concentrations is seen at a depth of 70 -80 cm.

The core of 9th February shows enhanced concentrations of CH$_3$I, C$_2$H$_5$I, CHBr$_3$ and CH$_2$Br$_2$ at the ice-atmosphere interface. Another peak in halocarbon concentrations is also seen at a depth of 1 m, however this data should be treated with caution. Where the ice is over 1 m thick, two cores must be taken as the SIPRE corer is only 1 m long. It is possible that the peak in concentrations at 1 m for this core corresponds to processes associated with having to make two cores, i.e. brine pouring into the core hole from the surrounding ice, brine draining out of the first core as it removed from the ice, and the pressure of the seawater below the ice pushing water / brine up through the lower section of the ice before it is removed. Thus this 'peak' may be an artefact of the sampling method.
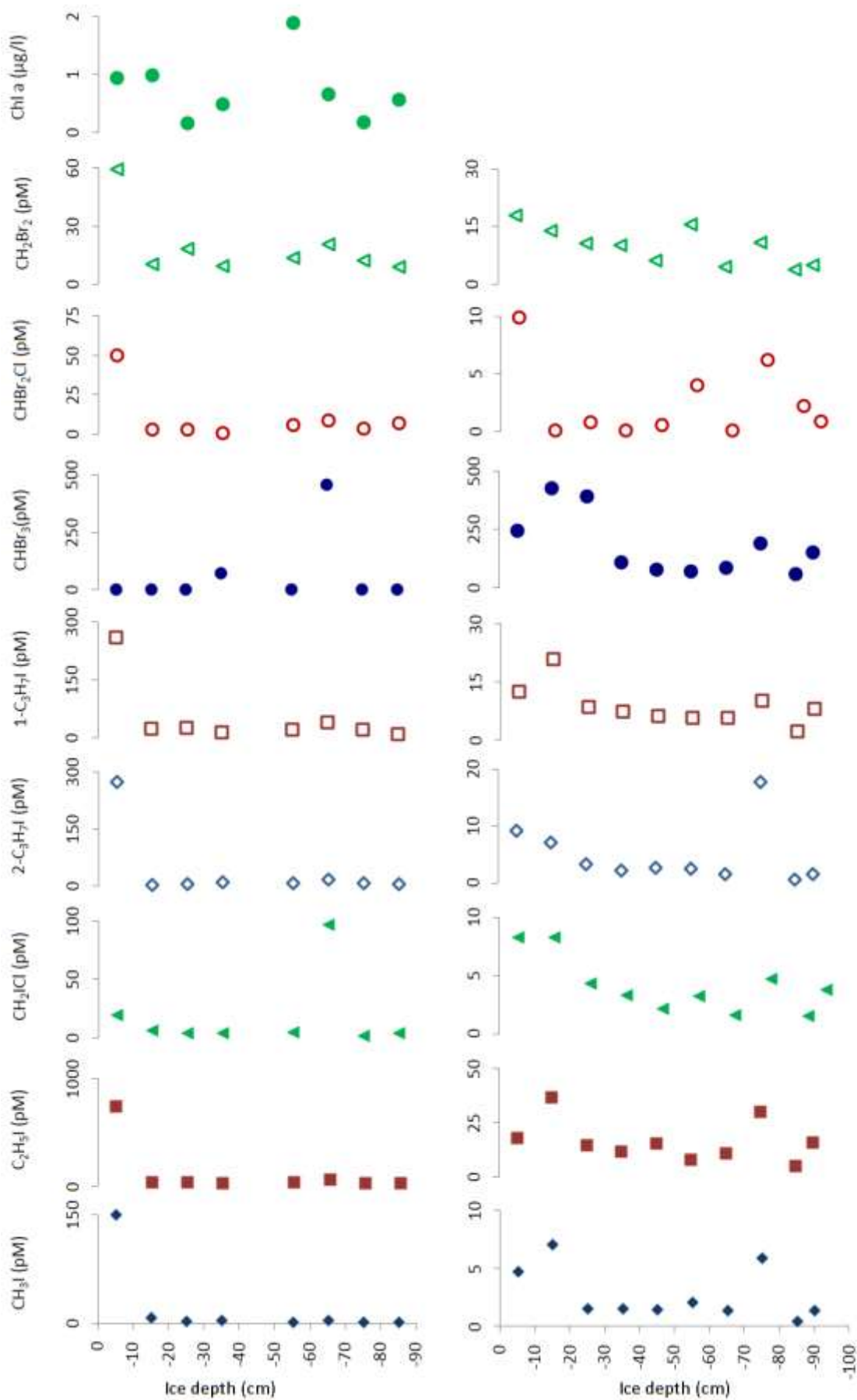
Figure 45. Vertical profiles of Chl *a* and halocarbons in sea ice on 5th Feb (left panel) and 7th Feb (right panel), Values have been normalised to brine volume and salinity corrected as described in the text. CH₂IBr concentrations were below the LoD. Note the change in scale.
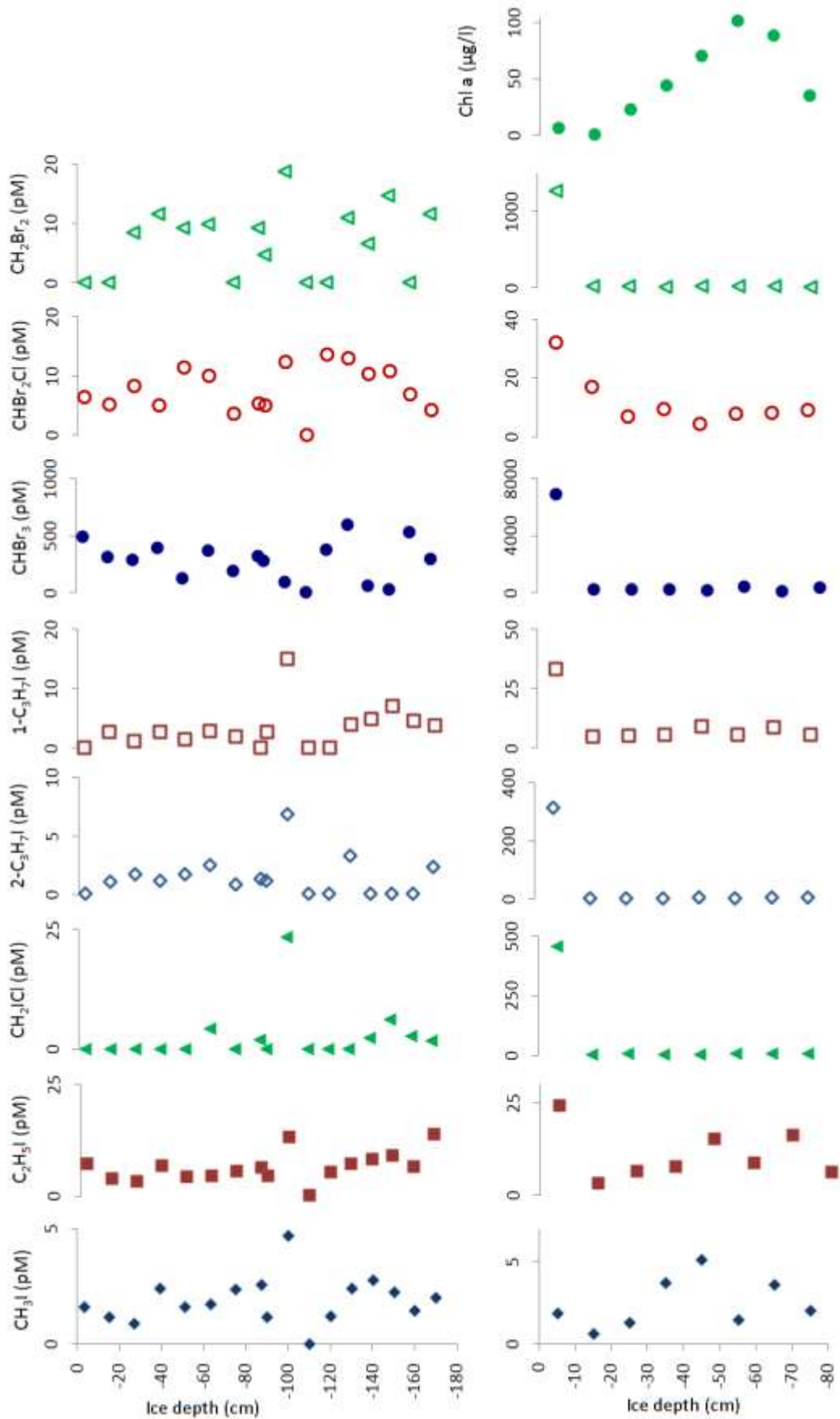
Figure 46. Vertical profiles of Chl *a* and halocarbons in sea ice on 9th Feb (left panel) and 13th Feb (right panel). Values have been normalised to brine volume and salinity corrected as described in the text. CH₂IBr concentrations were 406 pM in the top section of the core of 13th Feb and below the LoD in all other samples. Note the change in scale.

The core of 13th February shows an enhancement in most compounds close to the surface of the ice. This core was collected in a slightly different way to the others – the small boat was used to get close to an ice floe where an area of high algal biomass was visible close to the ice–air interface. The core remained inside the corer until back on board the ship, where it was then cut up and subsamples were taken as before. Whilst the halocarbon concentrations would suggest that the diatom rich layer was sampled, the Chl *a* concentrations do not support this. However different species will dominate throughout the ice thickness which may not contain the same amount of Chl *a* so a comparison of the vertical profiles must be undertaken with caution. Also, horizontal migration of brine through the ice from the ice edge bloom may have occurred. Good agreement between CH_3I and C_2H_5I concentrations can be seen in the profiles for this core.

Water samples

Concentrations of halocarbons measured in samples taken from the ship's USW supply are shown in figure 47. $CHBr_3$ is the dominant bromocarbon and C_2H_5I is the dominant iodocarbon. Concentrations of bromocarbons and 1-C_3H_7I are similar to, or within the lower range of, measurements made by others in this area [*Chuck et al.*, 2005; *Fogelqvist and Tanhua*, 1995], whereas concentrations of the other iodocarbons are low (Table 1).

Concentrations of most compounds decrease as the campaign progresses, in agreement with declining atmospheric halocarbon concentrations (figure 49). The cluster of points on 5th March corresponds to the ship's passage through the Antarctic convergence zone, where concentrations of $CHBr_2Cl$ and CH_3I are enhanced.

Figure 48 compares halocarbon concentrations in water and ice samples; the potential for halocarbon concentrations to be enhanced in sea ice is clear. Mann-Whitney statistical analysis was carried on the water and ice data, iodocarbon concentrations in ice core and DRI samples are statistically similar (p values 0.32 – 0.49), whereas bromocarbon concentrations show less similarity (p values 0.029 – 0.32) whereas neither type of ice sample are similar to the seawater for any halocarbon (p values <0.0001 – 0.0044).

Air samples

Mixing ratios in air of those halocarbons which were above the LoD are shown in figure 49. The measurements made on the Brunt ice are discussed in more detail in section 5.4.4.

The concentrations of halocarbons in air appear to steadily decrease during the field campaign, with the exception of measurements made on 5th March. The steady decrease could be due to a reduction in freshly melted ice as the summer season progressed, and hence less release of halocarbons which had previously been stored in the ice. However, as the ship was moving around through variable ice cover, many other influencing factors on halocarbon release may have changed, such as phytoplankton productivity, seawater temperature, wind speed and wind direction.

On 5th March the ship sailed through the Antarctic convergence zone, the region where Antarctic seawater flowing north meets the warmer waters of the sub-Antarctic. As the cooler waters sink and the warmer waters rise, the subsequent upwelling brings nutrients to the photic zone and thus this region is very biologically productive. A wide range of halocarbon concentrations was measured on this day (figure 47), the higher concentrations may be reflective of the increased biological activity of the seas. However no clear trends were found along the ship's course or between compounds.
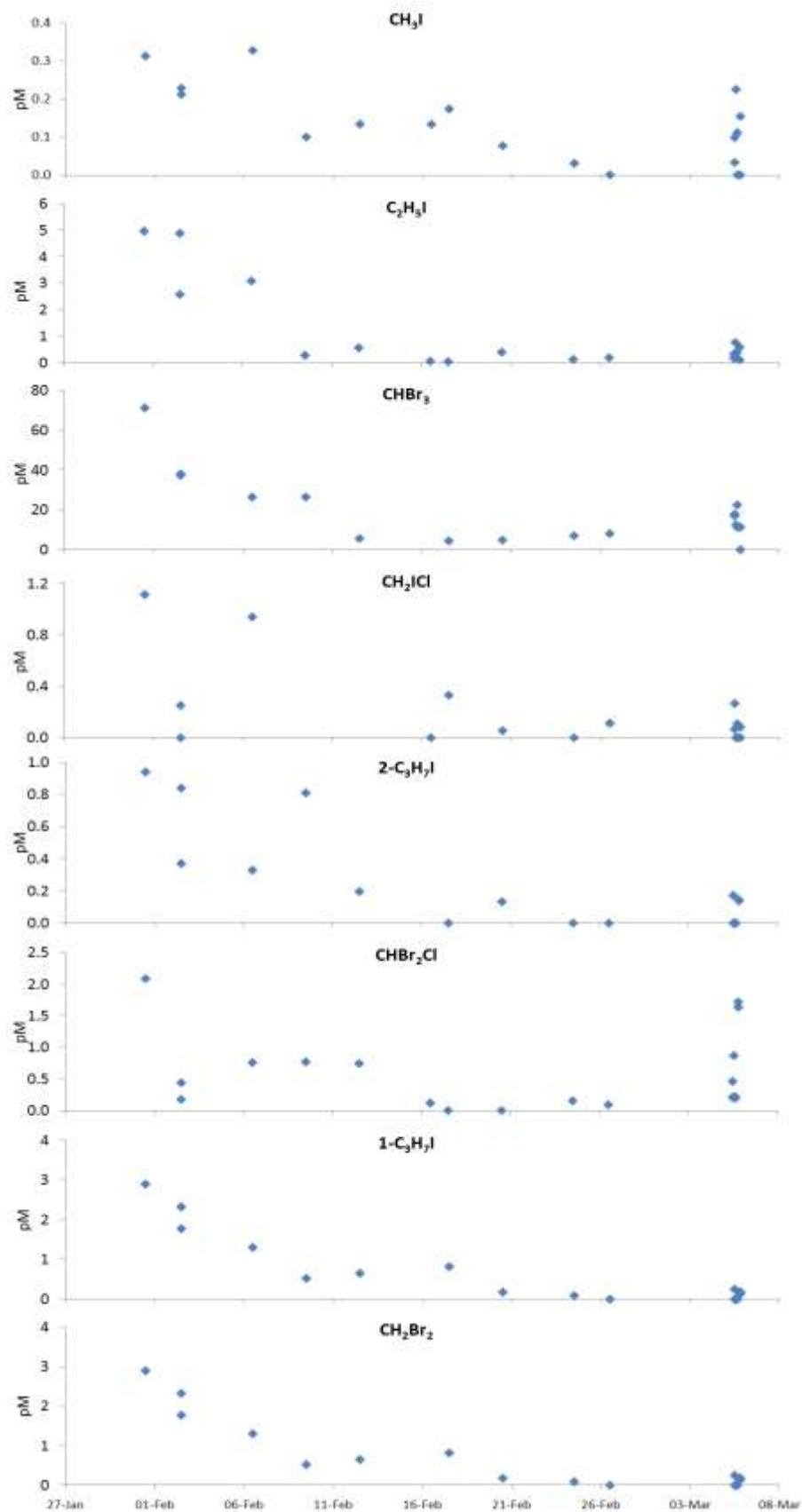
Figure 47. Halocarbon concentrations in samples taken from the ship's USW supply during the campaign. CH_2IBr was not present above the LoD in USW samples. The cluster of points on 5th March 2009 corresponds to the ship's passage through the Antarctic convergence zone.
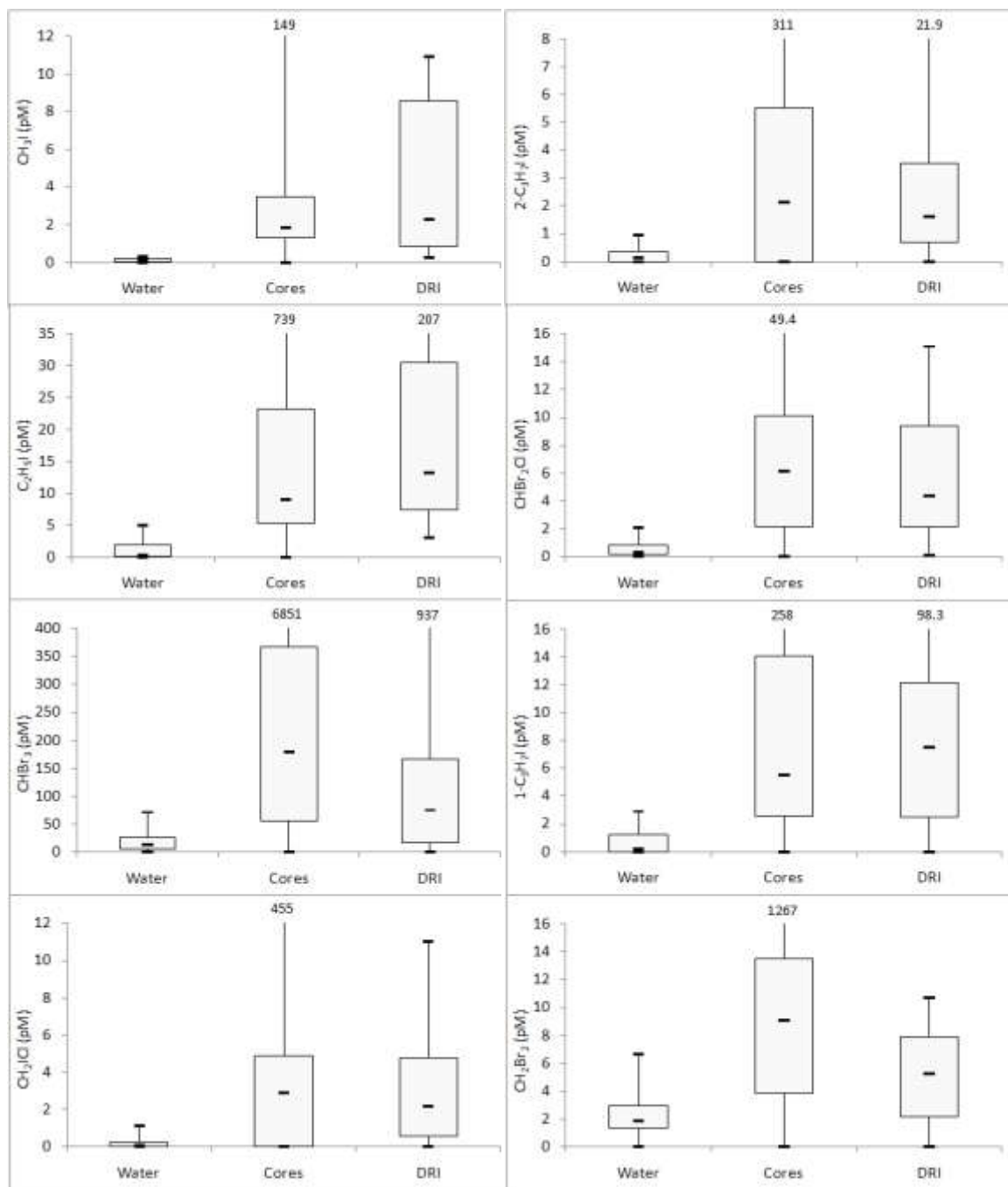
Figure 48. Box whisker plots of halocarbon concentrations in water and ice samples. Boxes represent 20th to 80th percentiles and the median is shown by the dash within the box. Where no cap is present on the range bars, the value is off the scale and given above.
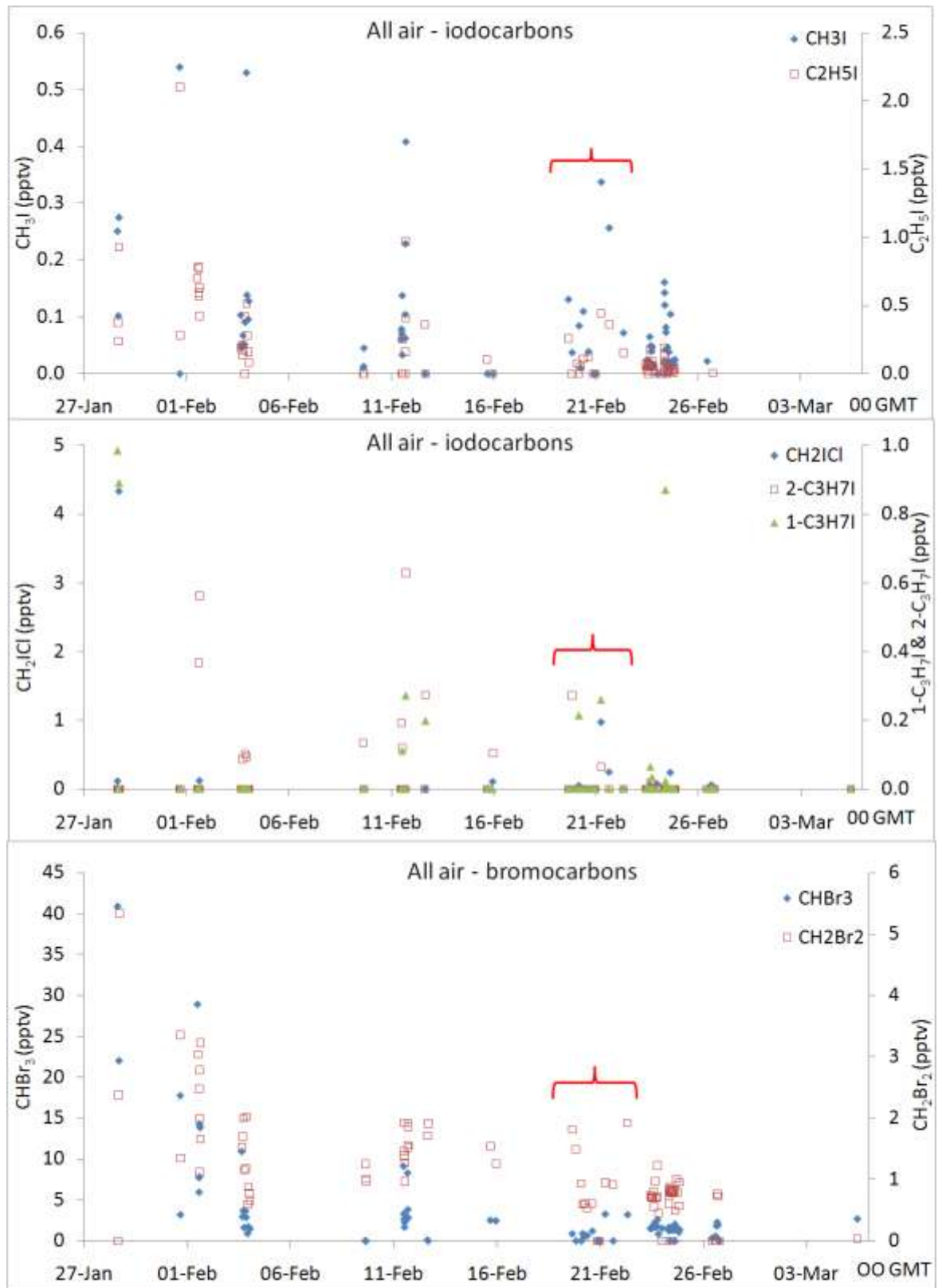
Figure 49. Halocarbon mixing ratios in air over the Weddell Sea and Southern Ocean. Measurements were made on board the ship except those denoted ⌐‿⌐ which were made on the Brunt ice shelf.

Measurement	No of samples	LoD	Average	Max	Min
I$_2$ in air (pptv)	24 x 3hours	0.095	9.8	30.9	5.9
AIC in air (pptv)	24 x 3 hours	0.029	1.9	3.8	0.7
Chl *a* in ice (µg / L)	22	0.01	2.27	9.03	0.004
Chl *a* in water (µg / L)	4	0.01	0.14	0.22	0.05
Iodide in ice (nM)	10	0.08	10.0	38.0	3.9
Iodide in water (nM)	2	0.08	61.3	97.6	25.1
Iodate in ice (nM)	10	30	19.1	50.0	5.5
Iodate in water (nM)	2	30	358	364	351
IO in air (pptv)	36 days	0.3	5.1	6.6	2.7

Table 14.Complementary measurements to the GCMS analysis during the Weddell Sea cruise.

5.4.3 Inorganic iodine compounds measured with denuder tubes

AIC (HOI + ICl) and I$_2$ mixing ratios in air were measured via denuder tubes throughout the campaign. Results are shown in figures 50 and 51 respectively. Concentrations remained reasonably constant throughout apart from a peak during the ice shelf experiment, discussed in more detail in section 5.4.4. Concentrations of the inorganic iodine compounds are two orders of magnitude higher than iodocarbon concentrations.

The mixing ratios of I$_2$ are similar to previous measurements in coastal locations where macroalgae beds are a known source of iodine. Up to 25 pptv I$_2$ was measured during the day at Mace Head, Ireland [*Saiz-Lopez and Plane*, 2004] with concurrent measurements of up to 7 pptv IO. Also at Mace Head, *Huang et al.* [2010] report daytime concentrations of I$_2$ of up to 29 pptv, with concurrent IO concentrations of up to 9.5 pptv. This however is the first time that such high I$_2$ concentrations have been made away from macroalgae beds exposed at low tide.

This technique is very new and it is not known whether some other species could be acting as an artefact in the measurement, causing artificially high data. Similar I$_2$ concentrations observed over open water and ice covered areas would suggest some

other species is giving a high background reading. If the source of the I_2 is the sea ice, then huge amounts would need to be produced for such high concentrations to be present at a height of 6 m (the height of the sampling tube on the ship). For the ice shelf experiment, the source strength would have to be higher than ever recorded. These questions are discussed further in section 5.4.9, where a modelling study has been carried out to further understand the data. If the data is to be believed, effective recycling mechanisms must be occurring which are not yet fully understood. Such large amounts of I_2, along with its much shorter photolytic lifetime, would mean this species is the dominant source of volatile iodine in the atmosphere above the Weddell Sea.
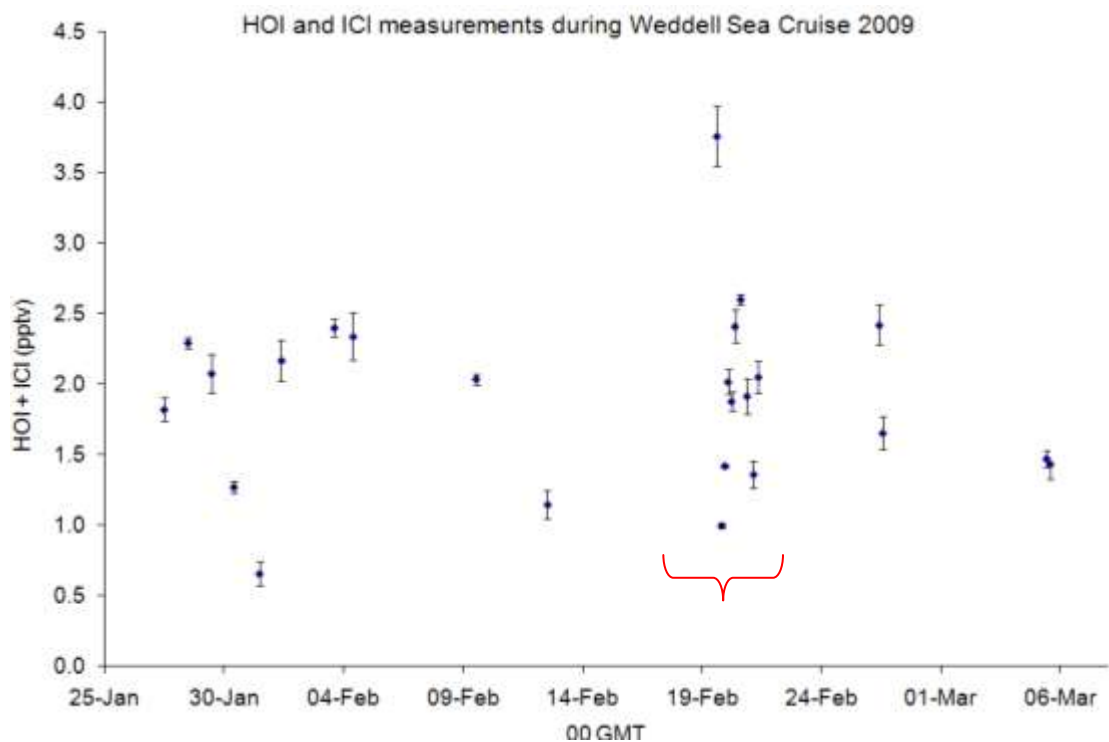
Figure 50. Atmospheric HOI and ICl concentrations during ES033. Measurements were made on board the ship except those denoted ⌣ which were made on the Brunt ice shelf. Each point denotes a 3 hour sample. Average values of pseudo-triplicate samples are shown, error bars represent 1 standard deviation.
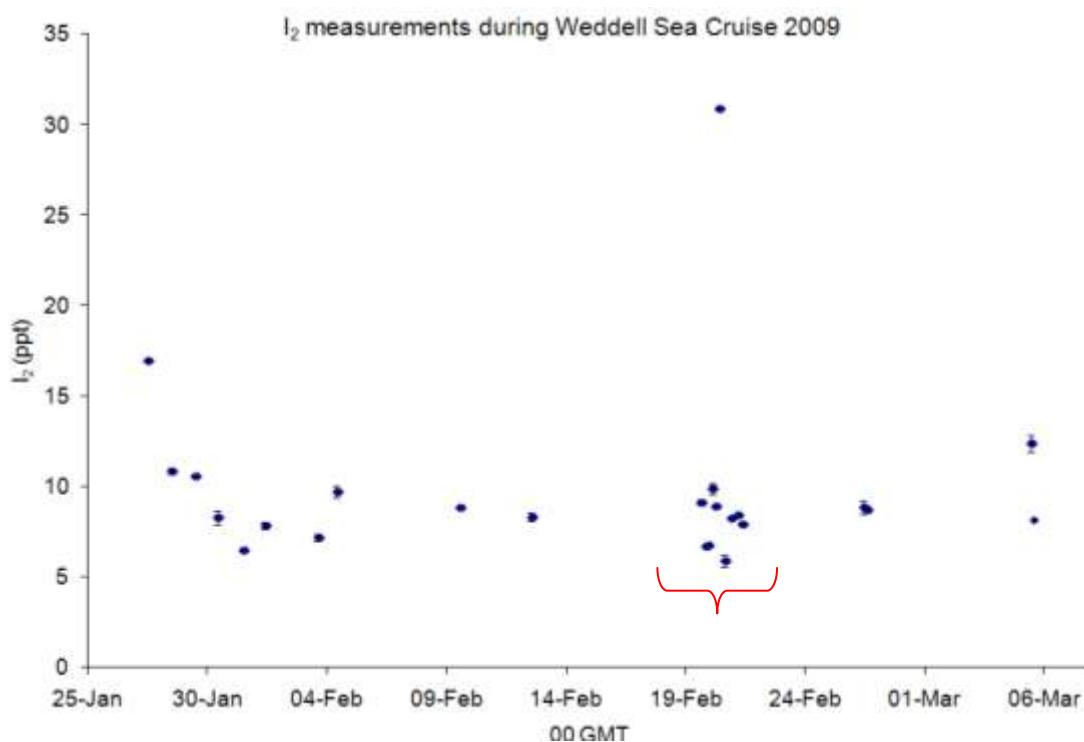
Figure 51. Atmospheric I_2 concentrations during ES033. Measurements were made on board the ship except those denoted ⌣ which were made on the Brunt ice shelf. Each point denotes a 3 hour sample. Average values of pseudo-triplicate samples are shown, error bars represent 1 standard deviation.

5.4.4 Air sampling on the Brunt ice shelf

Average mixing ratios of CH_3I, C_2H_5I, $CHBr_3$, CH_2ICl, $CHBr_2Cl$, and CH_2Br_2 in air measured on the Brunt Ice shelf were 0.09, 0.13, 0.89, 0.11, 0.48, and 0.87 pptv respectively, shown in more detail in figure 52. The iodocarbons 1- and 2-C_3H_7I were only observed above the LoD twice during this period, values were <0.3 pptv, and CH_2IBr was only observed above the LoD once at 0.06 pptv. The lower concentrations of the more labile iodocarbons are undoubtedly due to their shorter atmospheric lifetimes with respect to photolysis. CH_3I mixing ratios are in good agreement with those measured by Graham Mills (unpublished data via private communication, Anna Jones, BAS) during the CHABLIS field campaign, 13 km away from the sampling site used in this study (at the CASlab, 1 km SW of Halley) during 2004-2005. AIC and I_2 mixing ratios above the Brunt Ice shelf are shown in figure 53. Concentrations of AIC remain reasonably constant during the experiment; average mixing ratios are 2 pptv. I_2 mixing ratios also remain constant at around 8 pptv with the exception of the measurement made from 09:11 to 12:11 GMT on 20th February.

When the iodocarbon emissions are compared to wind direction and I_2 concentrations (figure 54), it looks as though the organic and inorganic iodine compounds have a similar source. When the wind is from the east concentrations of all compounds are low. The wind then swings round, via the south (and over the open water in between the ice shelf and the sea ice), to the south-west. This momentary southerly wind corresponds to a burst of I_2. AIC concentrations are enhanced during south westerly winds, concentrations of I_2 and iodocarbons remain low until another change in direction, again via the south, which corresponds to a burst in iodocarbons. Concentrations then drop back down to a low level.

It is possible that the peak in I_2 concentrations during the first burst of southerly wind had a corresponding enhancement in atmospheric iodocarbon concentrations which was not detected due to the different sampling times and frequencies (samples for halocarbon analysis were taken for 10 minutes once every 3 hours whereas air samples for I_2 analysis were continuous, with a new tube deployed every 3 hours). However a peak in halocarbon concentrations does not correspond to a peak in I_2, though a small peak may have been disguised by the longer sampling time.

As can be seen from figure 60, an area of open water is present in between the sea ice of the Weddell Sea and the ice shelf flowing off the Antarctic continent. Unique species of diatom flourish is this environment which may be responsible for I_2 emissions, this is discussed further in section 5.5. As the lifetime of I_2 is a few seconds or less at noon at this latitude, the source has to be extremely close to the sampling site, so the ice edge or the snowpack must be responsible.

The source of iodine compounds remains unknown over the Antarctic continent, but, whilst it is accepted that it is difficult to draw definite conclusions from one point, these measurements support the hypothesis that the continental snowpack may release reactive iodine, as inferred by recent measurements of extremely high concentrations of IO in Antarctic snow firn air [*Frieß et al.*, 2010]. One possible source is aerosol deposition and recycling on the snowpack, as suggested by a recent modelling study [*Saiz-Lopez et al.*, 2008] on data from IO concentrations of up to 20 pptv measured close to this location on the Brunt ice shelf [*Saiz-Lopez et al.*, 2007a]. Back trajectories, shown in figure 55, are in agreement with the wind direction data in figure 53.
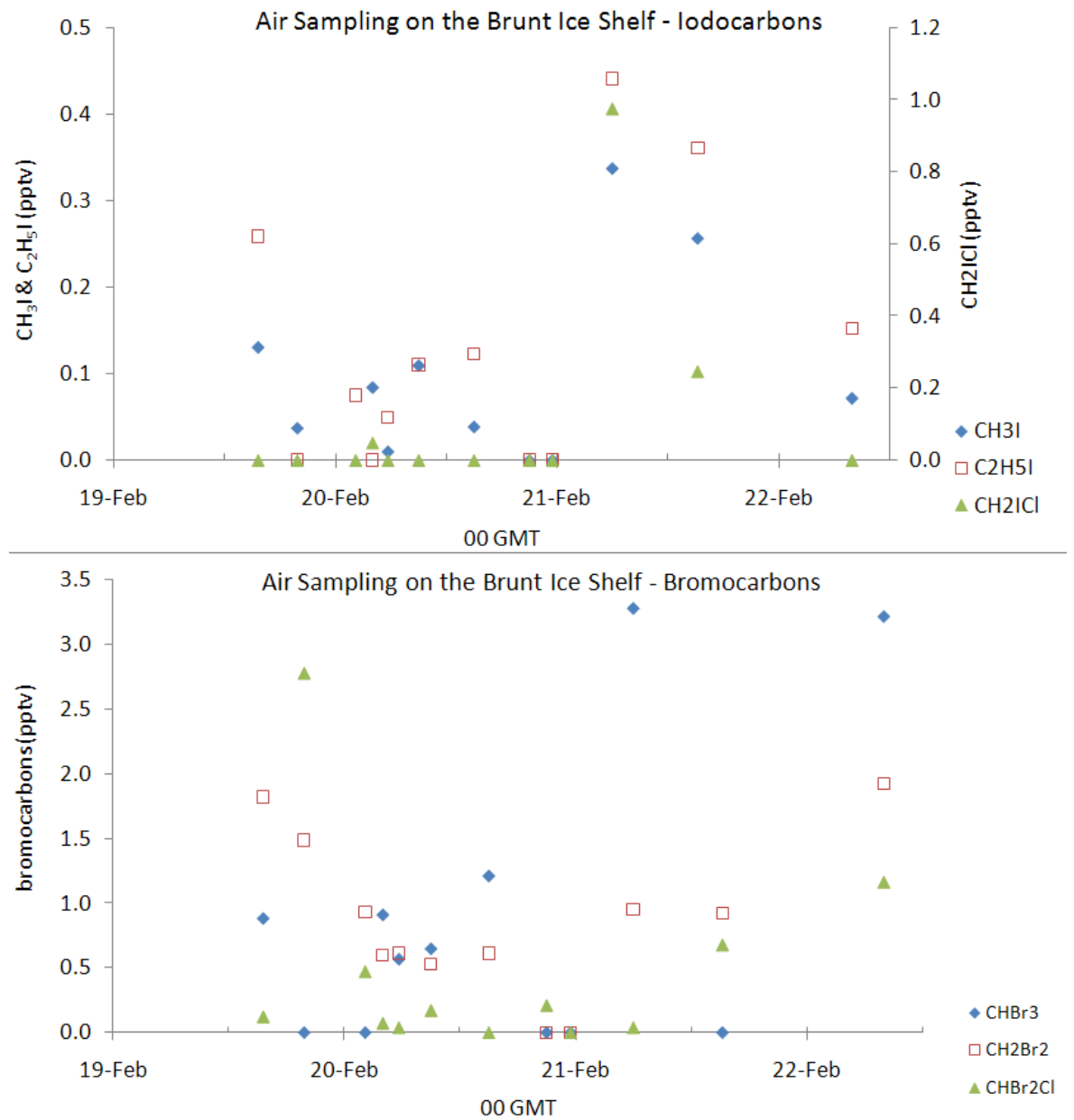
Figure 52. Iodocarbon (top panel) and bromocarbon (bottom panel) concentrations in air measured on the Brunt ice shelf at 75.4°S 26.6°W. Each sample represents average concentrations of a 10 minute sampling period.
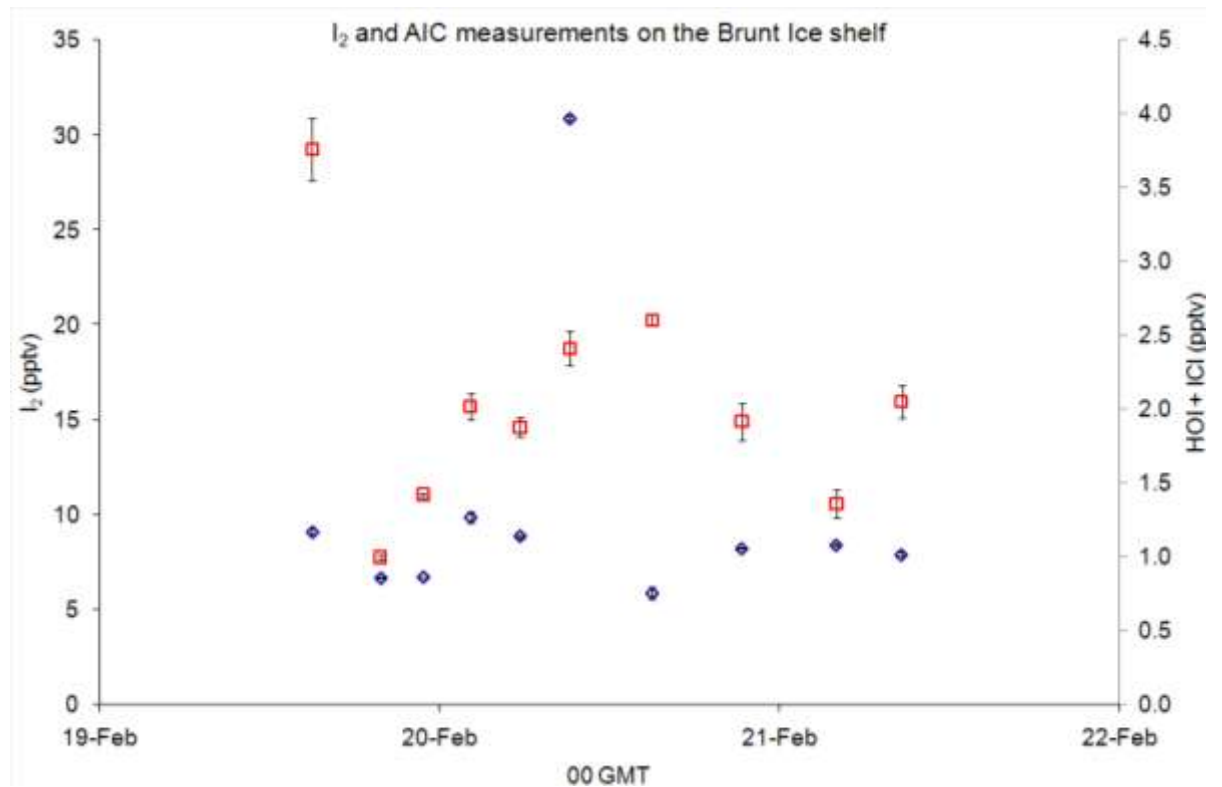
Figure 53. Concentrations of AIC (red squares) and I$_2$ (blue diamonds) in air measured on the Brunt ice shelf at 75.4°S 26.6°W. Each point denotes a 3 hour sample, the mid-sampling time is shown.

There are no pulses in ozone (figure 54) which would cause a burst in I$_2$ due to an increase in the reaction of iodide with ozone in surface seawater, instead, short ozone depletion events are witnessed, as would be expected from such high concentrations of atmospheric iodine. No major ozone depletion event is associated with the burst in I$_2$, but the ozone was measured from the ship, upwind of the air sampling site on the Brunt ice shelf; if the I$_2$ is being emitted from the snowpack the ozone depletion would thus not have been detected. Any I$_2$ emissions from the ice edge may not have yet depleted the ozone in the air mass before it reached the ship.
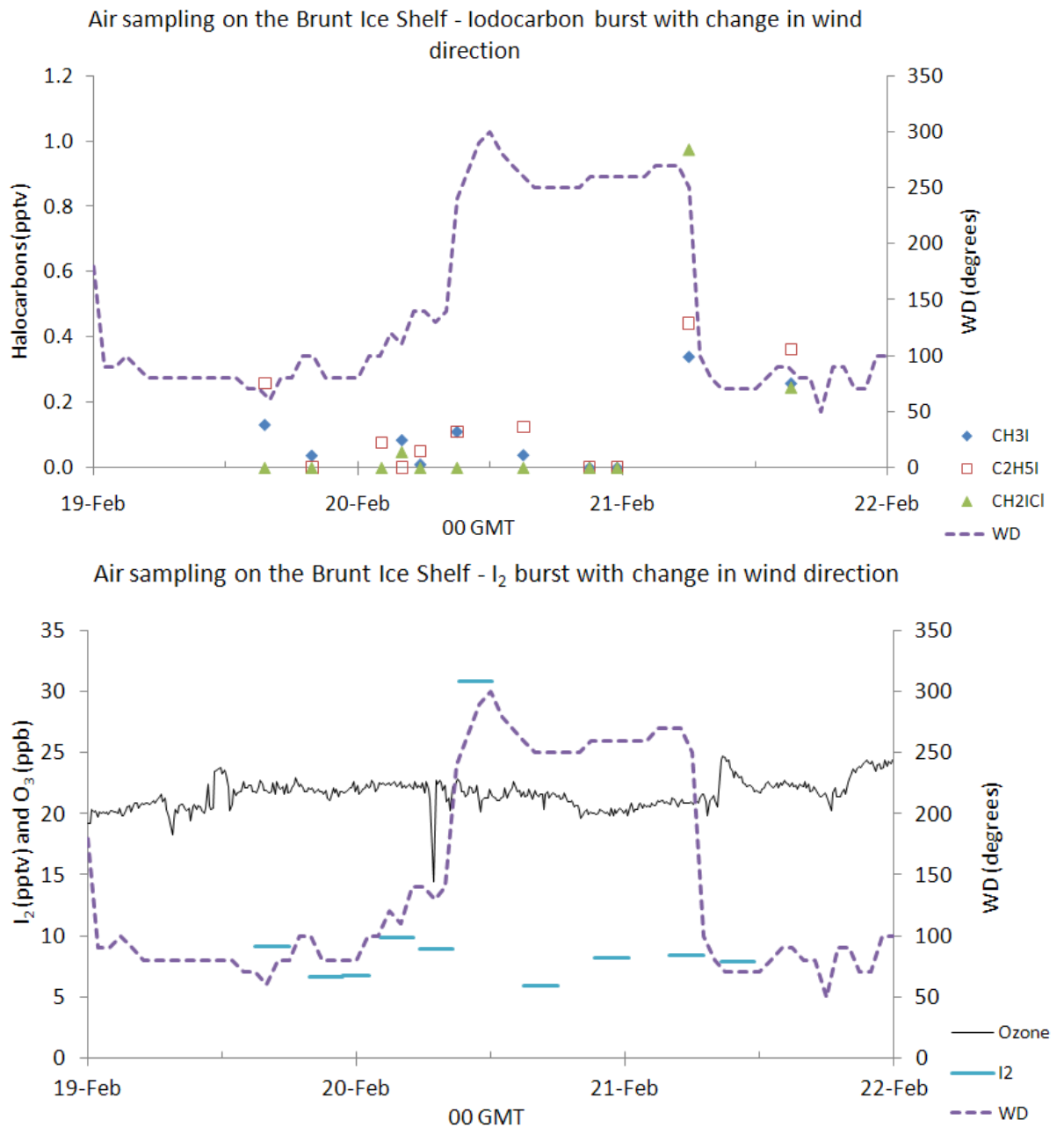
Figure 54. Atmospheric iodocarbon (top panel) and I_2 (bottom panel) concentrations with corresponding wind direction and ozone concentration. Back trajectories are shown in figure 55 for comparison.
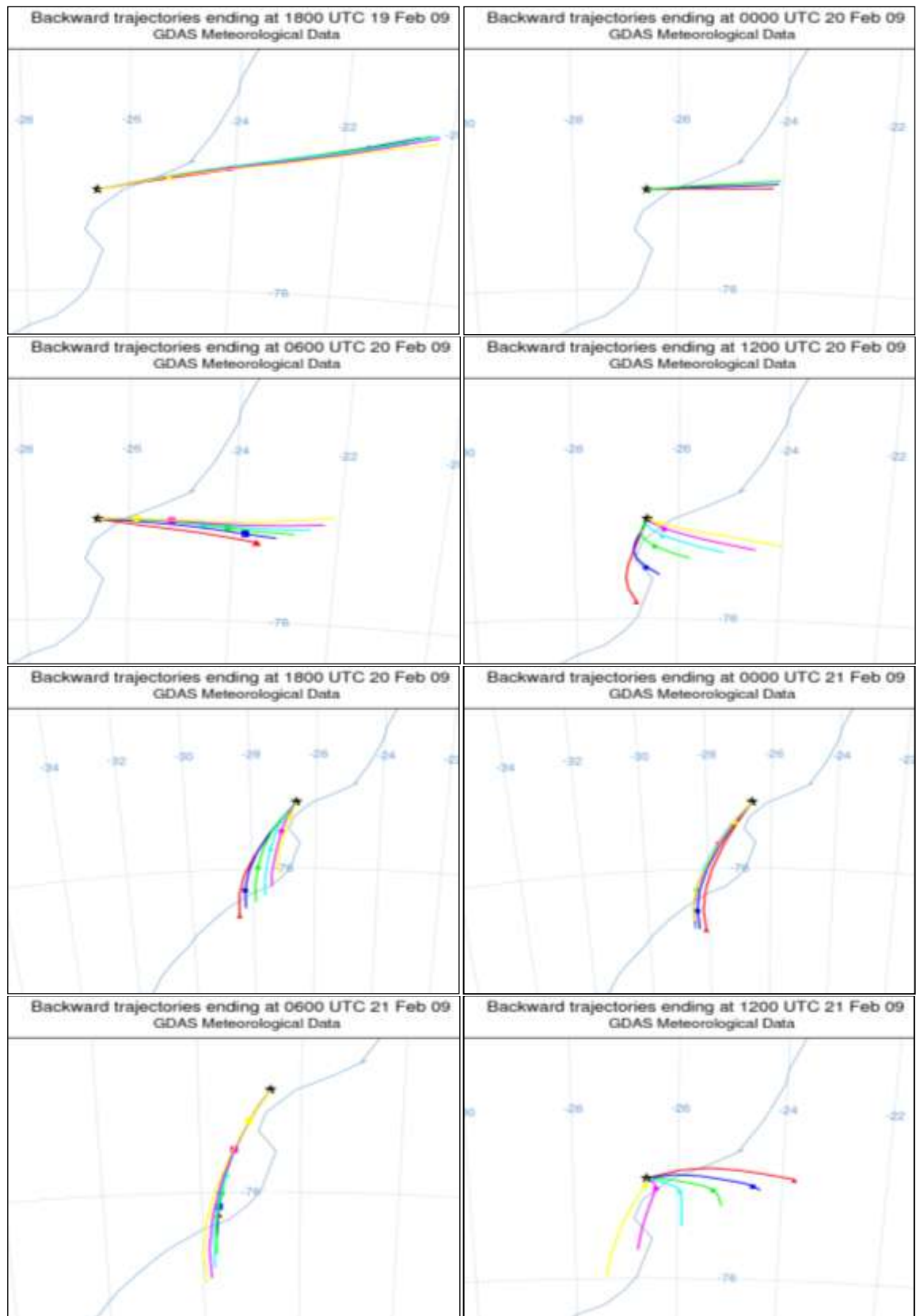
Figure 55. Hourly back trajectories for air masses reaching the Brunt ice shelf from 1200 GMT 19th Feb to 1200 GMT 21st Feb. The movement of the air parcels for 6 hours previous to: ▬ the time shown in the chart title, and ▬ 1 hour, ▬ 2 hours, ▬ 3 hours, ▬ 4 hours and ▬, 5 hours before this, respectively. Courtesy of the NOAA HYSPLIT model

Emissions from the snowpack?

Halocarbon concentrations measured via a sampling tube pushed 20 cm into the snowpack on the Brunt ice shelf are shown in figure 56. CH_3I and C_2H_5I concentrations show a diurnal profile with values of up to 0.48 and 0.98 pptv respectively. These concentrations are enhanced with respect to those measured 1 m above the snowpack (figure 54) at the same location. These results suggest the snowpack is a source of these compounds, and the lower concentrations at night are due to the lower solar flux as the sun is lower in the sky and lifetimes of the compounds will be longer. These measurements are in good agreement with those of *Swanson et al.* [2007], who measured enhanced concentrations of CH_3I and C_2H_5I in the snow interstitial air at the South Pole compared to the atmosphere above. Bromocarbon concentrations are similar to those in the boundary layer, and concentrations of the other halocarbons were below the LoD.
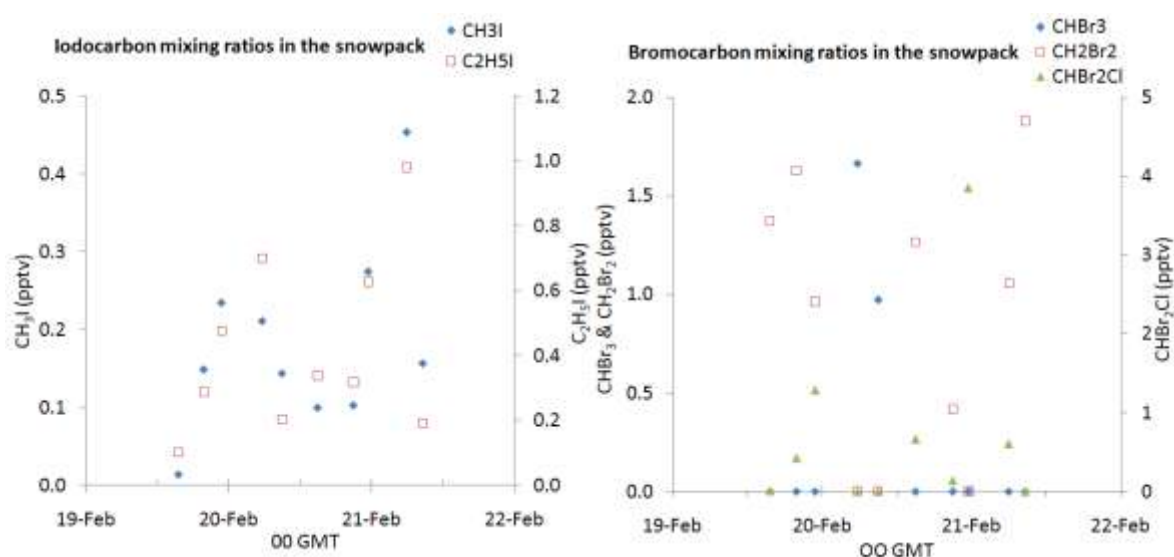
Figure 56. Halocarbon concentrations measured by drawing air through a Teflon-lined tube pushed 20cm into the snowpack of the Brunt ice shelf.

5.4.5 IO by mini MAX-DOAS

Figure 57 shows IO vertical column densities of $0.16 – 0.37 \times 10^{13}$ molecules / cm^2 in the boundary layer on sunny days. If IO were evenly distributed in a well mixed boundary layer, to 200 m altitude similar to that given by Renfrew & King (2002), this would result in 3 – 7 pptv IO. However, if the main contribution to IO is I_2 then the IO may not be well mixed in the boundary layer. Also, the assumption would have to be made that no recycling was occurring on snow and ice surfaces, and the results presented here suggest otherwise. It is however useful to consider IO mixing ratios

when the modelling study was employed (section 5.4.9) and when comparing this data to those of others.

Gaps in the IO measurements are due to bad weather, ship's motion causing the instrument to be directed at the water or ice, instrument failure, or the passage of people in front of the instrument, being positioned as it was close to a doorway.
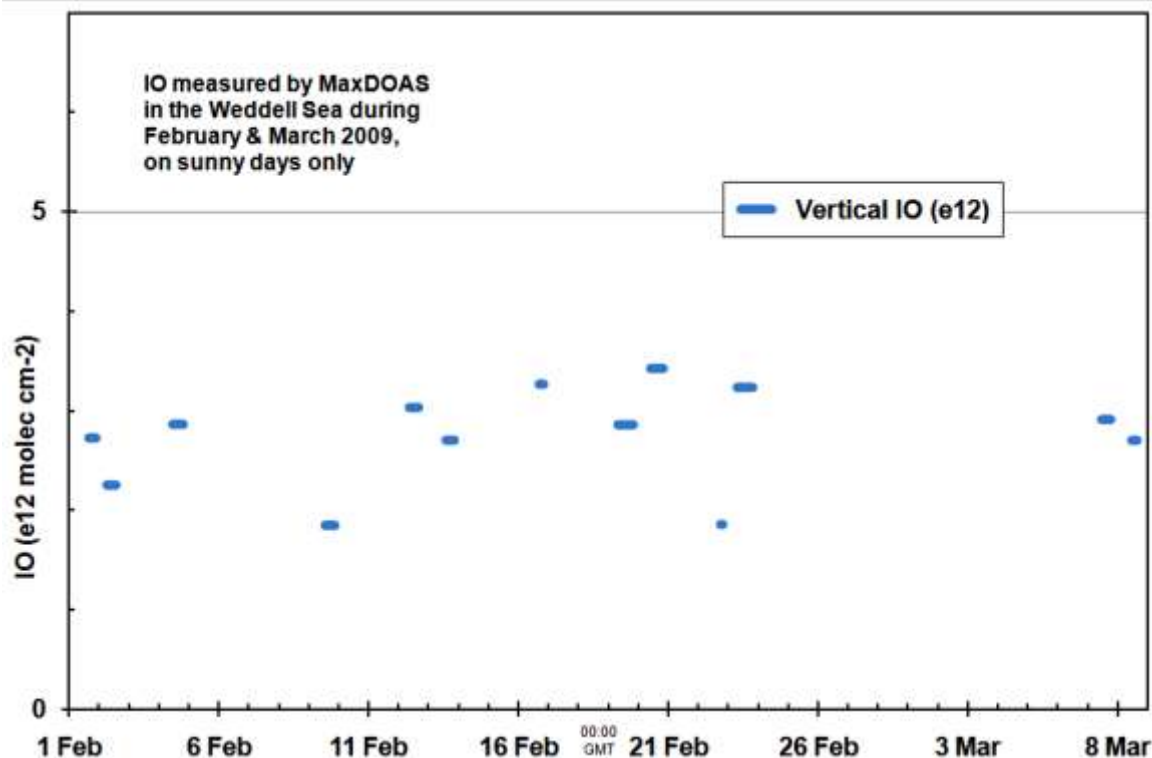
Figure 57. IO vertical column densities above the sea ice of the Weddell Sea.

5.4.6 IO by satellite

IO concentrations measured by the SCHIAMACHY instrumentation are shown in figures 58 and 59. Values of up to 1.8×10^{12} molecules cm^{-2} are lower than those measured by the ship-based MMD (of up to 3.7×10^{12} molecules cm^{-2}), the possible reasons for this are discussed in section 5.5. The satellite results reveal the striking agreement between IO mixing ratios (figures 58 and 59) and average ice area (figure 60) of the Weddell Sea during the campaign period.
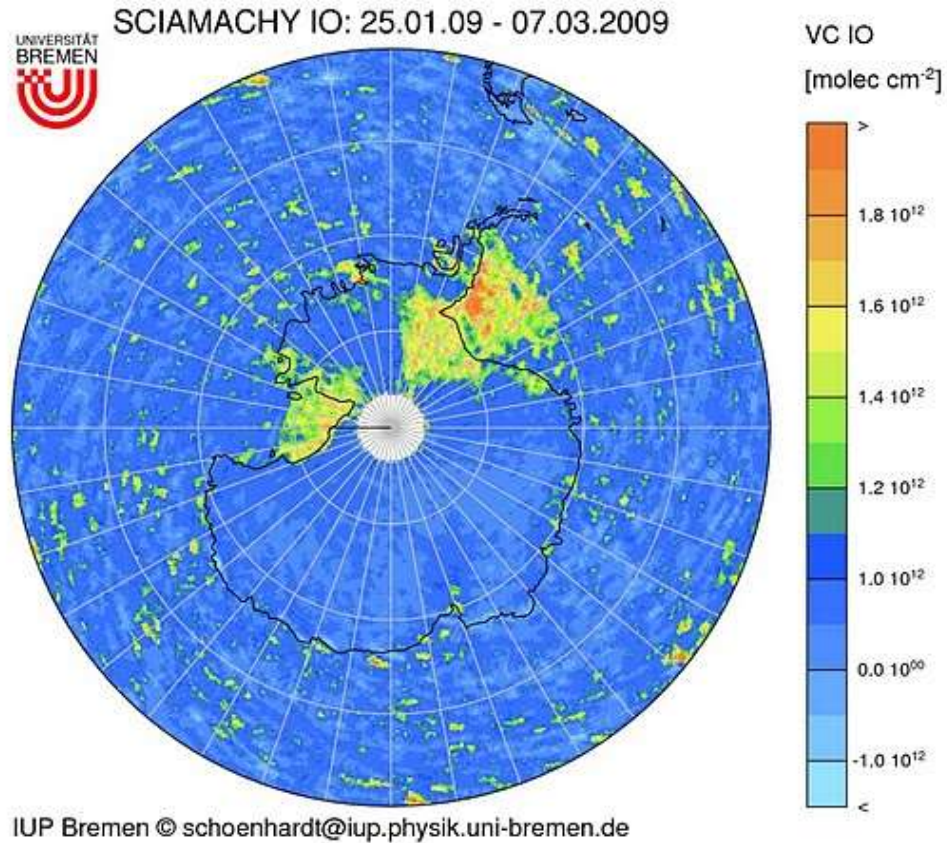
Figure 58. Average IO vertical column densities over Antarctica measured by satellite for the campaign period 25th January – 7th March 2009.
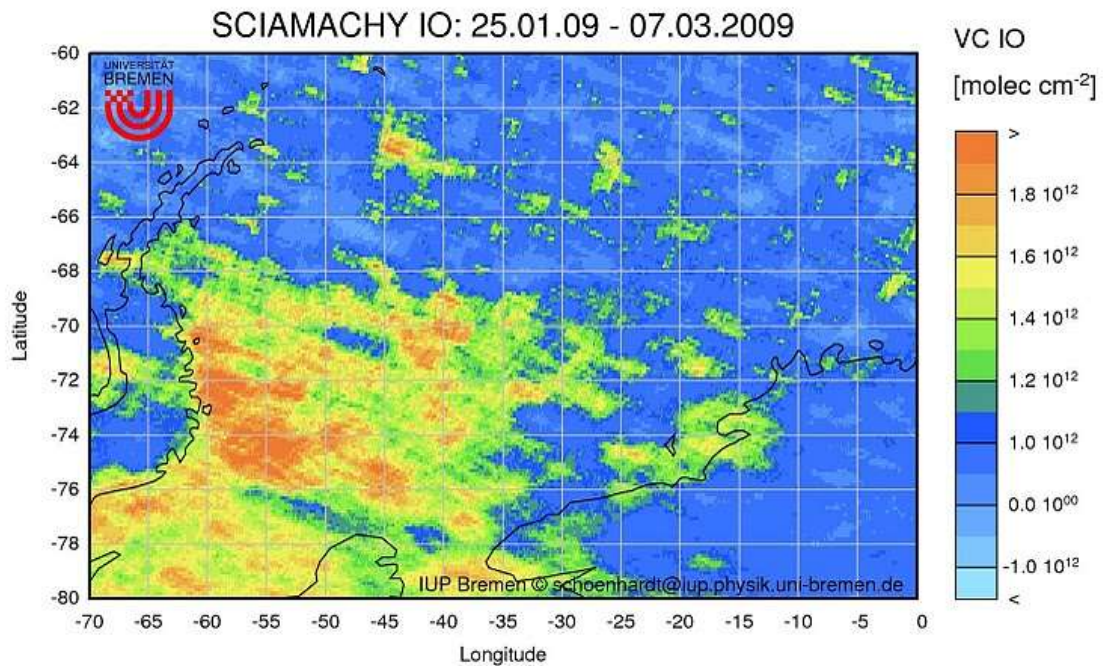
Figure 59. Average IO vertical column densities over the Weddell Sea measured by satellite for the campaign period 25th January – 7th March 2009.
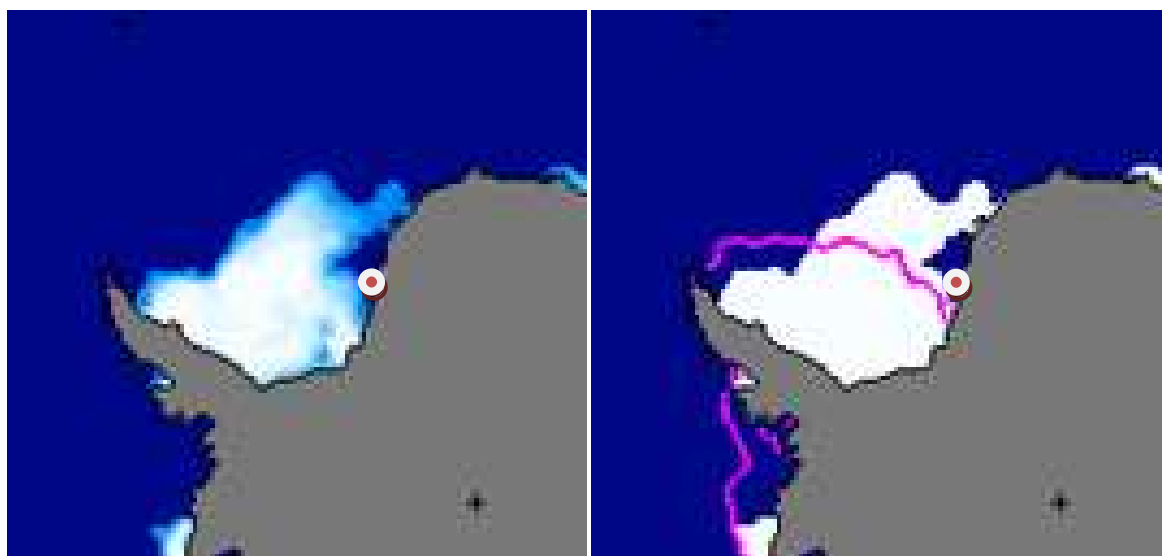
Figure 60. Average ice coverage (left hand panel) and extent (right hand panel) for February 2009, courtesy of NSIDC. The circle denotes the location of the sampling site.

5.4.7. Iodide / iodate concentrations

A selected number of samples were analysed for iodide and iodate concentrations by Rosie Chance (University of York and UEA). One ice core (13th Feb) comprising 8 samples corresponding to discrete 10 cm depths through the ice, 4 diatom-rich ice and 2 water samples from the ship's USW supply. Results from the core are shown in figure 61 and from the seawater in table 15. In the diatom-rich ice samples, iodide concentrations were 18.8 ± 9.9 nM (brine volume normalised and salinity corrected) in one sample, and below the LoD in the other three; iodate concentrations were below the limit of detection in all diatom-rich ice samples. Iodide concentrations in the underlying seawater were 25.1 ± 3.2 nM whereas iodate concentrations were 351 – 364 ± 9 nM. Therefore there is no enhancement of iodide in this ice, but there is severe depletion of iodate. This has been observed previously by others in sediments [*Francois*, 1987], and marine aggregates (*Hughes et al.* manuscript in preparation).

Results from the ice core show a C-shaped profile for iodide concentrations, typical of compounds produced by diatoms in Southern Ocean sea ice which is biologically rich both close to the surface and the ice-water interface. The converse is true for iodate concentrations, which are similar to those of the underlying seawater at 10-30 cm depth where Chl *a* is low, but depleted close to the surface and below 30 cm where Chl *a* is higher.

In the seawater samples, iodate remains constant at around 350nM, iodide concentrations are much higher on the 24th February than on the 16th February; this is interesting as the ship was sailing north up the ice edge on the 24th February, whereas on 16th February the ship was surrounded by sea ice. Chl *a* concentrations were four times higher on 24th February, 0.22 µg l^{-1} compared to 0.54 µg l^{-1} on 16th February.

In the most biologically rich samples (this core and DRI samples) total iodine is depleted by half or more with respect to background seawater concentrations. This could be due to previous volatilisation by the sea ice community as has been suggested by *Saiz Lopez and Boxe* [2008], uptake to the diatom particulate, or reaction with organics. The results are consistent with 'missing iodine' observed by *Chance et al.* [2007] and measurements made by *Bluhm et al.* [2010] which showed iodide depletion in surface waters when Chl *a* levels were high, the bloom was in progress and diatoms will have been in their exponential growth phase, backed up by laboratory studies.
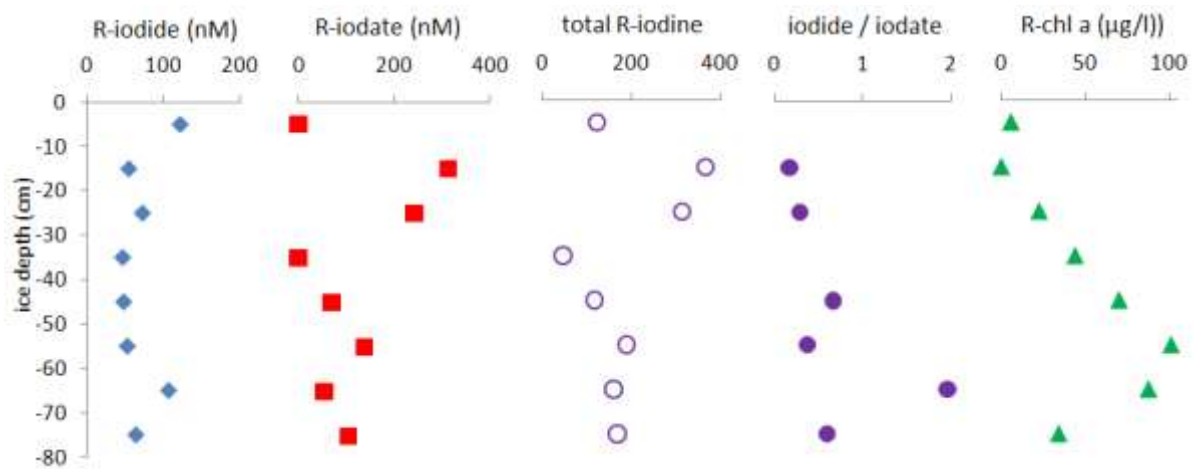
Figure 61. Rationalised iodide, iodate and Chl *a* concentrations in the ice core of 13th March. Values have been normalised to brine volume and corrected to salinity. Total iodine (iodide + iodate) and iodide / iodate ratios are also shown.

Date	iodide	error	iodate	error	total	error	iodide / iodate	error
16th Feb	25.1	3.2	364.1	9.7	389.2	50.4	0.069	0.009
24th Feb	97.6	6.3	351.2	9.6	449.8	31.4	0.278	0.019

Table 15. Iodide and iodate concentrations in two Weddell Sea water samples, all values are in nM.

5.4.8. Particles

A previous field campaign [*Davison et al.*, 1996a] in the Weddell Sea along a similar path found increased new particle formation in areas of broken Weddell Sea pack ice, and no clear correlation to dimethyl sulphide, which was assumed at that time to be the controlling chemical species in new particle bursts. It is now know that iodine oxides are capable of growing to form new particles [*O'Dowd et al.*, 2002]. Iodine emissions from sea ice diatoms disturbed by passage of the ship may be responsible, with a clear implication in polar regions if they become CCN and thus have a positive climate feedback role.

A few words about the effect on the ice as the ship travels thorough it are prudent here. The ice breaker forges a path through the ice by driving its bow up onto the ice, and the ice is broken under the weight of the ship. This often causes the surface of the ice to become flooded with seawater which is coloured orange-brown by diatoms. Often, the snow and upper ice layer slide off, exposing the gap layer beneath, and large blocks of ice may also be overturned, exposing bottom communities. Therefore, any compounds produced by the diatoms will have chance to escape.

Particle number and size data was measured throughout the cruise (by Dr B Davison, Lancaster University) using a Grimm SMPS with size measurements range of 9.8 to 1000 nm. Periods of particle production were identified by aerosol size spectra on nine days, with periods of known contamination and slow ship movement being taken into consideration. New particle production was observed generally as the ship travelled through sea ice. Figure 62 shows particles growing into the measured range >9.8nm followed by growth over approximately 30 minutes to an aerosol size of approximately 40 nm, in line with classic "banana-shaped" aerosol growth.

Particle number size distribution,13 Feb 2009
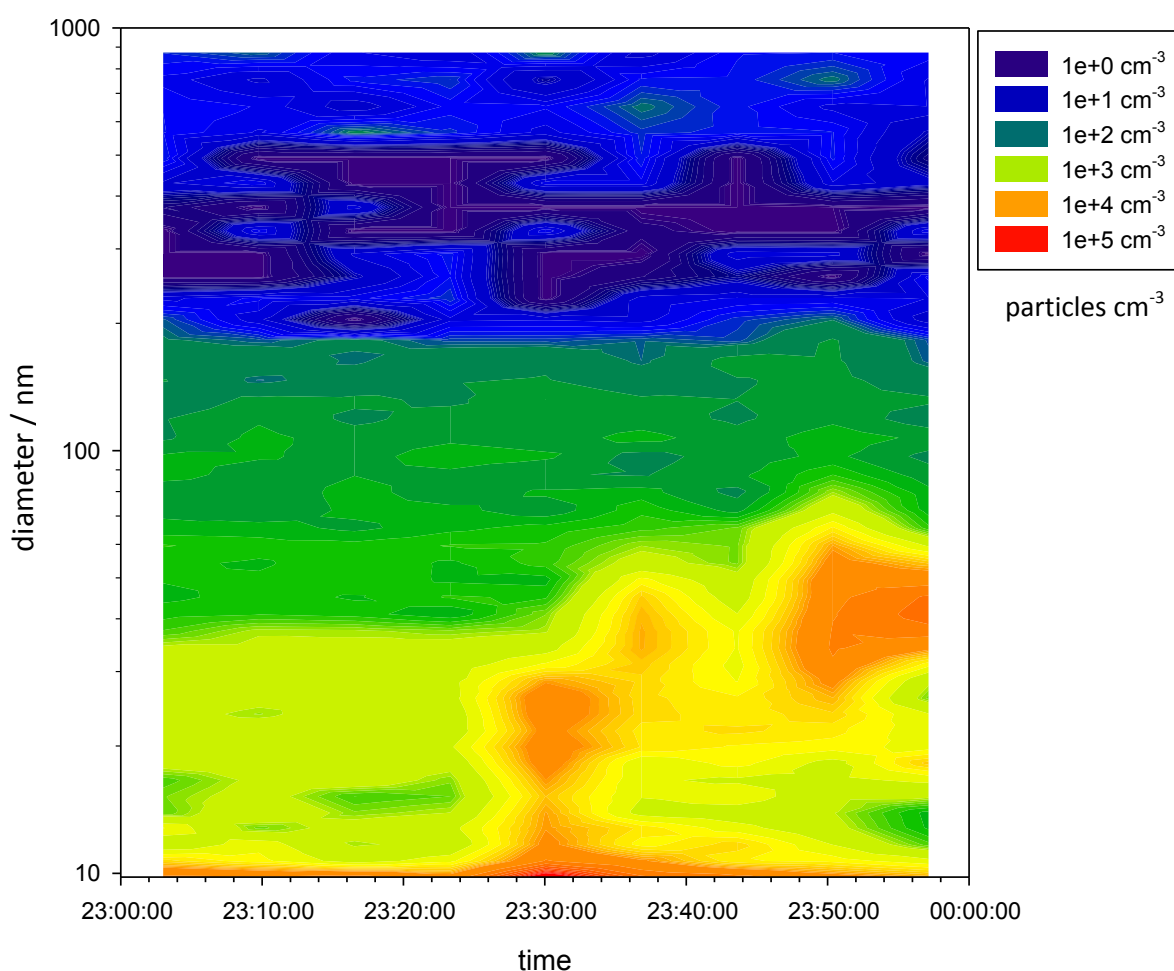
Figure 62. Particle number size distribution showing new particle formation the ship broke through the sea ice of the Weddell Sea on the 13th February. Courtesy B. Davison, Lancaster University.

5.4.9. Saturation anomalies, flux calculations and modelling results

Saturation anomalies are shown in table 16 and results from the flux calculations are shown in table 17. Average (and range) fluxes calculated for the iodocarbons were 0.6 (-0.1 to 3.8), 1.5 (-0.1 to 2.8), -1.3 (-15.2 to 2.9), 0.7 (-0.1 to 4.8) and 1.0 (0 to 3.8) nmol/m²/day for CH_3I, C_2H_5I, CH_2ICl, 2-C_3H_7I and 1-C_3H_7I respectively (CH_2IBr concentrations were below the LoD in most air and water samples) whereas average (and range) bromocarbon fluxes were -6.6(-130 to 110), -5.4 (-62 to 4.6) and -4.2 (-39 to 13) nmol/m²/day for $CHBr_3$, $CHBr_2Cl$ and CH_2Br_2 respectively. A negative flux represents an atmosphere to sea flux. The predominant trend is for iodocarbons (with the exception of CH_2ICl) to be released from the ocean and bromocarbons to be deposited from the atmosphere. This result may also go some way towards explaining the enhancement of iodine over bromine in the polar atmosphere.

	CH$_3$I	C$_2$H$_5$I	CHBr$_3$	CH$_2$ICl	2-C$_3$H$_7$I	CHBr$_2$Cl	1-C$_3$H$_7$I	CH$_2$Br$_2$
Ave	351	247	-21	-64	595	-37	479	95
Max	1683	674	31	-32	1761	240	715	954
Min	-38	-464	-67	-97	4	-305	243	-77

Table 16. Saturation anomalies (%) based on simultaneous air and water concentrations

	CH$_3$I	C$_2$H$_5$I	CHBr$_3$	CH$_2$ICl	2-C$_3$H$_7$I	CHBr$_2$Cl	1-C$_3$H$_7$I	CH$_2$Br$_2$
31/01	0.012	1.54	-11.5	-15.2	0.372	0.773	0.811	-1.48
01/02	3.82	2.80	-129	-0.424	0.137	-62.5	3.78	-38.8
03/02	0.596	2.18	-81.4	0.000	1.91	0.531	0.000	-12.3
09/02	0.667	2.25	110	0.000	4.76	2.77	3.25	-7.62
12/02	-0.101	-0.053	-9.32	0.000	0.008	-0.010	0.607	-2.94
16/02	0.511	0.175	-34.7	-0.828	-0.097	-2.23	0.000	5.82
20/02	0.052	0.844	1.86	0.124	0.326	-1.11	0.431	0.020
24/02	0.274	1.31	-6.73	0.000	0.000	2.31	1.15	-10.0
26/02	-0.153	2.28	62.8	1.179	0.000	0.878	0.000	13.2
05/03	0.463	2.00	32.6	2.890	0.000	4.64	0.000	12.7
Ave	0.614	1.54	-6.60	-1.23	0.742	-5.40	1.00	-4.15

Table 17. Results from flux calculations on the dates where simultaneous air and water measurements were made, all values are in nmol m^{-2} d^{-1}.

Flux calculations were also carried out using halocarbon concentrations in the uppermost sections of ice cores, or in samples of diatom rich ice. As the ice is very porous under these conditions, the brine in the channels is likely to be in contact with the atmosphere and thus halocarbon concentrations in the brine are assumed to be effective aqueous phase concentrations. Same-day air concentrations were used, and calculations were repeated as above. The total iodine atom flux to the atmosphere was then calculated, assuming steady state concentrations for atmospheric halocarbons, so that the sum of halocarbon fluxes from ice and water, F$_i$ and F$_w$ respectively, are equal to the iodine atom flux to the atmosphere. As can be seen from figure 63, there is potential for sea ice brine to provide a larger flux of iodine to the atmosphere, provided the same factors affect fluxes from a brine layer on the surface of sea ice as the surface microlayer on seawater, and providing the assumption of interconnected brine channels is valid. Whilst the latter is likely, the former is not at all known, and so these calculations are subject to large uncertainties. However to a first approximation it provides a useful comparison.

Quantifying halocarbon fluxes and understanding factors which control them is an important aspect of atmospheric modelling, but huge uncertainties still exist in halocarbon source strengths, atmospheric processes and sinks. For $CHBr_3$, the most studied of the halocarbons, the range of sea-to-air fluxes in the literature is 240–1760 Gg $CHBr_3$ a^{-1} [*Fogelqvist and Krysell*, 1991; *Liss*, 1986; *Quack and Wallace*, 2003] with large geographical and seasonal variations. Current estimates of iodocarbon fluxes are given in section 5.5.
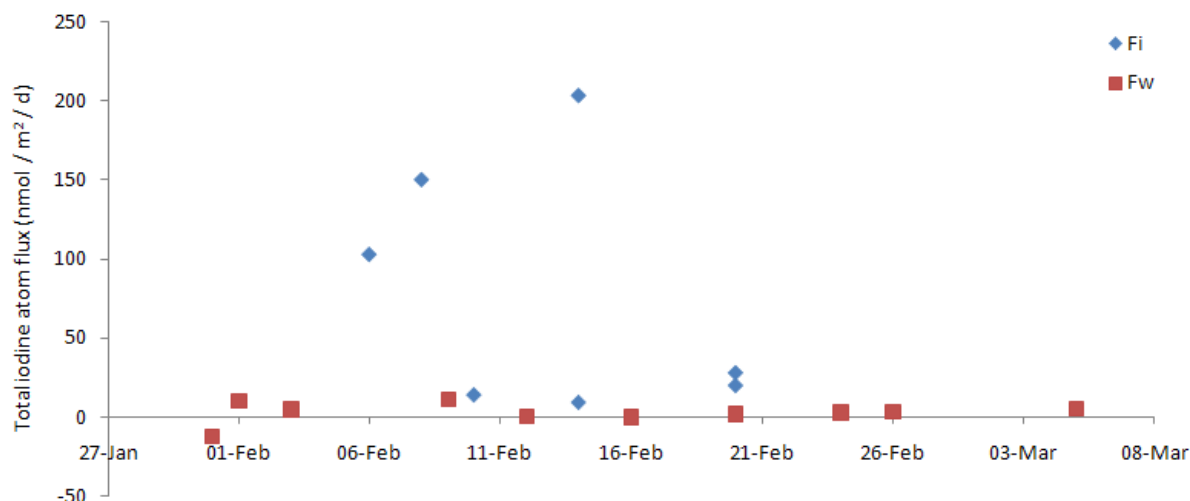
Figure 63. Total iodine atom flux to the atmosphere, based on the sum of all fluxes of iodocarbons from ice, F_i, and water, F_w, assuming atmospheric halocarbon concentrations maintain a steady state.

Contribution of reactive iodine species to IO budget

When calculating the contribution of volatile organic and inorganic compounds of iodine to IO mixing ratios in the boundary layer, the following considerations must be made: sources of iodine atoms to the atmosphere, assumed to be dominated by I_2, with some contribution from the iodocarbons. The breakdown of these compounds depends on photolysis rates; at the location of Halley at noon these rates are 0.853, 1.224×10^{-2}, 4.046×10^{-7}, 4.046×10^{-7}, 1.268×10^{-6}, 1.238×10^{-5}, 8.426×10^{-4} s^{-1} for I_2, ICl, CH_3I, C_2H_5I, C_3H_7I, and CH_2I_2 respectively (calculated using the model MISTRA, Zak Buys, BAS, personal communication), giving respective lifetimes of 1.2 s, 82 s, 29 days, 29 days, 9 days, 22 hours and 20 mins respectively. The reaction of iodine atoms with ozone will then form IO; the rate of this reaction is 2.3×10^{-11} cm^{-3} s^{-1} [*DeMore et al.*, 1997]. Loss processes of IO include photolysis, self reaction to form higher iodine oxides, uptake to aerosol, and dry deposition. Photolysis of IO to reform

I is rapid, with a rate of 0.201 s^{-1} (at Halley at noon) so a constant recycling between IO and I occurs.

The THAMO model was run, by Alfonso Saiz-Lopez and Anoop Mahajan at CIAC, to answer the following questions: what concentrations of IO result from the halocarbon fluxes in table 17? What atmospheric mixing ratios of I$_2$ would be necessary to reproduce the measured vertical column of IO (equal to 2.5 x 10^{12} molecule cm^{-2}, which, if evenly distributed over 200 m, would be 5 pptv of IO)?

As CH$_2$I$_2$ was not measured during this field campaign, an average previous CH$_2$I$_2$ flux, close to Southern Ocean sea ice, measured by a similar measurement technique and subsequent calculations, was used [*Carpenter et al.*, 2007]. CH$_2$I$_2$ is the most labile of the halocarbons, being photolysed in about 20 mins at this latitude at noon, and thus will contribute substantially to the iodine atom flux.

Results from the model runs are shown in figures 64 and 65. The maximum IO mixing ratio resulting from halocarbon fluxes is 0.035 pptv, much less than was observed.

In order to reproduce measured IO, the I$_2$ predicted at 10 m, at night time is 1 pptv, but during day time is only 0.2 pptv. This result would suggest the denuder tube method is massively overestimating I$_2$ mixing ratios.

The I$_2$ flux used was 2 x 10^{10} molecules cm^{-2} s^{-1}. This value is higher than previous fluxes based on similar measurements: a flux of 10^4 cm^{-3} s^{-1} I atoms was necessary to account for 4 pptv IO at Mace Head [*McFiggans et al.*, 2004], a flux of 5 x 10^7 cm^{-3} s^{-1} for new particle formation rates at Mace Head, and 10^9 cm^{-2} s^{-1} I atoms [*Saiz-Lopez et al.*, 2007a] for up to 20 pptv of IO in Antarctica. The I$_2$ concentrations suggested by the model are lower than observed, and using the same model it was estimated that 170 pptv IO (equally distributed over 200 m) would result from the observed I$_2$ concentrations.

New particle formation predicted by the model shows more agreement with measurements, with both predicting number densities of up to 1 x 10^5 cm^{-3} (figures 62 and 65). The field measurements however show particle growth to larger sizes than the model, the clusters produced in the model are formed rapidly but do not grow.

The model results also show that the assumption of well mixed IO in the boundary layer is flawed. This, and the discrepancies between modelled and measured values discussed above indicate the large gap in current understanding of atmospheric iodine chemistry, and more work is certainly needed to further interpret these measurements.
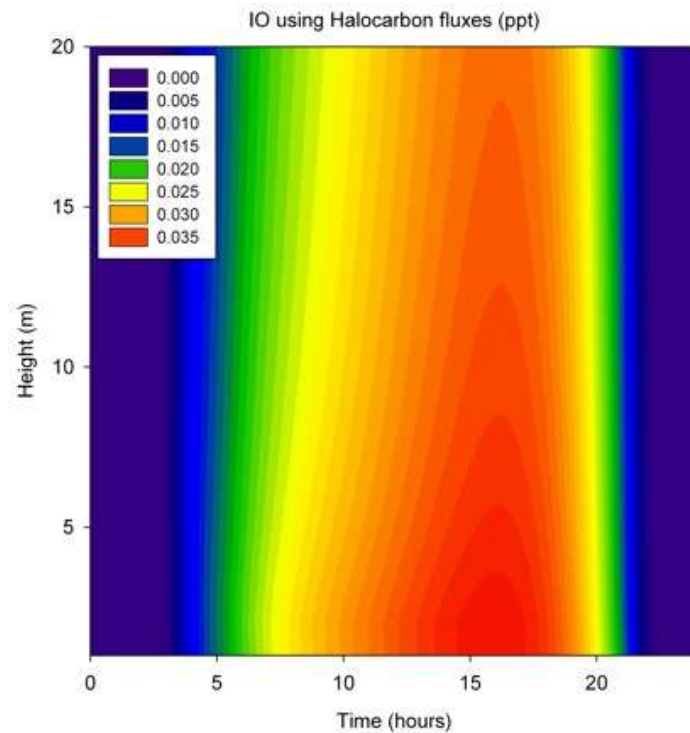
Figure 64. THAMO model results showing IO mixing ratios as a result of measured halocarbon fluxes. Courtesy CIAC.
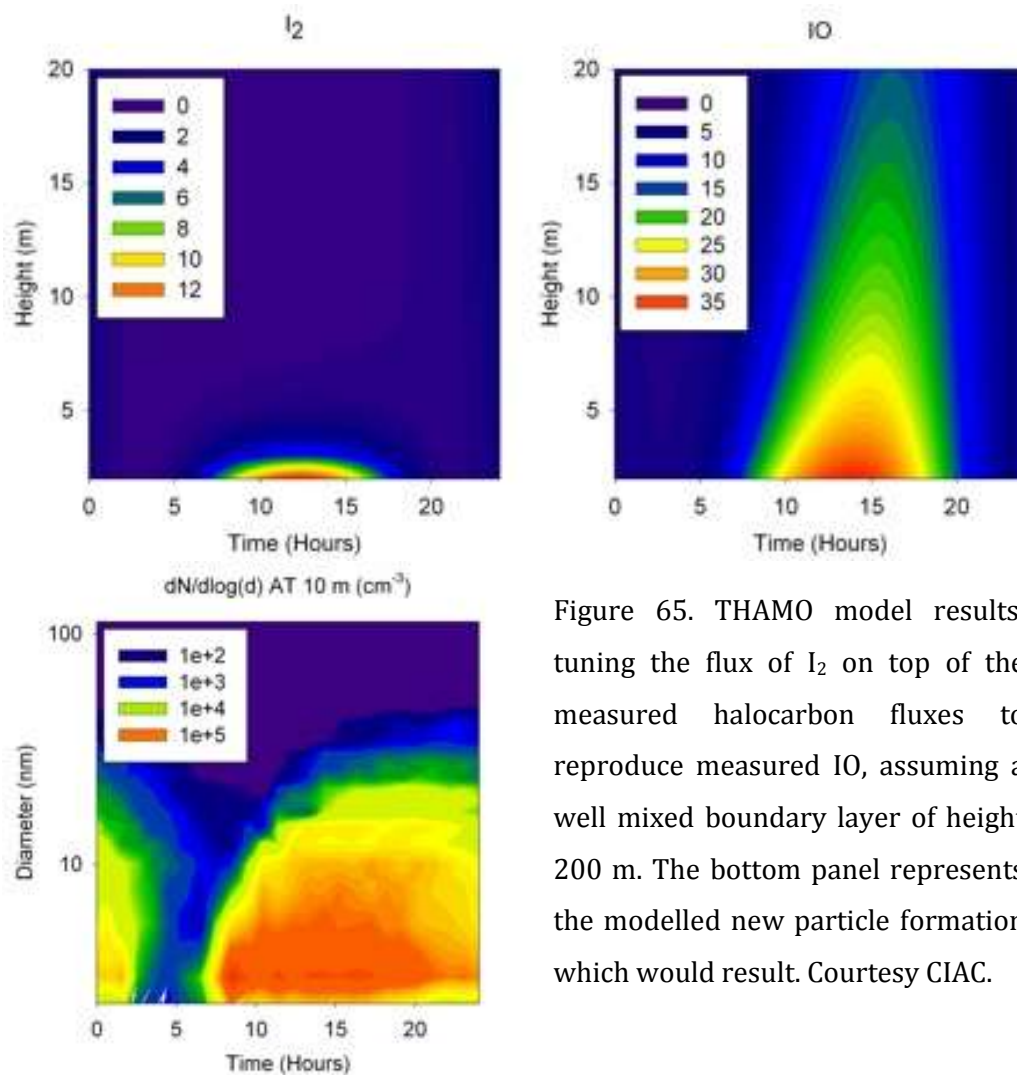
Figure 65. THAMO model results, tuning the flux of I_2 on top of the measured halocarbon fluxes to reproduce measured IO, assuming a well mixed boundary layer of height 200 m. The bottom panel represents the modelled new particle formation which would result. Courtesy CIAC.

5.5. Discussion

Sea ice measurements

The brine volume of the ice taken from ice cores ranged from 1.8 to 28% (average 11.8%) and from diatom-rich ice samples from 19 to 29% (average 25%). Whilst recent work by other groups has suggested gas transport though ice is negligible compared to that from open leads and cracks in the ice [*Loose et al.*, 2011, *Shaw et al.*, submitted], the measurements reported in this study were made in the warm austral summer month of February. The ice was very porous and well broken with many open leads.

The core of the 5th February, where only the first 1 m of much thicker ice could be retrieved due to a temporary problem with the corer, was the only core where brine volume was less than 5%, the threshold at which the brine channels close off to form isolated pockets. This happens at -5°C (the so-called rule of 5s, [*Golden et al.*, 1998]);

the porosity of sea ice increases exponentially above this temperature [*Cox and Weeks*, 1988]. The average ice temperature during this campaign was -1.8°C. This ice has survived much of the melt season and brine has had chance to drain, therefore its salinity is low and its melting point is close to 0°C. Thus, in all diatom-rich ice samples and 3 of 4 cores, the brine volume was such that the channels are assumed to be interconnected. Brine migration within the channels may then allow transport of dissolved ions and trace gases, providing a route from their sources in the ice to the atmosphere above.

Iodocarbons

Despite a pathway being present from sources to the atmosphere, high concentrations of halocarbons were measured in the sea ice brine, suggesting a local source. Ice core data show a trend for halocarbon concentrations to peak close to the ice/air interface, consistent with the distribution of algae in the ice in this area, where diatom-rich bands are seen in the ice close to the surface in so called 'gap layers' or infiltration layers, formed when sea water floods the surface of the ice, bringing fresh nutrients and thus promoting diatom growth. Enhanced halocarbon concentrations were also measured in diatom-rich ice samples.

The core of the 13th February in particular shows what enhancement in halocarbon concentrations is possible in these communities, this core was made from the small rescue boat and thus it was possible to make a core close to the edge of a small ice floe which was visibly discoloured by the sea ice community. Very high levels of halocarbons were found in this upper layer of ice, especially important as any halocarbons produced close to the surface of the ice will have more opportunity to escape to the atmosphere above. The prevalence of diatom bands close to the surface of the ice in the Weddell Sea could explain the high concentrations of atmospheric iodine observed in this region, though it may be that inorganic iodine compounds play a larger role than the iodocarbons.

Whilst bromocarbons were measured and have been discussed above, the focus of this study is on iodinated compounds, and the discussion in this section will cover iodocarbon concentrations measured, their significance, and comparison to previous measurements. Whilst the most studied iodocarbons are the mono-iodocarbons, and in particular CH_3I which was first measured by *Lovelock* [1975], the more labile poly-

iodocarbons are potentially more important in atmospheric processes due to their shorter photolytic lifetimes.

CH$_3$I

Average CH$_3$I concentrations in ice were 4.8 pM, enhanced with respect to the underlying water concentrations of average 0.4 pM. These measurements are much lower than similar previous field measurements of 38 pM in Weddell Sea ice brine (Fogelqvist and Tanhua 1995). Mixing ratios in air were average 0.08 pptv. Concentrations in firn air from the snowpack of the Brunt ice shelf showed a diurnal profile with mixing ratios reaching 0.5 pptv. In this region, previous measurements of CH$_3$I atmospheric mixing ratios have ranged from 0.3 to 7.9 pptv [*Bell et al.*, 2002 and references therein; *Reifenhauser and Heumann*, 1992]; our results are at the low end of this range. Despite the low concentrations, our flux calculations suggest average fluxes to be 0.6 (-0.5 to 3.8) nmol m^{-2} day^{-1}.

C$_2$H$_5$I

Average C$_2$H$_5$I concentrations in ice were 31 pM, higher than the underlying water concentrations of average 1.2 pM. These measurements are in agreement with those of *Fogelqvist and Tanhua* [1995] who measured C$_2$H$_5$I concentrations of 27 pM in Weddell Sea ice brine, 10 times higher than in the water below. Mixing ratios in air in this study were average 0.2 pptv. Concentrations in firn air from the snowpack of the Brunt ice shelf were correlated to CH$_3$I concentrations, showing a diurnal profile with mixing ratios reaching 1 pptv. C$_2$H$_5$I fluxes were more likely to be positive than those of the other halocarbons measured, with positive fluxes on 9 out of 10 occasions. Average fluxes were 1.5 (-0.05 to 2.8) nmol m^{-2} day^{-1}.

CH$_2$ICl

Average concentrations of CH$_2$ICl in ice were 9.6 pM, enhanced in comparison to the average underlying water concentration 0.2 pM (up to 1.1 pM). These measurements compare to those of *Carpenter et al.* [2007] (up to 2.4 pM, mean 0.7 pM). *Schall et al.* [1997] also measured CH$_2$ICl in the Southern Ocean, average values were 0.6 (range 0.05 to 1.8) pM, whereas *Klick and Abrahamsson* [1992] measured a mean Southern Ocean concentration of 1.4 (up to 22.7) pM. Thus our water concentrations are low, but the measurements in ice show how concentrations of this compound may be enhanced. Mixing ratios of CH$_2$ICl in air were on average 0.07 pptv. Flux calculations

show small positive fluxes on 3 occasions, but the potential for the flux of this compound to be strongly negative is shown by a negative flux of -15 nmol m^{-2} day^{-1} on one occasion. *Chuck et al.* [2005] found CH$_2$ICl flux to be positive in the open Atlantic, but close to zero in the Southern Ocean, whereas *Carpenter et al.* [2007] calculated a flux for CH$_2$ICl of 0.034–0.036 nmol m^{-2} day^{-1}.

CH$_2$ICl is formed in seawater via photolysis of CH$_2$I$_2$ with a yield of 25–35% [*Jones and Carpenter*, 2005], and field studies have investigated the relationship between these two compounds [eg *Carpenter et al.*, 2007]. It was a disappointment not to be able to measure CH$_2$I$_2$ concentrations during this campaign, but the presence of CH$_2$ICl suggests it may have been present.

2-C$_3$H$_7$I

Average 2-C$_3$H$_7$I concentrations in ice were 9.9 pM, enhanced with respect to the underlying water concentrations which were mostly below the LoD of 0.34 pM. This is in good agreement with measurements of 5.8 pM in Weddell Sea ice brine [*Fogelqvist and Tanhua*, 1995] who failed to measure 2-C$_3$H$_7$I above the LoD in seawater. 2-C$_3$H$_7$I was measured in air, average mixing ratios were 0.03 pptv, and fluxes were calculated to be positive on 6 out of 10 occasions, with an average (and range) flux of 0.7 (-0.1 to 4.8) nmol m^{-2} day^{-1}.

CH$_2$IBr

CH$_2$IBr was below the LoD of 0.12 pM in all water samples, and only detected in 9 of 99 air samples, where mixing ratios were average 0.03 pptv. A very high concentration (406 pM) was however detected in the top section of the ice core of 13th Feb, and CH$_2$IBr was detected in the diatom rich ice samples, where average concentrations were 3.22 pM (up to 28.9 pM). To our knowledge the only previous measurement of CH$_2$IBr in Antarctic waters was that of *Carpenter et al.* [2007] who measured concentrations of 0.7 (0.2 to 2.4) pM. These results show the importance of sea ice in the production of this compound, which may have a significant contribution to the iodine atom flux due to its short atmospheric lifetime.

1-C$_3$H$_7$I

Average ice 1-C$_3$H$_7$I concentrations were 14.3 pM, higher than average seawater concentrations of 0.9 pM. This is much lower than previous measurements of 235 pM

in Weddell Sea ice brine [*Fogelqvist and Tanhua*, 1995] where $1\text{-}C_3H_7I$ was not detected above the LoD of 0.33 pM in water samples. Average mixing ratios in air in this study were 0.08 pptv, and fluxes were calculated to be positive on 6 out of 10 occasions, with an average (and range) flux of 1.0 (0 to 3.8) nmol m^{-2} day^{-1}.

CH_2I_2

It was not possible to measure CH_2I_2 during this field campaign due to a contamination causing interference in the region of the chromatogram at which CH_2I_2 appears. A previous study at the ice edge of the Southern Ocean showed CH_2I_2 concentrations to range from 1.7 to 8.2 pM, and a range of fluxes of 0.02 to 6.1 nmol m^{-2} day^{-1}[*Carpenter et al.*, 2007].

I_2 and AIC

A unique feature of the campaign was the simultaneous measurement of I_2 and AIC (HOI and ICl) on board a ship in the sea ice zone. I_2 is unstable in seawater, reacting rapidly with organic material [*Truesdale*, 1974]. In the atmosphere I_2 is rapidly photolysed, subsequent iodine radicals may be taken up onto sea salt aerosols, and HOI may form, subsequent reaction with Br$^-$ and Cl$^-$ may produce further compounds of volatile iodine in the form of IBr and ICl.

High concentrations of both I_2 and AIC were observed, average mixing ratios were 9.8 (range 5.9 – 30.9) and 1.9 (range 0.65 – 3.76) pptv respectively. As discussed previously, these values are much higher than expected by consideration of the known atmospheric chemistry, and the modelling study employed has not been able to consolidate the I_2 and IO measurements.

The measurement of such high atmospheric concentrations of I_2, if this is what was measured with the denuder tubes, suggests processes are occurring in the sea ice zone which result in I_2 emissions. The depletion in total iodine in diatom-rich ice samples (compared to the underlying seawater) suggests the sea ice community may be able to volatilise and release iodine from the ocean. However the lack of a strong signal from ice covered areas, the presence of atmospheric I_2 over open water, and the high concentrations of I_2 measured above the snowpack of the Brunt Ice shelf, suggests other mechanisms are occurring which are not yet fully understood. These mechanisms may involve recycling on aerosol surfaces.

One source of I_2 could be the distinct types of diatom community found close to ice shelves. Platelet ice forms underneath congelation ice layer and is home to a unique array of ice algal species, which have been scavenged from the water column as platelets rise close to ice shelves [*Dieckmann et al.*, 1986]. The platelet layer forms due to the decreasing currents and sheer near an ice shelf. Nutrient supply in the platelet area is higher than in the interstitial area above, whereas radiation is lower; the differing physical environment owing to the nature of the ice crystals also contributes to making these quite different environments. The species which under these conditions do so in abundance, as has been observed in McMurdo Sound and the Weddell Sea [*Bunt*, 1964; 1968; *Palmisano and Sullivan*, 1985]. Platelet ice is the most porous of the sea ice-types; it ranges from a few cm to several m thick and is approximately 20% ice and 80% seawater. It is characterised by rapid nutrient exchange, high porosity and Chl *a* concentrations exceeding 1000 mg m^{-2} [*Bunt and Lee*, 1970]. If this significant habitat for sea ice biota contains diatoms capable of emitting I_2, this could be the source of high levels of I_2 recorded on the ice shelf, and the source of the high concentrations of IO in this region. Unique meteorology also occurs over open leads, where warm water is exposed, causing rapid vertical entrainment. This will be especially pronounced close to the cold Antarctic continent, and may explain such high levels of I_2 on the ice shelf ~27 m above sea level.

The results of this study show the potential for ice covered areas to be a source of reactive iodine in inorganic forms. Our understanding of the chemistry and mechanisms involved is far from complete, and further work is needed.

IO

Atmospheric IO was measured via the ship-based MMD and via satellite throughout the campaign, mixing ratios by MMD were 5.1 (range 2.7-6.6) pptv assuming a boundary layer height of 200m. Vertical columns by MMD were up to 3.8×10^{12} molecules / cm^2, higher than vertical columns measured by satellite of up to 1.8×10^{12} molecules / cm^2. The MMD was a point source measurement, located close to assumed sources, so it is expected that measurements will be higher than those averaged over a larger area. Further differences between the two measurement techniques may arise from the different geometries used to compensate between slant- and vertical- column densities and the quite different locations of the two instruments. Whereas the satellite-based instrument may struggle to see scattered

radiation from IO molecules in the lowest level of the atmosphere when much of the radiation has been scattered by the large volume of atmosphere above it, the MMD is ideally placed close to sea level. The SCHIAMACHY instrumentation has a much better signal/noise ratio for measurements over sea ice than open water, due to the different reflectivity of the two surfaces. Because of this, some of the signal over areas where much open water was present may not have been detected. Our results are in reasonable agreement with previous measurements of IO of up to 20 pptv on the Brunt ice shelf close to the location of this field campaign [*Saiz-Lopez et al.*, 2007a], backed up by satellite measurements [*Schönhardt et al.*, 2008].

The mechanism of iodine release

When sea ice forms, diatoms incorporated into the brine channels may accumulate iodine from the ocean. The production of halocarbons by diatoms was discussed in chapter 1, and it is likely that the compounds are emitted as a by-product of normal cell metabolism, possibly enhanced in the sea ice zone due to the stresses imposed by the harsh conditions. Haloperoxidase enzymes differ in their halogen specificity, and in the rate at which they are able to oxidise the halides. Bromoperoxidases catalyse the reaction of Cl^-, Br^- and I^- with organic material to produce poly-halogenated compounds, iodoperoxidases are I^- specific [*De Boer et al.*, 1986]. It is possible that the diatoms which colonise the sea ice of the Weddell Sea have iodoperoxidase enzymes, which favours the production of volatile iodine over volatile bromine, and more work is needed in order to ascertain this.

Furthermore, iodide is concentrated in the brine channels via the concentration effect of solvent volume reduction, and is a useful and easily available cell antioxidant in these extreme conditions. Any compounds of iodine which build up in reactive forms in sea ice brine channels will be released as the sea ice melts, in the form of iodocarbons and I_2, which are then photolysed, and high atmospheric concentrations of IO result.

The lack of a significant correlation between Chl *a* and halocarbon concentrations is not surprising, in ice cores or very diatom-rich ice samples. Species which reside close to the ice surface will be photo-adapted and therefore have less chlorophyll. Halocarbons may have escaped from this very porous ice, and the field campaign was carried out during the summer season when phytoplankton are at their stationary growth phase. Light and nutrient limitation influence Chl *a*, but not halocarbon

concentrations, and spot measurements such as these rarely show correlations as they give no indication of the history of the water and no account is taken of loss processes. For example, diatoms in the ice which could be responsible for halocarbon production could have since died off, and bacteria could be present which utilise halocarbons. Also both carbon/Chl *a* ratio and halocarbon production has been shown to vary widely between species [*Moore et al.*, 1996], and different species will be present at different levels in the ice. Halocarbon concentrations are a result of temporal variations in production and loss rates. It is also possible that the higher halocarbon concentrations are due to photochemical production and are not linked to diatoms.

The sea ice of the Weddell Sea is unusual for Antarctica in that some of it is multi-year; the Weddell Sea has a gyre system into which ice drifts and circles. Brine within this ice may not have been exposed to the atmosphere for some time. The low diffusivity of halogenated compounds through ice as opposed to through migration of brine and open leads [*Loose et al.*, 2011, *Shaw et al.,* submitted] therefore keeps the reactive iodine held in the ice until the ice is warm enough to allow brine migration.

Thus, the Weddell Sea may provide a constant source of IO to the atmosphere, trapping as it does very diatom rich ice. The presence of gap layers in this ice, held as they are close to the surface of the ice but often with a fresh-ice cap which will be very impermeable, may also facilitate a build up of reactive iodine, which will be easily released upon ice melt and break up. The high atmospheric levels of I_2 and IO, enhanced halocarbon concentrations in the sea ice brine, low total iodine in diatom-rich ice, and new particle formation as the ship moved though and broke up the ice all support this hypothesis.

A discussed in Chapter 1, recent work has however suggested that the enhancement of iodine compounds over Southern Ocean sea ice proceeds via accumulation of I^- by sea ice algae followed by I_2 release via the reaction HOI + I^- + H^+ $\rightarrow$ I_2 + H_2O [*Saiz-Lopez and Boxe*, 2008]. If this equilibrium exists, it will be driven in favour of the products by the high volatility of I_2. The total depletion in iodine in diatom rich ice and the high atmospheric concentrations of I_2 support this mechanism.

An alternative mechanism of I_2 release has been proposed from frozen seawater surfaces by *O'Driscoll et al.*[2008]. The mechanism involves nitrite and iodide which are both present in sea salt; protonation of HONO by H^+ ions, rejected from the ice

phase and concentrated in liquid micropockets, leads to H_2ONO^+ which may then react with I^- to release I_2 and NO. This reaction, had previously been known to occur in weakly acidic solutions, may therefore occur in neutral solutions which undergo a freeze thaw cycle. Our measurements therefore also support this mechanism

5.6. Summary

A large amount of data has been brought together during this field campaign. Sea ice rich in diatoms was sought out in the Weddell Sea, known to be an area in which iodine is effectively volatilised and released. Production of organic forms of iodine by sea ice diatoms was suggested by higher concentrations of iodocarbons in the sea ice brine than the underlying seawater. The influence of algal activity on the ratios of the inorganic forms of iodine in seawater, iodide and iodate, was also studied. The sea ice properties were measured to ascertain the continuity of the brine channel network, providing a pathway for compounds produced by ice algae to the atmosphere. Measurements were made of atmospheric mixing ratios of iodocarbons and I_2, the latter was found to dominate the budget of iodine atoms. The products of these reactions were also measured: IO was measured by ship-based instrumentation and qualified by satellite data; new particle formation, proposed to result from high atmospheric concentrations of IO, was observed as the ship broke through sea ice. On the Brunt ice shelf, enhanced concentrations of CH_3I and C_2H_5I were measured in the snow firn air, with a diurnal profile, suggesting the snow may be a source of these compounds. Saturation anomalies, flux calculations and a modelling study were used to interpret the measurements.

The key findings of this study are:

- Inorganic iodine compounds may be responsible for a larger iodine atom flux to the atmosphere than organic iodine compounds.
- Inorganic iodine compounds may thus provide a large contribution to IO formation, and may explain the high mixing ratios of IO observed over Antarctica.
- Higher concentrations of halocarbons in sea ice containing diatoms suggest the sea ice community is able to volatilise iodine from the ocean.
- Depletion of total iodine in sea ice containing diatoms suggests iodine which has been converted into volatile forms has subsequently been released to the atmosphere.

- Enhanced mixing ratios of halocarbons in snow firn air with respect to the atmosphere above suggests the snow may be a source of these compounds.
- Measurements of new particle formation as the ship broke through the sea ice have clearly shown the effect on the atmosphere of this reactive iodine chemistry.
- A modelling study has highlighted that our understanding is far from complete in this area, and further work is certainly needed.

Chapter 6. Halocarbons Associated with Arctic Sea Ice

6.1. Introduction

Halocarbons were measured in the brine of sea ice in the Arctic Ocean above the Greenland and Norwegian seas (∼81°N, 2-5°E), as a melting ice floe was followed for 9 days. Halocarbon concentrations are also reported from the water below, and air above, the ice floe as it drifted southwest and melted. Chl *a* was measured as an indication of ice algal biomass, and physical measurements of the sea ice were made. Ocean-atmosphere fluxes of halocarbons were calculated.

This ice was less than 1 m thick and very porous. As the Arctic ice melts, thins and retreats as the planet warms, the ice sampled is representative of that which will be typical in the Arctic, despite being sampled from the edge of the pack. Results are also reported from the COBRA field campaign where measurements were made on ice of the Canadian sub-Arctic in early spring, which was thicker, colder, and less porous.

This chapter includes a comparison of the ice properties, biomass and halocarbon concentrations in these two types of Arctic ice, and the results are further compared to the Antarctic data presented in chapter 5. This chapter enables further insight into how the brine volume and porosity of the ice influences the concentrations of trace gases in the brine, and how this may subsequently impact the products of atmospheric reactions involving halocarbons.

6.2. Materials and Methods

6.2.1. The Arctic Ocean - JR219

Measurements were made from 18th June to 10th July 2010 from the ice-strengthened RRS James Clark Ross, cruise JR219, legs 2 and 3, as shown in figure 66. During leg 2 the ship sailed from Longyearbyen, Svalbard 78°13'N, 15°36'E into the Arctic pack ice where the approximate average ice thickness was 1 m. The ship moored against a large ice floe (approximately 1300 m diameter) at 80°54'N, 5°25'E on 21st June 2010 where an 'ice station' was set up. Ice cores were made, sea ice brine was collected, air and water samples were taken regularly, until 1st July 2010, by which time the floe had drifted to 80°14'N, 2°70'E. Only air and water samples were collected during leg 3, in between Longyearbyen and the pack ice east of Greenland at 77°44'N, 005°38'W.
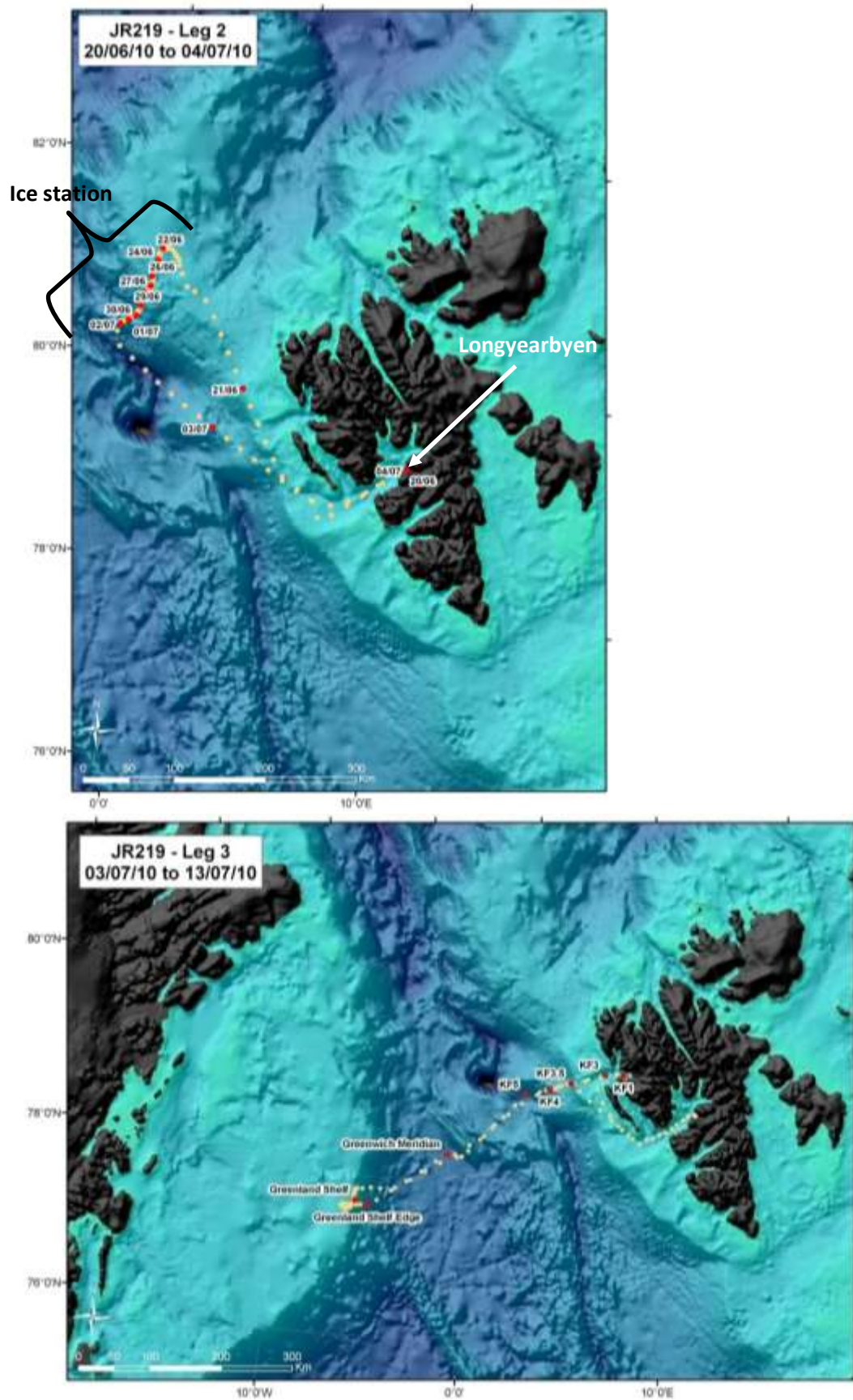
Figure 66. Cruise path of JR219, legs 2 (top panel) and 3 (bottom panel).

In order to understand where halocarbon production occurred, water samples were taken from the open ocean, approaching, underneath and within the sea ice.

Temperature-salinity profiles and Chl *a* data were used to interpret the trace gas measurements. Total halocarbons ejected to surface waters by melting sea-ice were estimated by multiplying halocarbon concentrations in ice brine with brine volume and ice melt. Using ice and water concentrations and simultaneous mixing ratios in air, saturation anomalies and ocean-atmosphere fluxes were calculated.

Sample collection – sea ice brine from ice cores

Collection of brine from sea ice without escape of volatile trace gases from the sample presents a considerable challenge. As an ice core is lifted out of the floe, the brine begins to drain out of the channels immediately. Two techniques were used to collect the brine during this campaign – a 9cm diameter SIPRE corer (as detailed in section 5.3.1) was used to make cores in the sea ice. The corer was then lifted from the ice, and immediately placed into a small plastic bucket. The hole left after core removal filled with brine from adjacent brine channels and pockets, which took between 2 and 32 seconds, depending on the depth of the core. The brine from the hole was collected into a 100 ml gas-tight syringe via a piece of Tygon tubing placed at the bottom of the hole to prevent collection of brine exposed to the atmosphere. The core remained inside the corer, and the bottom of the corer was in contact with the sides of the bucket until the brine had drained, the brine was then sampled from the bottom of the bucket as before. The two brine collections shall henceforth be known as 'drainage brine' and 'hole brine'.

Cores were made to different depths in the ice in order that a vertical profile of halocarbon concentrations through the ice could be made. Concerns regarding the drainage brine include the contribution from the entire length of the core, and the possibility of escape of the compounds during brine drainage. The issues surrounding the hole brine include the contribution from brine from anywhere in the surrounding ice, and the underlying seawater pushed up through the more porous ice below, and compound escape. For this reason, both techniques were used and the results were compared. In the shallower cores, concentrations of halocarbons were similar in both drainage brine and hole brine, whereas in deeper cores the hole brine concentrations were much lower. This is most likely due to the increasing porosity of ice with depth, leading to seawater being pushed up more easily.

The salinity of the sea ice brine was lower than that of the underlying seawater under these conditions, as freshwater ice melt infiltrates the brine channel network and

dilutes the brine. Figure 67 shows how the salinity of the hole brine is higher than that of the drainage brine, again confirming hole brine dilution by seawater. It is therefore clear that dilution of the hole brine by seawater from below may result in a dilution of the halocarbons, and results will only be reported from the core brine drainage. The values reported are not from discrete depths but are rather from the entire ice core removed, however this is preferable to being influenced by an unknown quantity of brine from the surrounding ice and underlying seawater.
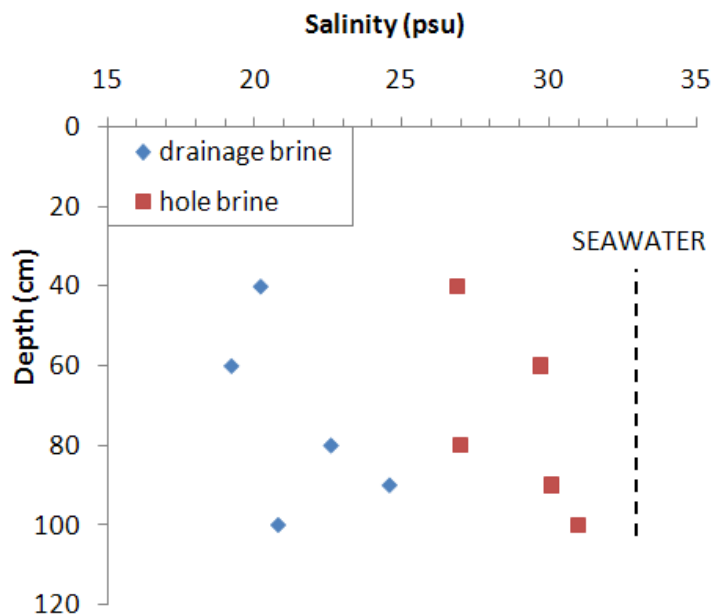
Figure 67. Salinity measurements of drainage brine and hole brine from ice cores made to discrete depths. The hole brine salinity is closer to that of the underlying seawater, which demonstrates the tendency for the hole brine to be influenced by seawater pushed up through the brine channel network from below.

The temperature of the ice was measured with a handheld temperature probe after drilling small holes in the side of the core with a cordless drill. The salinity of the bulk ice samples was measured after ice melt as described in section 2.7. The melting point of sea ice is higher than its freezing point due to it being more less saline after brine drainage.

Sea ice brine for incubations

1 m² holes were made in the sea ice to allow access for the dive team. These holes were made by chainsawing through the ice and manually hauling out blocks approximately 0.25 m³ volume. Whilst this work was being carried out, the opportunity was taken to collect large volumes of sea ice brine. The ice blocks were

placed in large plastic containers, allowed to drain, and transferred to gas tight syringes within 10 minutes in order that incubations could be carried out.

Water samples

Water sampling was carried out in a number of different ways during the campaign. Samples were taken from Niskin bottles used for routine CTD (conductivity, temperature, depth) measurements, results are also reported from under-ice seawater collected via a dedicated sampling site and from samples collected by the dive team. These results have been separated out and will be discussed individually, then a comparison of all water samples will be undertaken in order that the different processes which contribute towards halocarbon concentrations can be assessed.

CTD water samples were collected from the surface and from the depth of chlorophyll maximum (DCM) which ranged from 14 to 57 m. Though the CTD Niskin bottles were sampled by other cruise participants, samples for GCMS analysis were taken first, to limit the exposure of the water to the atmosphere. A 100 ml gas-tight syringe with a piece of Tygon tubing attached was connected to the bottom valve of the Niskin bottle. Samples were taken occasionally when time permitted during leg 2 and daily during leg 3. CTD water measurements were made in ice covered waters during leg 2 on 25th and 28th June (Arctic Ocean) and during leg 3 on 8th and 9th July (Greenland Shelf).

Under-ice water samples were collected from a dedicated water sampling site, labelled 'hole A', set up away from other activities at the ice station. This comprised of a 2.5 m long Teflon tube going from the ice-water interface, up through the ice, attached to bamboo pole, with a plastic valve on the end. A gas-tight syringe was used to draw water up from underneath the ice. A triplicate sample was taken daily whilst the ship was moored against the ice floe.

Under-ice water samples from the dive team were collected as depicted in figure 68. Two types of diatom community were present underneath the ice: the epontic community which reside within the bottom layer of the ice (the lighter brown patches in figure 68) and those which hang underneath the ice, and are comprised of dead and decaying plankton which clump together after draining from the melting ice (as seen in figure 68 insert). Three types of water sample were collected by the divers: (A) under ice water; (B) water / brine collected by drawing water into a gas-tight syringe

held against the underside of the ice which was visibly discoloured by diatom communities, and algae could be seen to be entering the syringe during sample collection; and (C) large mats of dying diatoms placed into the syringe with the surrounding seawater.

Therefore measurements made during this study are representative of different types of sea ice diatom community: core drainage water containing brine channel communities; under-ice water samples which may represent algal blooms underneath the ice (or water from ice melt); bottom ice samples collected by the dive team represent the epontic community and the dead and dying algae communities which have drained from the brine channels. In total 23 water samples from CTD bottles and 9 under-ice water samples were collected, 18 brine samples from 3 ice cores and 9 samples collected by the dive team were also analysed. Most sea ice brine samples were made in duplicate, except where limited by sample volume in the shallowest cores. CTD water samples, water from underneath the ice, and air samples were made in triplicate, except for the full CTD profile of the 28th June, where duplicate samples were made due to time constraints.
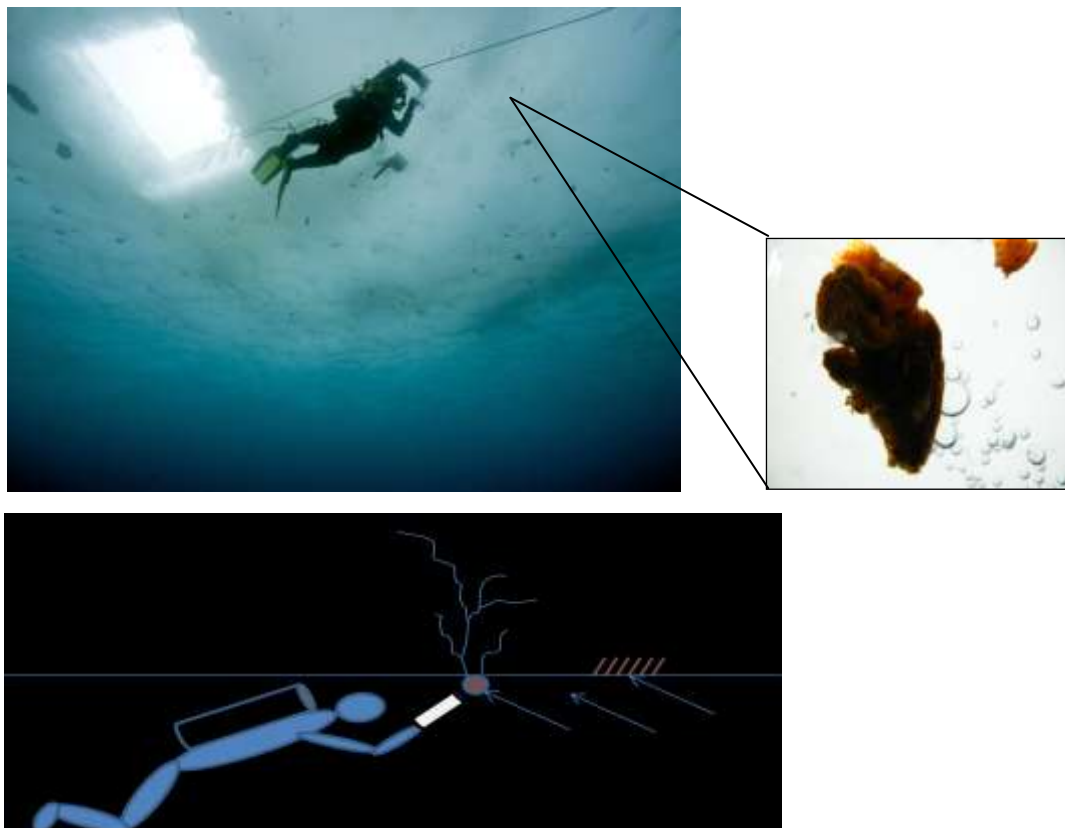
Figure 68. Sample collection by the dive team – under-ice water and brine samples collected from: (A) water underneath the ice, (B) ice algae communities associated with the bottom of the ice and (C) algae mats from draining brine channels (picture shown in insert).

Air samples

An air sample was collected daily (on 19 days) from the deck of the ship facing into the wind by drawing air through a Markes sorbent tube at a rate of <100ml min^{-1} with a gas-tight syringe. Triplicate samples were made; results are presented as average and range.

Sample preparation and analysis

Brine and water samples were gently filtered through 47μm Whatman GF/F filter papers directly into the glass tube at the start of the GCMS run as detailed in section 2.1, with the Markes thermal desorption unit used as the trapping method, for **halocarbon** analysis. Care was taken to avoid introduction of bubbles into the sample. The filter papers were wrapped in aluminium foil and stored at -80°C on the ship for **Chl *a*** analysis back in the UK.

In total 8 halocarbons were measured, shown in table 18, with retention times and limit of detection. A calibration was carried out at the start and end of the campaign. R^2 values for all calibration curves were above 0.98. Liquid standards were prepared in the UK, as detailed in section 2.1, stored at -20°C, and used within 3 months. Measurement precision, determined by repeat analysis of known concentrations of halocarbons in water, was between 0.5% and 8.0%.

	CH_3I	C_2H_5I	$CHBr_3$	CH_2ICl	$2\text{-}C_3H_7I$	CH_2IBr	$1\text{-}C_3H_7I$	CH_2Br_2
m/z	142	156	173	176	170	222	170	174
LoD	1.6	0.094	1.5	1.2	0.49	1.08	1.1	0.06
RT	6.74	8.7	12.8	10.5	9.8	11.8	10.5	10.1

Table 18. Halocarbons analysed by GCMS, showing mass / charge ratio (m/z), limit of detection (LoD) in pM, and retention times (RT) in minutes. The LoD improved during the course of the campaign for most compounds, LoD at the start of the campaign is given.

Chl *a* was measured on ice core and under ice water samples as detailed in section 2.3 within 6 months of the campaign, samples were stored at -80°C during this time. Chl *a* concentrations for CTD water samples were measured with a Chelsea Aqua 3 fluorometer on board the sampling rosette which was not calibrated, so values should be taken as relative values only. The **brine volume** of the sea ice was calculated as detailed in section 2.7; **Sea surface temperature** and **salinity** data used for flux calculations were taken from the ship's underway seawater (USW) supply logger at a

depth of 6m; salinity measurements on water samples agree with CTD sampler within 0.7‰. Chl *a* was also monitored via fluorescence by the USW logger, and this data is shown in figure 69. **Wind speed** and **wind direction** data recorded by the ship are also shown.
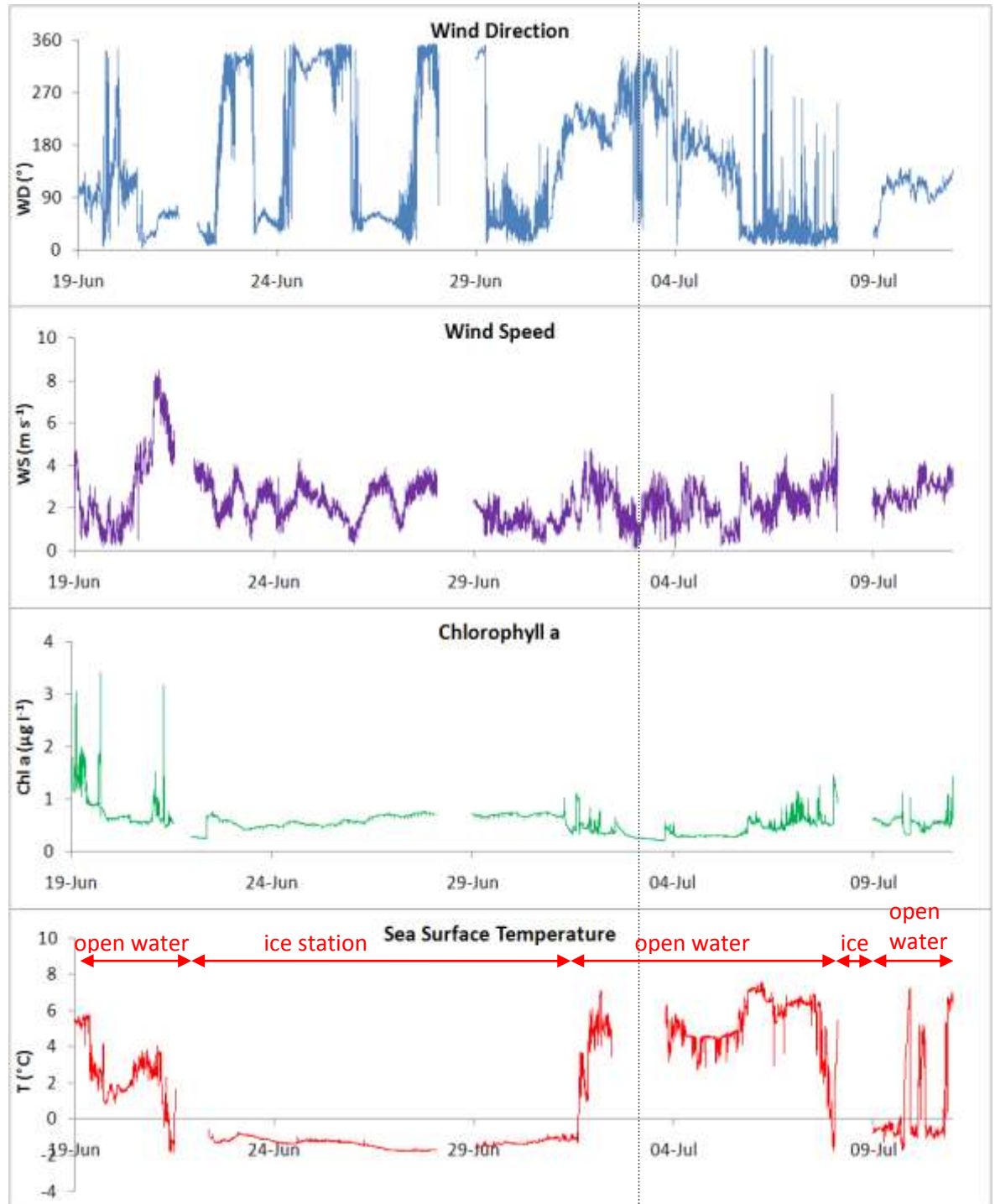
Figure 69. Supporting information from the ship's logger, with SST and Chl *a* recorded via the USW supply. The dashed line represents the transition from leg 2 to leg 3 of the cruise, and the annotation in red denotes water and ice conditions.

Incubations

Brine collected from ~0.25 m^3 pieces of sea ice was incubated for 48 hours under semi-transparent plastic screens which allowed transmission of 100%, 14% and 1% solar radiation, designed to be representative of light intensities in surface waters, mid way and underneath one metre thick sea ice respectively. For each light intensity, a gas tight syringe was filled with 100 ml brine, and a replicate was filled with brine which had been filtered at 0.2 µm under a light vacuum to remove phytoplankton. The syringes were held in flowing seawater tanks on the ship's deck, the water temperature was -1.8°C to –1.5°C.

6.2.2. COBRA

The site at which extremely high concentrations of atmospheric halocarbons had previously been measured [*Carpenter et al.*, 2005] was close to the town of Kuujjuarapik, on the east coast of Hudson Bay in the Canadian sub-Arctic (figure 70). As discussed in section 1.6, these measurements were made in the absence of open leads and an abiotic mechanism was proposed for their production. The site was revisited and in this study results are reported of halocarbon concentrations in the sea ice sampled during the 6 week COBRA field campaign which took place during January – March 2008. Mixing ratios of atmospheric halocarbons and IO have been reported elsewhere [*Mahajan et al.*, 2010b]
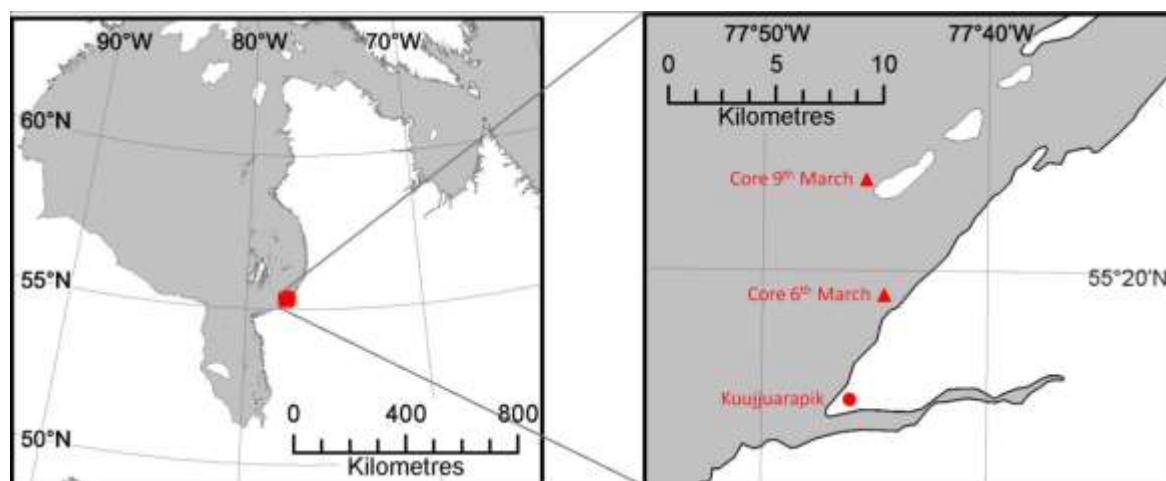
Figure 70. The location of the COBRA field campaign, red triangles denote the location of the ice cores from which samples were taken for halocarbon analysis

Sample collection –ice cores

The ice properties and meteorological conditions during the COBRA field campaign necessitated a different method of sea ice brine sample collection. As mentioned previously, the ice was much thicker here (up to 1.8 m) and the influence of the outflow of the Great Whale River close by reduced the salinity of the underlying water and hence the ice. This weakly saline and very cold ice did not contain interconnected brine channels, and any channels or pockets of brine which may have drained froze up instantly upon core removal, as the air temperature was mostly below -25°C. For this reason, bulk ice samples were collected. Cores on the 6th March 2008 (at 55°18'N, 77°44'W) and 9th March 2008 (at 55°21'N, 77°44'W) (see Figure 70) were made with same corer as described in section 2.1.1, and cut into 10 cm or 3 cm long sections with a stainless steel saw. The middle section of the ice core was removed with a custom-made stainless steel 'mini-corer' with dimensions to exactly match those of the inside of a 100ml gas-tight syringe. The mini core was then immediately transferred to a syringe and left to melt at 4°C in the dark. This method limited escape of the compounds as much as possible before the ice was placed in the syringe.

Sample preparation and analysis

Water (and melted ice) samples were gently filtered through a 0.47 μm mini-sart filter in a nylon housing with a luer-lock fitting directly from the gas-tight syringe into the purge tube. **Halocarbon** analysis was carried out in collaboration with York University using a Perkin Elmer (USA) Clarus 600 GCMS interfaced with a Perkin Elmer Turbomatrix Thermal Desorption Unit (TDU). The GC incorporated a 60 m x 0.53 mm internal diameter wall coated open tubular (WCOT) non polar DB-5 (Supelco) capillary column and used CP grade helium (BOC gases) as a carrier gas (3.0 ml min^{-1}). Following injection, the GC oven temperature was held at 35°C for 3 minutes, ramped up to 180°C at a rate of 10°C min^{-1}, held at 180°C for 1 min, ramped up to 200°C at a rate 25°C min^{-1}, and held at 200°C for 1 minute for adequate conditioning between sample runs.

The sensitivity of the GCMS was monitored with a National Physics Laboratory standard containing 14 chlorinated hydrocarbons, of which only $CHCl_3$ and CCl_4 were monitored. The GCMS was calibrated with stock standard solutions (>99% purity, Sigma Aldrich), in methanol (Fisher HPLC grade), diluted with sparged H_2O, and

applied to a pressurised, heated gas-tight purge tube and sparged into a passivated 10 L electropolished aluminium lined cylinder (Aculife) with zero grade nitrogen gas.

Following removal of the sample used for halocarbon analysis, the remainder of the core was left to melt at room temperature in the dark, then gently filtered under vacuum through a 0.47 μm Whatman GF/F filter paper. The filter papers were stored at -20°C at the research station before frozen transport back to the UK for **Chl *a*** analysis. Some filter papers were used to confirm the presence of diatoms via microscopy: a small number were seen, no other organisms were found in the ice.

Chl *a* measurements were made with a Turner TD-700 fluorometer following the method of *Strickland and Parsons* [1968] following overnight extraction in 10 ml acetone (Sigma-Aldrich) at 4°C. Chl *a* from spinach (Fluka) dissolved in acetone (Sigma-Aldrich) was used as a standard for calibration, the concentration of the standard was determined with a Unicam 5625 UV/Vis spectrophotometer. The Chl *a* values were not corrected for pheopigments due to the low salinity of the samples. Measurement precision, determined by repeat analysis of identical standard concentrations, was <1% error. Errors due to random and pseudo-random effects on calibration averaged to 18%, determined by standard deviation from straight-line fits to calibration curves.

6.3. Results from the Arctic cruise (JR219)

The temperature of the ice ranged from -0.1 to -1.6°C, and brine volumes in the ice ranged from 11 to 51% (figure 71), well above the 5% threshold for brine network connectivity in columnar ice.

Chl *a* concentrations ranged from 0.006 – 0.094 μg l^{-1} in the ice, 0.013 to 1.09 μg l^{-1} in the water underneath and up to 3.35 μg l^{-1} at the DCM in waters in which the phytoplankton bloom was well underway. The diatom communities in the ice and in the water were dominated by small pennate diatoms (figure 72).

Halocarbon concentrations in the sea ice brine are presented in section 6.3.1, concentrations in seawater and air are discussed in sections 6.3.2 and 6.3.3 respectively. Saturation anomalies, flux calculations and the relative contributions of the physical and biological processes affecting halocarbon production in sea ice and the impact on the surrounding ocean are then discussed.
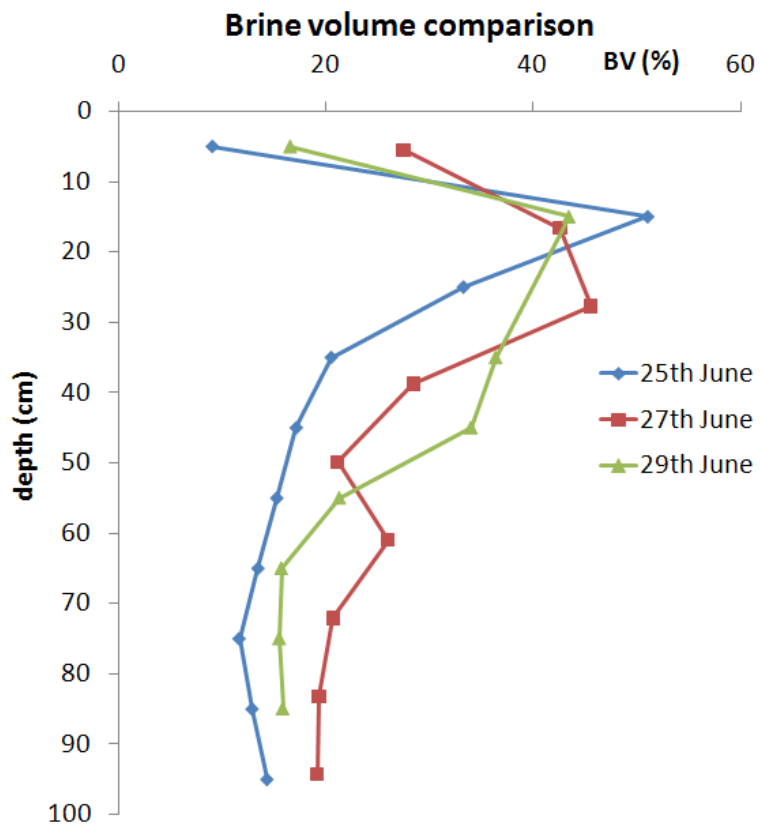
Figure 71. Brine volume in three ice cores collected during cruise JR219.
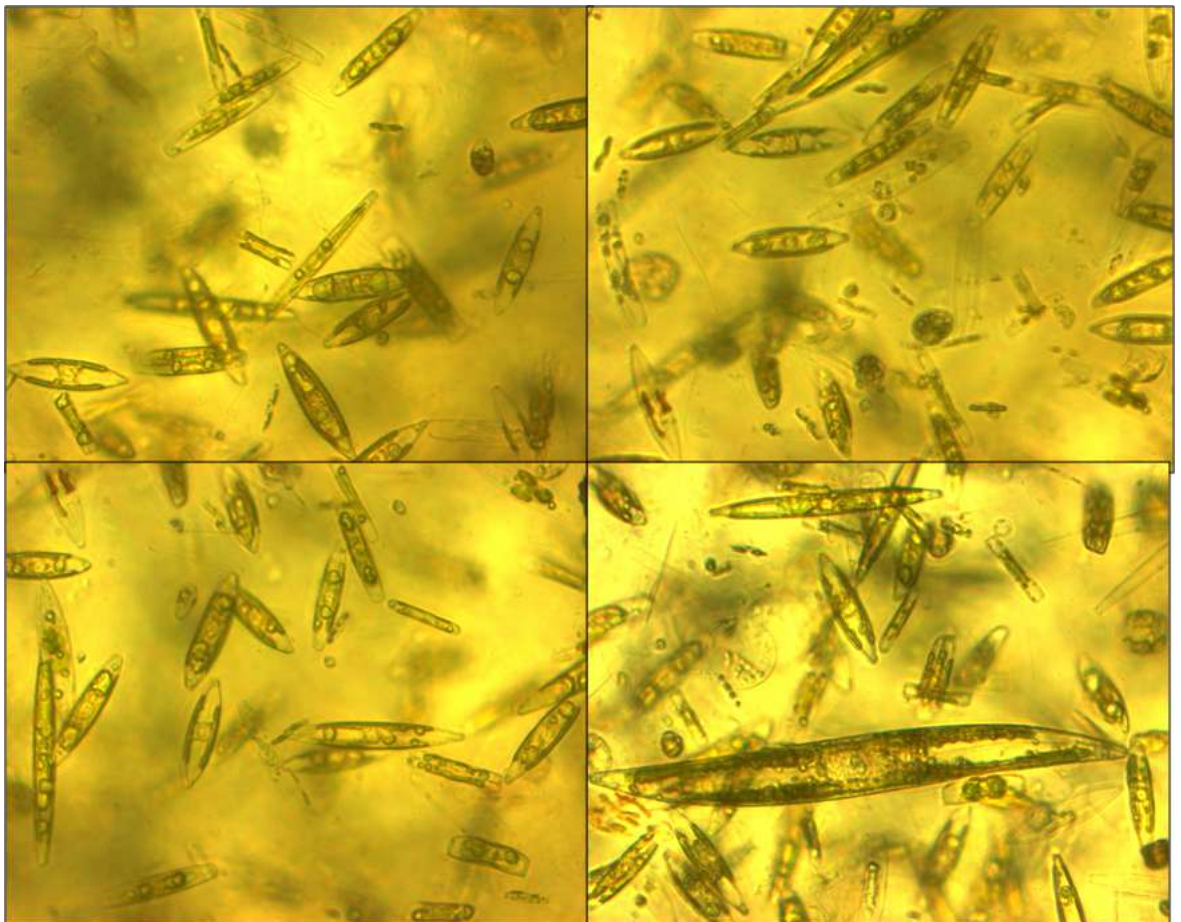
Figure 72. Four photographs of diatoms under the microscope from cruise JR219.

6.3.1. Halocarbon concentrations in sea ice brine

Vertical profiles of halocarbons throughout the ice are shown in figure 73. The concentrations which would be expected from the concentration effect, that is by the reduction in the volume of the liquid phase of the sea ice, are shown for comparison. The seawater concentrations used to calculate this are surface water values close to the ice, given in table 19. Whilst these concentrations may have been affected by emissions from the ice, the values are as close to a representation of the water frozen when the ice formed as it is possible to obtain. Under-ice water concentrations were not used as these are more likely to be influenced by emissions from the under-ice bloom. As well as the errors intrinsic in this estimation, further errors due to brine drainage i.e. rejection of the hypersaline solution and dissolved halocarbons from the ice column to the underlying water during freezing, and fresh water melt influx to the brine channels make these concentration effect calculations an educated guess at best. However, it is useful to qualitatively consider whether halocarbons are enhanced or reduced compared to that expected solely from passive transport of seawater through sea-ice brine to the sea-ice surface. Where concentrations are larger than those expected by the concentration effect, in-situ production of halocarbons could be occurring, whereas loss processes may dominate when values are lower.

Compound	CH_3I	C_2H_5I	$CHBr_3$	CH_2ICl	$2\text{-}C_3H_7I$	CH_2IBr	$1\text{-}C_3H_7I$	CH_2Br_2
Concentration (pM)	2.3	0.3	20	0.1	0.4	0.1	1.2	10

Table 19. Seawater concentrations which have been multiplied by brine volume to give brine concentrations expected via the concentration effect.

Chl *a* concentrations are also shown in figure 73 as an approximate indication of diatom distribution in the ice. Average halocarbon concentrations in the core brine drainage are shown in table 20, previous similar measurements are shown for comparison.

In the cores of the 25th Feb (left panel of figure 73), $CHBr_3$ and CH_2Br_2 concentrations were enhanced beyond the concentration effect close to the surface of the ice and close to the ice water interface, as was Chl *a*. C_2H_5I and CH_2ICl were slightly enhanced, with CH_2ICl showing a similar pattern to $CHBr_3$, but the other iodocarbons (1- and 2-

C_3H_7I and CH_2IBr) were either similar or depleted compared to calculated concentrations, possibly indicating specific loss processes for these compounds.

An interesting feature of the cores of 27th Feb (middle panel of figure 73), is the high Chl *a* close to the surface. Only CH_2ICl concentrations closely match this trend, although as before, $CHBr_3$ and CH_2Br_2 are generally enhanced compared to the "concentration effect" calculations, whereas CH_3I, 1- and 2-C_3H_7I and CH_2IBr show variability around the calculated profile.

The cores of the 29th Feb (right panel of figure 73), show a different trend, with the mono-iodocarbons showing a much larger enhancement than the bromocarbons, but no enhancement of CH_2ICl and strong depletion of CH_2IBr. These results show how complex this system is, with many different factors competing to influence halocarbon concentrations, which are a product of both production and loss processes. Production by the sea ice community and photochemical reactions compete with uptake to the diatom particulate, consumption by bacteria, loss to the water below and gas exchange with the atmosphere; therefore the brine channels are not inert pathways.

	CH_3I	C_2H_5I	$CHBr_3$	CH_2ICl	2-C_3H_7I	CH_2IBr	1-C_3H_7I	CH_2Br_2
Ave (A)	30.9	27.7	128	2.1	5.6	2.8	4.8	172
Max (A)	145	225	593	14.8	25.8	26.1	29.8	573
Ave (W)	5.7	30.4	351	16.1	16.4	9.4	14.3	38.7
Max (W)	149	739	6850	455	311	406	258	1270
Ave (F)	38.0	27.3	22		7.1		235	
Max (F)	40.9	26.2	23				259	

Table 20. Average (Ave) and maximum (Max) halocarbon concentrations (pM) measured in sea ice brine during this study (labelled A), measurements made in the Weddell Sea as presented in Chapter 5 (labelled W), and by *Fogelqvist and Tanhua* [1995] in the Weddell Sea (labelled F).
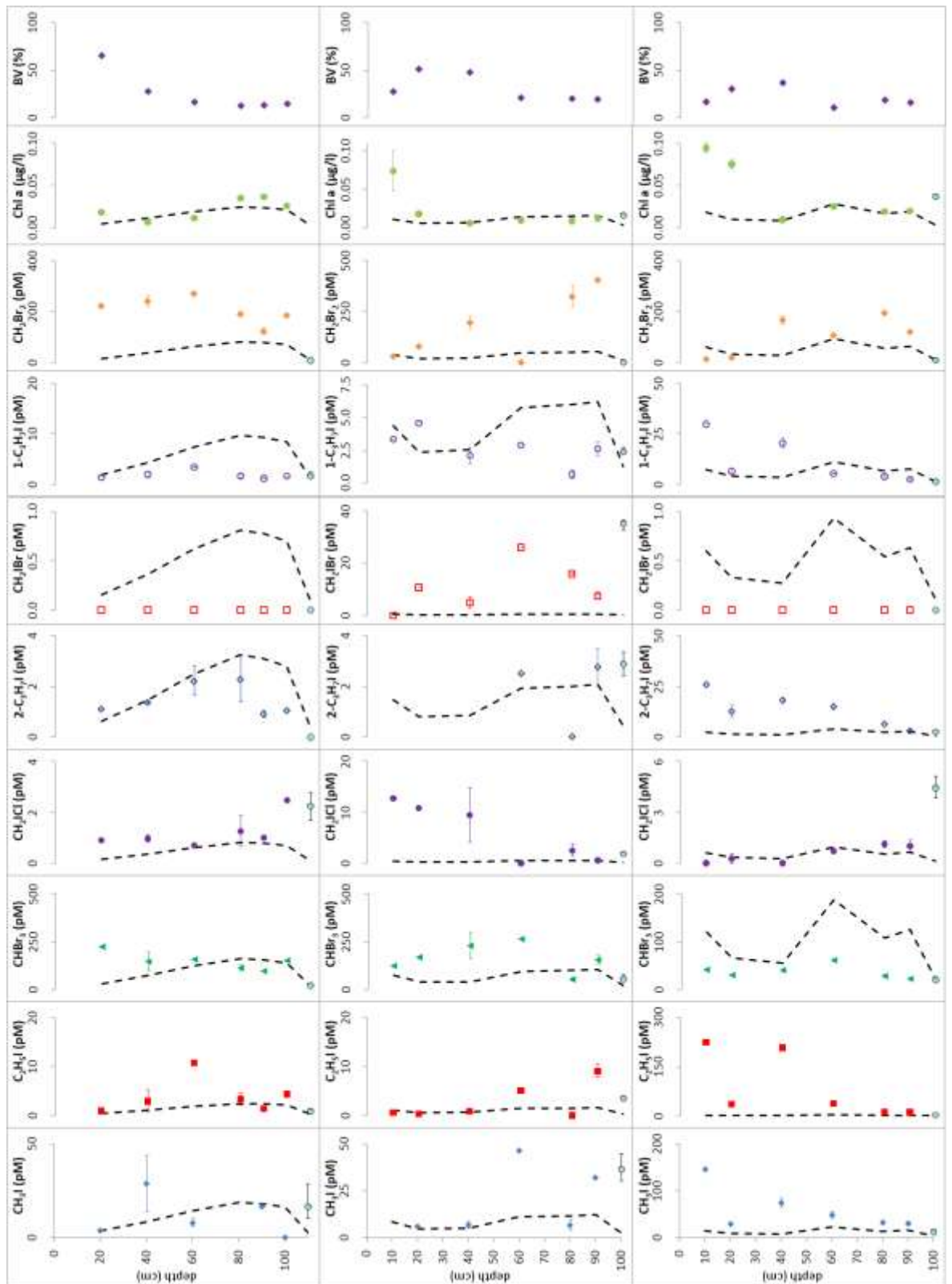
Figure 73. Halocarbon concentrations in sea ice brine from cores made on 25th June (left panel), 27th June (middle panel) and 29th June (right panel), the lower point on each graph represents halocarbon concentrations in the underlying seawater. Average and range of duplicate samples are shown. The dashed line shows the expected halocarbon concentrations via the concentration effect as described in the text. Note the change in scale.

6.3.2 Halocarbons in seawater

Halocarbon concentrations in water underneath the ice floe taken from hole A are shown in figures 74 and 75. The decrease in thickness of the ice floe, observed by other cruise participants (Gavin Turner, private communication) confirmed the ice was melting at a rate of approximately 3 cm day^{-1}. CH_2ICl concentrations increased during the time spent at the ice station. For the other compounds, an increase in most concentrations is observed, followed by a gradual decrease towards the end of the time spent at the ice station. This can be explained by consideration of the ice melt and water currents. The end of the Teflon tube used to sample the water was set up be level with the ice-water interface on the 22nd June. As the ice melted from below, the water sampled will have been ever further away from the ice-water interface. If under-ice blooms produce halocarbons, the peak in concentrations will occur a little distance from the ice, as ice meltwater has the greater influence closer to the ice, and loss to deeper waters occurs at depth. Therefore a concentration gradient moving away from the ice can be calculated (an example of this is shown in the lower panel of figure 75). The exception to this trend is CH_2ICl, which steadily increases as the ice floe melts. This is consistent with production of this compound by algae not associated with the ice.

These data are compared to CTD water samples taken throughout the cruise in figures 74 and 75. The larger range bars on the under-ice water samples reflect the variability in the water as 3 discrete samples were taken, whereas samples taken from the CTD Niskin bottles are triplicate samples of the same water mass. Chl *a* concentrations in the water samples are shown in figure 76.

The full depth profile of halocarbons through the water column, taken during a CTD cast whilst moored at the ice station is shown in figure 77. The profiles of C_2H_5I, 1- and 2-C_3H_7I concentrations show a strong peak at 10 m, just above the mixed layer depth at 12 m. Previous measurements [*Hughes et al.*, 2008] have shown these compounds to be produced by marine aggregates which are likely to collect here, as they sink from the upper photic zone due to gravity, but are prevented from sinking further due to the pycnocline barrier. CH_2Br_2 is the only compound which shows a similar profile to Chl *a*. Iodocarbon concentrations in seawater are lower during leg 3 when away from the Arctic pack ice, apart from CH_2ICl which shows a significant increase in concentration at the DCM in open waters. CH_2ICl shows a good correlation

to Chl *a* throughout the campaign (Figure 78). Concentrations of the other halocarbons tend to be higher in water underneath the ice, especially the iodopropanes. No correlation was seen between the other compounds and Chl *a.*
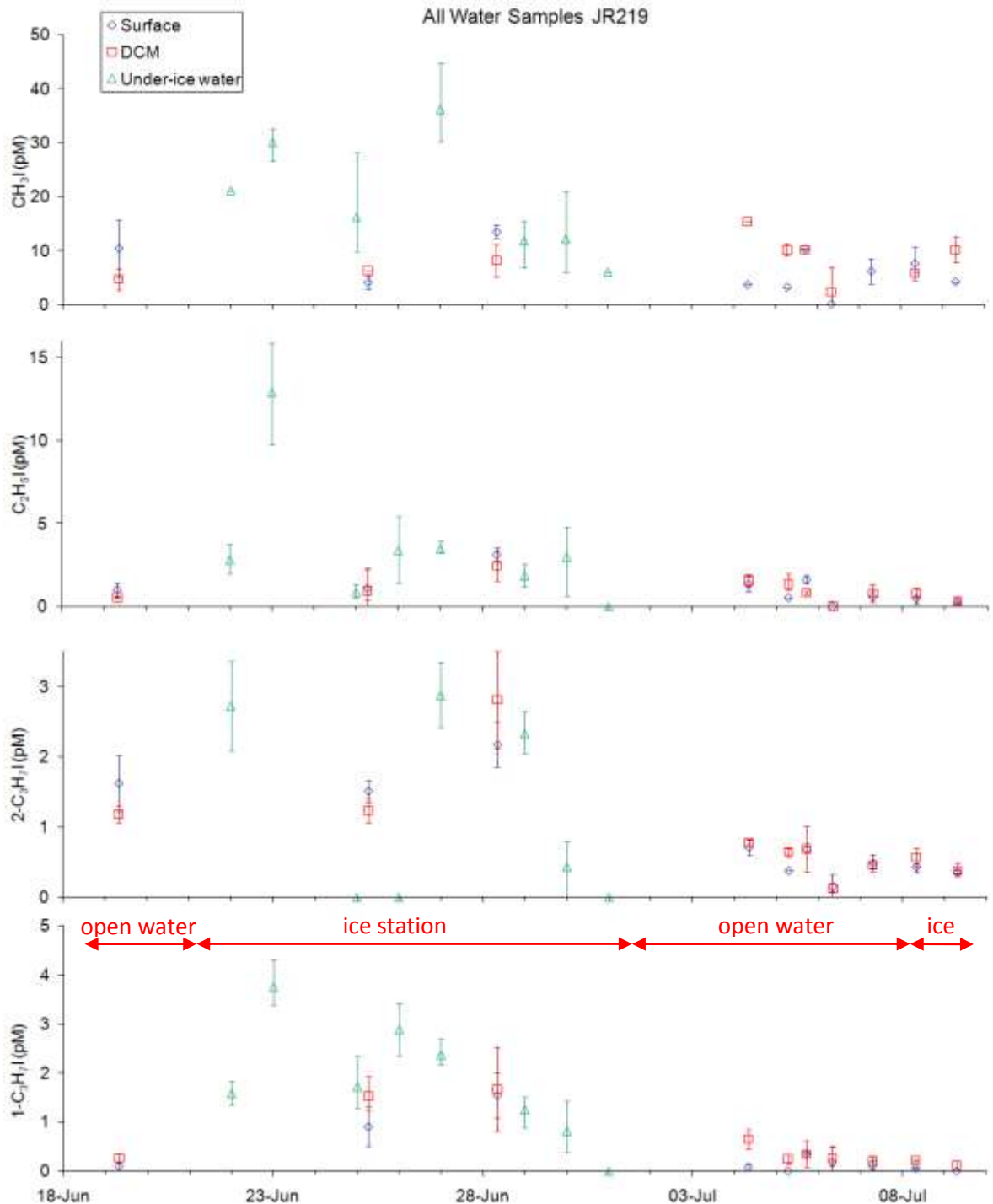
Figure 74. Halocarbon concentrations in water sampled via CTD Niskin bottles within the top 1m of the water column and the DCM. Water samples from underneath the ice are also shown from the time period the ship was moored at the ice station, from 21st June to 1st July. On 8th and 9th July the ship was close to the pack ice east of Greenland.
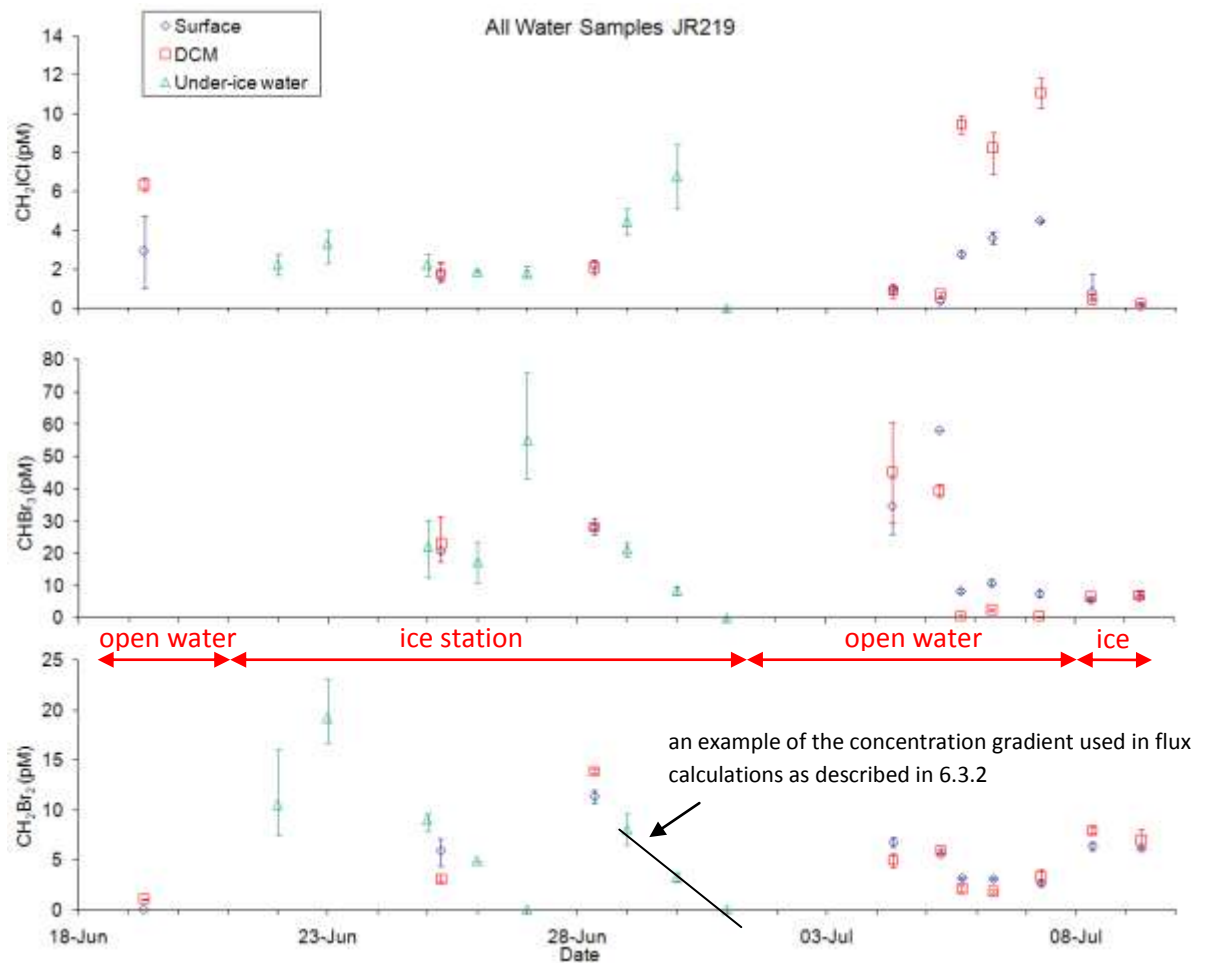
Figure 75. Halocarbon concentrations in water sampled via CTD Niskin bottles within the top 1m of the water column and the DCM. Water samples from underneath the ice are also shown from the time period the ship was moored at the ice station, from 21st June to 1st July. On 8th and 9th July the ship was close to the pack ice east of Greenland. CH_2IBr only measured above LoD in one under-ice water sample on 27th June where concentration was 35 (32.5 – 36.5) pM, and in 4 CTD water samples, made from 4th – 7th July where concentrations were up to 2.2 pM.
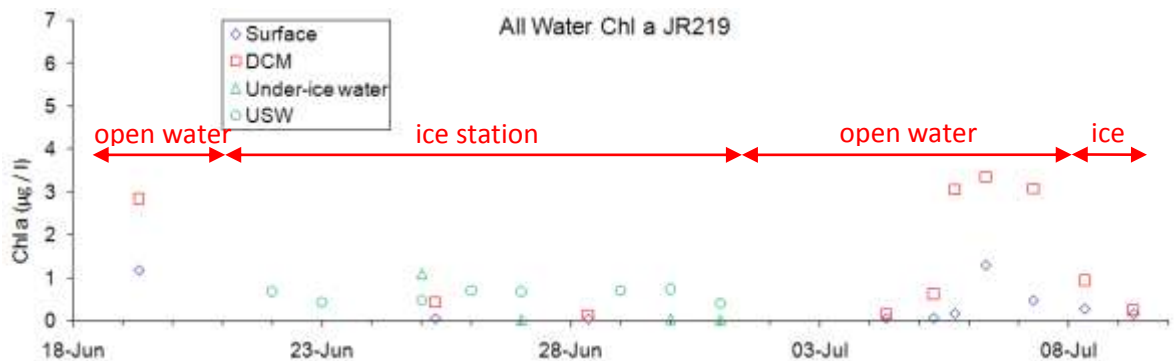
Figure 76. Chlorophyll a concentrations of water samples. The open water samples taken on 19th June and 4th – 7th July show a clear difference in biomass between surface and DCM, whereas concentrations in ice covered waters are similar at the different depths, and are on average lower.
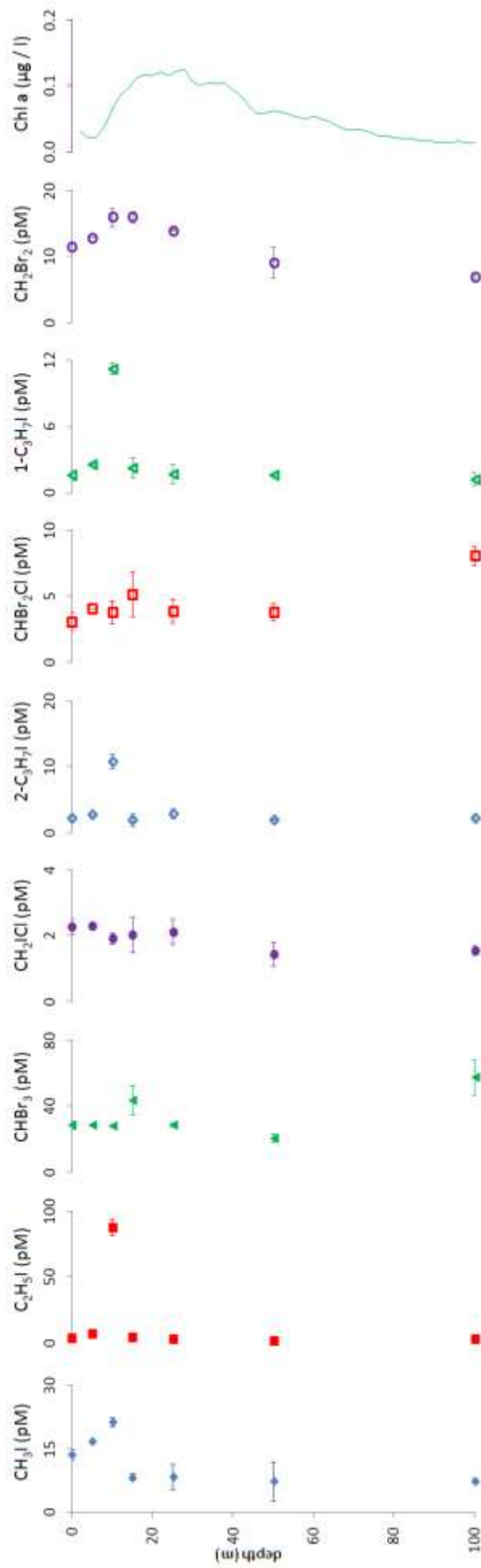
Figure77. Full profile of halocarbon concentrations through the water column whilst at the ice station on 28th June, sampled via CTD Niskin bottles.
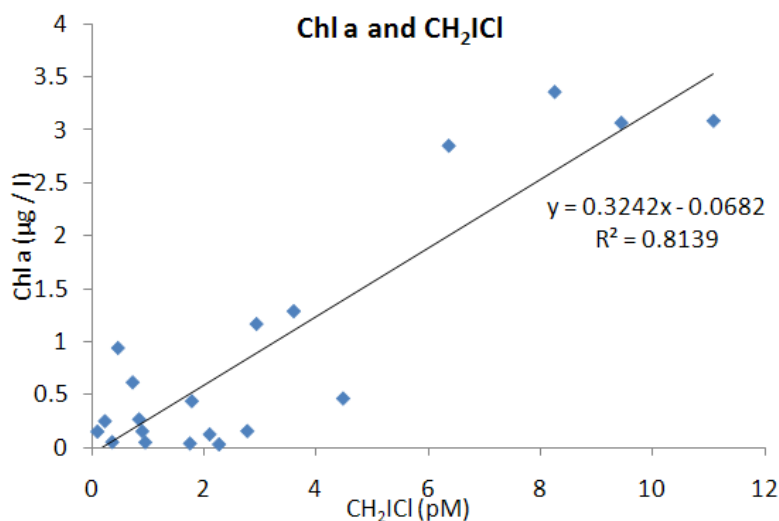
Figure 78. Chlorophyll *a* and CH_2ICl concentrations in water samples

The water sampled during the campaign (depicted in figure 74 - 76) can be subcategorised as follows: 19th June is open water west of Svalbard; 22nd June – 1st July is water sampled while the ship was surrounded by the Arctic pack ice; 4th – 7th July is open water sampled during the transect from Svalbard to Greenland; 8th – 9th July again represents ice covered waters, this time east of Greenland. In figure 69, the sea surface temperature can be seen to drop when in ice, and the Chl a concentrations show much less variability.

The only compound which follows the same trend as Chl *a* concentrations in water samples is CH_2ICl, this compound seems to be produced by organisms not associated with the ice. Concentrations of all other halocarbons are higher in sea ice brine and in ice covered waters. This may be due to production of halocarbons by different phytoplankton species, with higher production rates by ice diatoms, or by processes occurring in the ice itself which is not related to diatoms, for example the concentration effect. Work by other groups has shown that the activity of the enzymes responsible for halocarbon production is more active in polar and ice-associated diatoms [*Arrigo and Thomas*, 2004; *Hill and Manley*, 2009]

Waters in which CTD casts were made can be separated into 4 distinct types, as depicted in figures 79 and 80: CTD casts made whilst the ship was moored at the ice station; station KF3, close to Svalbard as shown in figure 66; station KF4 in deeper waters further out to sea; and over the Greenland shelf. As can be seen, CH_3I and C_2H_5I concentrations are variable and values overlap across all water masses. Concentrations of the iodopropanes are higher in water close to the Arctic pack ice, and CH_2ICl show much higher concentrations at KF4, especially at the DCM.
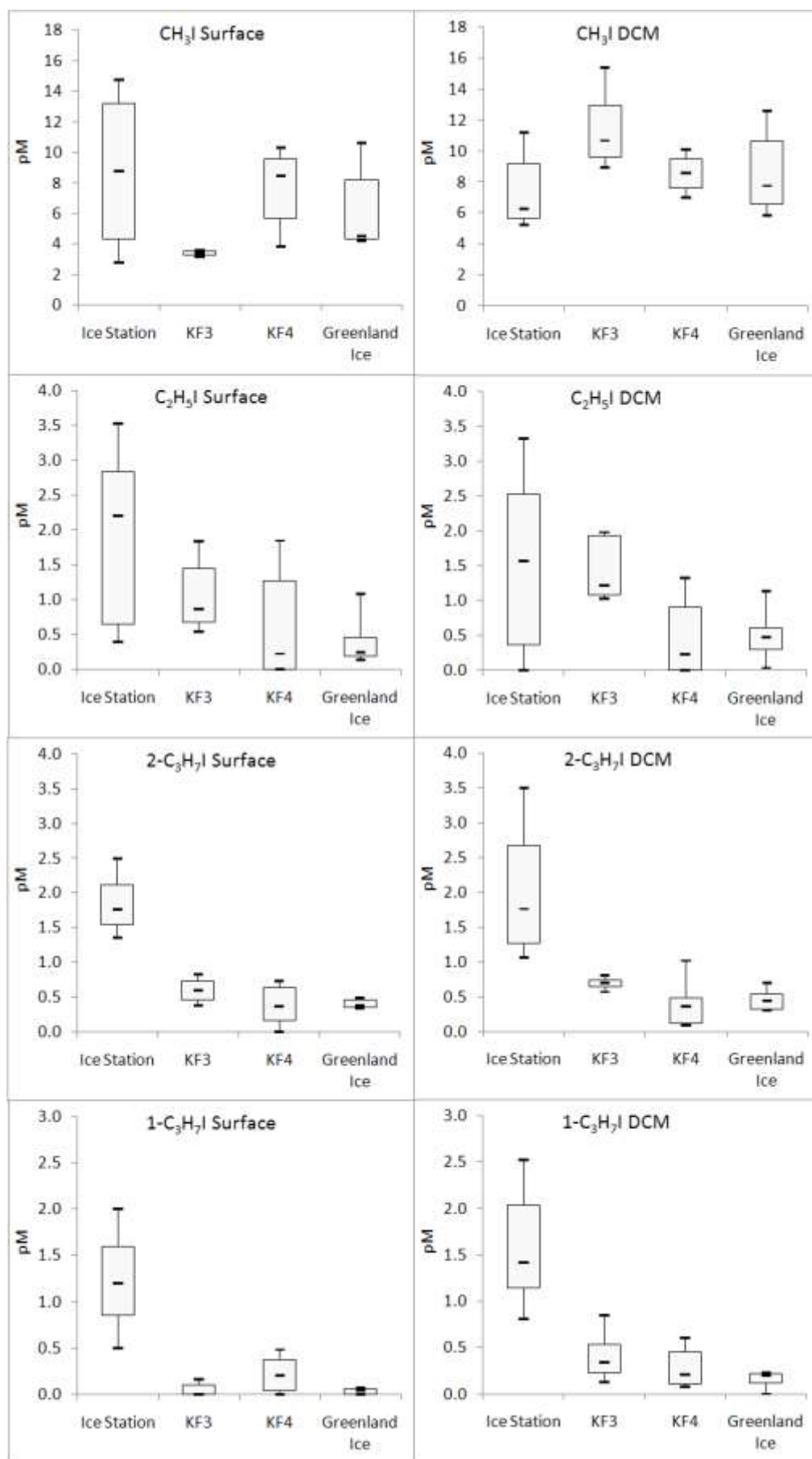
Figure 79. Box whisker plots showing halocarbon concentrations in water samples from CTD casts of different areas. The boxes represent the 20th and 80th percentiles, the dash represents the median and the range bars show the maximum and minimum concentrations.
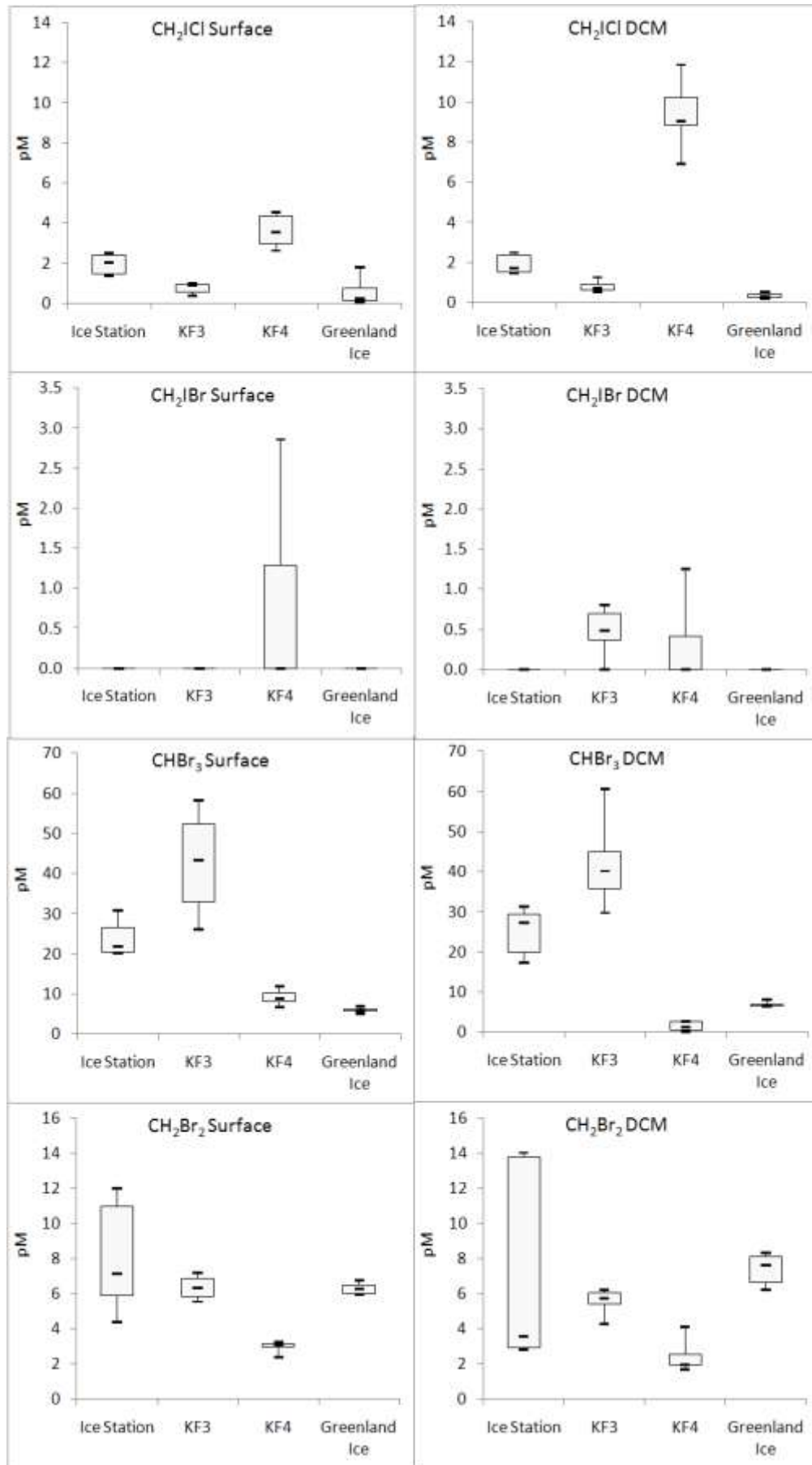
Figure 80. Box whisker plots showing halocarbon concentrations in water samples from CTD casts of different areas. The boxes represent the 20th and 80th percentiles, the dash represents the median and the range bars show the maximum and minimum concentrations.

As can be seen from the Chl *a* concentrations in figure 76, the most biologically productive waters were sampled west of Svalbard, and the ice edge algae bloom in this region is clearly seen in the satellite image in figure 81 (courtesy Andrew Fleming, BAS, from the SeaWifs dataset).
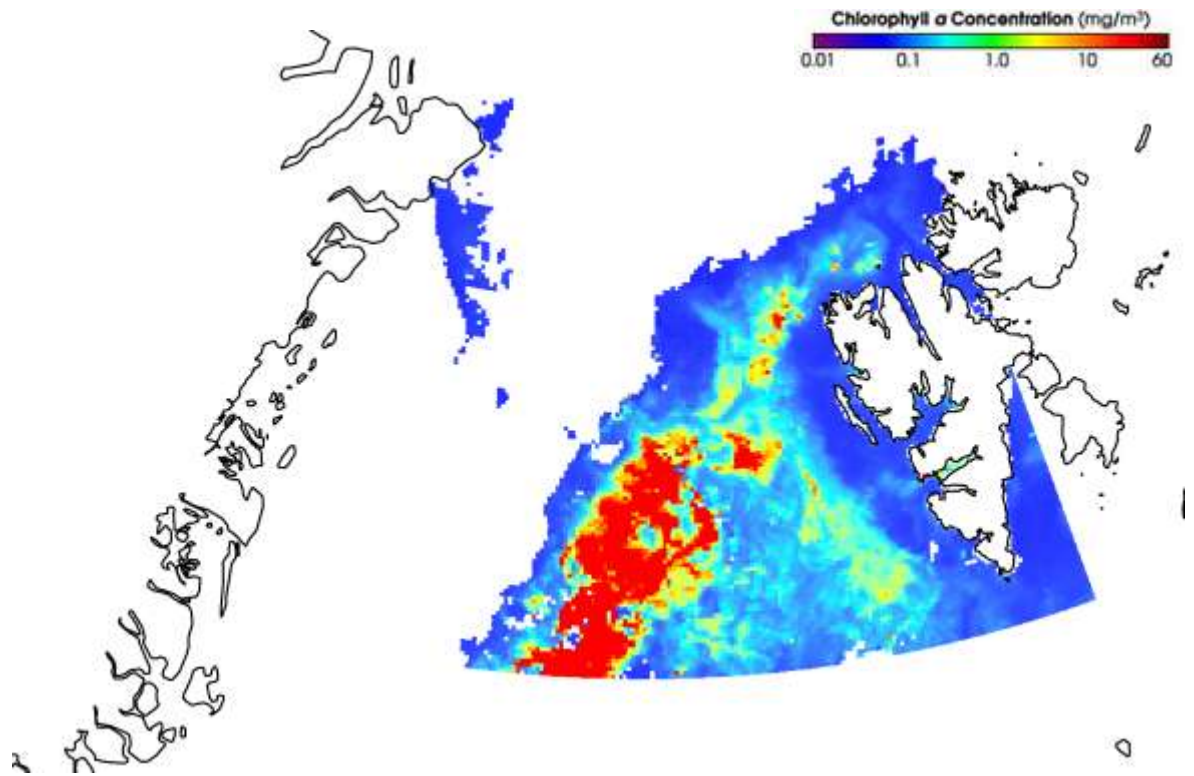
Figure 81. Satellite imagery showing the phytoplankton bloom west of Svalbard in June 2010 (courtesy Andrew Fleming BAS, from SeaWifs data)

Halocarbon concentrations in the dive samples are shown in table 21 and figure 82. The larger concentrations of $CHBr_3$, CH_2Br_2 and CH_3I suggests these compounds are released from dead /dying algae draining from the ice. Concentrations of the other halocarbons are not enhanced in these diatom-rich samples. Previous work monitoring production of halocarbons over the life cycle of diatoms has shown the production is highest during exponential growth, and less during stationary and dying phases [*Moore et al.*, 1996], which explains a lower halocarbon concentration ratio between the ice brine and dense algae mats than the cell density ratio.

		Average	Max	Min
CH₃I	close to ice	30.0	33.5	25.8
	bottom ice algae	23.8	30.7	15.6
	algae mats	49.3	70.4	37.9
C₂H₅I	close to ice	16.3	20.3	11.0
	bottom ice algae	11.5	15.5	6.1
	algae mats	21.0	26.6	17.1
CHBr₃	close to ice	32.3	36.6	29.7
	bottom ice algae	28.6	30.7	25.3
	algae mats	203.2	309.4	72.4
CH₂ICl	close to ice	3.7	4.0	3.1
	bottom ice algae	3.2	3.9	2.8
	algae mats	6.1	9.9	3.1
2-C₃H₇I	close to ice	5.4	7.7	3.7
	bottom ice algae	4.3	4.5	3.8
	algae mats	6.2	7.4	5.2
1-C₃H₇I	close to ice	3.8	4.2	3.2
	bottom ice algae	3.9	4.2	3.4
	algae mats	6.0	7.7	4.2
CH₂Br₂	close to ice	11.9	12.4	11.5
	bottom ice algae	12.5	17.3	9.4
	algae mats	39.7	58.4	24.9

Table 21. Halocarbon concentrations (pM) in water samples collected by the dive team, as depicted in figure 68. Three samples of each type were collected.
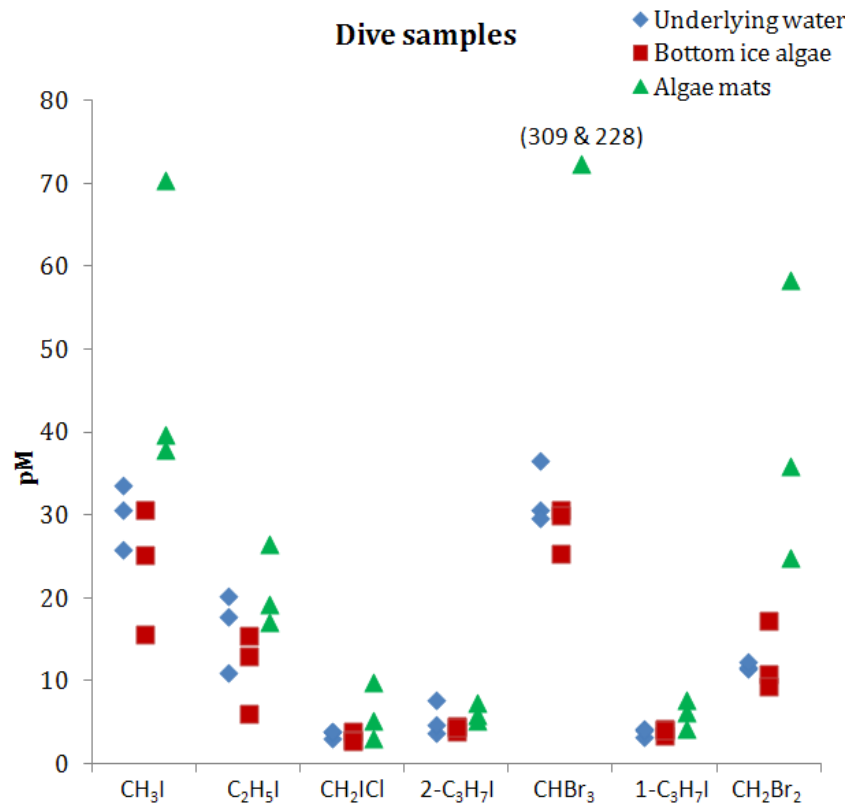
Figure 82. Halocarbon concentrations in the three types of water samples collected by the dive team. (Concentrations of $CHBr_3$ from two algae mat samples are off the scalee at 309 and 228 pM).

When halocarbon concentrations in the different sample types collected at the ice station are compared (figure 83), the potential for some halocarbons to be enhanced in the sea ice brine channel network is clear, though the range is large and overlaps with the water concentrations. Production underneath the ice, flushing of the brine channels with seawater and fresh ice melt all contribute to halocarbon concentrations, along with consumption by bacteria and loss to the atmosphere. These processes are discussed further in section 6.4.
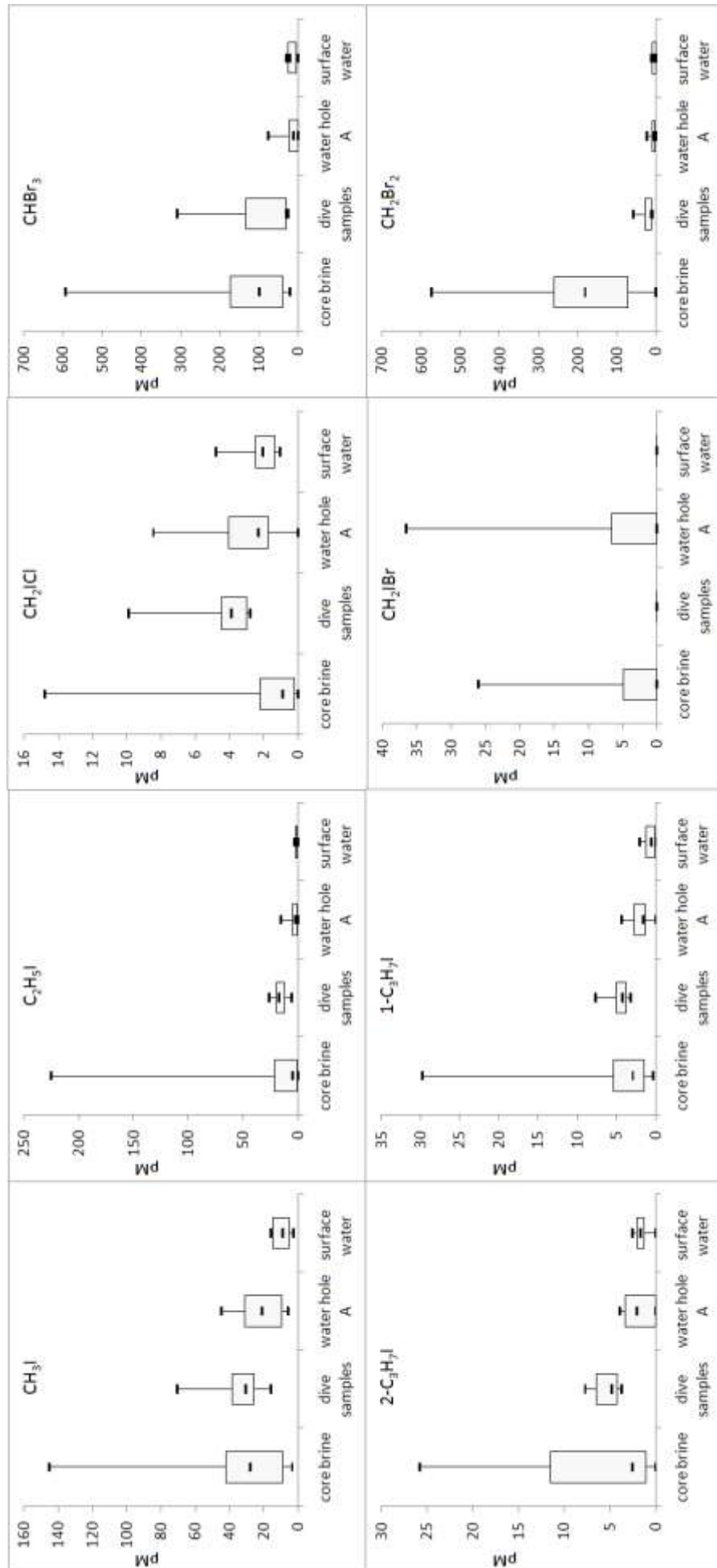
Figure 83. Summary of halocarbon concentrations in water and sea ice brine samples collected at the ice station. The boxes represent the 20th and 80th percentiles, the dash represents the median and the range bars show the maximum and minimum concentrations.

6.3.3. Halocarbons in air

Triplicate air samples were made every day, results are shown in figure 84. Higher mixing ratios are observed above the sea ice of the Arctic Oceans. As can be seen from back trajectories in figure 85, and wind direction data in figure 69, the wind was predominantly from the north. The low air concentrations for all compounds on the 19th June (figure 84) could be due to the air mass having originated over Svalbard (figure 85) where potential halocarbon sources are less likely.

Bromocarbon mixing ratios are similar to previous measurements by others [*Chuck et al.*, 2005; *Class and Ballschmiter*, 1987; *Quack and Wallace*, 2003]. CH_3I mixing ratios are higher than previous measurements in polar regions (table 2), but similar to measurements made at Mace Head [*Carpenter et al.*, 1999] close to kelp beds. C_2H_5I and CH_2ICl concentrations are very high compared to previous measurements, though the latter are in the same range as those of Jones *et al.* in the Outer Hebrides, also close to kelp beds.

The larger variability of halocarbon concentrations in air samples over ice (figure 84) potentially reflects temporal variation in source strengths in the ice area. For example open leads in the ice pack may cause a 'hot spot' in concentrations in the air mass reaching the ship, which may not be sampled during all three air samples which are taken over approximately 15 mins each, total sampling time approximately 45 mins. The smaller error bars for air measurements made over open water reflect the more well mixed air parcel, as source strengths will be less variable from the ocean. However open ocean data does exhibit fairly large variability between sampling events. This is because concentrations are dependent on wind speed, wind direction, boundary layer height, temperature and solar radiation as well as source strength.
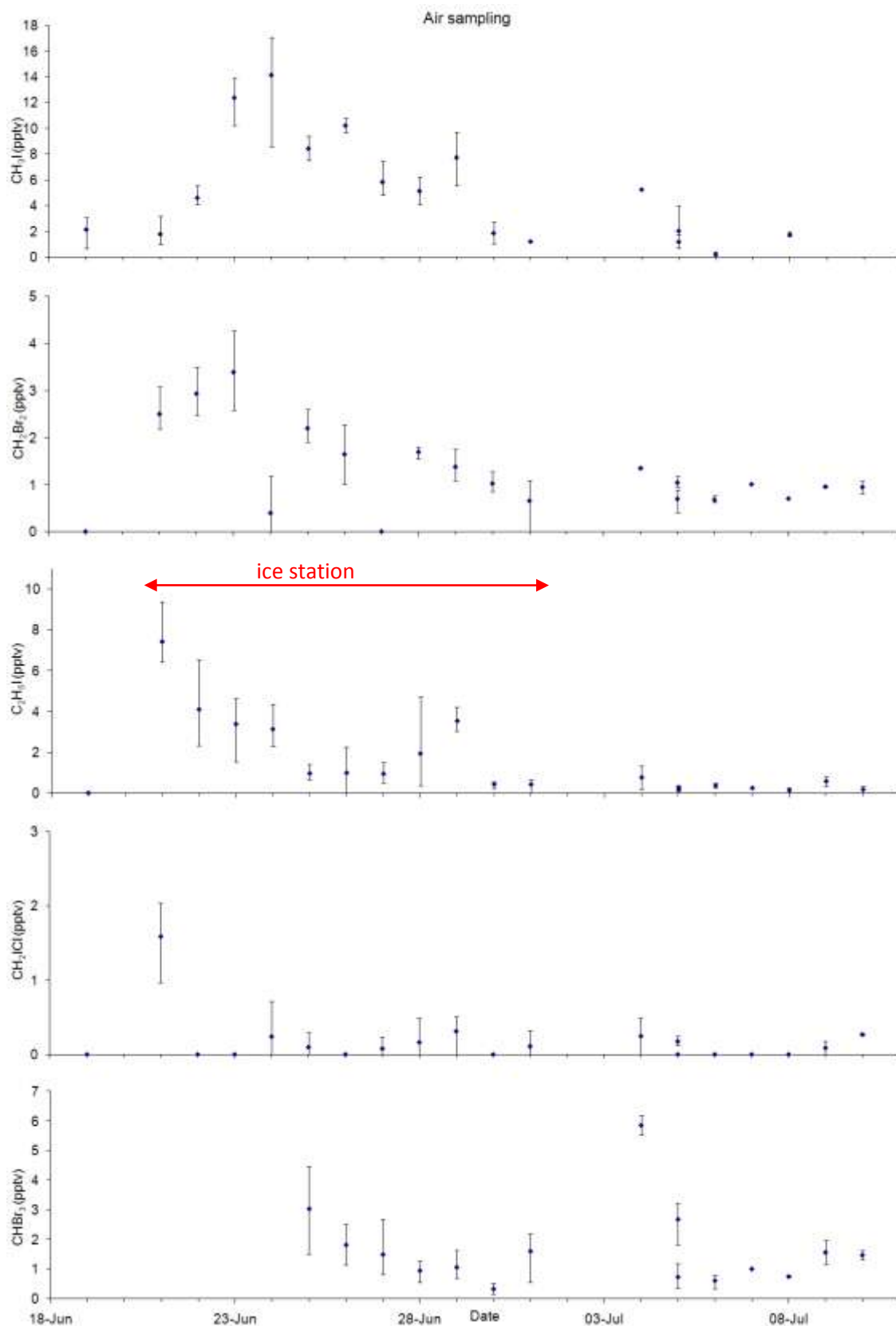
Figure 84. Atmospheric mixing ratios of CH₃I, CH₂Br₂, C₂H₅I, CH₂ICl and CHBr₃ during the JR219 field campaign. CH₂IBr was only measured above the LoD on 21st and 22nd June, and from 5th – 7th July, 1- and 2-C₃H₇I were below the LoD in all air samples.
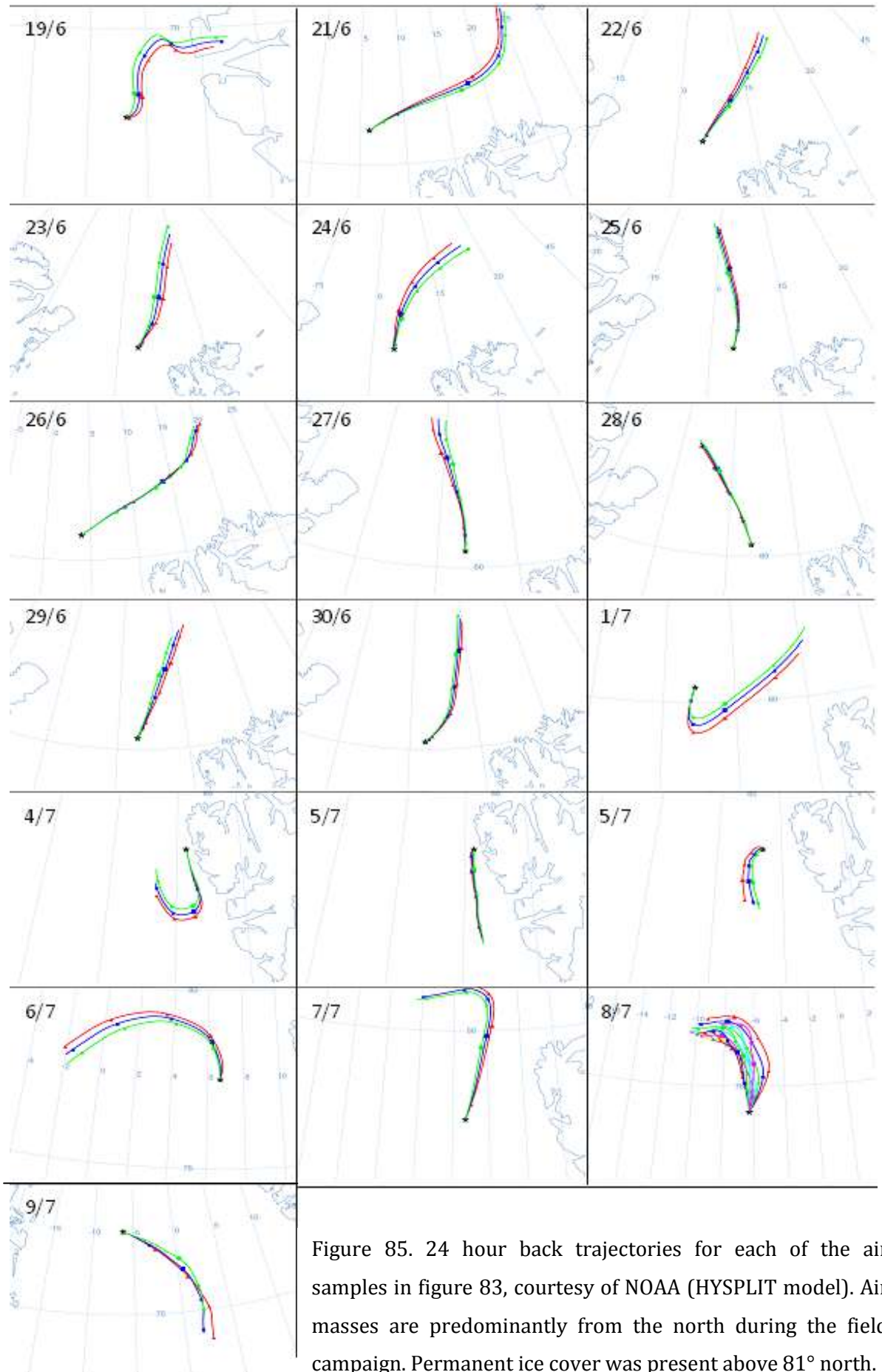
Figure 85. 24 hour back trajectories for each of the air samples in figure 83, courtesy of NOAA (HYSPLIT model). Air masses are predominantly from the north during the field campaign. Permanent ice cover was present above 81° north.

The movement of the air parcels for 6 hours previous to: ▇▇ the time shown in the chart title, and ▇▇ 1 hour, ▇▇ 2 hours, ▇▇ 3 hours, ▇▇ 4 hours and ▇▇, 5 hours before this.

6.3.4. Incubations

Brine collected whilst holes were being made in the ice to allow access for the dive team was incubated for 48 hours. The conditions were designed to be representative of those in surface waters, and also mid way and underneath one metre thick sea ice (as detailed in section 6.2.1).

No enhanced levels of iodocarbons or bromocarbons were observed in the brine samples, compared to the filtered controls. However, algae colonies were visible in the ice long after the brine had drained (figure 86) suggesting the brine collected did not contain the brine channel communities, so the lack of halocarbon production in the brine is not surprising. A better way of repeating these incubations would be to melt the lower ice sections in the ice pore water collected and some underlying seawater, thus simulating sea ice melt. These results do however indicate halocarbon production is not occurring in the sea ice brine by abiotic processes.

Figure 86. Large pieces of sea ice cut to make holes for the dive team. Large volumes of brine were collected from these $\sim 0.25 m^3$ pieces of brine for incubation studies, however as is clear from the photograph, the diatom colonies did not drain from the ice with the brine.

6.3.5 Saturation anomalies and flux calculations

Results from this study show that halocarbon concentrations may be enhanced in the sea ice brine and in under-ice water samples. This may be due to emissions from algae within- and underneath the ice. Saturation anomalies and fluxes were calculated in order to estimate the importance of this regional chemistry on the atmosphere above, as detailed in section 5.3.4.

Results from the calculations of saturation anomalies are shown in table 22. CH_3I and C_2H_5I are always supersaturated in surface waters, which will lead to an ocean-atmosphere flux. $CHBr_3$, CH_2ICl and CH_2Br_2 are predominantly supersaturated in surface waters, though occasions do exist when undersaturation occurs and therefore these halocarbons may be deposited to the ocean. These results show how CH_3I and C_2H_5I have the highest mixing ratios in air (figure 84).

Saturation anomalies were also calculated using concentrations measured in water underneath the ice to assess whether exposure of these waters would lead to greater fluxes of halocarbons. The flow of water underneath the ice flow will ensure these waters do become exposed to the atmosphere. Results, shown in table 23, show a slight increase in saturation anomaly in the under-ice water, with the exception of CH_2Br_2.

$$\text{Saturation anomaly} = 100\% \times (C_w - C_a/H)/(C_a/H) \qquad (7)$$

	CH_3I	C_2H_5I	$CHBr_3$	CH_2ICl	CH_2Br_2
ave	1290	869	143	355	107
max	2198	2528	334	753	203
min	136	28	-39	-60	-10

Table 22. Saturation anomalies (%) based on simultaneous air and surface water concentrations. CH_2IBr 1- and 2-C_3H_7I were not measured above the LoD in enough air samples for these calculations to be carried out.

	CH_3I	C_2H_5I	$CHBr_3$	CH_2ICl	CH_2Br_2
ave	1845	656	186	585	51
max	4698	1902	422	745	109
min	391	-93	9	426	8

Table 23. Saturation anomalies (%) based on simultaneous air and under-ice water concentrations.

The statistical language R was used for flux calculations as detailed in *Johnson* [2010]. Briefly, equation $F = K_w(C_a/H - C_w)$ was used where F is the flux, K_w is the transfer velocity, C_a is the air concentration, C_w the simultaneous water concentration, and H the Henry's law constant as above. Transfer velocities are dependent on wind speed, salinity and water temperature; 7-day average wind speed values were used.

Simultaneous (same day) air and surface (CTD) water samples were used in flux calculations. For the period of time the ship was moored at the ice station, under-ice water concentrations were used, in order to calculate a flux at the ice edge when these water masses are exposed to the atmosphere. Fluxes were also calculated using halocarbon concentrations in the uppermost sections of the ice cores, in order to calculate fluxes from the ice to the atmosphere. The assumption is made here that the concentrations in the brine channels in the top 10 cm of the ice are representative of the concentrations in the liquid film on the ice surface, as under these conditions the brine channels are connected and brine migration transports dissolved ions and trace gases to the ice-atmosphere interface. This method assumes the same factors affect fluxes from a brine layer on the surface of sea ice as affect the surface microlayer on seawater. This is not known, but to a first approximation it provides a useful comparison.

Results (figures 87 and 88) show how ocean-atmosphere fluxes are potentially much larger when waters underneath the ice are transported to the ice edge and become exposed to the atmosphere. Also, fluxes from the surface of sea ice to the atmosphere may be much larger than those from the ocean. Both of these higher fluxes explain why atmospheric mixing ratios of halocarbons are higher in air which has travelled over sea ice (figure 84).
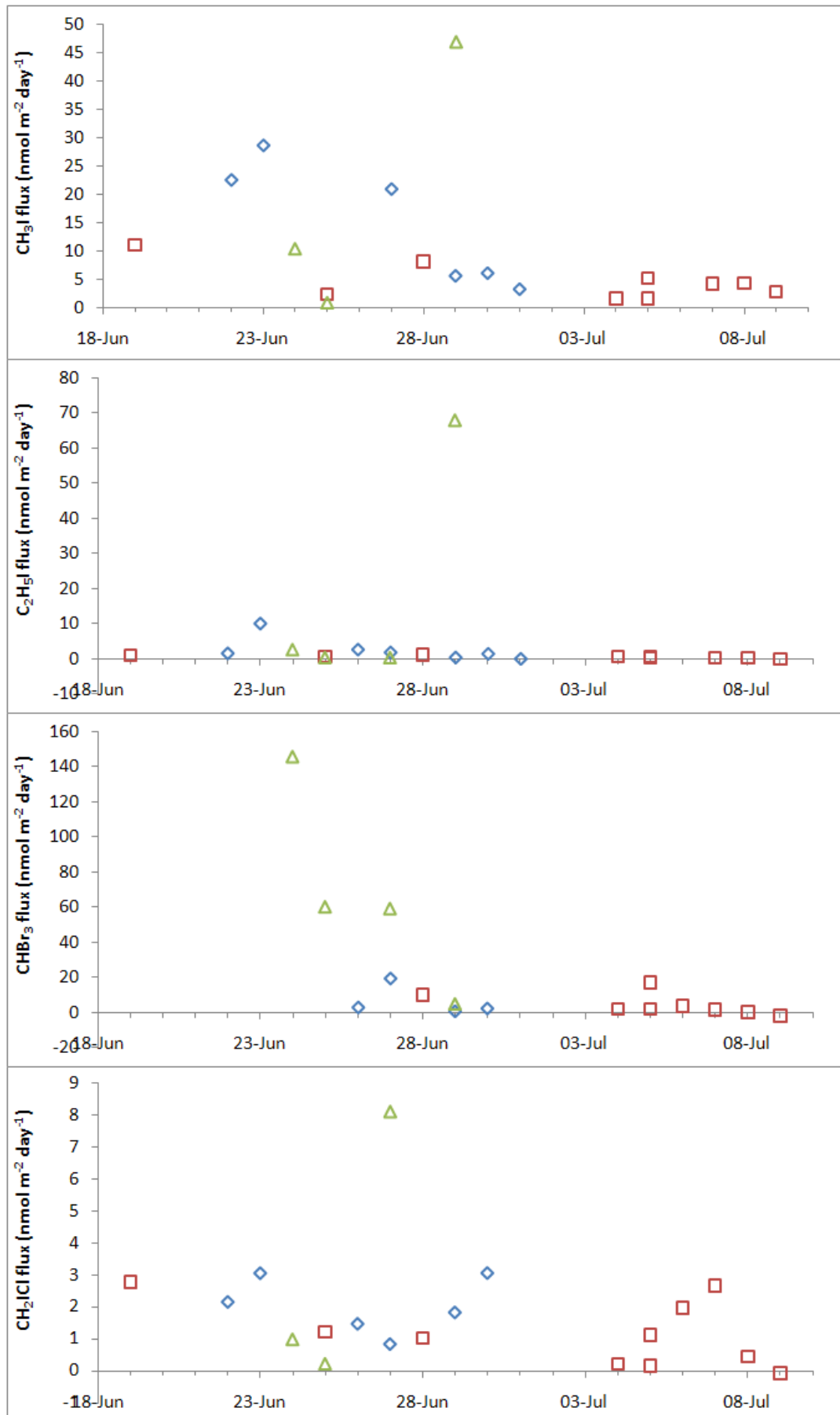
Figure 87. Fluxes of halocarbons using under-ice water concentrations (blue diamonds), surface seawater concentrations (red squares), uppermost ice core brine concentrations (green triangles) and same day air mixing ratios.
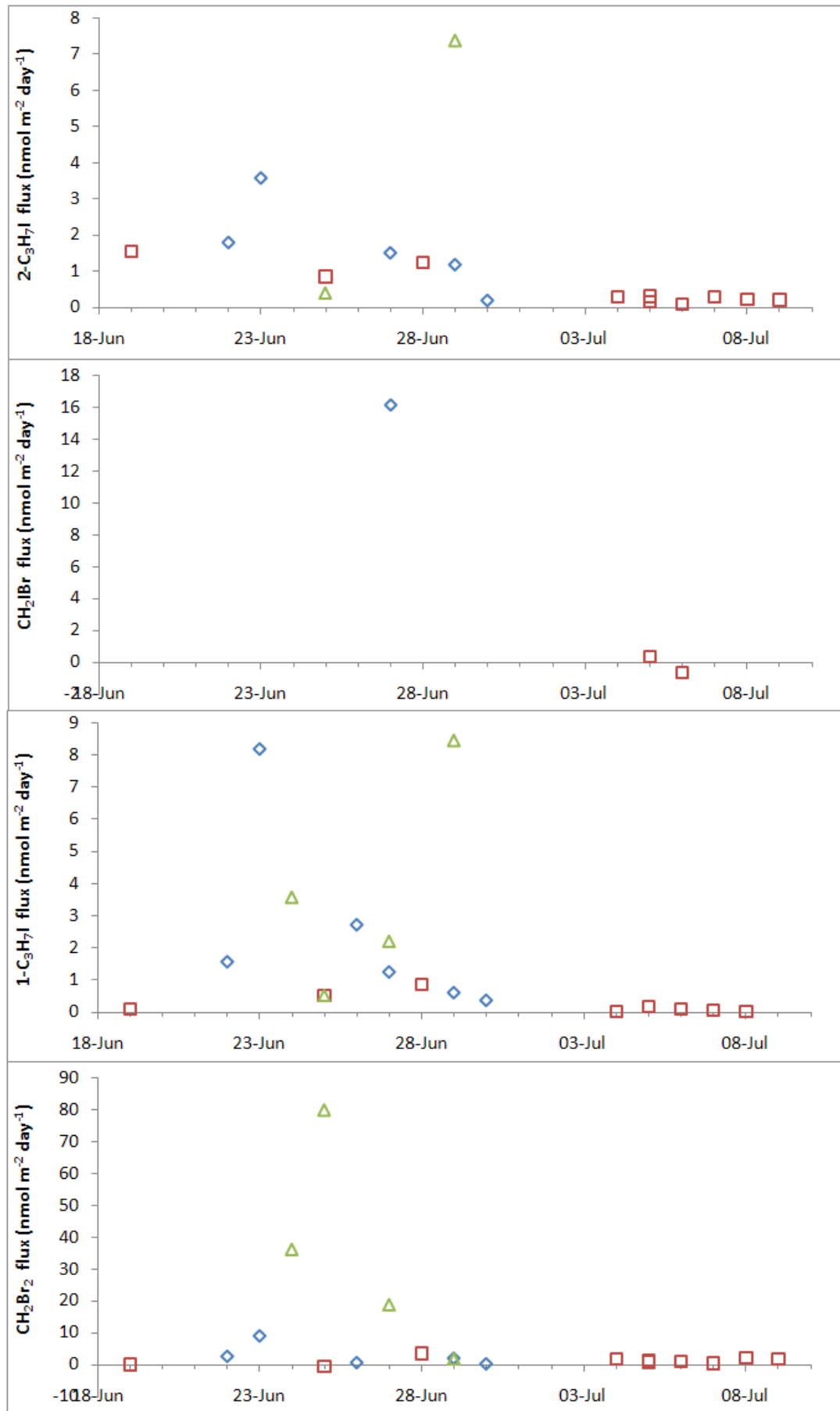
Figure 88. Fluxes of halocarbons using under-ice water concentrations (blue diamonds), surface seawater concentrations (red squares), uppermost ice core brine concentrations (green triangles) and same day air mixing ratios.

Fluxes from the ice to the water below

When sea ice forms, salts are expelled from the growing ice matrix and hyper-saline brine drains from the ice, forming a network of channels. When the ice starts to melt, freshwater dilutes this brine, eventually making it less saline than the seawater underneath. When this point is reached, brine no longer drains from the channels and a stratified regime takes over. From this point onwards, solute exchange is mainly controlled by molecular diffusion [*Tison et al.*, 2010].

From the ice core data in figure 73, it would appear that a concentration gradient exists in the core of the 29th June (right panel) for all compounds except CH_2ICl and CH_2IBr. This would result in a flux of halocarbons from the higher concentrations within the centre of the core to the lower concentrations in the underlying seawater, controlled by molecular diffusion and driven by the concentration gradient. For this reason, the concentration gradient in these cores, and the molecular diffusion coefficient of seawater at 0°C of 1×10^{-9} m^2 s^{-1} [*Yuan-Hui and Gregory*, 1974] was used to calculate a flux due to brine channel drainage. From Fick's first law of diffusion, flux = $-D(\delta C/\delta t)$, where $(\delta C/\delta t)$ is the concentration gradient and D is the diffusion coefficient. The results range from 9.1×10^{-8} to 8×10^{-6} nmol m^{-2} day^{-1}, much slower than sea to air and ice to air fluxes. Therefore, it is expected that following brine drainage (when the brine salinity was higher than that of the underlying seawater), the very slow process of molecular diffusion then keeps halocarbon concentrations relatively constant in the ice. To calculate the contribution from the brine channels due to ice melt, the average concentration in the lower section of the ice brine has been multiplied by brine volume and the average rate of ice melt (3 cm day^{-1}). Results range from 0.003 to 2.4 nmol m^{-2} day^{-1}, much larger than those due to molecular diffusion discussed above.

The results from the two brine channel fluxes were then compared to the flux calculated from the concentration gradients, calculated from the measured fluxes from hole A. This latter flux was calculated by multiplying the change in under-ice water concentrations from hole A by the distance the sampling tube moved away from the ice. This measured flux should take into account the ice melt, brine channel contribution from molecular diffusion and production by the bottom- and under- ice water community. Therefore by calculating the difference between the two values, *in-situ* production (possibly by diatoms) underneath the ice can be inferred. It is

accepted that the values are only an approximation and certain factors have not been taken into account, such as water currents and exchange with the underlying seawater. This last approximation is valid as a stratified water column was observed during the depth profile of the 28th June. Production by diatoms underneath the ice is therefore calculated to be 0.2, 0.06, 0.9, 0.004, 0.02, 0.03, 0.02 and 2.4 nmol m^{-2} day^{-1} for CH_3I, C_2H_5I, $CHBr_3$, CH_2ICl, $2\text{-}C_3H_7I$, CH_2IBr, $1\text{-}C_3H_7I$ and CH_2Br_2 respectively.

6.4. Discussion of halocarbon concentrations and fluxes during JR219

A complex ecosystem network affects halocarbon concentrations, including production by diatoms [*Sturges et al.*, 1992], uptake by bacteria [*Goodwin et al.*, 1997; *Goodwin et al.*, 1998], and fluxes between the ice, air and atmosphere. Results from the ice cores show how halocarbon concentrations are enhanced in the sea ice brine, and enhanced concentrations in under-ice water samples show how the under-ice bloom may also produce halocarbons. In order to estimate the contribution of these processes, the various production and loss processes have been considered as depicted in figure 89.

F_i and F_w have been calculated in section 6.3.5, along with contributions from the ice algae. Assuming similar factors affect fluxes from a liquid brine layer on the surface of sea ice, ice-atmosphere fluxes have the potential for a greater contribution to the atmospheric halogen budget than the seawater, however the flux at the ice edge due to waters influenced by the ice edge and under-ice communities may supply a similar flux.

Factors affecting fluxes from the ice are however not known, much more work is needed in this area. One factor which could affect these fluxes is the presence of a snow layer. Whilst one may think that the presence of snow would suppress fluxes, snow is very porous, and very cold temperatures and ice surfaces may actually increase halogen reactivity [*Cho et al.*, 2002]. The presence of halogen radicals or ions in the so-called quasi-liquid layer may make them more available for reaction due to their highly polarisable electron field, which will be particularly pronounced for the large iodide ion.

The largest halocarbon flux to the water underneath the ice is from ice melt and under-ice diatom community production, whereas brine channel drainage contributes little under these conditions. The reasons for halocarbon production have

not been conclusively determined, but one possibility is in response to grazing [*Manley*, 2002], and enhanced halocarbon concentrations in the sea ice brine channels may occur as ice melts and brine channels widen, hence allowing small zooplankton to enter and grazing pressure on the ice communities to increase.
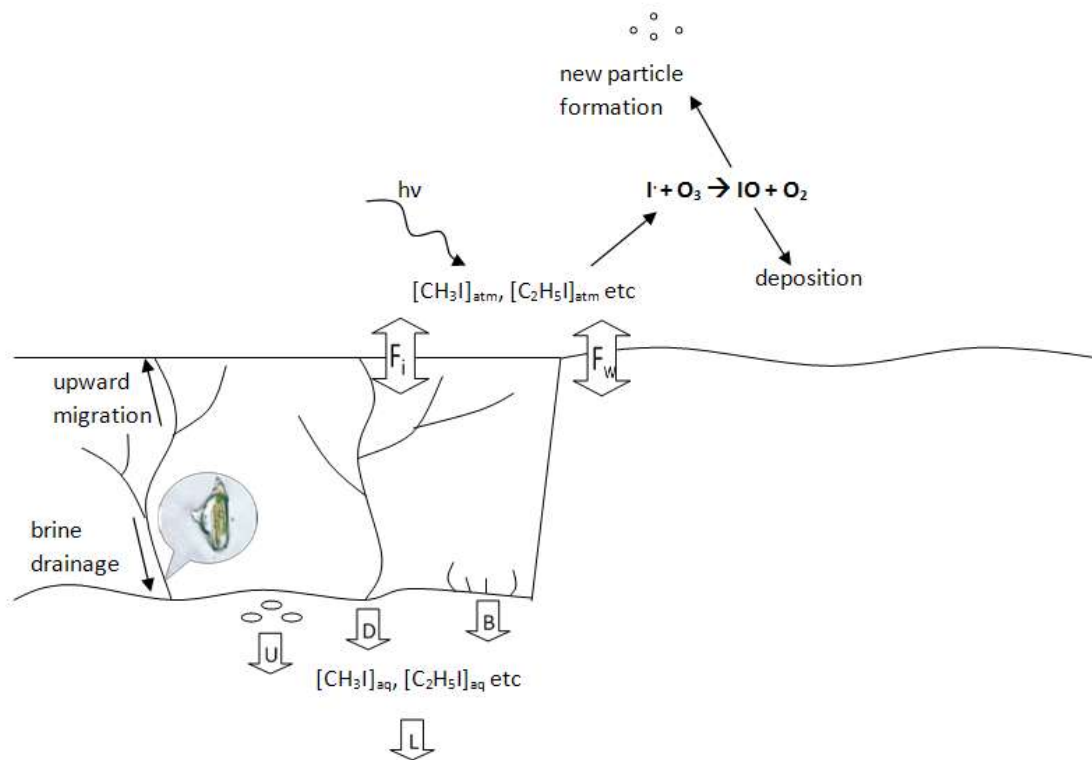
Figure 89. The different processes contributing to halocarbon concentrations, where F_i and F_w are ice- and water-atmosphere fluxes respectively, U is production by the under-ice bloom, D is brine channel drainage, B is production by the bottom ice community and L is loss to the underlying seawater and other loss processes as discussed in the text.

6.4.1. Correlations between halocarbon concentrations

Within the sea ice brine, a correlation was found between concentrations of the iodocarbons CH_3I, C_2H_5I, 1- and 2-C_3H_7I (R^2 values 0.76 to 0.94); a similar trend was found between these compounds across water samples but R^2 values are lower (0.42 to 0.62). *Schall et al.* [1997] showed a correlation between $CHBr_3$ and CH_2Br_2, no such correlation was found between the bromocarbons in this study.

Others have noted a low correlation between the bromocarbons close to sources [*Carpenter and Liss*, 2000; *Hughes et al.*, 2009]. *Schall et al.* [1997] showed bromocarbon concentrations were linked to Chl *a* but iodocarbons were not, however in this study only a correlation between Chl *a* and CH_2ICl is found. The difficulty in

this comparison is that Chl *a* is not necessarily a reliable indication of total biomass as different species fluoresce by different amounts, and halocarbon production is also species dependent. The picture is further complicated when studying the ice, as when the brine drains from the ice the diatoms remain stuck to the walls of the brine channel network, as has been observed by others [*Krembs et al.*, 2002].

Though it was not possible to measure CH_2I_2 on this campaign, CH_2ICl can be formed by a reaction of CH_2I_2 + Cl- [*Class and Ballschmiter*, 1987; *Moore and Tokarczyk*, 1993]. *Moore et al.* [1996] showed a decline in CH_2I_2 and concurrent increase in CH_2ICl concentrations in *Porosira Glacialis* stocks after diatom growth. *Jones and Carpenter* [2005] have recently reported CH_2ICl production from CH_2I_2 photolysis in a yield of 35±20%, so the presence of CH_2ICl may be indicative of the presence of CH_2I_2, and it can be estimated that CH_2I_2 concentrations would have been at least double those of CH_2ICl. Quantum yield of photodissociation of CH_2I_2 is 0.62 ± 0.09 [*Jones and Carpenter*, 2005].

6.5. Results COBRA

As depicted in figure 70, the core of the 6th March 2008 was made close to shore where the salinity of the seawater was very low (range 3.7 to 5.9 psu), due to the outflow of the Great Whale River and other smaller tributaries close by. The stretch of islands approximately 2.5 km out to sea, the southern-most of which being Bill of Portland Island, closes in an area known as Manitounuk Sound where the brackish water is prevented from mixing with the more saline waters in Hudson Bay. The core of the 9th March was made on the west side of Bill of Portland Island where the water was more saline (19.1 to 21.7 psu). Bulk salinity was 0.9 – 2.8 psu and 3.4 – 7.4 psu, and brine volume was 0.6 – 1.6% and 0.8 – 8.2% for the cores of 6th and 9th March 2008 respectively (figure 90). All brine volume measurements except the lowermost section of the core of 9th March were below the percolation threshold of 5%.

As described in section 6.2.2, bulk ice was sampled during the COBRA field campaign, and values have been normalised to sea ice brine volume and corrected to salinity as described in section 2.8. This then allows a comparison of concentrations in the two types of Arctic ice. In order to further compare the ice concentrations, the expected concentrations in the ice due to the concentration effect have been calculated, using the seawater values used for similar calculations in the JR219 data. It was not deemed appropriate to use the seawater concentrations in water sampled below the ice

during the COBRA campaign as the values were mostly below the limit of detection. Also, as the ice was very thick here, very little sunlight will have penetrated through the ice, therefore under-ice water halocarbon concentrations will not have been representative of the water from which the ice formed.

Agreement between measured and expected halocarbon concentrations is good for some compounds (figure 90), especially for the bromocarbons. CH_3I, C_2H_5I and CH_2IBr are enhanced beyond the concentration effect, suggesting local sources.

Average concentrations of Chl a were 0.5 (range 0. 1 to 1.4) µg l^{-1} and 0.32 (range 0.01 to 2.5) µg l^{-1} in the ice cores, and 0.25 and 0.34 µg l^{-1} in the underlying seawater, on 6th and 9th March respectively. These measurements compare well with those of *Gosselin et al.* [1986] who measured Chl a in the ice of this area (both in Manitounuk Sound and west of Bill of Portland Island) in April and May; the range was 0.1 to 25 µg l^{-1}. The measurements made in this study are at the low end of this range, which is to be expected earlier on in the season where the ice is thicker and solar radiation is less intense; these measurements were made well before the ice melt and start of the spring bloom.

Hsiao [1980] studied species of microalgae in brackish ice and waters similar to this environment the Canadian Arctic. The sea ice communities (consisting mainly of diatoms, mostly of the pennate form) were found to develop in late fall when the ice started to form, growing slowly through the winter months, increasing exponentially in early spring to peak just before the ice thaw and declining rapidly in summer as the ice melts. The most biologically abundant area of the ice was the bottom, where the concentrations of species, mainly diatoms, were one to two orders of magnitude greater than in the upper levels of the ice, and between 50 and 500 times greater than the seawater below. Figure 91 shows how, even this early on in the season, Chl a concentrations are highest in the lowest ice section.

As the core of the 9th March is believed to be more representative of the ice of Hudson Bay due to the environmental conditions discussed above, discussion will be limited to these concentrations (see figure 90 bottom panel). C_2H_5I, and $CHBr_3$ follow a similar profile, the enhancement in concentrations close to the bottom of the ice could be due to production by diatoms at the ice-water interface. The enhancement at the top could be due to brine being expelled upwards during freezing, or surface flooding due to tidal cracks. CH_2I_2 and CH_2IBr have a similar profile through the ice, implying a

common source. The concentration of CH_2IBr is surprisingly high, this is interesting as this compound was the most abundant iodocarbon in the atmosphere in the 2005 campaign.

CH_3I and $1-C_3H_7I$ are only present close to the surface of the ice, suggesting a photochemical source. No enhanced concentrations are seen in areas of high Chl *a* biomass at the ice–water interface, for the same reasons as discussed in section 6.4.1. Photochemistry has previously been suggested as a route to alkyl iodides, for example on snow surfaces in Greenland [*Swanson et al.*, 2002]. Sea ice is much more opaque to UV than seawater ($1/k_D$ seawater (300 nm) $\sim$ 5 m) so any photochemical reactions will be confined to the uppermost part of the ice; the presence of any snow will further reduce the light transmission.

Halocarbons were detected in air during the COBRA field campaign [*Mahajan et al.*, 2010b], mostly during the night-time, with concentrations of 3.83 pptv CH_3I, 0.11 pptv CH_2IBr, CH_2ICl 0.165 pptv, in air masses which had passed over open leads or polynyas. IO was also measured in amounts up to 3.4±1.2ppt in the boundary layer in the same air masses. Hence it is likely that halocarbons remain trapped in the ice, and may only escape when the ice is melting and porous, or when leads open in the ice.
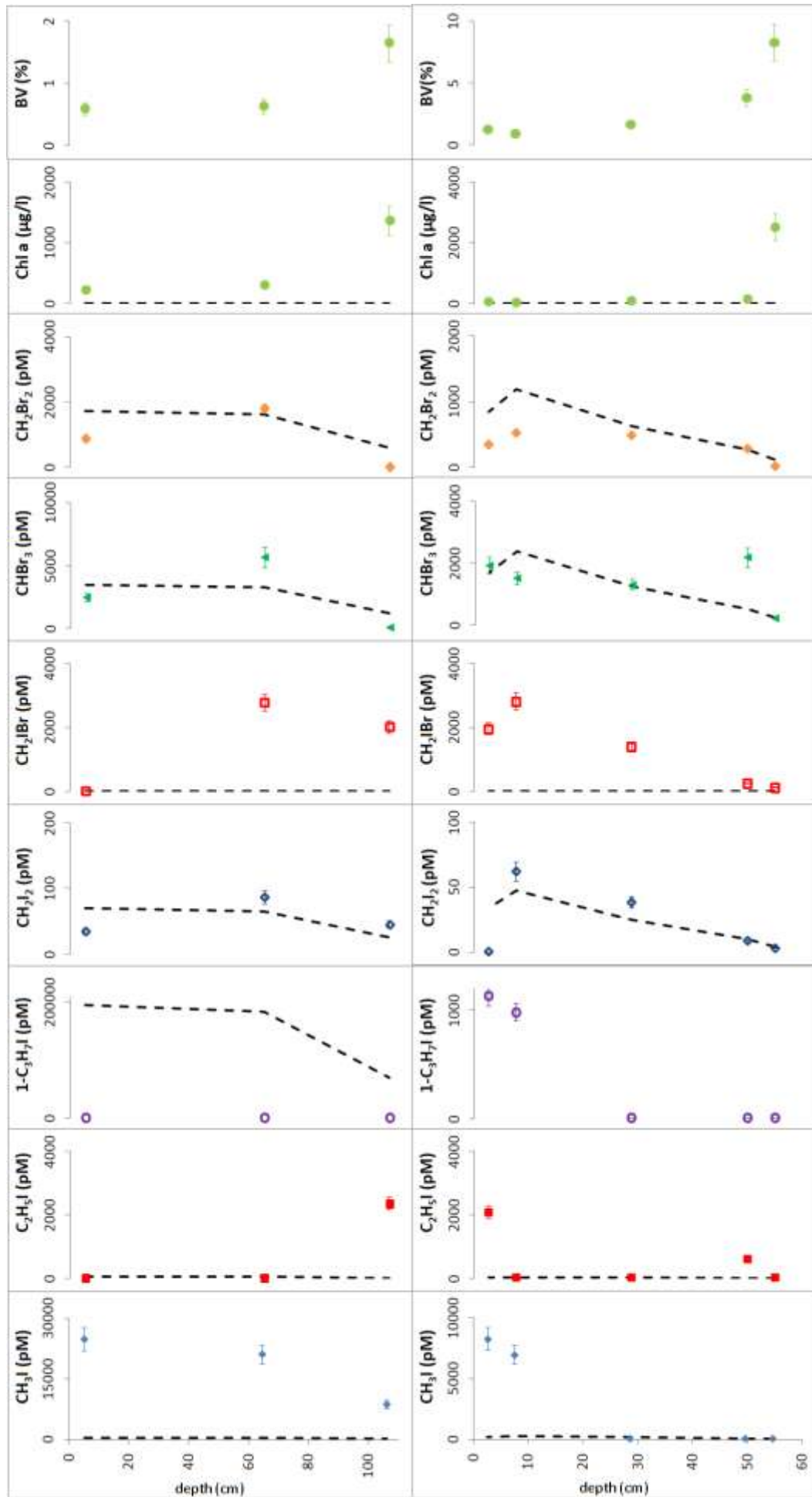
Figure 90. Halocarbon concentrations, normalised to brine volume, during the COBRA campaign on 6th March (top panel) and 9th March (bottom panel). The dashed line shows expected concentrations had the ice formed from seawater containing concentrations equal to low open ocean values measured during JR219.
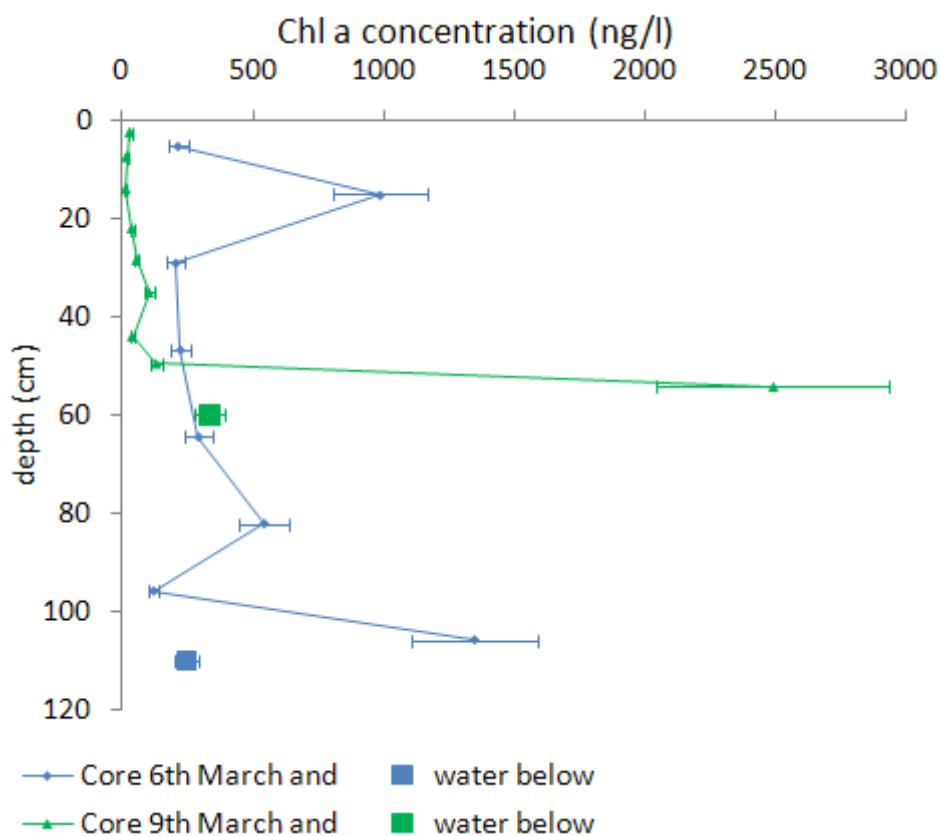
Figure 91. Chl *a* concentrations in the ice cores collected during the COBRA field campaign, error bars represent one standard deviation across repeated calibration curves.

6.5.1. Potential ice-seawater fluxes during ice melt

The maximum rate of ice melt in Hudson Bay is 4.2 cm day^{-1} [*Wang et al.*, 1994]; using the maximum halocarbon concentrations found during the COBRA campaign, ice-water fluxes of CH_3I, C_2H_5I, $CHBr_3$, CH_2IBr, 1-C_3H_7I and CH_2Br_2 during ice melt could be as high as 4.3, 1.2, 1.0, 0.7, 0.4 and 0.3 nmol m^{-2} day^{-1}. These values are similar to those calculated for the JR219 campaign, as, although the concentrations in the ice of Hudson Bay are high, this is due to their extreme concentration in the brine channels of this very cold ice, so the compounds become very much diluted upon ice melt. If the brine were to be pushed up to the surface of the ice by the pressure of the water below once the ice had melted enough for the brine channels to be interconnected, then the potential impact on the atmosphere above will be greater. This may well have been the source of the atmospheric halocarbons measured in the earlier campaign in the same location [*Carpenter et al.*, 2005].

Flux calculations carried out on COBRA IO and atmospheric halocarbon data [*Mahajan et al.*, 2010b] estimate fluxes from open leads of CH_2IBr, CH_2ICl, CH_3I (and CH_2I_2 which was not measured here) required to sustain the observed halocarbons

were 2880, 72, 293 (and 1.4) nmol m^{-2} day^{-1}. These values are much larger than the estimated fluxes from the measurements in this study.

Leads opening in the ice may allow the escape of some compounds from the water below, but until brine channel connectivity is re-established, compounds in the ice will remain trapped. New ice formation following the opening of leads, and the subsequent concentrating of dissolved trace gases in the brine, may provide one mechanism by which halocarbons are released from patches of open water in the ice, as brine is expelled upwards as well as downwards during ice formation, resulting in a concentrated brine on the surface of the ice which may be rich in dissolved halocarbons.

6.6. Summary

Average halocarbon concentrations in sea ice brine of the Arctic Ocean were 30.9, 27.7, 128, 2.1, 5.6, 2.8, 4.8 and 172 pM for CH_3I, C_2H_5I, $CHBr_3$, CH_2ICl, 2-C_3H_7I, CH_2IBr, 1-C_3H_7I and CH_2Br_2 respectively. The ice was warm, very porous and halogenated gases will have had chance to escape. Nevertheless, the high concentrations in the sea ice brine suggest a local source. One possibility is the concentration effect of brine volume reduction. Another is production by anti-oxidative enzymes in organisms which make up the sea ice community, which may be particularly active in the harsh environment experienced in the brine channels. Halocarbon production may also be related to a defence mechanism, in response to grazing [*Manley*, 2002], so enhanced halocarbon concentrations in the sea ice brine channels may occur as ice melts and brine channels widen, hence allowing small zooplankton to enter and grazing pressure on the ice communities to increase.

Ice- and water-atmosphere fluxes were calculated; it is clear that the ice-atmosphere flux has the potential for a greater contribution to the atmospheric halogen budget than the seawater, however waters influenced by the ice edge and under-ice communities may supply a similar flux.

Estimations of halocarbon fluxes from the sea ice to the water below have suggested the largest contribution is from ice melt and under-ice diatom community production, whereas brine channel drainage contributes little under these conditions.

The halocarbon concentrations in sea ice brine are similar to those measured in sea ice with similar physical properties in the Weddell Sea, Antarctica, as presented in

Chapter 5. The water below the ice also showed high halocarbon concentrations, due to ice melt and production by underwater diatom communities. $1\text{-}C_3H_7I$, $CHBr_3$, C_2H_5I, $2\text{-}C_3H_7I$, and CH_2Br_2 showed significant enhancement in concentration in the sea ice brine, of an average order of 2.5, 3, 7, 7, and 23 times respectively, when compared to the water below the ice. Iodocarbon concentrations in the under-ice water were enhanced with respect to concentrations in surrounding waters in the Arctic Ocean. Open ocean measurements showed enhanced halocarbon concentrations may also be found in areas influenced by the phytoplankton bloom associated with the melting sea ice.

The sea ice studied during JR219 was very porous first year ice. These results have been compared to thicker, less porous ice from Hudson Bay, in the Canadian sub-Arctic. The much higher halocarbon concentrations in Hudson Bay ice are due to the concentration effect of brine volume reduction for the bromocarbons, whereas additional sources must be present to account for further enhancement of CH_3I, C_2H_5I and CH_2IBr. Photochemical reactions or biological production may be responsible, but the Chl *a* biomass in this ice was very low.

Halocarbons remain concentrated and trapped in this cold, weakly saline ice, where brine channels do not form a continuous network. This is not the mechanism by which halogenated compounds are released into the atmosphere under these conditions. Percolation through sea ice may provide a route, but rates are slow and not sufficient to account for atmospheric concentrations. Measurements of halocarbons in air during the COBRA campaign [*Mahajan et al.*, 2010b] suggest halogenated compounds may be released into the atmosphere when leads open in the ice, allowing compounds to be released.

During JR219, concentrations of halocarbons were high in the Arctic atmosphere, especially whilst at the ice station when the wind was predominantly from the north. Recent work has suggested trace gas transport though ice is negligible compared to that from open leads and cracks in the ice ([*Loose et al.*, 2011], *Shaw et al.*, submitted). However the ice station was situated on the edge of the Arctic pack ice in the warm summer months of June and July, the ice was very porous and well broken with many open leads. Hence any volatile dissolved gases in the liquid brine and ice meltwater will have had chance to escape to the atmosphere.

As the Arctic warms and the ice becomes thinner and more porous, the potential for trace gases dissolved in the brine to be released to the atmosphere above is greater. Also, processes occurring within and underneath the ice such as diatom growth, grazing pressure, and photochemical reactions, which cause halocarbon formation, will have more impact on the overlying atmosphere if the brine channels are interconnected and the trace gases may travel with brine migration. The enhanced concentrations of the halocarbons due to the concentration effect may also lead to increased halocarbon fluxes to the atmosphere in an area which contains porous ice, especially if the brine is pushed up to the surface of the ice by the pressure of the underlying seawater.

Chapter 7. Iodocarbons on the Antarctic Peninsula

7.1 The Rothera Time Series

Chapters 2 and 3 include results of controlled laboratory experiments carried out at Rothera, a research station on the Antarctic Peninsula shown in figure 6. Field measurements were also carried out, as part of the Rothera Oceanographic and Biological Time Series (RaTS) data set. Previous measurements made by others during the RaTS project have shown bromocarbon concentrations in the seawater and atmosphere to be correlated to the phytoplankton bloom in Ryder Bay (Hughes *et al.* 2009). Ongoing work aims to elucidate the impact of climate change-induced sea ice retreat on halocarbon emissions.

Whilst the data for surface and 15 m depth seawater bromocarbon concentrations, and atmospheric mixing ratios, will be reported elsewhere (Hughes *et al.,* in preparation), the opportunity to present more detailed profiles of bromocarbon concentrations through the water column has been taken in the form of this thesis chapter. Iodocarbon concentrations in seawater are also reported; this the first time such measurements have been made in the waters of the Antarctic Peninsula.

Atmospheric mixing ratios of IO were also measured, in order to further understand the distribution of IO in Western Antarctica. These measurements are also a first.

7.2 Materials and methods

The Rothera research base is located on Adelaide Island on the Western Antarctic Peninsula as shown in figure 6. Measurements were made from mid November 2009 to early March 2010. Seawater samples have been collected from the RaTS sampling sites (figure 6) at surface at 15 m depth since October 2004, and bursts in Chl *a,* indicative of the phytoplankton bloom, have shown a strong correlation to bursts in seawater bromocarbon concentrations. A full description of the project and the measurements made can be found in Hughes *et al.* [2009]. The collection, preparation and analysis of the Chl *a* samples are as detailed in Clarke *et al.* [2008]. The data presented here is complimentary to these measurements, and helps understand how iodocarbon emissions may be concurrent with bromocarbon emissions, in a region in which the presence of atmospheric iodine was not previously known.

For halocarbon analysis, the Markes adsorption tube method of trapping and thermal desorption system, and Agilent GCMS set up was identical to that detailed in section 3.2. LoD and retention times are identical, as are calibration details.

Water samples were collected in triplicate from the side of a small boat. Surface water samples were collected by lowering a 500 mL amber glass stoppered bottle to just below the water surface, rinsing three times, and filling whilst ensuring no bubbles were introduced. Water samples at 5 m, 10 m, 15 m, 25 m, 50 m and 100 m were collected using Niskin bottles hand-winched to the required depth. Water was drained from the bottom of the Niskin bottle via a section of Tygon tubing which ran to the bottom of the 500 mL amber glass stoppered bottle, which ensured the bottle was filled from the bottom up. Once full, the bottles were allowed to overflow for a few seconds. This filling method avoids losses and contamination. Samples were collected between 19th November 2009 and 22nd February 2010, and were analysed within 4 hours of collection. Full depth profiles were made when time and weather permitted, on other occasions it was only possible to sample at surface and 15 m.

Atmospheric IO mixing ratios over Ryder Bay were monitored during the course of the campaign with a mini-max DOAS, as detailed in section 2.6. The instrument was mounted on the roof of a shipping container at 67°34'12.72"S, 68°07'30.69"W with a custom-made steel support, levelled, and set to face south across Ryder Bay. The instrument was protected from precipitation with a plastic sheet with a hole cut out for the viewing lens. Elevation angles were 2°, 4°, 15° and 90°.

7.3 Results

$CHBr_3$ and CH_2Br_2 profiles throughout the water column from surface to 100 m are shown in figure 93. The phytoplankton bloom was very late in this season, occurring mid to late February 2010. Up until this time, bromocarbon concentrations throughout the water column varied little with depth and values were less than 74 pM $CHBr_3$ and less than 17 pM CH_2Br_2. On the 15th Feb, when samples were only taken at surface and 15 m, $CHBr_3$ concentrations reached 243 pM CH_2Br_2 concentrations reached 21 pM, with both compounds slightly enhanced at 15 m. On the 22nd February, the increase in $CHBr_3$ concentrations is huge, with values reaching 744 pM. It is clear from the depth profile that $CHBr_3$ production is occurring in the upper 25 m of the water column, with a pronounced peak at 5 m. CH_2Br_2 production also increases, though by a smaller degree of magnitude; concentrations reach 32 pM.

CH_2Br_2 concentrations peak at 15 m, this could be due to production by different species of phytoplankton which reside at a slightly lower depth in the water column to those which produce $CHBr_3$.
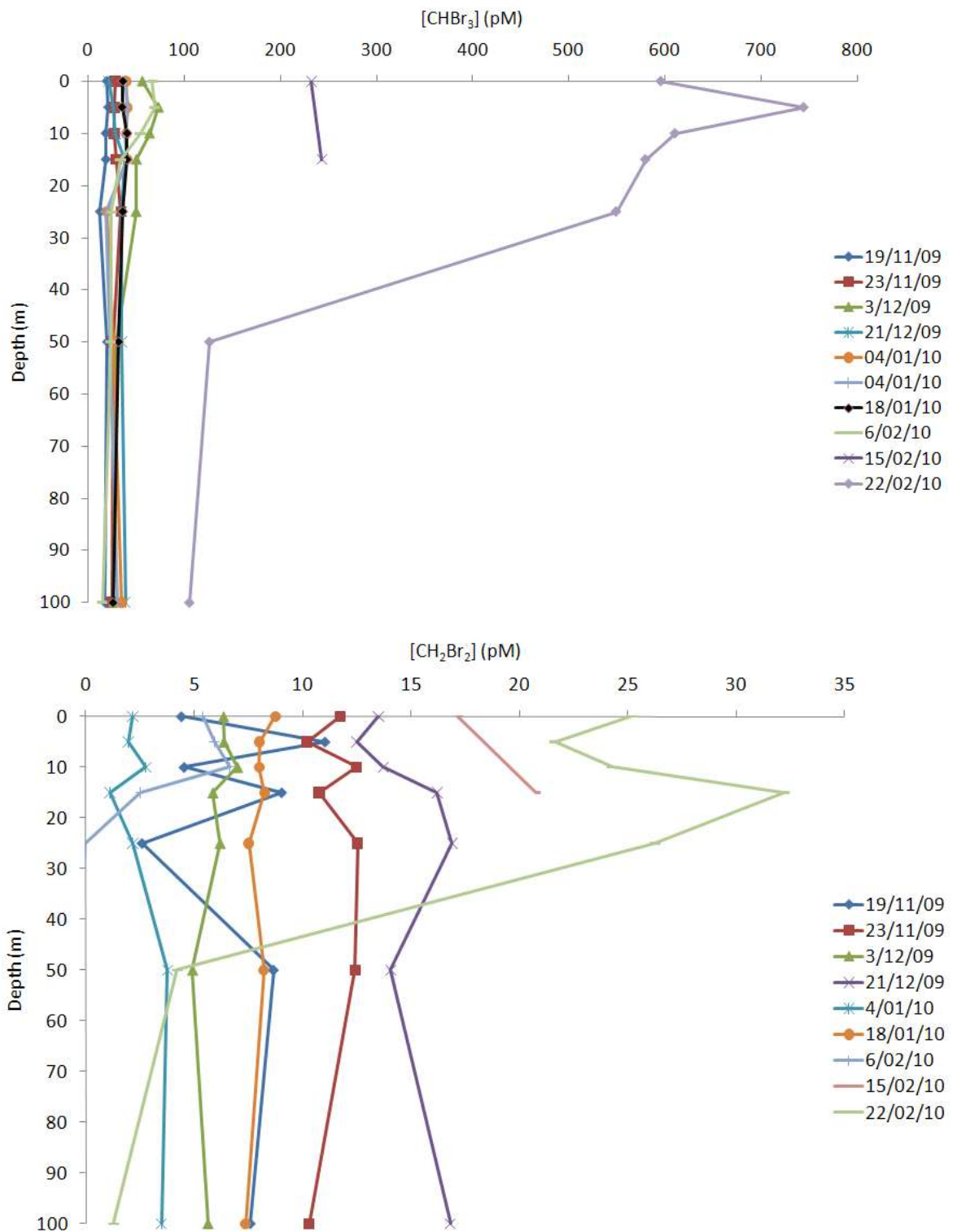
Figure 92. Bromocarbon profiles through the water column throughout the 2009/10 field campaign. Dates the water samples were collected are shown in the legend.

Seawater iodocarbon concentrations were also measured throughout the field campaign. CH_3I and C_2H_5I were present all season, at levels of up to 5 pM and up to 2 pM respectively. No increase in C_2H_5I concentrations was observed to be coincident with the phytoplankton bloom and subsequent increase in bromocarbon concentrations. CH_3I concentrations did however peak during the bloom, with up to 14 pM measured at 25 m depth on 22nd February 2010. Figure 94 compares a typical profile through the water column, made on 21st December 2009, with measurements made on 22nd February 2010.

The iodocarbons CH_2I_2, CH_2IBr, CH_2ICl, 2-C_3H_7I and 1-C_3H_7I were not observed above the limit of detection of the GCMS until 22nd February 2010. On this date values reached 0.3 pM, 0.5 pM, 0.3 pM, 0.2 pM and 0.8 pM respectively (figure 95). All compounds show a maximum between 15 m and 25 m depth; CH_2IBr is present only in the region 10m – 25 m. CH_2I_2 and CH_2ICl concentrations show a similar profile. The sub-surface maximum is typical of biotic halocarbon concentrations, as production occurs in the upper photic zone, but loss to the atmosphere depletes surface waters.
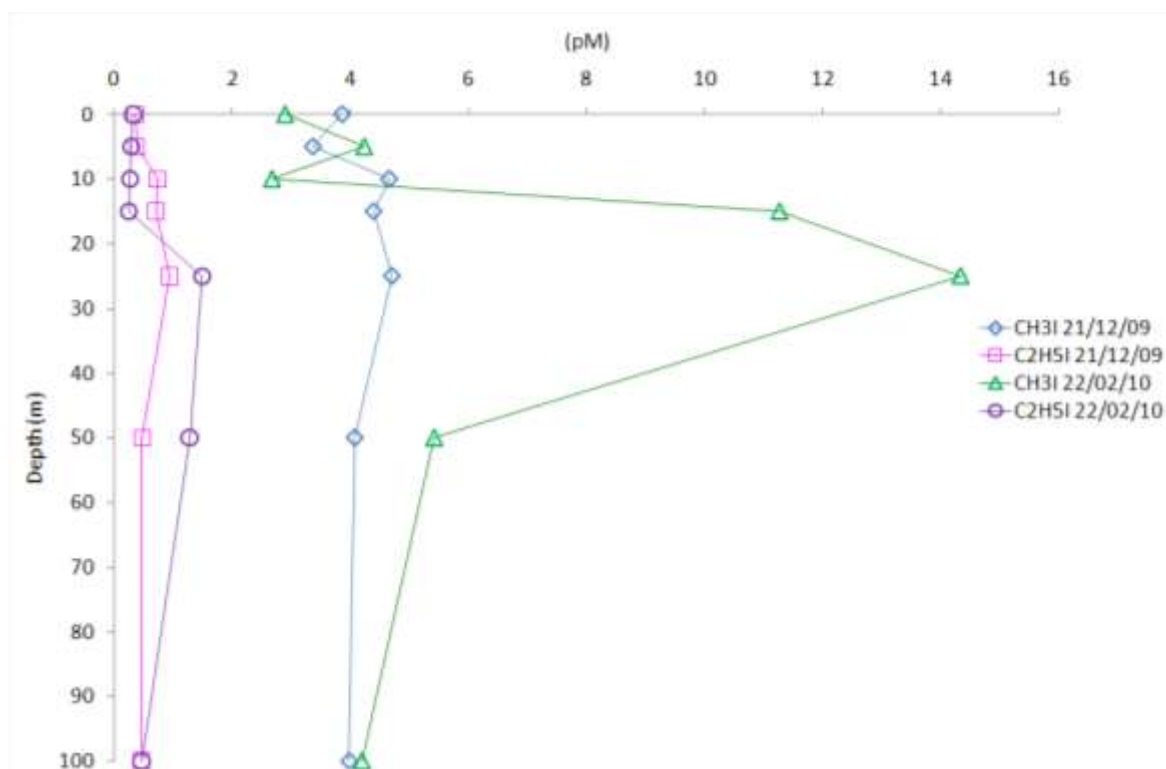
Figure 93. Seawater iodocarbon concentrations in Ryder Bay at the start of the summer season (December 2009) and during the phytoplankton bloom (February 2010).
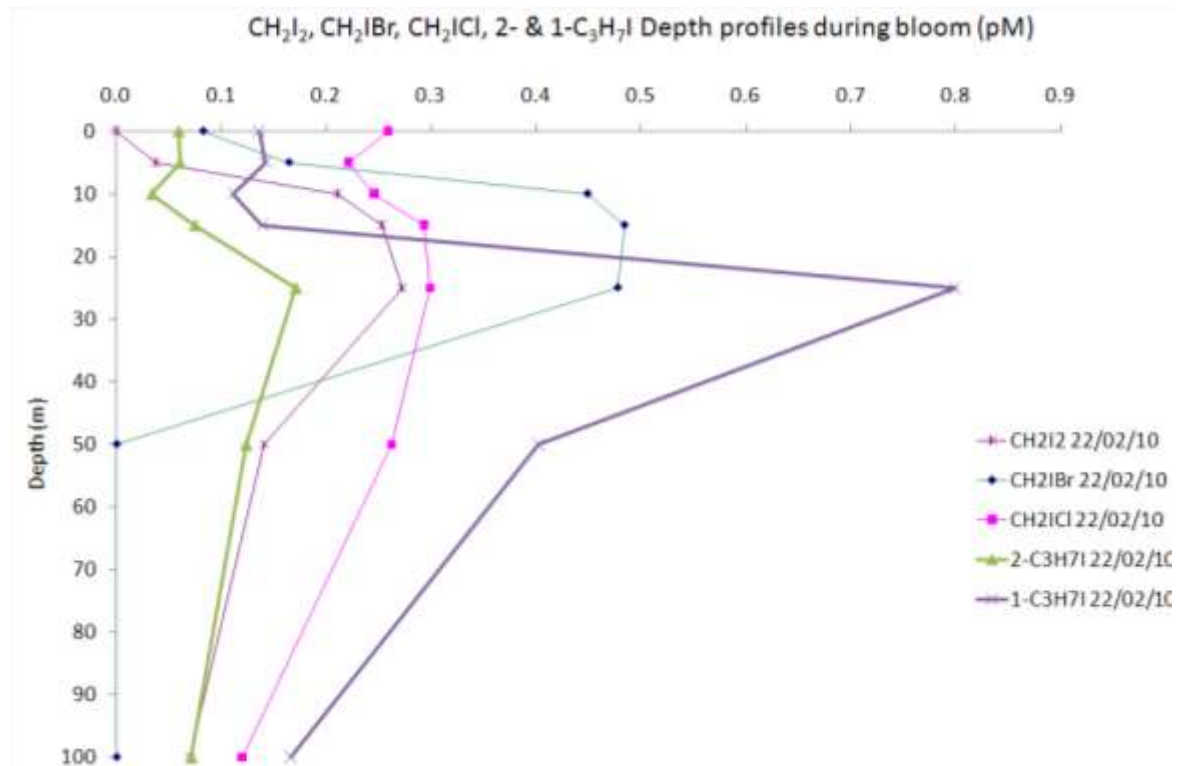
Figure 94. Seawater iodocarbon concentrations in Ryder Bay during the phytoplankton bloom.

Results for atmospheric IO mixing ratios are shown in figure 96, alongside Chl *a* concentrations at 15 m depth, in order to determine whether IO concentrations increase due to the increase in iodine atom precursors which may result from an increase in iodocarbon emissions from phytoplankton. No correlation is seen between atmospheric IO mixing ratios and Chl *a* concentrations in seawater. However IO concentrations will be affected by many factors, the most important of which will be air mass origin and history. The mini MAX-DOAS was located within a few hundred metres of the water sampling sites, so any iodocarbons emitted from the water may not have been photolysed by the time the air mass was sampled. Therefore, any IO which may have formed following emissions of iodine from the seawater may not have been detected by the mini-max DOAS.
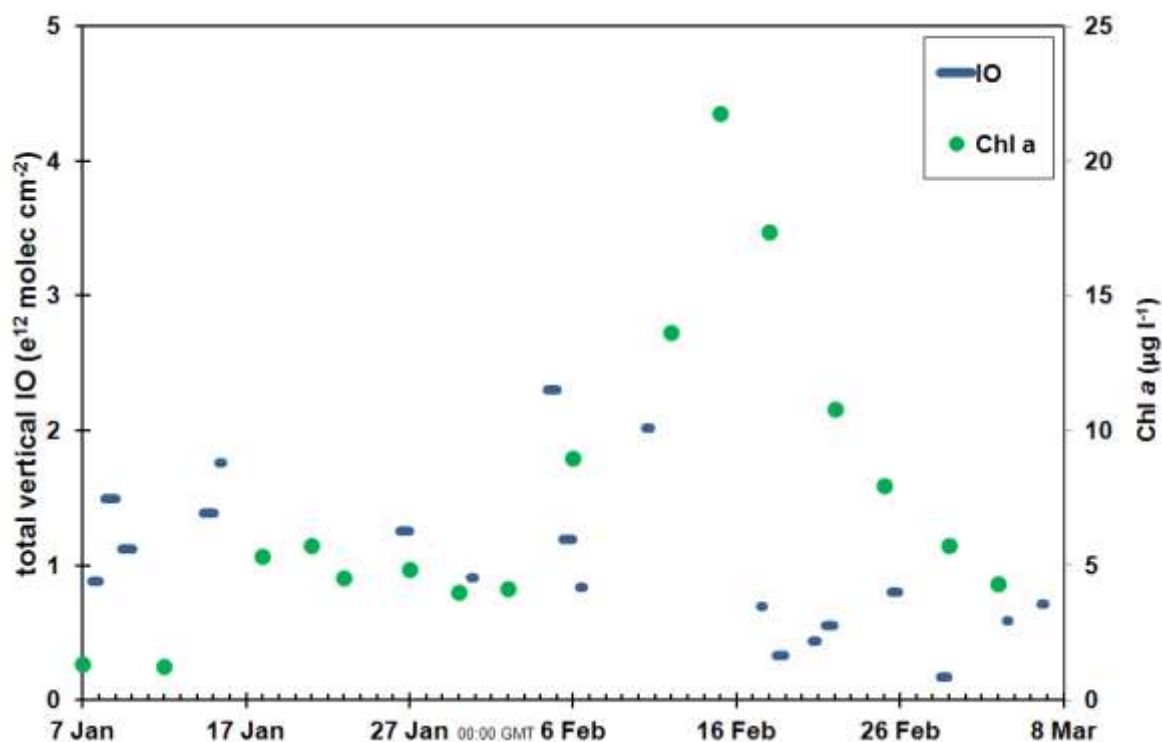
Figure 95. IO mixing ratios measured on the Antarctic Peninsula with the mini MAX-DOAS Jan – March 2010, compared to Chl *a* concentrations at 15 m depth seawater which is indicative of the phytoplankton biomass.

7.4 Summary

It has been shown that $CHBr_3$ and CH_2Br_2 production increases during the phytoplankton bloom in Ryder Bay, with a larger increase observed for $CHBr_3$ than CH_2Br_2 concentrations. Furthermore, $CHBr_3$ concentrations show a pronounced peak at 5 m, whereas CH_2Br_2 concentrations peak at 15 m, this could be due to production of the two bromocarbons by different species of phytoplankton which reside at slightly different depths in the water column.

It has also been demonstrated that iodocarbon production occurs in the waters of the Western Antarctic Peninsula. CH_3I, present throughout the season, increased in concentration during the phytoplankton bloom. C_2H_5I was the only other iodocarbon consistently found in seawater, this compound showed no increase in concentration during the bloom. The iodocarbons CH_2I_2, CH_2IBr, CH_2ICl, $2-C_3H_7I$ and $1-C_3H_7I$ were only observed during the phytoplankton bloom, where all compounds show a maximum between 15 m and 25 m depth; the sub-surface maximum is typical of compounds produced by phytoplankton, as production occurs in the upper photic zone, but loss to the atmosphere depletes surface waters.

The presence of atmospheric IO on the Antarctic Peninsula has also been demonstrated, with no increase in mixing ratios associated with the phytoplankton bloom.

This is a small dataset, but it nevertheless shows the presence of compounds of iodine in the region of the Antarctic Peninsula. Furthermore, the enhancement of iodocarbons due to the phytoplankton bloom in the bay has been demonstrated.

Chapter 8. Synthesis and further work

8.1 Conclusions

In Chapter 1, an introduction was given to the atmospheric chemistry of iodine, and the importance of its study. Reactive atmospheric iodine species are broken down in the atmosphere to yield iodine radicals. The radicals react with ozone, destroying it catalytically to form IO [*Chameides and Davis*, 1980]. IO may self react to form stable clusters, these may grow to become CCN and hence impact climate via increased scattering of sunlight [*O'Dowd et al.*, 2002].

The ability of algal activity to concentrate and volatilise iodine from the ocean was discussed, and it was shown how diatoms living in sea ice may play a role. Diatoms are known to emit iodocarbons [*Sturges et al.*, 1992; *Tokarczyk and Moore*, 1994], and the focus of many previous measurements of atmospheric iodine has been on organic precursors. Such measurements made in the polar regions were summarised (tables 1 and 2).

Recent work [*Huang et al.*, 2010; *Mahajan et al.*, 2010a] has shown the importance of molecular iodine in so-called 'hotspots', coastal areas where kelp beds exposed at low tide emit pulses of iodine compounds, and where ozone depletion and new particle formation have been demonstrated. Phytoplankton, and in particular diatoms, have been shown to have similar iodine-pathways in their metabolism, though their biomass is much more disperse than kelp in the oceans, leading to lower release rates. Diatoms are however ubiquitous throughout all bodies of water, so the emission of these compounds is potentially more significant due to their widespread distribution.

One area of high emissions of volatile forms of iodine may be those covered in sea ice, where diatom numbers have the potential to become more concentrated. If similar mechanisms are occurring in micro-and macro-algae then sea ice could be another iodine hotspot.

The high atmospheric mixing ratios of IO measured over Southern Ocean sea ice by satellite [*Schönhardt et al.*, 2008], and in particular the Weddell Sea, would suggest this is the case. The lack of high concentrations over Arctic sea ice may be due to the physical properties of the ice and the oceanography in the polar regions. These factors, along with differences in the communities within the ice were discussed in

chapter 1. For example, the presence of gap layers in the sea ice of the Weddell Sea – diatom rich layers close to the surface of very porous ice [*Meguro*, 1962]– may go some way to explaining why iodine emissions from ice algae are more easily released into the Antarctic atmosphere. Previous studies, both of concentrations of iodine compounds made during polar field campaigns, and production rates of iodocarbons by polar diatoms in the lab, were summarised.

The overarching aim of this study was to investigate why such high mixing ratios of IO are present over Antarctica, with particular focus on the Weddell Sea area where the highest IO levels are found. An iodine–selective mechanism must exist which concentrates and volatilises iodine in preference to bromine in the ocean: bromide is at least 1000 times more abundant than iodide in seawater, whereas atmospheric mixing ratios of (up to 20 pptv) IO are similar to those of bromine monoxide (BrO) in Antarctica.

Competing theories exist as to how iodine compounds may become enhanced in the atmosphere above sea ice. One proposed mechanism is iodocarbon or I_2 emissions from sea ice algae, migration of these compounds through the sea ice, driven by a concentration gradient [*Saiz-Lopez and Boxe*, 2008], and subsequent release from the ice surface. Diatoms have also been shown to be capable of accumulating iodide [*de la Cuesta and Manley*, 2009], releasing hypoiodous acid (HOI) [*Hill and Manley*, 2009], and to play a role in the conversion of iodate to iodide [*Chance et al.*, 2007].

An alternative abiotic mechanism has recently been proposed [*Carpenter et al.*, 2005], supported by laboratory experiments, for the production of CH_3I, C_2H_5I and CH_2I_2 via the reaction of HOI with humic material in the quasi-liquid layer (QLL) on the surface of sea ice. The origin of HOI in the QLL was suggested to be atmospheric deposition or from reactions of the type $HOBr + I^- \rightarrow HOI + Br^-$.

With a view to investigating these competing theories, laboratory experiments on sea ice and associated diatoms have been carried out which have aimed to elucidate how halocarbons may become enhanced in sea ice. To further understand the enhancement of iodine in sea ice and the polar atmosphere, field measurements have been carried out in four different polar areas, with a focus on sea ice diatoms, ice properties, and measurements of an array of iodine compounds.

Laboratory Experiments

As the highest concentrations of atmospheric IO are observed over the sea ice of the Weddell Sea during spring when the ice is melting [*Schönhardt et al.*, 2008], with another peak in autumn during ice formation, a logical place to start this investigation was with the formation of sea ice. As the sea ice forms, diatoms which live in the brine channels will be subjected to decreasing temperatures and an increase in availability of halide ions. Therefore, experiments were carried out to ascertain whether it was in response to this stressful environment that forms of volatile iodine compounds were produced.

These stress experiments were carried out under controlled laboratory conditions on *Porosira Glacialis*, an ice-associated diatom which has a bipolar distribution [*Hasle*, 1976], two Antarctic ice diatoms, *Fragilariopsis Cylindrus and Fragilariopsis sp.*, collected from the Weddell Sea and Antarctic Peninsula respectively, and on a naturally occurring ice algae community on the Antarctic Peninsula. The experiments using the latter community were important, to show these results are not confined to the laboratory, which may not be representative of the natural environment, but rather may be applied to native systems. These diatoms were first frozen in Tedlar sampling bags, and halocarbon concentrations were monitored during the freezing and melting of the seawater.

Further stress experiments then explored what factors of the freezing process may be responsible for a change in halocarbon concentrations. Cultures of *Porosira Glacialis*, *Fragilariopsis Cylindrus and Fragilariopsis sp.* were subjected to varying salinities, iodide and bromide concentrations, and halocarbon concentrations in the medium were monitored. Physiological measurements were made to understand how the diatoms survive under these extreme conditions.

Another question investigated during this study was whether higher concentrations of iodocarbons may be found in sea ice brine due to a "concentration effect" of volume reduction of liquid in which compounds are dissolved, or whether diatoms subjected to the stresses of a sea ice environment may be more likely to emit halocarbons.

Field measurements

Field campaigns were then carried out in the ice of the both Arctic and Antarctic, where the concentrations of compounds of iodine (and bromine) were measured in

sea ice, brine, seawater and air, as detailed in table 4. Physical measurements of the ice were made to determine whether the brine channels form a continuous network which could provide a transport route from organisms living in the ice to the ice-atmosphere interface.

8.2 Summary

Results from the freezing of seawater containing diatoms in Tedlar bags, carried out both at UEA and on the Antarctic Peninsula, were presented in **chapter 3**. Bromocarbon production rates were observed to be mostly independent of temperature; increases in concentration at very low temperatures were due to the concentration effect of brine volume reduction during sea ice formation. Some iodocarbon concentrations showed a greater potential to become more concentrated in sea ice.

CH_3I concentrations at low temperature were lower than those expected via the concentration effect, suggesting loss processes are occurring. One such loss mechanism could be nucleophilic substitution by Cl^-, the rate of which increases with increasing salinity [*Elliott and Rowland*, 1993]. C_2H_5I concentrations consistently increased upon ice melt which is an interesting result - abiotic reactions could be occurring which are not understood, but release of this compound from the material of the bag is also possible.

The more reactive iodocarbons, CH_2ICl, CH_2I_2, CH_2IBr, 1- and 2-C_3H_7I all showed the potential to be produced in larger quantities under sea ice conditions, exceeding concentrations expected via the concentration effect. CH_2ICl production increased under frozen conditions in the naturally occurring Antarctic communities, concentrations of CH_2I_2 and CH_2IBr increased in both *Porosira Glacialis* cultures and the natural community on the Antarctic Peninsula, whereas 1- and 2-C_3H_7I production only increased in *Porosira Glacialis* cultures.

Both the increase in iodocarbon production and the concentration effect provide a mechanism by which halogens may be volatilised and released in the sea ice zone.

Porosira Glacialis, which is a relatively large diatom, did not survive when frozen in a seawater medium to -15°C. After the seawater was melted again, cell volume had halved and cell number doubled, suggesting the diatoms were crushed during ice formation. However, the much smaller *Fragilariopsis Cylindrus*, which may be more

easily incorporated into the brine channel network when seawater freezes, did survive. Though the photosynthetic efficiency was greatly reduced at -15°C, the diatom recovered upon ice melt.

Less ice formation was observed in bags containing *Fragilariopsis Cylindrus* than *Porosira Glacialis* at the same temperature. This suggests the ice diatom *Fragilariopsis Cylindrus* secretes an ant-freeze agent which helps it to survive in the sea ice brine channel network.

The increase is iodocarbon concentrations in the sea ice brine may be due to increased production by diatoms under stressful conditions as they utilise iodide in this extreme environment. Concentrations may also become enhanced in the seawater medium when the diatom frustules break open upon cell death, and intracellular compounds are released.

These findings are important in understanding how the concentrations of iodine compounds are enhanced in sea ice brine channels. The measurements made on sea ice collected from Ryder Bay on the Western Antarctic Peninsula showed enhanced concentrations of iodocarbons, but not bromocarbons, in the brine. When the sea ice is porous enough to allow these compounds to escape, this provides a mechanism by which iodine may be enhanced in the atmosphere above sea ice.

Chapter 4 sought to understand what aspects of the freezing process may contribute to an increase in halocarbon concentration, by varying salinity and concentrations of bromide and iodide independently. The key findings from experiments using *Porosira Glacialis* were the decreased bromocarbon production but increased iodocarbon production when diatoms were salinity stressed halide ion concentrations were increased.

Production of the bromocarbons was greatest when salinity, bromide and iodide concentrations were all low. In contrast, salinity changes and the presence of iodide cause iodocarbon concentrations to increase. Maximum production rates of CH_3I, C_2H_5I and $1\text{-}C_3H_7I$ were observed when *Porosira Glacialis* was salinity stressed and iodide concentrations were enhanced. CH_2ICl, $2\text{-}C_3H_7I$, and CH_2IBr production increased with increasing iodide concentration, though very high salinities suppressed production.

Cell lysis at extreme salinity caused CH_3I, C_2H_5I, $1-C_3H_7I$ and CH_2IBr concentrations to increase. suggesting these compounds reside within the diatom cell.

The different responses of different enzyme types were clear, with the same patterns of production for monoiodocarbons (methyl transferase) and polyiodocarbons (iodoperoxidase).

These results have implications for the sea ice environment. As seawater freezes, trace gases and dissolved ions become concentrated in brine. The channels which form as the brine drains from the ice are home to diatoms, which may use iodide as a cellular anti-oxidant, and the anti-oxidative enzymes which utilise iodide and produce iodocarbons may be particularly active in this harsh environment. The iodocarbons may be a byproduct of the anti-oxidative metabolism of the cell.

Therefore, the conditions inside the brine channels may lead to increased production of iodocarbons, but not bromocarbons, by sea ice algae. These processes may help us to understand why iodine compounds are concentrated and released in the sea ice environment, as any labile compounds released by sea ice diatoms may be released to the atmosphere if the ice is porous enough to allow the compounds to escape.

This work agrees well with that of *Fogelqvist and Tanhua* [1995] who found enhanced iodocarbon, but not bromocarbon, concentrations in sea ice brine in the Weddell Sea.

No increase in halocarbon production was observed in cultures of *Fragilariopsis Cylindrus and Fragilariopsis sp.* under any experimental conditions in chapter 4. This result shows how halocarbon production is dependent on species and environment.

Chapter 5 reported results from a ship-based field campaign in the Weddell Sea, Antarctica. Organic and inorganic compounds of iodine were measured in the seawater, ice brine and the atmosphere.

Concentrations of halocarbons in the sea ice were enhanced with respect to the water below. Enhancement ratios in the ice were greater for the iodocarbons than the bromocarbons, with average ice concentrations being 48, 26, 25, 16, 12, 11, 8 and 7 times higher than average seawater concentrations for CH_2ICl, C_2H_5I, $2-C_3H_7I$, $1-C_3H_7I$, CH_3I, $CHBr_3$, CH_2Br_2 and $CHBr_2Cl$ respectively. Physical properties of the ice determined the continuity of the brine channel network, providing a source-to-

atmosphere pathway for the iodine compounds, and halocarbons were detected in the atmosphere.

Atmospheric mixing ratios of inorganic iodine compounds, especially I_2, were much higher than those of the iodocarbons, suggesting this compound is the main source of atmospheric IO above the sea ice of the Weddell Sea. Doubts do however exist as to the validity of the measurement technique. The pulse of I_2 over the ice shelf was particularly unexpected. Mechanisms may be occurring which are yet unknown which involve recycling over the snowpack.

IO and new particle formation were measured to assess the subsequent impact of these iodine emissions on the atmosphere. IO concentrations measured from the ship were in reasonable agreement with satellite data, and new particle formation was observed as the ship broke through sea ice.

Saturation anomalies, flux calculations and a modelling study were used to interpret the measurements. Flux calculations on simultaneous water concentrations and mixing ratios in air showed the predominant trend was for iodocarbons (with the exception of CH_2ICl) to be released from the ocean to the atmosphere, but bromocarbons to be deposited to the ocean. Furthermore, there is potential for iodocarbons, enhanced in concentration in the brine channels of sea ice, to be released to the atmosphere if the brine is pushed up to the surface of sea ice by the pressure of the underlying seawater.

A modelling study was used to further interpret the measurements. The IO mixing ratio resulting from measured halocarbon fluxes was less than was observed; whereas that resulting from the measured I2 was much greater than observed. In order to reproduce the measured IO, the I_2 mixing ratio was less than that measured. These results suggest an additional iodine atom source to the halocarbons must exist, which is probably I_2, however the denuder tube method seems to be massively overestimating mixing ratios. New particle formation predicted by the model showed more agreement with measurements, however field measurements exhibited particle growth to larger sizes than the model.

Measurements of iodine (iodide and iodate) in seawater showed total iodine is depleted by half or more in diatom rich ice samples with respect to background seawater concentrations. This finding supports the mechanism proposed by *Saiz*

Lopez and Boxe [2008] as the iodide could have been previously volatilised and released by the sea ice community.

The results from chapter 5 may help explain the larger enhancement of iodine than bromine from the ocean to the polar atmosphere. The atmospheric mixing ratios of I_2, AIC and IO are similar to measurements made at coastal iodine 'hot spots' close to exposed macroalgae beds. It has been demonstrated that, like these coastal locations, iodine chemistry may be responsible for bursts of new particles. Thus, the Weddell Sea is another iodine 'hotspot'. The modelling study used to interpret this data has highlighted that further work is needed to further our understanding of the complex chemistry of this region.

Chapter 6 presented results from two field campaigns in the Arctic –JR219, a ship-based campaign in the Arctic Ocean above the Greenland and Norwegian seas, and COBRA, in the Canadian sub-Arctic on the east coast of Hudson Bay, Quebec. The focus of these campaigns was halocarbon concentrations in sea ice brine, measurements were also made in seawater and air.

The ice properties in the two campaigns were quite different: the ice in JR219 was less than 1 m thick and very porous, whereas the ice in the COBRA field campaign was thicker, colder, and less porous. These different ice properties enabled a further investigation of the concentration effect, and higher concentrations of halocarbons were found in the brine of the colder ice, despite much lower algal activity. The halocarbon measurements during the COBRA campaign demonstrate how the halogenated trace gases, concentrated by brine volume reduction during sea ice formation, remain trapped in the ice when the ice is fresher, colder and in which brine channels are not interconnected.

The ice in the JR219 campaign was very warm and very porous and ever-more typical of the ice of the Arctic as the planet warms and sea ice retreats. Despite its high porosity, high concentrations of halocarbons were measured in the sea ice brine suggest a local source, one possibility is in response to grazing pressure.

Flux calculations carried out on simultaneous halocarbon concentrations in sea-water / ice brine and mixing ratios in air on the JR219 data again showed the potential for enhanced fluxes from the sea ice, though a number of assumptions have been made regarding the factors which affect such halocarbon fluxes. There is some debate as to

the correct methodology for these calculations, and this will be discussed further in section 8.2.

During JR219, very high atmospheric mixing ratios of halocarbons were measured, for some compounds the highest ever recorded. Mixing ratios were especially high whilst the ship was moored at the ice station, when the wind was predominantly from the north and hence originating from over the Arctic pack. As the Arctic warms and the ice becomes thinner and more porous, the potential for trace gases dissolved in the brine to be released to the atmosphere above is greater. Thinner ice also leads to more light penetration and hence more algal growth.

An increase in the number of diatoms and their subsequent halocarbon emissions, along with photochemical reactions which cause halocarbon formation, will have more impact on the overlying atmosphere if the brine channels are interconnected and the trace gases may travel with brine migration. The enhanced concentrations of the halocarbons due to the concentration effect may also lead to increased halocarbon fluxes to the atmosphere in an area which contains porous ice, especially if the brine is pushed up to the surface of the ice by the pressure of the underlying seawater.

Similar concentrations of halocarbons in Antarctic and Arctic sea ice brine with similar physical properties (Weddell Sea and JR219) suggests similar processes are occurring involving organic halogens associated with sea ice in both polar regions. However, species of diatom present will be quite different in these two areas, and many other factors affect halocarbon concentrations. CH_2ICl for example showed the greatest enhancement in the sea ice of the Weddell Sea, but showed the greatest enhancement in waters away from the sea ice during the Arctic cruise. This again demonstrates how different species are produced in different amounts by different species.

As the climate warms and the ice of the Arctic becomes more like that of the Antarctic (thin, porous and mostly first year) it is interesting to consider how this may affect halocarbon concentrations associated with the ice brine. As discussed in chapter 1, the enhancement of iodine over the sea ice of the Weddell Sea may be partly due to ice properties. More porous ice has additional space for algal colonisation, thinner ice lets more light penetrate to under-ice diatoms. Furthermore, gap layer formation may become more likely in Arctic sea ice which is no longer one consolidated pack. If the

production of halocarbons by diatoms is increased due to the stresses of the sea ice environment then there is potential for increased fluxes to the atmosphere.

It could be argued that less ice leads to more open water and an increase in sunlight penetration, which may lead to an increase in phytoplankton growth, resulting in increased halocarbon production. However, in the polar regions, the phytoplankton bloom is often preceded by the retreat of sea ice; if the warming climate leads to a greater inter-annual variability in sea ice cover, this increases the area potentially affected by a bloom, and so may lead to bursts of halocarbon fluxes associated with the bloom as the ice-edge retreats. An increase in iodine atom flux to the atmosphere will result, with a subsequent increase in tropospheric ozone depletion and new particle formation.

Chapters 3 and 4 showed how the stresses of the sea ice environment may increase iodocarbon production by diatoms, especially mono-iodocarbon production by the anti-oxidative methyl transferase enzymes. Chapter 5 showed how the volatilisation of iodine in seawater may release iodocarbons and result in depletion of total iodine in diatom-rich ice. Measurements of I_2, though as yet invalidated, hint as to the potential of the Weddell Sea to be another iodine "hot-spot". IO measurements and new particle formation demonstrated the impact on the overlying atmosphere. Chapter 6 reported high concentrations of halocarbons in sea ice brine and the overlying atmosphere of the Arctic. Flux calculations have suggested an increase in halocarbon emissions from thinning Arctic sea ice which is more porous.

Another interesting area of investigation of this study was that of the concentration effect on trace gases of brine volume reduction. Chapter 3 demonstrated how this was possible in the laboratory, and results from the COBRA field campaign showed how these higher concentrations may remain trapped in the ice when the ice is fresher, colder and in which brine channels are not interconnected.

8.3. Further work

8.3.1. Laboratory experiments

The controlled laboratory experiments carried out in this study have involved three species of cultured diatoms and a natural community from one area, with particular emphasis on *Porosira Glacialis,* which was already known to produce halocarbons. This work and studies by other groups [*Moore*, 2003] have shown a variety of

halocarbons are produced in different quantities by different species. More work is needed on a wider range of species from a variety of locations in order that these results can be extrapolated to the global scale. It is not known what fraction of diatom species produce halocarbons, and though there is more evidence in the literature for production by polar species, this could simply be a reflection of the variety of species tested.

Many more experiments could be carried out with the Tedlar bags used as reported in chapter 3, involving a wider range of temperatures and light intensities. It would also be useful to investigate the effect of freezing known concentrations of halocarbon standards in seawater with no marine organisms, to separate out the processes which are due to diatom activity. The release of C_2H_5I upon ice melt in the experiments involving the Tedlar bags could be due to reactions not yet understood, and it would be interesting to investigate this further using reaction vessels of different materials.

Stress experiments have been carried out during this study, which have often involved sudden changes in conditions. Whilst diatoms may experience this during ice melt as they drain from a weakly saline brine channel, influenced by melting ice, into the ocean, for most of their life cycle they will experience milder and more gradual changes. Experiments carried out over long time scales with more gradual changes in conditions would ascertain how halocarbon production would be affected. It would be interesting to grow diatoms under different conditions and then measure halocarbon production, for example growing diatoms at high iodide concentrations to check for iodide accumulation and the subsequent effect on halocarbon production.

As recent work, here (Chapter 6) and by others [*Huang et al.*, 2010; *Mahajan et al.*, 2010a] has suggested I_2 emissions play a large role in the transfer of iodine from the oceans to the atmosphere it would also be interesting to repeat these experiments with a focus on inorganic iodine compounds. An experiment to measure I_2 emissions from diatoms collected from the Weddell Sea, and particularly the waters close to the Brunt Ice Shelf, should be carried out. It is possible that the diatoms which colonise the sea ice of the Weddell Sea have iodoperoxidase enzymes, which favours the production of volatile iodine over volatile bromine, and more work is needed in order to ascertain this.

As discussed in Chapter 6, the transfer velocity used in ice-atmosphere flux calculations is not known, and though some work by the York group [*Shaw et al.,*

submitted] has improved our understanding of the factors which may affect it, these were carried out on artificial sea ice grown in a laboratory chamber, and more work is needed in the field. The flooding of the surface of sea ice by ice brine pushed up through the ice by the pressure of the underlying seawater is a particularly important aspect, further laboratory experiments could be designed to investigate how this may affect fluxes. An artificial sea ice chamber could be made in which porous ice was grown. A pressure applied to underlying seawater containing halocarbons in order to flood the surface, and simultaneous halocarbon analysis of the air above, would enable further quantification of the factors affecting fluxes form sea ice.

8.3.2. Field measurements

An uncertainty in the discussion of halocarbon concentrations in sea ice brine is the initial concentrations in seawater at the point of ice formation. A useful way to resolve these questions is a field campaign in the marginal ice zone spanning a year. Halocarbon concentrations could be monitored in the water before freezing, in sea ice brine as the brine becomes more, and then less concentrated as the ice grows and then melts, and again in the seawater following ice melt. Halocarbon measurements in air would determine whether increased fluxes to the atmosphere resulted from concentrating the halocarbons in the sea ice brine, this would be especially important during initial ice formation when brine is expelled upwards.

The measurement of high concentrations of I_2 close to an ice shelf next to an open lead in sea ice was a significant finding of this study. More work is definitely needed to validate these measurements. As discussed in chapter 5, this region has unique types of ice and of diatom species, so experiments measuring I_2 emissions from diatoms collected in this area of the Weddell Sea would resolve how such high concentrations of I_2 come to be present in the atmosphere.

It would be useful to carry out another field campaign on board a ship in the Arctic Ocean to measure the fluxes of CH_2I_2, which unfortunately could not be measured during cruise JR219, as this compound may have a more significant contribution to iodine fluxes than the other iodocarbons due to its shorter photolytic lifetime. Simultaneous measurements of IO in the Arctic sea ice zone would give more information as to the impact of iodine chemistry. Furthermore, I_2 and AIC measurements would also be useful to assess the impact of inorganic iodine compounds in the Arctic atmosphere. Much more work is needed to understand how

the changing ice properties of the Arctic Ocean ice will impact the marine and atmospheric chemistry of this region.

References

Ackley, S. F., K. R. Buck, and S. Taguchi (1979), Standing crop of algae in the sea ice of the Weddell Sea region, *Deep Sea Research Part A. Oceanographic Research Papers*, *26*(3), 269-281.

Ackley, S. F., G. Dieckmann, and H. Shen (1987), Algal and foram incorporation into new sea ice, *Eos*, *68*(50), 1736.

Ackley, S. F., J. Bengtson, P. Boveng, M. Castellini, K. Daly, S. Jacobs, G. Kooyman, J. Laake, L. Quetin, and R. Ross (2003), A top–down, multidisciplinary study of the structure and function of the pack-ice ecosystem in the eastern Ross Sea, Antarctica, *Polar Record*, *39*(03), 219-230.

Allen, A. G., J. L. Grenfell, R. M. Harrison, J. James, and M. J. Evans (1999), Nanoparticle formation in marine airmasses: contrasting behaviour of the open ocean and coastal environments, *Atmospheric Research*, *51*(1), 1-14.

Arrigo, K. R., and C. W. Sullivan (1992), The influence of salinity and temperature covariation on the phytophysiological charachteristics of Antarctic sea ice microalgae 1 *Journal of Phycology*, *28*(6), 746-756.

Arrigo, K. R., and D. N. Thomas (2004), Large scale importance of sea ice biology in the Southern Ocean, *Antarctic Science*, pp. 471-486.

Arrigo, K. R., D. L. Worthen, P. Dixon, and M. P. Lizotte (1998), Primary productivity of near surface communities within Antarctic pack ice, *Antarctic Research Series*, *73*, 23-43.

Bari, S., and J. Hallett (1974), Nucleation and growth of bubbles at an ice-water interface, *J Glaciol.* 13, 489.

Barlow, R. G., M. Gosselin, L. Legendre, J. C. Therriault, S. Demers, R. F. C. Mantoura, and C. A. Llewellyn (1988), Photoadaptive strategies in sea-ice microalgae, *Marine ecology progress series*, pp. 145-152.

Barrie, L. A., J. W. Bottenheim, R. C. Schnell, P. J. Crutzen, and R. A. Rasmussen (1988), Ozone destruction and photochemical reactions at polar sunrise in the lower Arctic atmosphere, *Nature*, *334*(6178), 138-141.

Bell, N., L. Hsu, D. Jacob, M. Schultz, D. Blake, J. Butler, D. King, J. Lobert, and E. Maier-Reimer (2002), Methyl iodide: Atmospheric budget and use as a tracer of marine convection in global models, *J. Geophys. Res*, *107*(10.1029).

Bergström, B., G. Hempel, H. P. Marschall, A. North, V. Siegel, and J. O. Strömberg (1990), Spring distribution, size composition and behaviour of krill *Euphausia superba* in the western Weddell Sea, *Polar Record*, *26*(157), 85-89.

Bluhm, K. (2010), The influence of marine phytoplankton on iodine speciation in the Tropical and Southern Atlantic Ocean. PhD Thesis, der Christian-Albrechts-Universität zu Kiel

Boyd, P. W. (2002), Environmental factors controlling phytoplankton processes in the Southern Ocean 1, *Journal of Phycology*, *38*(5), 844-861.

Buinitsky, V. K. (1977), Organic life in sea ice, *Polar oceans. Arctic Institute of North America*, 301-306.

Bunt, J. (1964), Primary productivity under sea ice in Antarctic waters, influence of light and other factors on photosynthetic activities of Antarctic marine microalgae, *Biology of the Antarctic seas*, 27.

Bunt, J. (1968), Some characteristics of microalgae isolated from Antarctic sea ice, *Antarctic Research Series 11*, pp1-14

Bunt, J., and C. Lee (1970), Seasonal primary production in Antarctic sea ice at McMurdo Sound in 1967, *J. Mar. Res*, *28*, 304-320.

Burkholder, J., J. Curtius, A. Ravishankara, and E. Lovejoy (2004), Laboratory studies of the homogeneous nucleation of iodine oxides, *Atmospheric Chemistry and Physics*, *4*(1), 19-34.

Campos, M., A. Farrenkopf, T. Jickells, and G. Luther (1996), A comparison of dissolved iodine cycling at the Bermuda Atlantic Time-series Station and Hawaii Ocean Time-series Station, *Deep Sea Research Part II: Topical Studies in Oceanography*, *43*(2-3), 455-466.

Carpenter, L. J., and P. S. Liss (2000), On temperate sources of bromoform and other reactive organic bromine gases, *J. Geophys. Res.*, *105*(D16), 20539-20547.

Carpenter, L. J., W. T. Sturges, and S. Penkett (1999), Short-lived alkyl iodides and bromides at Mace Head, Ireland- Links to biogenic sources and halogen oxide production, in *Journal of Geophysical Research*, pp. 1679-1689.

Carpenter, L. J., D. J. Wevill, C. J. Palmer, and J. Michels (2007), Depth profiles of volatile iodine and bromine-containing halocarbons in coastal Antarctic waters, *Marine Chemistry*, *103*(3-4), 227-236.

Carpenter, L. J., J. R. Hopkins, C. E. Jones, A. C. Lewis, R. Parthipan, D. J. Wevill, L. Poissant, M. Pilote, and P. Constant (2005), Abiotic Source of Reactive Organic Halogens in the Sub-Arctic Atmosphere?, *Environmental Science and Technology*, edited, pp. 8812-8816.

Cavalieri, D., C. Parkinson, P. Gloersen, J. Comiso, and H. Zwally (1999), Deriving long-term time series of sea ice cover from satellite passive-microwave multisensor data sets, *Journal of Geophysical Research*, *104*(C7), 15803-15815.

Chameides, W. L., and D. D. Davis (1980), Iodine- Its possible role in tropospheric photochemistry, *Journal of Geophysical Research*, pp. 7383-7398.

Chance, R., G. Malin, T. Jickells, and A. R. Baker (2007), Reduction of iodate to iodide by cold water diatom cultures, *Marine Chemistry*, pp. 169-180, Elsevier.

Cho, H., P. B. Shepson, L. A. Barrie, J. P. Cowin, and R. Zaveri (2002), NMR Investigation of the Quasi-Brine Layer in Ice/Brine Mixtures, *The Journal of Physical Chemistry B*, *106*(43), 11226-11232.

Chuck, A. L., S. M. Turner, and P. S. Liss (2005), Oceanic distributions and air-sea fluxes of biogenic halocarbons in the open ocean, *Journal of geophysical research*, edited, pp. 10022-10022

Class, T., and K. Ballschmiter (1987), Chemistry of organic traces in air IX: Evidence of natural marine sources for chloroform in regions of high primary production, *Fresenius' Journal of Analytical Chemistry*, *327*(1), 40-41.

Cox, G. F. N. and W. F. Weeks (1982), Equations for Determining the Gas and Brine Volumes in Sea Ice Samples, in *Journal of Glaciology*, DTIC Research Report ADA122779.

Cox, G. F. N. and W. F. Weeks (1988), Numerical Simulations of the Profile Properties of Undeformed First-Year Sea Ice During the Growth Season, *J. Geophys. Res.*, *93*(C10), 12449-12460.

Daly, K. L. (1990), Overwintering development, growth, and feeding of larval Euphausia superba in the Antarctic marginal ice zone, *Limnology and Oceanography*, *35*(7), 1564-1576.

Daly, K. L., W. O. Smith, G. C. Johnson, G. R. DiTullio, D. R. Jones, C. W. Mordy, R. A. Feely, D. A. Hansell, and J. Z. Zhang (2001), Hydrography, nutrients, and carbon pools in the Pacific sector of the Southern Ocean: Implications for carbon flux, *Journal of Geophysical Research - Oceans,* 106 (C4), 7107-7124.

Davis, D., J. Crawford, S. Liu, S. McKeen, A. Bandy, D. Thornton, F. Rowland, and D. Blake (1996), Potential impact of iodine on tropospheric levels of ozone and other critical oxidants, in *Journal of Geophysical Research - Atmospheres*, 101 (D1), pp. 2135-2147.

Davison, B., C. N. Hewitt, J. A. Lowe, M. H. Smith, M. Schwikowski, U. Baltensperger, and R. M. Harrison (1996a), Dimethyl sulfide, methane sulfonic acid and physicochemical aerosol properties in Atlantic air from the United Kingdom to Halley Bay, *Journal of Geophysical Research*, 101 (D17) pp. 22855-22867.

Davison, B., C. N. Hewitt, C. D. O'Dowd, J. A. Lowe, M. H. Smith, M. Schwikowski, U. Baltensperger, and R. M. Harrison (1996b), Dimethyl sulfide, methane sulfonic acid and physicochemical aerosol properties in Atlantic air from the United Kingdom to Halley Bay, *Journal of Geophysical Research. D. Atmospheres*, *101*, 22855-22867.

De Boer, E., M. G. M. Tromp, H. Plat, G. E. Krenn, and R. Wever (1986), Vanadium (V) as an essential element for haloperoxidase activity in marine brown algae: purification and characterization of a vanadium (V)-containing bromoperoxidase from Laminaria saccharina, *Biochimica et Biophysica Acta (BBA) - Protein Structure and Molecular Enzymology*, 872, pp. 104-115.

de la Cuesta, J., and S. L. Manley (2009), Iodine assimilation by marine diatoms and other phytoplankton in nitrate-replete conditions, *Limnol. Oceanogr*, *54*(5), 1653-1664.

Deming, J. W. (2002), Psychrophiles and polar regions, *Current Opinion in Microbiology*, *5*(3), 301-309.

DeMore, W., S. Sander, D. Golden, R. Hampson, M. Kurylo, C. Howard, A. Ravishankara, C. Kolb, and M. Molina (1997), Chemical kinetics and photochemical data for use in stratospheric modeling. Evaluation number 12, *JPL Publication 97-4*, 1-266.

Dieckmann, G., G. Rohardt, H. Hellmer, and J. Kipfstuhl (1986), The occurrence of ice platelets at 250 m depth near the Filchner Ice Shelf and its significance for sea ice biology, *Deep Sea Research Part A. Oceanographic Research Papers*, *33*(2), 141-148.

Duce, R. A., J. T. Wasson, J. W. Winchester, and F. Burns (1963), Atmospheric iodine, bromine, and chlorine, *Journal of Geophysical Research (US)*, *68*.

Eicken, H., and M. A. Lange (1989), Development and Properties of Sea Ice in the Coastal Regime of the Southeastern Weddell Sea, *J. Geophys. Res.*, *94*(C6), 8193-8206.

Eide, L., and S. Martin (1975), The formation of brine drainage features in young sea ice, *J. Glaciol*, *14*(70), 137-154.

El-Sayed, S. Z. (2005), History and evolution of primary productivity studies of the Southern Ocean, *Polar Biology*, *28*(6), 423-438.

Elliott, S., and F. S. Rowland (1993), Nucleophilic substitution rates and solubilities for methyl halides in seawater, *Geophys. Res. Lett.*, *20*(11), 1043-1046.

Fogelqvist, E. (1985), Carbon tetrachloride, tetrachloroethylene, 1,1,1-trichloroethane and bromoform in Arctic seawater, *J. Geophys. Res.*, *90*(C5), 9181-9193.

Fogelqvist, E. and Krysell (1991), Naturally and anthropogenically produced bromoform in the Kattegatt, a semi-enclosed oceanic basin, *Journal of Atmospheric Chemistry*, *13*(4), 315-324.

Fogelqvist, E. and T. Tanhua (1995), Iodinated C1-C4 hydrocarbons released from ice algae in Antarctic, *Naturally Produced Organohalogens*, 295-307.

Francois, R. (1987), The influence of humic substances on the geochemistry of iodine in nearshore and hemipelagic marine sediments, *Geochimica et Cosmochimica Acta*, *51*(9), 2417-2427.

Frankenstein, G., and R. Garner (1967), Equations for determining the brine volume of sea ice from-0.5 C to-22.9 C, *Journal of Glaciology*, *6*, 943-944.

Frieß, U., T. Deutschmann, B. Gilfedder, R. Weller, and U. Platt (2010), Iodine monoxide in the Antarctic snowpack, *Atmos. Chem. Phys*, *10*, 2439-2456.

Fuge, R., and C. C. Johnson (1986), The geochemistry of iodine—a review, *Environmental Geochemistry and Health*, *8*(2), 31-54.

Furneaux, K., L. K. Whalley, D. E. Heard, H. M. Atkinson, W. J. Bloss, M. J. Flynn, M. W. Gallagher, T. Ingham, L. Kramer, J. D. Lee, R. Leigh, G. B. McFiggans, A. S. Mahajan, P. S. Monks, H. Oetjen, J. M. C. Plane and J. D. Whitehead (2010), Measurements of iodine monoxide at a semi polluted coastal location, *Atmospheric Chemistry and Physics*, *10*, 3645-3663.

Garrison, D. L. and K. R. Buck (1989), The biota of Antarctic pack ice in the Weddell sea and Antarctic Peninsula regions, *Polar Biology*, *10*(3), 211-219.

Garrison, D. L., M. O. Jeffries, A. Gibson, S. L. Coale, D. Neenan, C. Fritsen, Y. B. Okolodkov, and M. M. Gowing (2003), Development of sea ice microbial communities during autumn ice formation in the Ross Sea, *Marine Ecology Progress Series*, *259*, 1-15.

Genty, B., J. M. Briantais, and N. R. Baker (1989), The relationship between the quantum yield of photosynthetic electron transport and quenching of chlorophyll fluorescence, *Biochimica et Biophysica Acta (BBA)-General Subjects*, *990*(1), 87-92.

Golden, K., S. Ackley, and V. Lytle (1998), The percolation phase transition in sea ice, *Science*, *282*(5397), 2238.

Goodwin, W. J. North, and M. E. Lidstrom (1997), Production of bromoform and dibromomethane by giant kelp: factors affecting release and comparison to anthropogenic bromine sources, *Limnology and Oceanography*, 1725-1734.

Goodwin, J. Schaefer, and R. Oremland (1998), Bacterial oxidation of dibromomethane and methyl bromide in natural waters and enrichment cultures, *Applied and environmental microbiology*, *64*(12), 4629.

Gosink, T. A., J. G. Pearson, and J. J. Kelley (1976), Gas movement through sea ice, *Nature*, 263, 41-42.

Gosselin, M., L. Legendre, J. C. Therriault, S. Demers, and M. Rochet (1986), Physical control of the horizontal patchiness of sea-ice microalgae, *Marine Ecology,* 29, pp. 289-298.

Grant, W., and R. Horner (1976), Growth responses to salinity variation in four arctic ice diatoms [*Melosira juergensii, Porosira glacialis, Navicula transitans derasa, Coscinodiscus lacustris*], *Journal of Phycology, 12 (2) 180-185*.

Guillard, R. R. L., and J. H. Ryther (1962), Studies of Marine Planktonic diatoms: I. *Cyclotella Nana Hustedt,* and *Detonula Confervacea (Cleve) Gran*, *Canadian Journal of Microbiology*, 8(2), 229-239.

Guillard, R. R. L., W. Smith, and M. Chanley (1975), Culture of phytoplankton for feeding marine invertebrates, *Culture of Marine Invertebrates.*, 26-60.

Haas, C., D. N. Thomas, and J. Bareiss (2001), Surface properties and processes of perennial Antarctic sea ice in summer, *Journal of Glaciology*, *47*(159), 613-625.

Hannach, G., and A. C. Sigleo (1998), Photoinduction of UV-absorbing compounds in six species of marine phytoplankton, *Marine Ecology Progress Series*, *174*, 207-222.

Hasle, G. R. (1976), The biogeography of some marine planktonic diatoms, *Deep Sea Research and Oceanographic Abstracts*, *23*(4), 319-338, IN311-IN316.

Hemmingsen, E. (1959), Permeation of gases through ice, *Tellus*, *11*(3), 355-359.

Hetzel, B. S., J. T. Dunn, and J. B. Stanbury (1987), *The prevention and control of iodine deficiency disorders*, Elsevier Publishing Company.

Hill, V. L., and S. L. Manley (2009), Release of reactive bromine and iodine from diatoms and its possible role in halogen transfer in polar and tropical oceans, *Limnology and Oceanography*, *54*(3), 812-822.

Hönninger, G., and U. Platt (2002), Observations of BrO and its vertical distribution during surface ozone depletion at Alert, *Atmospheric Environment*, *36*(15-16), 2481-2489.

Horner, R., S. F. Ackley, G. S. Dieckmann, B. Gulliksen, T. Hoshiai, L. Legendre, I. A. Melnikov, W. S. Reeburgh, M. Spindler, and C. W. Sullivan (1992), Ecology of sea ice biota. I: Habitat, terminology, and methodology, *Polar Biology*, 12 (3-4) pp. 417-427, Springer.

Hoshiai, T. (1977), Seasonal change of ice communities in the sea ice near Syowa Station, Antarctica. *Polar Oceans*, Calgary, *Arctic Inst. North Am*, 307-317.

Hsiao, S. I. C. (1980), Quantitative composition, distribution, community structure and standing stock of sea ice microalgae in the Canadian Arctic, *Arctic*, *33*(4), 768-793.

Huang, R.-J., K. Seitz, J. Buxmann, D. Pöhler, K. Hornsby, L. Carpenter, U. Platt, and T. Hoffmann (2010), In situ measurements of molecular iodine in the marine boundary layer: the link to macroalgae and the implications for O_3, IO, OIO and NO_x, *Atmos. Chem. Phys*, *10*, 4823-4833.

Huang, R. J., and T. Hoffmann (2009), Development of a coupled diffusion denuder system combined with gas chromatography/mass spectrometry for the separation and quantification of molecular iodine and the activated iodine compounds iodine monochloride and hypoiodous acid in the marine atmosphere, *Analytical chemistry*, *81*(5), 1777-1783.

Hughes, C., G. Malin, C. Turley, B. Keely, P. Nightingale, and P. Liss (2008), The production of volatile iodocarbons by biogenic marine aggregates, *Limnology and Oceanography*, *53*(2), 867-872.

Hughes, C., A. L. Chuck, H. Rossetti, P. J. Mann, S. M. Turner, A. Clarke, R. Chance, and P. S. Liss (2009), Seasonal cycle of seawater bromoform and dibromomethane concentrations in a coastal bay on the western Antarctic Peninsula, *Global Biogeochemical Cycles*, *23*(2), GB2024.

Jickells, T., S. Boyd, and A. Knap (1988), Iodine cycling in the Sargasso Sea and the Bermuda inshore waters, *Marine Chemistry*, *24*(1), 61-82.

Johnson, M. (2010), A numerical scheme to calculate temperature and salinity dependent air-water transfer velocities for any gas, *Ocean Sci*, *6*, 913–932.

Jones, C. E., and L. J. Carpenter (2005), Solar photolysis of CH2I2, CH2ICl, and CH2IBr in water, saltwater, and seawater, *Environmental science & technology*, *39*(16), 6130-6137.

King, J., and P. Anderson (1994), Heat and water vapour fluxes and scalar roughness lengths over an Antarctic ice shelf, *Boundary-Layer Meteorology*, *69*(1), 101-121.

Klick, S., and K. Abrahamsson (1992), Biogenic volatile iodated hydrocarbons in the ocean, *Journal of Geophysical Research*, *97*(C8), 12683-12612,12687.

Kreher, K., P. Johnston, S. Wood, B. Nardi, and U. Platt (1997), Ground based measurements of tropospheric and stratospheric BrO at Arrival Heights, Antarctica, *Geophysical Research Letters*, *24*(23), 3021-3024.

Krembs, C., H. Eicken, K. Junge, and J. Deming (2002), High concentrations of exopolymeric substances in Arctic winter sea ice: implications for the polar ocean carbon cycle and cryoprotection of diatoms, *Deep Sea Research Part I: Oceanographic Research Papers*, *49*(12), 2163-2181.

Kristiansen, S., and E. Syvertsen (1990), Sea ice algae in the Weddell Sea during austral spring 1988, *EOS, Trans. A m. Geophys. U nion*, *71*, 79.

Küpper, F. C., N. Schweigert, E. Ar Gall, J. M. Legendre, H. Vilter, and B. Kloareg (1998), Iodine uptake in Laminariales involves extracellular, haloperoxidase-mediated oxidation of iodide, *Planta*, *207*(2), 163-171.

Lange, M., S. Ackley, P. Wadhams, G. Dieckmann, and H. Eicken (1989), Development of sea ice in the Weddell Sea, *Annals of Glaciology*, *12*, 92-96.

Liss, P. S. (1986), *NATO ASI*, *185*, 283–294.

Loose, B., P. Schlosser, D. Perovich, D. Ringelberg, D. Ho, T. Takahashi, J. Richter Menge, C. Reynolds, W. McGillis, and J. L. Tison (2011), Gas diffusion through columnar laboratory sea ice: implications for mixed layer ventilation of CO_2 in the seasonal ice zone, *Tellus B - Chemical and Physical Meteorology,* 63, 1, pp 23-39.

Lovelock, J. E. (1975), Natural halocarbons in the air and in the sea, *Nature* 256, 193-194

Luther, G. W., C. B. Swartz, and W. J. Ullman (1988), Direct determination of iodide in seawater by cathodic stripping square wave voltammetry, *Analytical chemistry*, *60*(17), 1721-1724.

Luther, G. W., J. Wu, and B. Cullen John (1995), Redox Chemistry of Iodine in Seawater, *Aquatic Chemistry*, pp. 135-155

Mahajan, M. Sorribas, J. Gómez Martín, S. MacDonald, M. Gil, J. Plane, and A. Saiz-Lopez (2010a), Concurrent observations of atomic iodine, molecular iodine and ultrafine particles in a coastal environment, *Atmospheric Chemistry & Physics Discussions*, *10*, 27227-27253.

Mahajan, M. Shaw, H. Oetjen, K. E. Hornsby, L. J. Carpenter, L. Kaleschke, X. Tian-Kunze, J. D. Lee, S. J. Moller, and P. Edwards (2010b), Evidence of reactive iodine chemistry in the Arctic boundary layer, *Journal of Geophysical Research*, *115*(D20), D20303.

Mahajan, A., J. Plane, H. Oetjen, L. Mendes, R. Saunders, A. Saiz-Lopez, C. Jones, L. Carpenter, and G. McFiggans (2010), Measurement and modelling of tropospheric reactive halogen species over the tropical Atlantic Ocean, *Atmos. Chem. Phys*, *10*, 4611-4624.

Manley, S. (2002), Phytogenesis of halomethanes: A product ofselection or a metabolic accident?, Biochemistry, 60, 2, 163-180, pp. 163-180

Manley, S. and J. L. de la Cuesta (1997), Methyl iodide production from marine phytoplankton cultures, *Limnology and Oceanography*, *42*(1), 142-147.

Martino, M., G. P. Mills, J. Woeltjen, and P. S. Liss (2009), A new source of volatile organoiodine compounds in surface seawater, *Geophysical Research Letters*, *36*(1), L01609.

McConnell, J. C., G. S. Henderson, L. Barrie, J. Bottenheim, H. Niki, C. H. Langford, and E. M. J. Templeton (1992), Photochemical bromine production implicated in Arctic boundary layer ozone depletion, *Nature*, *355*, 150-152.

McFiggans, G., R. A. Cox, B. J. Allan, and J. M. C. Plane (2002), Active chlorine release from marine aerosols: Roles for reactive iodine and nitrogen species, in *Journal of Geophysical Research,* 107, p. 4271

McFiggans, G., C. Bale, S. Ball, J. Beames, W. Bloss, L. Carpenter, J. Dorsey, R. Dunk, M. Flynn, and K. Furneaux (2010), Iodine-mediated coastal particle formation: an overview of the Reactive Halogens in the Marine Boundary Layer (RHaMBLe) Roscoff coastal study, *Atmospheric Chemistry & Physics*, *10*, 2975-2999.

McFiggans, G., H. Coe, R. Burgess, J. Allan, M. Cubison, M. R. Alfarra, R. Saunders, A. Saiz-Lopez, J. M. C. Plane, D. Wevill, L. J. Carpenter, A. R. Rickard, and P. S. Monks (2004), Direct evidence for coastal iodine particles from Laminaria macroalgae - linkage to emissions of molecular iodine, *Atmos. Chem. Phys.* 4, 701–713.

Meguro, H. (1962), Plankton ice in the Antarctic Ocean, *Antarctic Record*, pp. 1192-1199.

Moline, M. A., and B. B. Prezelin (1996), Long-term monitoring and analyses of physical factors regulating variability in coastal Antarctic phytoplankton biomass, in situ productivity and taxonomic composition over subseasonal, seasonal and interannual time scales.

Moore, R. M. (2003), Marine Sources of Volatile Organohalogens, *The Handbook of Environmental Chemistry* Vol. 3, Part P (2003): 85–101.

Moore, R. M. and R. Tokarczyk (1993), Volatile biogenic halocarbons in the northwest Atlantic, *Global Biogeochemical Cycles*, *7*(1), 195-210.

Moore, R. M., M. Webb, R. Tokarczyk, and R. Wever (1996), Bromoperoxidase and iodoperoxidase enzymes and production of halogenated methanes in marine diatom cultures, *Journal of Geophysical Research* 101, C9, pp. 20899-20908

Moore, R. M., and O. C. Zafiriou (1994), Photochemical production of methyl iodide in seawater, *Journal of Geophysical Research,* 99, D8, 16415-16420.

Nakayama, E., T. Kimoto, K. Isshiki, Y. Sohrin, and S. Okazaki (1989), Determination and distribution of iodide-and total-iodine in the North Pacific Ocean-by using a new automated electrochemical method, *Marine Chemistry*, *27*(1-2), 105-116.

O'Dowd, C. D., J. L. Jimenez, R. Bahreini, R. C. Flagan, J. H. Seinfeld, K. Hameri, L. Pirjola, M. Kulmala, S. G. Jennings, and T. Hoffmann (2002), Marine aerosol formation from biogenic iodine emissions, *Nature*, *417*(6889), 632-636.

O'Driscoll, P., N. Minogue, N. Takenaka, and J. Sodeau (2008), Release of nitric oxide and iodine to the atmopshere from the freezing of sea-salt aerosol components, *Journal of Physical Chemistry A*, *112*(8), 1677-1682.

Palmisano, A., and C. Sullivan (1985), Growth, metabolism, and dark survival in sea ice microalgae, in: Horner, R. A. *Sea ice biota*, pp 131-146

Pechtl, S., E. Lovejoy, J. Burkholder, and R. Von Glasow (2006), Modeling the possible role of iodine oxides in atmospheric new particle formation, *Atmospheric Chemistry and Physics*, *6*(2), 505-523.

Pirjola, L., C. O'Dowd, Y. J. Yoon, and K. Sellegri (2005), Modelling Iodine Particle Formation and Growth from Seaweed in a Chamber, in *Environmental Chemistry*, pp. 271-281.

Platt, U., and C. Janssen (1995), Observation and role of the free radicals NO_3, ClO, BrO and IO in the troposphere, *Faraday Discuss.*, *100*, 175-198.

Platt, U., D. Perner, and H. Pätz (1979), Simultaneous measurement of atmospheric CH_2O, O_3, and NO_2 by differential optical absorption, *Journal of Geophysical Research*, *84*(C10), 6329-6335.

Quack, B., and D. W. R. Wallace (2003), Air-sea flux of bromoform: Controls, rates, and implications, *Global Biogeochem. Cycles*, *17*(1), 1023.

Rankin, A. M., E. W. Wolff, and S. Martin (2002), Frost flowers: Implications for tropospheric chemistry and ice core interpretation, in *Journal of Geophysical Research*, 10, D23, p. 4683.

Read, K. A., A. S. Mahajan, L. J. Carpenter, M. J. Evans, B. V. E. Faria, D. E. Heard, J. R. Hopkins, J. D. Lee, S. J. Moller, and A. C. Lewis (2008), Extensive halogen-mediated ozone destruction over the tropical Atlantic Ocean, *Nature*, *453*(7199), 1232-1235.

Reifenhauser, W., and K. G. Heumann (1992), Determinations of methyl iodide in the Antarctic atmosphere and the south polar sea, in *Atmospheric environment, Part A,* 24, 9, pp. 2905-2912.

Renfrew, I. A., and J. C. King (2000), A Simple Model Of The Convective Internal Boundary Layer And Its Application To Surface Heat Flux Estimates Within Polynyas, *Boundary-Layer Meteorology*, *94*(3), 335-356.

Saiz-Lopez, A., and J. M. C. Plane (2004), Novel iodine chemistry in the marine boundary layer, in *Geophysical research letters*, 31, L04112.

Saiz-Lopez, A., and C. S. Boxe (2008), A mechanism for biologically-induced iodine emissions from sea-ice, *Atmos. Chem. Phys. Discuss.*, *8*(1), 2953-2976.

Saiz-Lopez, A., A. S. Mahajan, R. A. Salmon, S. J. B. Bauguitte, A. E. Jones, H. K. Roscoe, and J. M. C. Plane (2007a), Boundary Layer Halogens in Coastal Antarctica, *Science*, 317, p 348.

Saiz-Lopez, A., J. Plane, G. McFiggans, P. Williams, S. Ball, M. Bitter, R. Jones, C. Hongwei, and T. Hoffmann (2006), Modelling molecular iodine emissions in a coastal marine environment: the link to new particle formation, *Atmospheric Chemistry and Physics*, *6*(4), 883-895.

Saiz-Lopez, A., J. M. C. Plane, A. S. Mahajan, P. S. Anderson, S. J. B. Bauguitte, A. E. Jones, H. K. Roscoe, R. A. Salmon, W. J. Bloss, and J. D. Lee (2007b), On the vertical distribution of boundary layer halogens over coastal Antarctica: implications for O_3, HO_x, NO_x and the Hg lifetime, *ACPD* pp. 9385-9417.

Sander, R. (1999), Compilation of Henry's law constants for inorganic and organic species of potential importance in environmental chemistry, *Max-Planck Institute of Chemistry*, Air Chemistry Dept.

Saunders, and J. M. C. Plane (2006), Fractal growth modelling of I_2O_5 nanoparticles, *Aerosol Science 37* pp. 1737-1749

Saunders, R. Kumar, J. Martin, A. Mahajan, B. Murray, and J. Plane (2010), Studies of the formation and growth of aerosol from molecular iodine precursor, *Z. Phys. Chem*, *224*, 1095–1117.

Schall, C., K. Heumann, and G. Kirst (1997), Biogenic volatile organoiodine and organobromine hydrocarbons in the Atlantic Ocean from 42 N to 72 S, *Fresenius' Journal of Analytical Chemistry*, *359*(3), 298-305.

Schönhardt, A., A. Richter, F. Wittrock, H. Kirk, H. Oetjen, H. K. Roscoe, and J. P. Burrows (2008), Observations of iodine monoxide columns from satellite, *Atmos. Chem. Phys.*, *8*(3), 637-653.

Simpson, W. R., et al. (2007), Halogens and their role in polar boundary-layer ozone depletion, *Atmos. Chem. Phys.*, *7*(16), 4375-4418.

Slingo, A. (1990), Sensitivity of the Earth's radiation budget to changes in low clouds, *Nature*, *343*(6253), 49-51.

Spindler, M. (1990), A comparison of Arctic and Antarctic sea ice and the effects of different properties on sea ice biota, *Geological history of the Polar Oceans: Arctic Versus Antarctic. Kluwers Academis Publishers*, 173-186.

Spokes, L. J., and P. S. Liss (1996), Photochemically induced redox reactions in seawater, II. Nitrogen and iodine, *Marine Chemistry*, *54*(1-2), 1-10.

Strickland, J., and T. Parsons (1968), A practical handbook of seawater analysis, *Bull. Fish. Res. Bd. Can*, *167*, 311.

Sturges, G. F. Cota, and P. T. Buckley (1992), Bromoform emission from Arctic ice algae, *Nature*, *358*(6388), 660-662.

Sturges, G. F. Cota, and P. T. Buckley (1997), Vertical profiles of bromoform in snow, sea ice, and seawater in the Canadian Arctic, *Journal of Geophysical Research*, *102*(C11), 25073-25025,25083.

Sutherland, P. C. (1852), *Journal of a voyage in Baffin's Bay and Barrow Straits: in the years 1850-1851 performed by HM Ships Lady Franklin and Sophia under the command of Mr. William Penny, in search of the missing crews of HM Ships Erebus and Terror*, Longman, Brown, Green and Longmans.

Swanson, A. L., N. J. Blake, J. E. Dibb, M. R. Albert, D. R. Blake, and F. Sherwood Rowland (2002), Photochemically induced production of CH_3Br, CH_3I, C_2H_5I, ethene, and propene within surface snow at Summit, Greenland, *Atmospheric Environment*, *36*(15-16), 2671-2682.

Swanson, A. L., N. J. Blake, D. R. Blake, F. Sherwood Rowland, J. E. Dibb, B. L. Lefer, and E. Atlas (2007), Are methyl halides produced on all ice surfaces? Observations from snow-laden field sites, *Atmospheric Environment*, *41*(24), 5162-5177.

Thomas, D. N. and G. Dieckmann (2002), Antarctic sea ice-a habitat for extremophiles, *Science*, *295*(5555), 641.

Thomas, D. N., S. Papadimitriou, and C. Michel (2010), Biogeochemistry of Sea Ice, in *Sea Ice, Second Edition*, Wiley Blackwell, pp 425-467

Tison, J. L., F. Brabant, I. Dumont, and J. Stefels (2010), High-resolution dimethyl sulfide and dimethylsulfoniopropionate time series profiles in decaying summer first-year sea ice at Ice Station Polarstern, western Weddell Sea, Antarctica, *J. Geophys. Res.*, *115*(G4), G04044.

Tokarczyk, R., and R. M. Moore (1994), Production of volatile organohalogens by phytoplankton cultures, *Geographical Research Letters*, *21*(4), 285-288.

Truesdale, V. (1974), The chemical reduction of molecular iodine in seawater, *Deep Sea Research and Oceanographic Abstracts*, *21*(9), 761-766.

Truesdale, V. (1995), Effect of iodide concentration upon the kinetics of disproportionation of hypoiodous acid in borate buffer, *Journal of the Chemical Society, Faraday Transactions*, *91*(5), 863-866.

Truesdale, V. and C. P. Spencer (1974), Studies on the determination of inorganic iodine in seawater, *Marine Chemistry*, *2*(1), 33-47.

Tsunogai, S., and T. Sase (1969), Formation of iodide-iodine in the ocean, *Deep Sea Research and Oceanographic Abstracts*, *16*(5), 489-496.

Vincent, W. F., and S. Roy (1993), Solar ultraviolet-B radiation and aquatic primary production: damage, protection, and recovery, *Environ. Rev*, *1*, 1-12.

Vogt, R., P. J. Crutzen, and R. Sander (1996), A mechanism for halogen release from sea-salt aerosol in the remote marine boundary layer, *Nature*, *383*(6598), 327-330.

Vogt, R., R. Sander, R. von Glasow, and P. J. Crutzen (1999), Iodine Chemistry and its Role in Halogen Activation and Ozone Loss in the Marine Boundary Layer: A Model Study, *Journal of Atmospheric Chemistry*, *32*(3), 375-395.

Wadhams, P., M. A. Lange, and S. F. Ackley (1987), The Ice Thickness Distribution Across the Atlantic Sector of the Antarctic Ocean in Midwinter, *J. Geophys. Res.*, *92*(C13), 14535-14552.

Wang, J., L. A. Mysak, and R. G. Ingram (1994), A Numerical Simulation of Sea Ice Cover in Hudson Bay, *Journal of Physical Oceanography*, *24*(12), 2515-2533.

Weeks, W. F., and S. F. Ackley (1982), The growth, structure, and properties of sea ice *Rep.*, Cold Regions Research and Engineering Lab Hanover HN

Weissenberger, J., G. Dieckmann, R. Gradinger, and M. Spindler (1992), Sea Ice: A Cast Technique to Examine and Analyze Brine Pockets and Channel Structure, *Limnology and Oceanography*, *37*(1), 179-183.

Welch, H. E., and M. Bergmann (1989), Seasonal development of ice algae and its prediction from environmental factors near Resolute, NWT, Canada, *Canadian journal of fisheries and aquatic sciences*, *46*(10), 1793-1804.

Wong, G. (1991), The marine geochemistry of iodine, *Rev. Aquat. Sci*, *4*(1), 45-73.

Yuan-Hui, L., and S. Gregory (1974), Diffusion of ions in sea water and in deep-sea sediments, *Geochimica et Cosmochimica Acta*, *38*(5), 703-714.